TESIS DOCTORALES

INSTITUTO ESPAÑOL
DE OCEANOGRAFÍA

Fluxes, trends and decadal changes in the subtropical North Atlantic

Alicia María Lavín Montero

INICIO / START

SALIDA / EXIT

MINISTERIO
DE CIENCIA
Y TECNOLOGÍA

Título anterior de la serie *(Formerly titled)*:
MICROFICHAS
INSTITUTO ESPAÑOL DE OCEANOGRAFÍA

ISSN: 1578-410X
Núm. 15
Págs. 241
Madrid, España 2001

TESIS DOCTORALES. INSTITUTO ESPAÑOL DE OCEANOGRAFÍA

Publicación científica de periodicidad no regular destinada a la edición de tesis doctorales realizadas por investigadores del Instituto Español de Oceanografía sobre Ciencias Marinas. Las tesis se publican tal como han sido presentadas en las universidades.

An aperiodical scientific publication, whose purposes is to publish doctoral theses regarding the marine sciences by researchers from the Instituto Español de Oceanografía. These theses are published just as they were presented at university.

Para información sobre publicación de originales, suscripciones, intercambios y solicitud de ejemplares, por favor, dirigirse a *(For information regarding publications of papers, subscriptions, exchange of issues and back issues please contact)*:
INSTITUTO ESPAÑOL DE OCEANOGRAFÍA
Avda. de Brasil, 31. 28020 Madrid, España. Tel.: 91-417 54 11. Fax: 91-597 47 70
E-mail: publicaciones@md.ieo.es
Dirección en Internet *(Website)*: http://www.ieo.es

La responsabilidad por las opiniones emitidas en esta publicación corresponde exclusivamente al autor *(The opinions expressed herein are those of the author).*

Título abreviado de esta publicación *(Running title)*: Tesis Dr. Inst. Esp. Oceanogr.

Derechos de autor *(Copyright)*

MINISTERIO DE CIENCIA Y TECNOLOGÍA
INSTITUTO ESPAÑOL DE OCEANOGRAFÍA

Edita *(Published by)*: INSTITUTO ESPAÑOL DE OCEANOGRAFÍA

Depósito Legal: M-40353-2001
ISSN: 1578-410X
NIPO: 406-01-006-1
Diseño de cubierta *(Cover design)*: Omega. Ramón Azorín, 2. 28047 Madrid, España
Imprime *(Printed by)*: Microdata Micrografía e Informática, S.A. Montesa, 12. 28006 Madrid, España

TESIS DOCTORALES

INSTITUTO ESPAÑOL
DE OCEANOGRAFÍA

Fluxes, trends and decadal changes in the subtropical North Atlantic

Alicia María Lavín Montero

Centro Oceanográfico de Santander
INSTITUTO ESPAÑOL DE OCEANOGRAFÍA
Apdo. 240. 28080 Santander (Cantabria), España

Received December 1999. Accepted December 2000

MINISTERIO DE CIENCIA Y TECNOLOGÍA
INSTITUTO ESPAÑOL DE OCEANOGRAFÍA

Edita (Published by): INSTITUTO ESPAÑOL DE OCEANOGRAFÍA
Avda. de Brasil, 31. 28020 Madrid, España

ISSN: 1578-410X
Núm. 15
Págs. 241
Madrid, España 2001

UNIVERSIDAD DE CANTABRIA

DEPARTAMENTO DE CIENCIAS Y TÉCNICAS
DEL AGUA Y MEDIO AMBIENTE

TESIS DOCTORAL

Fluxes, trends and decadal changes in the subtropical North Atlantic

Flujos, tendencias y cambios decenales en la zona subtropical del Atlántico norte

Alicia María Lavín Montero

Datos técnicos *(Technical data)*

Presentación *(Presentation)*: Santander, enero de 1999
Fecha de lectura *(Reading date)*: 29 de abril de 1999
Directores *(Tutors)*: Gregorio Parrilla Barrera
Íñigo Losada Rodríguez
Tribunal *(Committee)*:
Presidente *(Chairman)*: Joaquín Tintoré Subirana
Secretario *(Secretary)*: Raul Medina Santamaría
Vocales *(Members)*: Harry Bryden
José Ramón Pascual Domínguez-Gil
José Luis Pelegrí Llopart

Notas *(Notes)*

En la presentación de esta tesis en la Universidad de Cantabria se incluyó una versión abreviada en español para dar cumplimiento a la disposición para presentación de tesis doctorales en lengua extranjera en dicha universidad *(The version of this thesis originally presented at the University of Cantabria included an abridged Spanish translation, to meet the university's regulations on presenting doctoral theses in foreign languages).*

A Mac

Y a mi familia para compensar la falta de dedicación

A Ana, Pedro, Raquel, Fernando y a Claudia que fue bautizada con agua de 3500 m de profundidad de la estación 100 (24º 37.41'N, 75º 19.12'W) en la Western Boundary, proveniente de los mares de Groenlandia, Islandia y Noruega, con una temperatura potencial de 2.217ºC, salinidad 34.915, oxígeno disuelto 6.19 ml/l, CFC-11 0.072 pmole/kg y CFC-12 0.216 pmole/kg. Que esto le proporcione la curiosidad necesaria para dedicarse a la investigación.

Agradecimientos

Quiero mostrar mi agradecimiento en primer lugar a Rafael Robles, Alvaro Fernández y Orestes Cendrero, director y subdirector entonces del Instituto Español de Oceanografía y director del C. Oceanográfico de Santander que me autorizaron una estancia de 2 años en el Instituto Tecnológico de Massachusettss (MIT) donde realicé parte de este trabajo. A la Fundación Marcelino Botín que mediante una beca de postgrado me financió dicha estancia. A Federico Fernández de Castillejo y Jose Ramón Pascual del IEO y Miguel Losada de la Universidad de Cantabria que en ese momento me apoyaron. A los profesores Carl Wunsch del MIT, Harry Bryden del Southampton Oceanographic Centre (R. U.) y a Robert Millard de la Woods Hole Oceanographic Institution con los que trabajé los capítulos 2 y 3. A los compañeros que me ayudaron y me animaron durante mi estancia en el MIT como Alison Macdonald, Jim Gunson, Gwyneth Hutfford y el apoyo técnico de Charmaine King. Al jefe de campaña Gregorio Parrilla y a todos los participantes en la campaña A-5 del WOCE, especialmente a Harry Bryden, María Jesús García, Bob Millard, Joaquín Molinero, Rafael Molina, Pepe Escánez, Tomeu Amengual, Pepe Braun, Antonio Cruzado, Zoila Velazques, Bill Smethie, Aida Ríos, Gabriel Rosón, Juan Alonso, Pilar Sánchez, Enrique Alvarez, y Alan Cantos con los que he seguido en contacto y me han animado. Al capitán, oficiales y tripulación del *Hespérides.* Organismos que financiaron la campaña como el IEO, la CICYT, NSF y NOAA, así como los que financiaron posteriormente el tratamiento de los datos como el IEO y el NERC (R. U.). El trabajo posterior a Harry Bryden, Gregorio Parrilla, María Jesús García, Bob Millard, Bill Smethie y Mike Griffiths. A Mary Woodgate-Jones el análisis de datos de sales nutritivas. A Mike Griffiths por algunas de sus gráficas. A Gregorio Parrilla, investigador principal del proyecto 'Transportes a través del paralelo 24º 30'N Atlántico, A-5 WOCE' del IEO y a María Jesús García investigadora de dicho proyecto, por las facilidades y su dedicación prioritaria al trabajo en los momentos necesarios a pesar de sus múltiples ocupaciones. A mis colegas José Manuel Cabanas, Guillermo Díaz del Río, Juan Alonso y Luis Valdés por su comprensión durante el último periodo de elaboración de esta tesis. A los colegas del IEO que me han ayudado en la elaboración del software y figuras como Pablo Barquín, Joaquín Molinero y Xabier Moreno-Ventas. A Concha Mosquera en la redacción. A Pilar Pereda, Begoña Villamor, Charo López y Victoria Ortiz de Zárate por su apoyo. A los

profesores y doctorandos del Grupo de Ingenieria Oceanográfica y de Costas de la Universidad de Cantabria por su ánimo y ayuda. A mi primer director de tesis Miguel Losada, por su insistencia y apoyo. A mis directores de tesis Gregorio Parrilla e Iñigo Losada por su esfuerzo y dedicación. Especialmente a Iñigo la paciencia e interés en ir resolviendo los puntos que han ido surgiendo. Y de nuevo y finalmente al Dr. Bryden, por su apoyo en momentos difíciles y por ser el principal acicate en el análisis de la sección.

Where does the water come from, where does it go, and what happens along its path? These seemingly simple questions about the ocean's semi-permanent circulation are at the heart of physical oceanography. Answers are sought from hydrographic data, direct current observations, tracers measurements and satellite observations. The North Atlantic is the most completely observed and extensively studied of all the world's oceans and yet it still resists thorough description and rationalisation.

Schmitz and McCartney

Contents

Resumen y palabras clave

Para estudiar los flujos, tendencias y cambios decenales en algunas características de las masas de agua, se han analizado tres campañas hechas sobre la misma sección a lo largo del paralelo 24,5º N, en la zona central del giro subtropical del Atlántico norte. La sección sobre los 24,5º N tiene una importante significación en los estudios climáticos puesto que se ha cubierto en tres ocasiones, durante el Año Geofísico Internacional de 1957, en 1981 y finalmente en 1992 denominada sección A-5 del Experimento de Circulación Oceánica Global (WOCE). La comparación de las temperaturas entre las tres campañas muestra que las aguas entre 700 y 2500 m se han calentado significativamente entre 1957 y 1992 y que este calentamiento desde 1957 es peculiarmente uniforme a lo largo de toda la extensión de la sección. El máximo calentamiento ocurre a 1000 m y es de 0,28±0,05º C. En la termoclina principal ha habido un incremento continuado de salinidad desde 1957 a 1992. En aguas intermedias, entre 800 y 1500 m, también se incrementa la salinidad entre 1981 y 1992, 0,025 a profundidad, temperatura potencial y superficies de densidad constantes. A través de la columna de agua hasta los 2000 m de profundidad la temperatura y la salinidad se han incrementado en todo lo largo de la sección en superficies de densidad constante. Por debajo de los 2000 m aparece un ligero enfriamiento y una disminución de la salinidad en las superficies de densidad constante. Los cambios decenales en temperatura y salinidad entre 1981 y 1992 se han separado en una componente debido al movimiento vertical de las isopicnas y otra debido a los cambios de temperatura y salinidad de las isopicnas. El notable calentamiento interior, a presión constante, es debido a ambos procesos: entre 1957 y 1981 se debió principalmente al movimiento de las isopicnas, de unos 50 db hacia el fondo, y entre 1981 y 1992, se debió a cambios en las características de las masas de agua. Aunque se ha detectado cambios en la temperatura y la salinidad, los campos de velocidad y el transporte meridional, promediado zonalmente, presentan gran similitud a escalas grandes. El transporte de calor, calculado siguiendo la misma metodología para las tres campañas, se mantiene invariable dentro de la incertidumbre de las medidas, a pesar de los cambios que se han producido en temperatura, salinidad y masas de agua. El transporte de agua en dirección sur a través de la sección a 24,5º N es de –1,23 Sv. La mayor contribución al flujo de calor hacia el Polo es la baroclínica, es decir el flujo de agua cálida hacia el norte en capas someras y su retorno hacia el sur, más fría, en capas profundas. La circulación horizontal, en la que aguas someras con bajo contenido de oxígeno fluyen hacia el norte, por los estrechos de

Florida y el borde occidental, y aguas con mayor contenido fluyen hacia el sur en la parte central y oriental de la sección, es la mayor contribución al transporte neto de oxígeno hacia el sur. El principal mecanismo del transporte de sales nutritivas es el transporte baroclínico, debido a un agua superficial con baja concentración de elementos nutritivos, fluyendo hacia el norte y la circulación de retorno hacia el sur con altas concentraciones. Con el fin de ajustar el balance global de silicato, es preciso cambiar los niveles de referencia de las velocidades geostróficas que se establecieron para el cálculo de la circulación oceánica. El balance de transportes obtenido en la cuenca del Atlántico norte a través de la sección en 24,5º N es el siguiente: un flujo de calor de 1,47 ± 0,40 PW de los cuales 0,14 PW se deben al efecto estacional, de sal –26,2 ± 11,5 × 10^6 kg s^{-1}, de oxígeno –2760 ± 530 kmol s^{-1}, de silicato -125 ± 250 kmol s^{-1}, de nitrato -87 ± 120 kmol s^{-1} y de fosfato –10,3 ± 7,6 kmol s^{-1}.

Palabras clave: Agua profunda del Atlántico norte, aguas intermedias, análisis espacial objetivo, Atlántico norte subtropical, balance de silicato disuelto, balances de transportes, calentamiento oceánico, calibración de los datos de la batisonda, cambio climático, cambios decenales, circulación meridional de retorno, flujos, fosfato, giro subtropical del Atlántico norte, masas de agua, mecanismos de transporte oceánico, nitrato, oxígeno, salinidad, silicato, temperatura, tendencias, transporte de agua, transporte de nutrientes, transporte de oxígeno transporte en clases de temperatura, transporte oceánico de calor.

Abstract and key words

Three transatlantic hydrographic sections across 24.5º N, the centre of the subtropical gyre of the North Atlantic Ocean, are analysed for fluxes, trends and decadal changes. The 24.5º N section is well suited for studies of climate change because it has been surveyed three times, during the International Geophysical Year of 1957, during 1981 and in 1992 as the WOCE A-5 section. Comparison of temperature from the three cruises show that the waters between 700 and 2500 m depth have consistently warmed over those 35 years and that the warming since 1957 is remarkably uniform across the zonal extend of the North Atlantic. The zonal mean maximum warming amounts to 0.28±0.05º C and occurs at 1000 m depth. In the main thermocline, there has been a steady increase in salinity from 1957 to 1981 and 1992. In the intermediate waters between 800 and 1500 m salinity has also increased from 1981 to 1992 by 0.025 on constant depth, constant potential temperature and constant density surfaces. Throughout the water column down to 2000 m and across the zonal section, salinity and temperature have broadly increased on density surfaces. Below 2000 m, there has been slight cooling and freshening on isopycnal surfaces since 1981. Decadal changes in temperature and salinity from 1981 to 1992 have been separated into a component due to vertical motion of the isopycnals and a component due to the changes in temperature and salinity on isopycnals. The remarkable interior warming at constant depth is due to both processes, from 1957 to 1981 mainly to downward displacement of isopycnals by about 50 db and from 1981 to 1992 mainly to changes in water masses characteristics. Since 1981 the continued cooling of deep water has been due to changes in water mass characteristics. Even though the temperature and salinity have changed, the three cruises exhibit similar features in the large-scale velocity fields and similar zonally averaged meridional transport. Ocean heat transport performed by similar calculations on the three cruises are indistinguishable. Total southward freshwater transport through the 24.5º N section accounts for –1.23 Sv. The different components of the fluxes, Ekman and its barotropic compensation, baroclinic and horizontal, have been evaluated for the fluxes of heat, salt, oxygen and nutrients. The baroclinic contribution due to overturning circulation is responsible for the largest amount of poleward heat transport, with warmer waters flowing poleward and cooler deep water flowing equatorward. The barotropic flow associated to the Bering Straits, net precipitation and Ekman transport is the main component in the salt transport. Horizontal transport is the main contribution to southward oxygen flux, and the large scale gyre circulation is

responsible for this. In the case of nutrients, baroclinic transport due to overturning circulation is the main factor for the southward transport of all nutrients. Consideration of the physical mechanisms of silica transport at 24.5º N in the North Atlantic in conjunction with the silica budget of the Atlantic Ocean basin requires small modifications of the geostrophic reference levels. Finally, the heat transport through the 24.5º N section is calculated to be 1.47 ± 0.40 PW, about 0.14 PW could be considered due to the seasonal effect, salt transport including Bering Straits and net precipitation -26.2 ± 11.5 × 10^6 kg s^{-1}, oxygen transport –2760 ± 530 kmol s^{-1}, silica transport -125 ± 250 kmol s^{-1}, nitrate transport -87 ± 120 kmol s^{-1} and phosphate transport of –10.3 ± 7.6 kmol s^{-1}.

Key words: Climatic change, CTD data calibration, decadal changes, dissolved silica budget, fluxes, freshwater transport, intermediate waters, mechanisms of ocean transport, meridional overturning circulation, nitrate, North Atlantic Deep Water, North Atlantic subtropical gyre, nutrient transport, objective mapping, ocean heat transport, ocean warming, oxygen, oxygen transport, phosphate, salinity, silica, subtropical North Atlantic, temperature, transport in temperature classes, transport budgets, trends, water masses.

List of figures

Figure 2.7. Zonal section of phosphate (µm kg^{-1}) across 24.5ºN from the hydrographic stations taken aboard *Hespérides* in July-August 1992. The upper plot has expanded vertical scale.

Figure 3.1. Difference of temperature at 24.5ºN using spline fitting and interpolating values each 0.5º of longitude. Differences were smoothed using a gaussian filter with e-folding scale of 300 km. Differences were calculated for A) 1981-1957 B) 1992-1981, and C) 1992-1957. Values are in ºC. Shading in colour indicates positive difference. The top plot has expanded vertical scale.

Figure 3.2. Difference of salinity (multiplied by 100) at 24.5ºN using spline fitting and interpolating values each 0.5º of longitude. Differences were smoothed using a gaussian filter with e-folding scale of 300 km. Differences were calculated for A) 1981-1957 B) 1992-1981, and C) 1992-1957. Shading in colour indicates positive difference. The top plot has expanded vertical scale.

Figure 3.3. Correlation function (equation 3.20) for the North American basin (o), Mid-Atlantic Ridge (+) and Canary basin (*) for depths A) 100 m, B) 900 m and C) 5000 m.

Figure 3.4. Signal correlation function (same as Fig 3.3, but with eddy motion filtered out) for the North American basin (o), Mid-Atlantic Ridge (+) and Canary basin (*) for depths A) surface, B) 1200 m and C) 4250 m.

Figure 3.5. 1992 cruise Temperature (ºC) at 5000 m depth, raw data (dashed), mapping data (solid) plus/minus the error in the mapping (dotted) for A) North American basin and B) Canary basin.

Figure 3.6. 1992 Temperature (ºC) section using objective mapping. The expected error in the temperature mapping in function of depth is shown on the right side. Below 3000 m, the error is given separately for the Canary (dotted) and North American (dashed) basins and values are multiplied by 10. Expected errors are inºC.

Figure 3.7. Salinity section for the 1992 cruise using objective mapping. The expected error in salinity mapping in function of depth is shown on the right side. Below 3000 m,

the error is given separately for the Canary (dotted) and North American (dashed) basins. Values are multiplied by 25.

Figure 3.8. Difference of temperature (ºC) by objective mapping, A) 1981-1957, B) 1992-1981 and C) 1992-1957. The expected error in the temperature difference in function of depth is shown in the right side. Below 3000 m, the error is given separately for the Canary (dotted) and North American (dashed) basins. Values are multiplied by 10. Expected errors are in ºC. Shading in colour indicates positive difference. The top plot has expanded vertical scale.

Figure 3.9. Difference of salinity (multiplied by 100) by objective mapping, A) 1981-1957, B) 1992-1981 and C) 1992-1957. The expected error in salinity difference in function of depth is shown in the right side. Below 3000 m, the error is given separated for the Canary (dotted) and North American (dashed) basins. Values are multiplied by 25. Shading in colour indicates positive difference. The top plot has expanded vertical scale.

Figure 3.10. Correlation function versus longitude for temperature (ºC) of a point situated at 50ºW for A) 500 m, B) 1200 m, C) 5000 m in the North American basin and D) 5000 m in the Canary basin.

Figure 3.11. Zonal average temperature differences (ºC) plotted ± the error estimate (colour shading) for A) 1981-1957, B) 1992-1981 and C) 1992-1957 from surface to 3000 m for all the Atlantic basin (upper plot) and deeper for the North American basin in the bottom left figure and for the Canary basin, bottom right.

Figure 3.12. Zonal average salinity differences plotted ± the error estimate (colour shading) for A) 1981-1957, B) 1992-1981 and C) 1992-1957 from surface to 3000 m for all the Atlantic basin (upper plot) and deeper for the North American basin in the bottom left figure and for the Canary basin, bottom right.

Figure 4.1. Change in pressure of isotherms from 1957 to 1992 at 24.5ºN. Zonally averaged temperature differences from 1957 to 1992 are divided by the average vertical potential temperature gradient to determine the zonally averaged change in pressure of the isotherms

Figure 4.2. Direction of the zonally averaged changes in potential temperature and salinity at fixed pressure from 1957 to 1992 for A) warm and thermocline waters between 8ºC and 20ºC and B) intermediate and upper deep waters between 3ºC and 8ºC. Potential density anomaly surfaces relative to 1000 dbar are indicated so the changes relative both to the zonally averaged potential temperature-salinity θ-S relationship and to the density surfaces at 24.5ºN can be assessed. The direction of the arrows is from the 1957 θ-S relationship towards the 1992 θ-S relationship.

Figure 4.3. Water mass characteristics of deep water in the eastern basin at 24.5ºN in the Atlantic. Salinity is plotted against potential temperature for all water masses in the eastern basin with potential temperature between 2 and 2.5ºC for the 1957 (+), 1981 (o) and 1992 (•) sections across 24.5ºN. Regressions lines are plotted for each section, as well as for Mantyla's (1994) recommended line for 24ºN and Saunders' (1986) suggested relationship for the eastern basin deep water. Details for the five lines are given in table 4.1.

Figure 4.4. Water mass characteristics of the thermocline waters at 24.5ºN in the Atlantic. Salinity is plotted against potential temperature for all water samples with θ between 12 and 17ºC for 1957 (blue +), 1981 (red o) and 1992 (black •) sections. A lineal least squares regression line is plotted for each section, and the details for each line are given in table 4.2.

Figure 4.5. Changes in the thermocline water mass characteristics along 24.5ºN from 1957 to 1992. The regression lines expressing the θ-S relationship in the thermocline for the 1957 and 1992 sections are drawn between 14ºC and 15ºC. The potential density surface passing through the median value for the 1957 regression at θ = 14.5ºC, S=35.9633 is drown and this surface intersects the θ-S regression at θ = 14.728ºC, S=36.0277. The change in water mass characteristics over time can be interpreted as a change in salinity at constant potential temperature of 0.0297, or as a combined change along a constant potential density surface of 0.064 in salinity and of 0.228ºC in temperature, and these alternatives are shown by arrows.

Figure 4.6. Potential temperature-salinity relationship by 10º-longitude bands across 24.5ºN for the 1992 hydrographic section. Potential temperature and salinity are determined at each station on a set of density anomalies surfaces. The density surfaces are taken to be potential density anomalies σ_0 referenced to sea surface pressure, at intervals of 0.05 from 25.50 to 26.85 kg m^{-3}, σ_1 (referenced to 1000 dbar) at intervals of 0.02 from 31.24 to 31.98, σ_2 (referenced to 2000 dbar) at intervals of 0.01 from 36.82 to 37.03; σ_4 (referenced to 4000 dbar) at intervals of 0.005 from 45.785 to 45.935. Averages of potential temperature and salinity on these density surfaces are made for all the stations within each 10º-longitude bands to create the θ-S curves. Several potential density anomaly surfaces (referenced to the surface) are also included to indicate the general slope of isopycnal surfaces.

Figure 4.7. Changes in potential temperature salinity relationships from 1981 to 1992 for the intermediate waters between 4ºC and 9ºC for A) western (65ºW to 75ºW) and B) eastern (25ºW to 35ºW) regions of the 24.5ºN hydrographic section. Average of potential temperature and salinity on σ_1 surfaces listed in the caption of figure 4.6 are made for all the stations within the 10º-latitude band. The heavy line denotes the 1992 relationship and the light line denotes the 1981 relationship. Potential density anomaly surfaces referenced to 1000 dbar are also indicated.

Figure 4.8. Zonal section of chlorofluorocarbon (A:CFC-11, and B:CFC-12) across 24.5ºN from the hydrographic stations taken aboard Hespérides in July-August 1992Units are pmole kg^{-1}. The distribution of stations positions is indicated by tics along the top.

Figure 4.9. Potential temperature-salinity relationship for North Atlantic Deep Water between 65ºW and 75ºW near the western boundary. Continuous curves for 1992 (black line) and 1981 (red line) represent averages on density surfaces listed in the caption for figure 4.6 over all the stations within the 10º-longitude band. Isolated values are indicated for all 1957 water samples (+) with potential temperature between 2ºC and 5ºC between 65ºW and 75ºW.

Figure 4.10. Distribution of Antarctic Bottom Water banked up against the western side of the Mid-Atlantic Ridge in 1957 (blue line, +), 1981 (red line, o) and 1992 (black line, •). The 1.8ºC isotherm is chosen here to represent the shape of the AABW layer.

Figure 4.11. Average changes from 1981 to 1992 A) in salinity and B) in potential temperature (ºC) in isopycnal surfaces over 10º-longitude bands. The changes are calculated by finding the salinity, potential temperature and pressure for the set of isopycnals listed in the caption of figure 4.6 for each within the 10º-longitude band, and then averaging the salinities, potential temperature, and pressure over all stations within the band. The differences (1992-1981) in salinity and potential temperature are then plotted against the averaged pressure of the isopycnal surfaces. Thus, these profiles of changes in water mass characteristics on density surfaces are presented linearly versus pressure (left axis), but the corresponding density anomaly values are also indicated (right axis).

Figure 4.12. Zonal sections of the differences (1992-1981) in (A) potential temperature (ºC), (B) salinity and (C) oxygen (ml l^{-1}) on isopycnal surfaces across 24.5ºN in the subtropical Atlantic Ocean. For each station the salinity, potential temperature and pressure are found for the set of isopycnals surfaces listed in the caption of figure 4.6. Values from the individual stations are gridded at 0.5º-longitudeintervals from 24.5ºW to 75.5ºW. Differences are filtered zonally with a 300-km Gaussian filter. The gridded averaged pressure of the isopicnal surfaces for 1992 and 1981 are also filtered and used as vertical coordinate.

Figure 4.13. Profiles of zonally averaged differences in (A) potential temperature (ºC), (B) salinity, (C) pressure (db) and (D) oxygen (ml l^{-1}) on isopycnal surfaces across 24.5ºN in the subtropical Atlantic Ocean. For each station, the salinity, potential temperature, pressure and oxygen are found on the set of isopycnals surfaces listed in the caption of figure 4.6, and the values are then gridded at 0.5º-intervals from 24.5ºW to 75.5ºW for each of the 3 sections. The averaged differences, 1992-1981 and 1981-1957, are then calculated and plotted against the average 1992 and 1981 pressures. Thus, these profiles of change in water mass characteristics on isopycnal surfaces are presented linearly versus pressure (left axis), but the corresponding density anomaly values are also indicated (right axis).

Figure 5.1. Zonally-averaged geostrophic meridional volume transport per unit depth at 24.5ºN across the transatlantic section for the three cruises, 1992 (solid blue), 1981 (dashed red) and 1957 (dotted green).

Figure 5.2. Zonally-averaged potential temperature (A) and salinity (B) profiles for the 24.5ºN transatlantic section for the three cruises, 1992 (solid blue), 1981 (dashed red) and 1957 (dotted green).

Figure 5.3. Vertical profiles of zonally-averaged potential temperature (A) and salinity (B) differences for the 24.5ºN transatlantic section for 1992-1957 (black), 1981-1957 (blue) and 1992-1981 (red).

Figure 5.4. Northward transport (Sv) across 24.5ºN transatlantic section as a function of potential temperature for A:1957, B:1981 and C:1992. Transport are determined over temperature intervals of 1.0 ºC from 2.5ºC to 30ºC and 0.7ºC below 2.5ºC.

Figure 5.5. Northward transport (Sv) of deep and bottom waters across 24.5ºN transatlantic section as a function of potential temperature below 2.5ºC for A:1957, B:1981 and C:1992. Transports are determined over temperature intervals of 0.05ºC.

Figure 6.1A. Magnitude of northward (positive) and southward (negative) geostrophic velocities at each station all across the Mid-ocean section and Florida Straits. Velocities are plotted every 20 m depth throughout the water column; for example velocities calculated between station 90 (70ºW) and 91 (70.67ºW) are plotted as dots at the mean longitude (70.34ºW). Note that there is a gap between the mid-ocean (15ºW to 75ºW) and the Florida Straits sections (79.2ºW to 80.1ºW).

Figure 6.1B. Velocity from 1200 to 5000 m depth.

Figure 6.1C. Velocity from 5000 to the bottom. Most of the water deeper than 5000 m appears in the North American basin, with small contribution from the Canary basin mostly between 30ºW and 39ºW.

Figure 6.1D. Velocity from 5600 to the bottom. Most of the water deeper than 5600 m appear between 54ºW and 71ºW in the North American basin.

Fig 6.2. Silicate (A) and nitrate (B) concentration from 5600m to bottom. Units are μmol kg^{-1}.

Figure 6.3. Overall volume transport through the 24.5ºN section by depth classes of 200 m, including Florida Straits, Ekman layer and mid-ocean section. Units are Sv (10^6 m^3s^{-1}).

Figure 6.4. Velocity separation: A) zonally average velocity profile <v> superimposed on section averaged velocity <v(z)>, and deviations from zonal average v'(x,z) for B) Florida Straits and C) the total 24.5ºN section.

Figure 6.5. Potential temperature separation: A) zonally average potential temperature profile <θ> superimposed on section averaged potential temperature <θ(z)>, and deviations from zonal average θ'(x,z) for B) Florida Straits and C) the total 24.5ºN section.

Figure 6.6. Salinity separation: A) zonally averaged salinity profile <salinity (z)> superimposed on section averaged <salinity>, and deviations from zonal average S'(x,z) for B) Florida Straits and C) the total 24.5ºN section.

Figure 6.7. Oxygen separation: A) zonally averaged oxygen profile <oxygen (z)> superimposed on section averaged <oxygen>; and deviations from zonal average oxygen'(x,z) for B) Florida Straits and C) the total 24.5ºN section.

Figure 6.8. Silicate separation: A) zonally average silicates profile < silicate(z) > superimposed on section averaged silicates < silicate >; and deviations from zonal average silicate' (x,z) for B) Florida Straits and C) the total 24.5ºN section.

Figure 6.9. Nitrate separation: A) zonally average nitrates profile < nitrate(z) > superimposed on section averaged nitrate < nitrate >; and deviations from zonal average nitrate' (x,z) for B) Florida Straits and C) the total 24.5ºN section.

Figure 6.10. Phosphate separation: A) zonally average phosphate < phosphate(z) > superimposed on section averaged phosphate < phosphate>; and deviations from zonal average phosphate'(x,z) for B) Florida Straits and C) the total 24.5ºN section.

Figure 6.11. Salt fluxes by components: barotropic flow balancing Ekman flow, Bering Strait flow and net precipitation (blue :), baroclinic (green -), horizontal (red --)

Figure 6.12. Heat fluxes by components: barotropìc balancing Ekman, Bering Strait and net precipitation (blue--), baroclinic: (green -), horizontal (red --).

Figure 6.13. Oxygen fluxes by components: Ekman and its compensating barotropic flux (blue :), baroclinic (green -), horizontal (red--). Units are mol s^{-1}.

Figure 6.14. Silica fluxes by components: Ekman and its compensating barotropic flux (blue :), baroclinic (green -), horizontal (red--). Units are mol s^{-1}.

Figure 6.15. Nitrate fluxes by components: Ekman and its compensating barotropic flux (blue :), baroclinic (green -), horizontal (red--). Units are mol s^{-1}.

Figure 6.16. Phosphate fluxes by components: Ekman and its compensating barotropic flux (blue:), baroclinic (green -), horizontal (red--). Units are mol s^{-1}.

Figure 6.17. Horizontal component of the heat transport on the mid-ocean section calculated for each station pair (dotted) and accumulated (solid) from the eastern end of the section.

Figure 6.18. Horizontal component of the oxygen transport on the mid-ocean section calculated for each stations pair (dotted) and accumulated (solid).

Figure 6.19. Horizontal component of the silica transport on the mid-ocean section calculated for each stations pair (dotted) and accumulated (solid) from the eastern end of the section.

Figure 6.20. Horizontal component of the nitrate transport on the mid-ocean section calculated for each stations pair (dotted) and accumulated (solid) from the eastern end of the section.

Figure 6.21. Barotropic velocity adjustment added to the previously discussed circulation to create an adjustment of 127 kmol s^{-1} of southward silica transport (Case 1: dotted yellow line) and a silica-conserving scheme (Case 2: solid green line). Maximum adjustments are only around 0.2 cm s^{-1} in the first case and of 0.5 cm s^{-1} for the second case.

List of tables

all samples with potential temperatures between 12 and 17ºC were least squares fitted to a line of the form

$$S=S_{14.5^oC} + B\ (\theta - 14.5^oC),$$

where $S_{14.5^oC}$ is the salinity at θ = 14.5ºC and B is the slope. The resulting regressions coefficients for $S_{14.5^oC}$ and B as well as the standard deviations of the samples from the fitted line are presented. In addition, the fitted values for salinity at 12ºC ($S_{12.5^oC}$) and 17ºC (S_{17^oC}) are given

Table 4.3. Spatial distribution of salinity at θ = 14.5ºC in the subtropical North Atlantic. Along 24.5ºN 10º-longitude averages on potential density surfaces were made for the 1981 *Atlantis II* cruise to determine the salinity at θ = 14.5ºC. For the meridional sections, overlaping 5º-latitude averages were made on potential density surfaces to determine the salinity at θ = 14.5ºC at 27, 24.5 and 22ºN from the 1984 *Endeavour* section along 66°W, the 1983 *Oceanus* section along 52°W and the 1983 *Knorr* section along 35°W.

Table 4.4. Spatial distribution of salinity at θ = 6.5ºC in the subtropical North Atlantic. Along 24.5ºN 10º-longitude averages on potential density surfaces were made for the 1981 *Atlantis II* cruise to determine the salinity at θ = 6.5ºC. For the meridional sections, overlaping 5º-latitude averages were made on potential density surfaces to determine the salinity at θ = 6.5ºC at 27ºN, 24.5ºN and 22ºN from the 1984 *Endeavour* section along 66°W, the 1983 *Oceanus* section along 52°W and the 1983 *Knorr* section along 35°W.

Table 5.1. Reference level transport (Sv), Area ($10^8 m^2$), Barotropic velocity (cm s^{-1}) and Total transport (Sv) for each of the cruises, 1957, 1981 and 1992.

Table 5.2. Meridional northward volume transport in mid-ocean in depth classes. Transport units are Sv.

Table 5.3. Geostrophic Mid-Ocean Circulation: Mean circulation, eddy and total heat transport across the mid ocean section. Units are 10^{15} W and velocity-weighted average temperature in ºC. In each case the total southward volume transport is 34.9 Sv.

Table 5.4. Components of the heat fluxes, transport, difference of temperature, northward heat transport and net heat transport across 24.5ºN for 1957, 1981 and 1992.

Table 6.1. Transport (Sv) by classes of depth (0-600, 600-1200, 1200-3000, 3000-4900, 4900-bottom) for some parts of the section: Western Boundary (75ºW-69ºW), North American Basin (69ºW-45ºW), Canary Basin (45ºW-25ºW) East Canary Basin (25ºW-16ºW), Florida Straits and Ekman layer.

Table 6.2. Transport of heat (PW), salt (10^6 kg s^{-1}), oxygen (kmol s^{-1}), silicate (kmol s^{-1}), nitrates (kmol s^{-1}) and phosphates (kmol s^{-1}) separated by components: Ekman and its barotropic compensation, baroclinic, horizontal, and net transport

Table 6.3. Velocity weighted average concentration of oxygen, silicate, nitrate and phosphate in the Mid-Atlantic, Ekman layer and Florida Straits. Units are μmol kg^{-1}.

Table 6.4. Components of the fluxes of oxygen, silicate, nitrate+nitrite and phosphate, transport, difference of property with Mid-Ocean, transport due to difference of property with Mid-Ocean concentration and with Ekman and Florida Straits transport and total transport given by equation. 6.21.

Table 6.5. Transport of heat, oxygen, silicate, nitrate+nitrite and phosphate for the three 1992, 1981 and 1957 sections by authors: 1992 results of this work (1), 1981 Rintoul and Wunsch, (1991) results (2), 1957 Hall and Bryden (1982) results (3) and 1957 Brewer *et al*., (1989) results (4).

Table 6.6. Transport (Sv) by classes of depth (0-600, 600-1200, 1200-3000, 3000-4900, 4900-bottom) and for different regions: Western Boundary (75ºW-69ºW), North American basin (68ºW-45ºW), Canary basin (45ºW-25ºW) East Canary basin (25ºW-16ºW), Florida Straits and Ekman layer; for a) Silica adjustment to 127 kmol s^{-1} and b) not silica transport. Table 6.1 gives similar information without any constraints.

Table 6.7. Transport (Sv) by classes of depth (0-600, 600-1200, 1200-3000, 3000-4900, 4900-bottom) for the three cases: case 0: mass conservation only, case 1: silica transport = 127 kmol s^{-1} and case 2: no silica transport.

Table 6.8. Ekman and its barotropic compensation, baroclinic, horizontal and net transport for Heat, Salt, Oxygen, Silica, Nitrate, and Phosphate for a) silica transport of 127 kmol s^{-1} and b) no silica transport. Same information with only mass conservation constraint (case 0) is given in table 6.2.

Table 6.9. Total transport for heat, salt, freshwater, oxygen, silica, nitrate and phosphate for the three cases: mass conservation only, silica transport of 127 kmol s^{-1} and not silica transport.

List of acronyms

AABW	Antarctic Bottom Water
AAIW	Antarctic Intermediate Water
ACC	Anthropogenic Climat Change
CFC	Chlorofluorocarbons
CICYT	Comisión Interministerial de Ciencia y Tecnología
CLIVAR	Climate Variability and Predictability Program
CTD CTDO2	Conductivity, Temperature, Depth, dissolved Oxygen (O_2) Profiling Instrument.
DecCen	Decadal-to-Centennial
DSOW	Denmark Strait Overflow Water
DWBC	Deep Western Boundary Current
ECMWF	European Centre for Medium Range Weather Forecast
EG&G	EG&G Marine Instruments, Cataumet, USA
ERS	European Radar Satellite
IEO	Instituto Español de Oceanografía
IGY	International Geophysical Year
IPTS-48	International Practical Temperature Scale 1948
IPTS-68	International Practical Temperature Scale 1968
LNADW	Lower North Atlantic Deep Water
LSW	Labrador Sea Water
MAR	Mid Atlantic Ridge
MEDDY	Eddy of Mediterranean Water
MIT	Massachusetts Institute of Technology
MOC	Meridional Overturning Circulation
MW	Mediterranean Water
NADW	North Atlantic Deep Water
NAO	North Atlantic Oscillation
NBIS	Neil Brown Instrument Systems
NEADW	North Eastern Atlantic Deep Water
PSS-78	Practical Salinity Scale

SMW	Subpolar Mode Water
SOC	Southampton Oceanographic Centre, U. K.
SST	Sea Surface Temperature
UNADW	Upper North Atlantic Deep Water
WBUC	Western Boundary Under Current
WHOI	Woods Hole Oceanographic Institution
WOCE	World Ocean Circulation Experiment

Introduction

As scientific understanding of the causal mechanisms for environmental changes improves, there is an accompanying public awareness of the susceptibility of the present environment to significant regional and global change. Understanding the basic mechanisms of climate is a key to early detection of change in the earth's climate system.

Since the ocean-atmosphere system is driven by the sun's radiation, it is important to know what the response of the system is to the known radiative input. The ocean carries a significant fraction of the meridional heat flux that makes the middle latitudes of the earth habitable. Vonder Haar and Oort (1973) found that in the region of maximum net northward energy transport by the ocean-atmosphere system (30-35ºN) the ocean transports 47% of the required energy (1.7×10^{22} cal $year^{-1}$). At 20ºN, where the ocean transport peaks, they estimated that the ocean accounts for 74% of the total meridional heat transport.

In the description of the role of the ocean in the planetary climate system, there are three basic components: the circulation of the heat, freshwater and chemicals, the formation and modification of water masses, and the statistics of the ocean variability. In regions where temporal variability is relatively small, repeated sections test the representativeness of the one-time hydrographic survey as an estimator of the mean circulation field. Measurements of the temporal evolution of the large-scale ocean circulation and fluxes of mass, heat and salt and chemicals can be achieved by repeat hydrographic observations.

The Atlantic Ocean is the most saline of all the world oceans. It has significant exchange of water masses, heat and salt with several marginal seas, regions in which important transformations of water masses take place. A complex thermohaline-driven circulation, moves water masses both northward and southward mostly along its western boundary regions. The Atlantic Ocean has been well surveyed in the twentieth century with various large scale surveys such as International Geophysical Year (IGY), Geochemical

Ocean Sections Studies (GEOSECS), Long Lines (LL), South Atlantic Ventilation Experiment (SAVE) and the World Ocean Circulation Experiment (WOCE). The Atlantic is the source of North Atlantic Deep Water (NADW), and in it can be found several important water masses: Mediterranean Water (MW), Antarctic Intermediate Water (AAIW) and Antarctic Bottom Water (AABW).

The 24.5ºN transatlantic section is an archetypal transoceanic hydrographic section. It is rich in water masses and crosses the North Atlantic in the middle of the subtropical gyre. It provides a census of major intermediate, deep and bottom water masses whose sources are in the Antarctic and far northern Atlantic as well as estimates of the thermohaline circulation of these water masses and of the wind-driven circulation in the upper water column. Furthermore, the 24.5ºN section crosses the northward flowing Gulf Stream in Florida Straits and the southward wind-driven Sverdrup flow in mid-ocean at essentially the latitude of maximum wind stress curl.

This section was measured in 1957 (IGY data) (Fuglister, 1960), and 1981 (Roemmich and Wunsch, 1985). Although hydrography is a traditional method for obtaining the geostrophic flow throughout the water column, the quantity and quality of the measurements have been dramatically increased since the use of electronic instrumentation such as CTD (Brown, 1974). This new technique has been used in the later periods of sampling.

From analysis of the 1957 section, Hall and Bryden (1982) determined that the Antarctic Intermediate water flows northward across 24.5ºN between 600 and 1100 m depth, North Atlantic Deep Water flows southward between 1200 and 4500 m, and Antarctic Bottom Water flows northward below 4500 m depth. They found a vertical meridional cell with a net northward flow across 24.5ºN of 18 x 10^6 m^3s^{-1} of warmer water in the upper 1000 m of the water column and a southward return as intermediate and deep water between 1000 and 4500 m depths. Roemmich and Wunsch (1985) reported a similar pattern of water masses and meridional flow on the 1981 section.

The 24.5ºN section was one of the sections planned to be repeated during WOCE (section A-5, WOCE Implementation Plan). Dr. Gregorio Parrilla from the Instituto Español de Oceanografía (IEO), proposed its realisation to the IEO and the Comisión

Interministerial de Ciencia y Tecnología. For this proposal, Parrilla had the important support of Harry Bryden and Robert Millard from Woods Hole Oceanographic Institution.

The cruise was carried out in July-August of 1992 with the participation of scientists from the Instituto Español de Oceanografía, Woods Hole Oceanographic Institution, and other Spanish and American institutions including Instituto de Investigaciones Mariñas of Vigo, Centro de Estudios Avanzados de Blanes, Facultad de Ciencias del Mar de la Universidad de Las Palmas, Universidad de La Coruña, Programa de Clima Marítimo from the Dirección General de Puertos, Ainco-Inter Ocean, Lamont Doherty Geological Observatory, and Rosenstiel School of Marine and Atmospheric Science of the University of Miami.

The objective of this work is to quantify the response of the ocean to the warmer atmospheric conditions of the 80's and beginning of the 90's and compare the conditions with previous surveys. After a description of the North Atlantic Ocean, in chapter two a view of the collected data from the three cruises is presented with the calibration procedures following the collected data mainly in temperature, salinity and oxygen. In chapter three the comparison between temperature and salinity for the two periods 1957-1981 and 1981-1992 is given and the used methodology is discussed. The procedure was as follows: First, the comparison was made using two methods based in cubic splines and objective mapping, then the differences between the cruises and the zonal average of the differences was calculated. A complete discussion of changes found in the three periods complete the chapter.

In the chapter four the decadal changes in potential temperature – salinity (θ-S) relationship are presented from 1957 to 1992. It is our intention to examine the characteristics of these water masses across 24.5°N from the three occupations of the section. Because the Antarctic Intermediate and Bottom Waters and the North Atlantic Deep Waters are quite far from their sources, changes in their characteristics may reflect longer term trends in their source strengths or in the conditions under which they are formed or in the conditions along their pathways. Surface and thermocline water types as well as the Mediterranean Water are generated closer to the 24.5°N section and hence changes in their characteristics may reflect more recent trends.

The purposes of the fifth chapter are to describe briefly the changes in the meridional circulation which have occurred at 24.5ºN and to use the data of the three sections to examine the meridional fluxes of mass and heat in the subtropical North Atlantic and their possible changes from 1957 to 1992. Bryden and Hall (1980) estimated the northward heat flux across 24.5ºN in the 1957 IGY section to be 1.2 x 10^{15}W. The same result was obtained by Roemmich (1980) using inverse calculations. Roemmich and Wunsch (1985) compared the 1957 data with the 1981 section and found the heat transport to be indistinguishable from computations of air-sea heat exchange. They attributed the steadiness of the heat transport to the invariance of the zonally averaged meridional circulation. Combining the Pacific heat transport with the established value of Atlantic heat transport across 24.5ºN, Bryden et al., (1991) estimated a total ocean heat transport of 2.0 x 10^{15}W, larger than the atmospheric heat transport of 1.7 x 10^{15}W.

In the sixth chapter, transport of freshwater, oxygen and nutrients are calculated through the 24.5ºN section from the 1992 cruise. Data are compared with previously published data from the section and discussed particularly with regard to the sources of silica into the Atlantic Ocean. Finally a model based on the silica budget in the Atlantic is adopted as representative for determining the circulation of heat, freshwater, oxygen, silica, nitrate and phosphate through the subtropical area at 24.5ºN in the North Atlantic.

This work has been performed during a series of years, and a large number of scientists contributed to it. First for the organisation of the cruise, Gregorio Parrilla was mainly responsible (Parrilla *et al.,* 1994b). During the cruise a total of 8 scientist were involved in CTD measurements, two more in salinity and oxygen sampling and determinations and another two for nutrients. After the cruise a part of this research (chapter 3) was worked on at Massachusetts Institute of Technology under Prof. Carl Wunsch's supervision, Woods Hole Institution of Oceanography with Robert Millard and the British Rennell Center for Ocean Circulation with Dr. Harry Bryden. Coming back to my job in the Instituto Español de Oceanografía, I have collaborated with colleagues Gregorio Parrilla and María Jesús García, and Harry Bryden (Southampton Oceanographic Centre), Robert Millard (WHOI), William Smethie (Lamontd-Doherty Geological Observatory, US). Some papers have already been published the 24ºN analysis such as Parrilla, Lavín, Bryden, García and Millard (1994), Bryden, Griffiths, Lavín, Millard, Parrilla and Smethie (1996) and Lavín, Bryden and Parrilla (1998). Communications to the

Annual Science conference of the International Council for the Exploration of the Sea (ICES) have been made in Lavín, Parrilla, Bryden, Wunsch, Millard and García (1993) and Lavín, Bryden, García and Parrilla (1994) and to the Annual Geophysical Conference (1995) and some posters at the WOCE Conference Halifax Canada, (May 1998) as Lavín, Bryden, Parrilla, Millard and García (1998) and Parrilla G., H. Bryden, A. Cruzado, M. J. García, J. Hernandez-Brito, A. Lavín, R. Millard, A. Rios, G. Rosón, W. Smethie, (1998). Other paper on the carbon transport through the section (also poster in the WOCE Conference, Rosón G., A. F. Ríos, A. Lavín, F. F. Pérez and H. L. Bryden, 1998) is in preparation. This thesis summarizes most of my research regarding the 1992 24.5ºN section. This work has been done with the help of a large number of people and try to represent an important contribution to the understanding of the climate change context.

Chapter 1

The North Atlantic

1.1 Introduction

The North Atlantic is the smallest of the six oceans, it contains 137 x 10^6 km ^{3} of water, almost exactly one-tenth of the volume of the world ocean. It is by far the warmest and most saline of the oceans, and appears to be the 'youngest' of them (Worthington, 1976). Large quantities of new deep and bottom water pour into it from the subpolar basins (Norwegian Sea, Irminger basin, Iceland basin) and Labrador Sea (McCartney and Talley, 1982), and as a consequence the North Atlantic has the highest oxygen and lowest nutrient concentration of all oceans.

1.2 Topographic features

The North Atlantic is mainly divided into two basins, eastern and western, separated by the Mid-Atlantic Ridge. The Ridge extends from Iceland to the Equator with depths (below sea level) between 1500 and 2000 m, sometimes with volcanic islands breaking the sea surface such as Iceland and the Azores. There are some deep gaps in the Ridge as the Charlie Gibbs in the north and Vema and Romanche fracture zones near the Equator, where sill depths are more than 4000 m. Meridionally a series of smaller basins are found in each main basin: in the eastern part are found the West European basin, Iberian basin, Canary basin and Cape Verde basin and in the western North Atlantic are found the Labrador basin, Newfoundland basin and the North American basin, the largest of all basins. Figure 1.1 gives the topographic view of the North Atlantic.

1.3 Water masses

The main water masses in the subtropical North Atlantic, following Worthington (1976), Schmitz and McCartney (1993) and Bryden *et al.*, (1996) are:

Figure 1.1. Topographic view of the North Atlantic (From National Geographic).

- Surface waters: Warmer (>22ºC) and saltier (>37) in the subtropical gyre. They are created by excess evaporation over the subtropical gyre, or are of southern Atlantic origin flowing across the Equator, through the Florida Straits into the North Atlantic.

- Thermocline waters, just below, from about 9º to 22ºC, generally considered to be made up of waters recently ventilated during late winter in northern regions of the subtropical gyre and subducted southward under the surface waters as part of the wind-driven Sverdrup circulation.

- Intermediate layers between 8 and 4ºC having two influences: towards lower salinity due to the northward penetration of Antarctic Intermediate Water (AAIW) in the subtropical region and towards higher salinity due to the mixing with Mediterranean Water (MW) coming out from the Straits of Gibraltar at 36ºN.

- North Atlantic Deep Water (NADW), in two layers, the upper one (UNADW) originates from the Labrador Sea (between 3º and 4ºC) and the lower (LNADW) with a range of 1.8 to 3ºC originates from the subpolar basins in the Greenland- Iceland-Norwegian sea.

- Antarctic Bottom water (AABW), typically considered waters colder than 1.9ºC in the North Atlantic, is restricted almost exclusively to the North American basin where its strongest signature lies on the western flank of the Mid-Atlantic Ridge.

1.4 Circulation on the North Atlantic

The circulation of the North Atlantic has been comprehensively described by Worthington (1976) and Schmitz and McCartney (1993). The main circulation is separate into a wind-driven circulation (that involves upper layers gyres) and a thermohaline or meridional overturning circulation that involves the transformation of warm to cold water at high latitudes.

Wind-driven flow or Sverdrup circulation is associated with purely geostrophic and Ekman layer dynamics. The curl of the wind stress produces convergence/divergence of the Ekman transport, which imposes pressure gradients on the water below. Convergent Ekman flow forcing the subtropical gyre and divergent forcing the subpolar gyre.

The subtropical gyre is a clockwise circulation forced by the wind and associated Ekman convergence with western intensification in the form of a western boundary current: the Gulf Stream. This gyre spans the width of the North Atlantic and extends roughly between 10ºN and 40ºN. There are also intermediate-scales flows called recirculation gyres that return water to the boundary currents. North of the subtropical gyre a counterclockwise gyre is called the subpolar gyre and also has western boundary currents: the East Greenland and Labrador currents.

The thermohaline circulation refers to the flow field associated with the sinking of water cooled by contact with cold air or associated with sources and sinks of salt water or fresh water. Waters sinking at high latitudes return equatorialward in a relative strong, narrow current called the Deep Western Boundary Current (DWBC). The transport of the DWBC may be increased by counterclockwise recirculation gyres and by additions of modified bottom or intermediate water. It has been pointed out that the formation of 13 Sv ($1Sv=10^6$ m ^{3} s^{-1}) of southward flowing NADW exiting the north Atlantic across the equator must be compensated in the upper ocean by northward cross-equatorial transport.

In figure 1.2, from McCartney (1997), a schema of the main advection pathways involved in the warm-to-cold water transformation (McCartney and Talley, 1984) within the North Atlantic part of the global thermohaline overturning circulation is presented. The basin-scale recirculations of the tropical, subtropical and subpolar circulations are suppressed to emphasise the warm water transformation pipeline of the upper ocean (red) and the compensating cold return flows at depth (green). The pipeline begins with the North Brazil current, bringing thermocline and intermediate waters from the South Atlantic to the Caribbean area; it also supplies the Florida Current, which transitions into the strong Gulf Stream. Southeast of Newfoundland the Gulf Stream bifurcates into eastward/southeastward flows and a northward-flowing North Atlantic Current. The North Atlantic Current turns northward into the eastern subpolar gyre, subsequently branching into the Norwegian Current. The westward flow moves across the subpolar gyre and

culminates the warm water transformation with the production of Labrador Sea Water. The blue area shows where the following two phenomena coexist. First, it is the domain of mode waters (McCartney and Talley, 1982) which are annually persistent thermostads formed by deep winter convection. It also is an area of subtropical recirculation where a significant fraction of the eastward flow of the Gulf Stream and North Atlantic Current along its northern edge is expelled into the subtropical gyre to return more slowly westward.

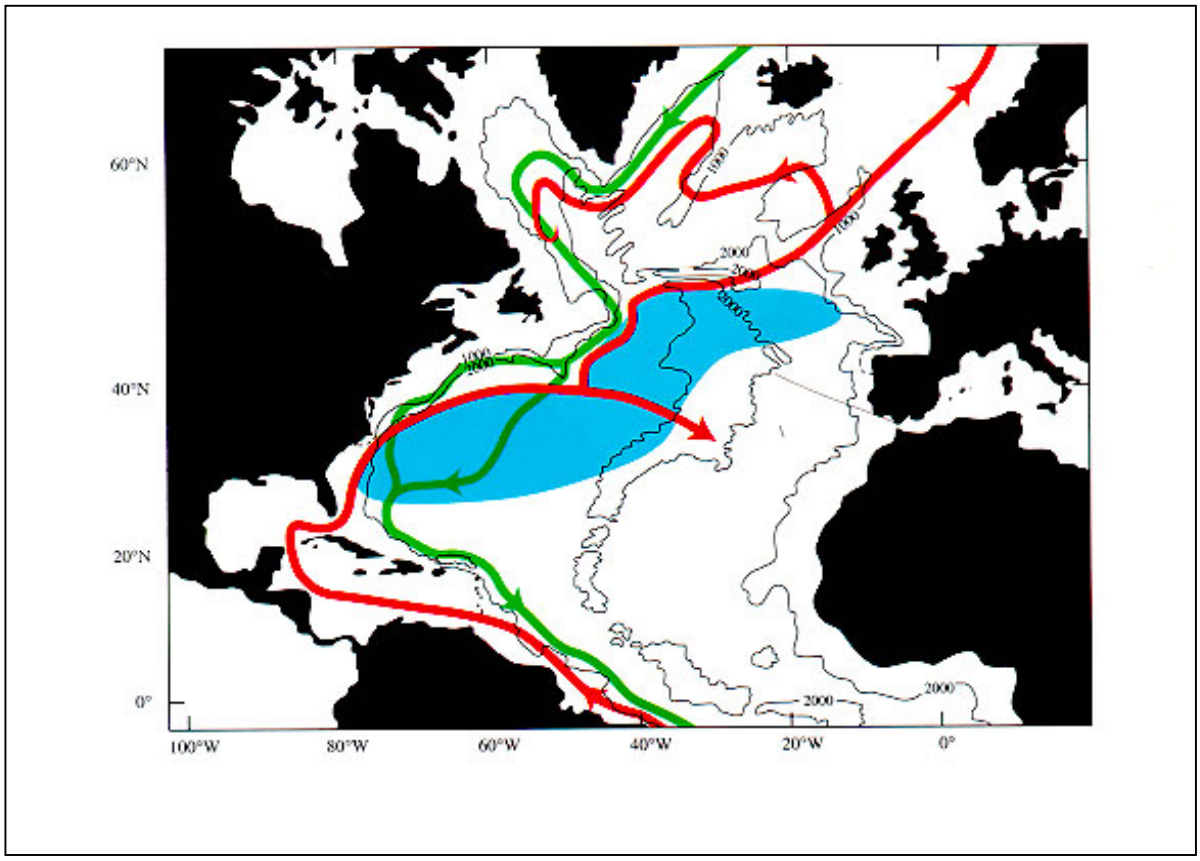

Figure 1.2. North Atlantic thermohaline overturning circulation. Red line represents warm waters pathway and green line cold waters pathway (From McCartney, 1997).

Chapter 2

Description of the data, calibration and characteristics of the 24.5º N section

2.1 Introduction

The objective of this work is to investigate the climatic variations of temperature, salinity, circulation, and transports over the subtropical North Atlantic Ocean from the surface to 6000 m depth from 1957 to 1992. The data used includes three oceanographic cruises carried out along a section on latitude 24.5ºN: the first one in October 1957, by the British R.R.S. *Discovery II* of the National Institute of Oceanography (Chief Scientist L.V. Worthington, Woods Hole Oceanographic Institution) during the International Geophysical Year (Fuglister 1960); the second one in August 1981, by the R.V. *Atlantis II* of the Woods Hole Oceanographic Institution (Chief Scientist D. Roemmich, at that time Woods Hole Oceanographic Institution) (Roemmich and Wunsch, 1985); the last one in July-August of 1992 by the Spanish B.I.O. *Hespérides* of the Armada Española, (Chief Scientist Gregorio Parrilla, Instituto Español de Oceanografía) (Parrilla *et al.,* 1994b).

The section chosen is situated in the central part of the subtropical gyre (Fig. 2.1). The transect was done each time downwind, westward from Africa to America. It began at the African continental shelf, which is quite flat, where depths increase slowly, reaching 4000 m around 20ºW, and 5500 m around 25ºW. The deepest part of the Canary basin is situated between 30º and 35ºW, west of this longitude the beginning of the Mid-Atlantic Ridge becomes apparent. The Mid-Atlantic Ridge is centred at about 45ºW and extends as far west as 53ºW, with the shallowest parts reaching 3000 m. West of the ridge, the bottom is smooth in the North American basin with depths between 5500 and 6500 m. The western boundary is quite steep from the 5000 m isobath up to the Bermuda Bank. The extent of both basins is 3000 km, but the North American basin is deeper on average than the Canary basin.

All the data are interpolated to a common set of depths. These depths are closely

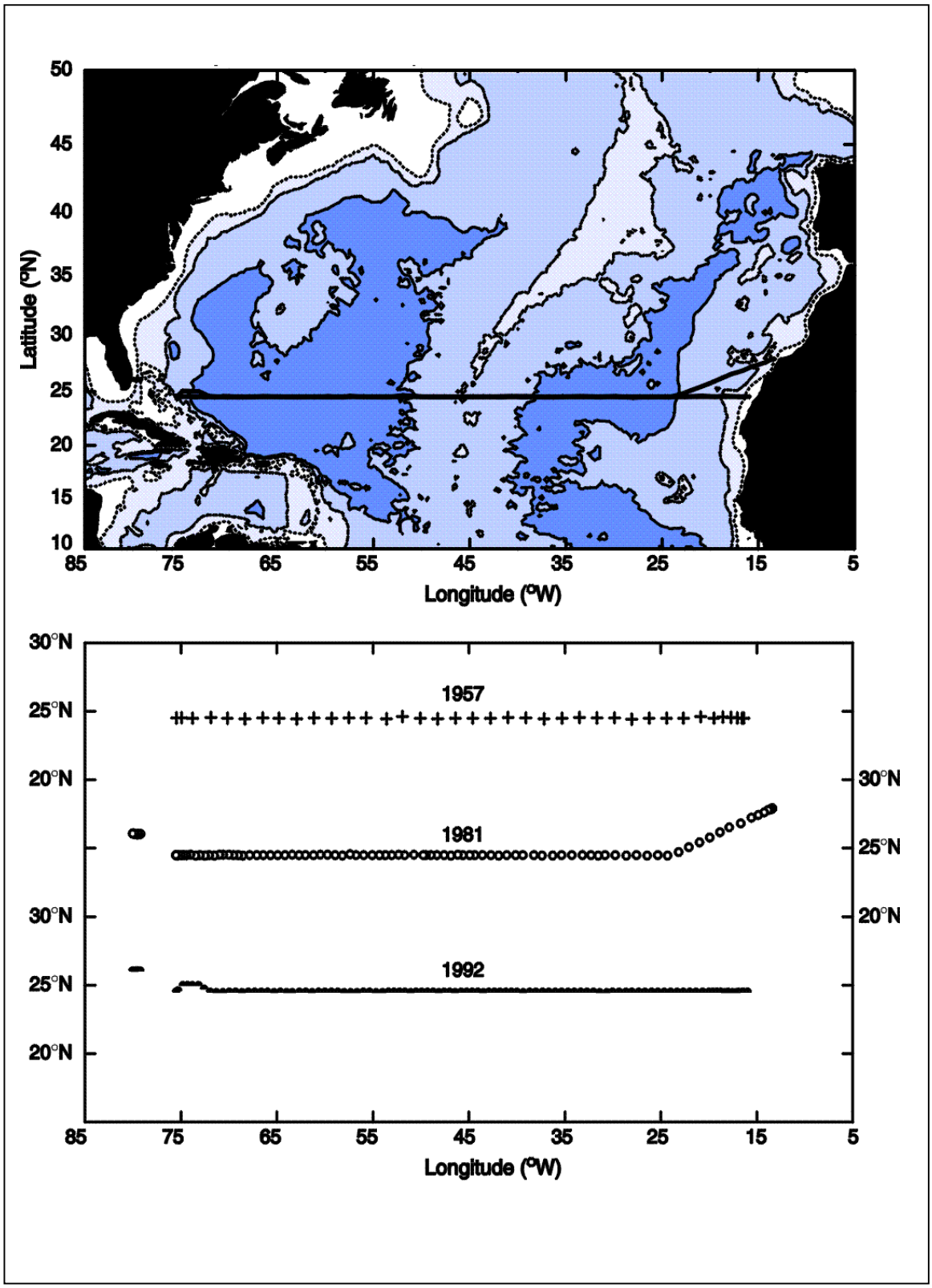

Figure 2.1. The 24.5ºN section. The section is indicated by the solid line in the chart of the North Atlantic on which the 500, 3000 and 5000 isobars are drawn. Station position for 1957 (+), 1981 (○) and 1992 (●) are shown below the chart.

spaced in the upper waters, with increasing separation toward the bottom (Table 2.1). The spacings are chosen to resolve the large structures of the general circulation and the mesoscale variability. Data and interpolation procedures are described here for each cruise.

nº	depth	interval
1	0	
2	50	
3	100	
4	150	50
5	200	
6	250	
7	300	
8	400	
9	500	
10	600	
11	700	
12	800	
13	900	100
14	1000	
15	1100	
16	1200	
17	1300	
18	1400	
19	1500	
20	1750	
21	2000	
22	2250	
23	2500	
24	2750	
25	3000	
26	3250	
27	3500	250
28	3750	
29	4000	
30	4250	
31	4500	
32	4750	
33	5000	
34	5500	
35	6000	500

Table 2.1 List of the standard depths.

2.2 Data

2.2.1 *Discovery II* 1957 IGY data

There is a detailed description of the cruise in Fuglister (1960). The cruise was carried out between October 6 and October 28, 1957, from 16º 20'W to 75º 28'W. The total number of stations was 38 (Fig. 2.1) and the sampling was done using reversing thermometers with Nansen bottles for water samples. Temperatures are stated to be accurate within ± 0.01ºC, depth is accurate within ± 5 m based on reading of paired protected and unprotected thermometers and salinity is accurate to ± 0.005.

Data were converted from depth to pressure using Saunders's formula (Saunders, 1981). Temperatures were based on IPTS-48 (International Practical Temperature Scale 1948), conversion to IPTS-68 (Barber 1969) is possible by Fofonoff and Bryden's (1975) formula. Differences, however are less than 0.01ºC in surface and less than 0.002ºC for temperatures lower than 4ºC. Such differences are lower than the accuracy of the measurements and therefore the 48 scale were used. All salinities presented in this thesis are according to the practical salinity scale (UNESCO, 1981). On this scale a salinity of 35 has approximately 35 grams of dissolved salts per kilogram of seawater; and a salinity difference of 0.001 is effectively a difference of 1 part per million. No units are used. Because the difference between the older and newer definitions of salinity is negligible in the oceanic range of salinity (UNESCO, 1991), no adjustments are made to the 1957 salinities due to the revised definition of salinity.

For the discrete bottle data, vertical linear interpolation was made, for each station, between adjacent data points to the standard depths. Data were plotted to check the values and detect errors in interpolation.

The IGY hydrographic sections were a watershed in oceanographic data quality, particularly for salinity, which was measured for the first time by conductivity techniques which are a factor of 4 more precise and accurate than the previous titration methods. Thus, the IGY temperatures and salinities are effectively at modern standards. The 1957 oxygens, however, are suspicious due to the use of an early technique that has been since

improved. While Worthington (1976) suggested that the IGY oxygens be multiplied by 1.048 to account for the difference between the old and new oxygen measurement techniques, we did not find such corrected oxygens to be reliable enough for meaningful comparisons with the 1981 and 1992 oxygen data sets.

2.2.2 *Atlantis II* 1981 long lines data

Detailed description of the 1981 cruise is given in Roemmich and Wunsch (1985). The cruise began August 11 from Las Islas Canarias with the first station off Cape Juby (Morocco). The last station was east of the Bahamas Bank on September 4 (Fig. 2.1). Two sections were made across the Florida Current at 26º 02' N and 27º 23' N to finish on September 6. The mid-ocean section was composed of 90 stations sampled by a Neil Brown Instrument $CTDO_2$. A 24-bottle rosette water sample was used for $CTDO_2$ calibrations (Millard, 1982). The 1981 CTD and water sample data sets are generally available at international oceanographic data centres. Simple averages of the nearly continuous $CTDO_2$ measurements were made to derive the standard depth values. The `window' was set 20 m above and 20 m below the standard depths. When the CTD did not reach the bottom to enable interpolation to all available standard depths, linear vertical extrapolation was allowed to estimate one more standard depth from the last two interpolated depths.

2.2.3 *Hespérides* 1992 WOCE data

The 1992 24.5ºN section, designated A-5 by WOCE (WOCE Implementation plan), was made by the Spanish B.I.O. *Hespérides* of the Armada Española, (Chief Scientist Gregorio Parrilla, Instituto Español de Oceanografía). The boat departed from Cádiz on July 14, sailing to Las Islas Canarias; six stations were made during this leg for testing the CTDs and rosette system.

We left Las Palmas on July 20 arriving at the first station (24º 29.97' N, 15º 58.08' W) the same day. The section ended at the Bahamas (24º 30' N, 75º 31' W) after 101 stations on August 14. On August 15, a section of 11 stations across of the Florida Current

at 26º 3' N was done. Figure 2.1 gives the location of the stations. Detailed description of the sampled stations is given by Parrilla *et al.* (1994b).

2.3 *Hespérides* 1992 CTD data calibration

Two NBIS EG&G Mark IIIb $CTDO_2$ underwater units each equipped with pressure, temperature, conductivity and polographic oxygen sensors were used throughout the cruise. Their serial numbers are 1100 and 2326. A General Oceanic rosette fitted with 24 Niskin bottles of 10 or 12 litre of capacity was used with the $CTDO_2$ for collecting water samples. In all cases, data were collected from the ocean surface to within a few meters of the bottom.

Both NBIS EG&G Mark IIIb CTDs were equipped with titanium pressure sensors manufactured by Paine Instrument. The temperature sensor was a Rosemount platinum # 171. The conductivity sensor was a 3-cm alumina cell manufactured by NBIS EG&G. The CTD work was supervised by G. Parrilla (IEO) and H. Bryden (WHOI), software and calibrations by R. Millard (WHOI) and hardware by J. Molinero (IEO) and G. Bond (WHOI).

Water sampling included measurements of salinity, oxygen, nutrients (silicate, nitrate+nitrite and phosphate), chlorofluorocarbons (CFC), pH, alkalinity, CO_2, particulate matter, chlorophyll pigments, ^{14}C and aluminum. Typically, 24 samples were obtained for each station. The water sample salinities were measured with a Guildline Autosal model 8400A salinometer by R. Molina (IEO). Oxygen determinations were carried out following the Winkler method primarily by J. Escánez and B. Amengual (IEO), (Parrilla *et al.,* 1994b).

Since in this research we have used mainly $CTDO_2$ data, only these observations will be described. Data acquisition and calibrations were done following the procedures given by Millard and Yang (1993). The EG&G data logging program CTDACQ was used to record down and up profiles and CTDPOST was used to flag spurious data. The remainder of the CTD post-processing was performed using the WHOI PC based CTD processing system as described by Millard and Yang (1993).

The $CTDO_2$ profiles require accurate calibration of conductivity, temperature, and pressure sensors in the laboratory. This is particularly important in deep water (below 1500 m) where variations in temperature and salinity are small. CTD pressure, temperature, and conductivity sensors for both CTDs were calibrated at WHOI before and after the cruise. The best fit NBIS EG&G Mark IIIb CTD sensor calibration is usually found to be linear in conductivity, quadratic in temperature, and quadratic for the titanium pressure transducer (Millard *et al.,* 1993). The polynomial coefficients to calibrate the raw sensor data are determined using standard least squares techniques.

Temperature calibrations are based on the International Practical Temperature Scale 1968 (IPTS-68, Barber, 1969). All the comparisons are made in this scale. In pressure, resolution is 0.1 db, with an accuracy of ±2.0 db for CTD number 1100 and ±5.0 db for CTD number 2326. The temperature resolution was 0.0005ºC with an accuracy better than ±0.0015ºC (Millard and Yang, 1993) over the range 0 to 30ºC. A comparison of pre-cruise and post-cruise calibration shows a large (0.01 to 0.015ºC) shift of temperature in the same direction in both CTDs. This shift was traced to a faulty pre-cruise laboratory temperature standardization, and was removed from the calibrations.

For calibration purposes, acquisition programs allow the operator to create a file of $CTDO_2$ observations at the time of bottle closure, and write averaged values of the raw, uncalibrated $CTDO_2$ sensor data around that point. An iterative fitting procedure has been developed for determining both conductivity and oxygen algorithm model coefficients (Millard and Yang, 1993) to minimize the differences between the CTD data and the water samples. Pre-cruise calibration data and *in situ* water sample salinity and oxygen were used on board to calibrate conductivity (salinity) and oxygen. These data were considered preliminary until the post-cruise laboratory calibration was completed.

The conductivity sensor resolution was 0.001 Ms cm^{-1} and an overall accuracy of the resulting CTD salinity calibrated to the rosette water bottle salinities is estimated as better than ±0.0025. CTD 1100 was used for stations 1-62, 74-80, 89-101 and the Florida Straits section; CTD 2326 was used for stations 63-71 and 81-88. The conductivity calibrations were examined closely at the change of instruments.

After acquiring the $CTDO_2$ data, the four post-processing steps are: editing, pressure averaging, calculation of calibrated data quantities, and pressure centring and data quality control. The raw station data were edited just after the finish of each station. Erroneous $CTDO_2$ observations were flagged and pressure-averaging programs replaced these observations. To match the conductivity data time response to that of the temperature data, an exponential recursive filter was applied to the conductivity sensor data (Millard, 1982). The edited raw $CTDO_2$ data was gridded to form a centred uniform pressure series with calibrated salinity and oxygen data in two steps. The pressure-averaging step replaced the erroneous input data, applied the conductivity-temperature sensor lags, and bin averaged the raw data in uniform pressure steps of 2 decibars. After that, a pressure centring step converted the data to physical units by applying the calculation polynomial and interpolated the pressure averaged observations to a uniform pressure series.

Data quality control was performed to check the integrity of the calibrations and water sample measurements. Temperature, salinity, oxygen, and potential density anomaly profiles versus pressure were examined, also salinity and oxygen versus potential temperature diagrams of consecutive stations are examined. Calibration data and quality control of this cruise has been done by R. Millard (WHOI), G. Parrilla (IEO), M. J. García (IEO), H. Bryden (SOC, U.K.) and the author.

The 1992 data set was collected under the World Ocean Circulation Experiment (WOCE) of the World Climate Research Programme, under which stringent quality control procedures have been instituted. The 1992 data set was submitted for evaluation to the WOCE Hydrographic Program Office in 1994 and the resulting comments have being incorporated to produce the final version of data. In the meantime, scientists who have requested the 1992 data have been provided with it, with the caveat that it was not yet in final WOCE form.

The 2-db temperature, salinity, and oxygen data have been smoothed with a binomial filter and then linearly interpolated (Mamayev *et al.,* 1991) as required to the standard levels (Table 2.1). When the CTD did not reach the bottom, to enable interpolation to all available standard depths, linear vertical extrapolation were used to estimate one more standard depth as for the 1981 cruise from the last two interpolated depths.

During the *Hespérides* 1992 cruise along 24.5ºN, dissolved inorganic nutrients (orthophosphate, nitrate+nitrite, and orthosilicate) were collected and analysed on board, using a continuous flow analyzer, by A. Cruzado (Parrilla *et al.*, 1994b) following methods adapted from Withledge *et al.,* (1981) (see Cruzado's addendum to Parrilla *et al.*, 1994b). Errors in oxygen determinations are 0.3 µmol kg^{-1}; errors in silicate determinations are 0.05 µmol kg^{-1}; errors in nitrate + nitrite determinations are 0.02 µmol kg^{-1}; errors in phosphate determinations are 0.01 µmol kg^{-1}. Since oxygen concentrations are high over the section, the determined concentrations of nitrate + nitrite are considered mostly as nitrate concentrations.

2.4 Characteristics of the 24.5ºN *Hespérides* section

2.4.1 Temperature

Potential temperature distribution (Fig. 2.2) presents highest surface values (>25ºC) in the western part decreasing eastward toward the African shelf where surface temperature is as low as 19.5ºC. This cold temperature is the signature of upwelling in the area. In the thermocline layer, temperature decreases quickly to reach 9ºC around 700 m in the Canary basin and deeper than 800 m in the North American basin. Tilting of isotherms gives indication of southern flux of thermocline waters over the section except the western boundary where fluxes reverse. At the base of the intermediate water range, 4ºC is reached at around 2000 m in the Canary basin and a little shallower in the North American basin. Influences of MW and AAIW temperature are hard to detect. UNADW ranging between 4ºC and 3ºC is the deepest water mass covering the entire section uninterrupted. The largest differences between basins are found in LNADW and AABW. In the North American basin, AABW, considered to be water colder than 1.9ºC, is restricted almost exclusively from 4000 m to the bottom near the western flank of the Mid-Atlantic Ridge, extending westward to 70ºW in the basin (where the 1.8ºC isotherm falls to the bottom) with very little influence to the west due to some recirculations in the area (Schmitz and McCartney, 1993, Lee *et al.*, 1996). LNADW occupies the rest of the basin between around 2500 m and the bottom and the AABW limit. The Canary basin is not directly

influenced by the AABW. The coldest water found has a potential temperature of 1.9ºC, and it is a blend of NADW and AABW (Saunders, 1986; Mantyla, 1994).

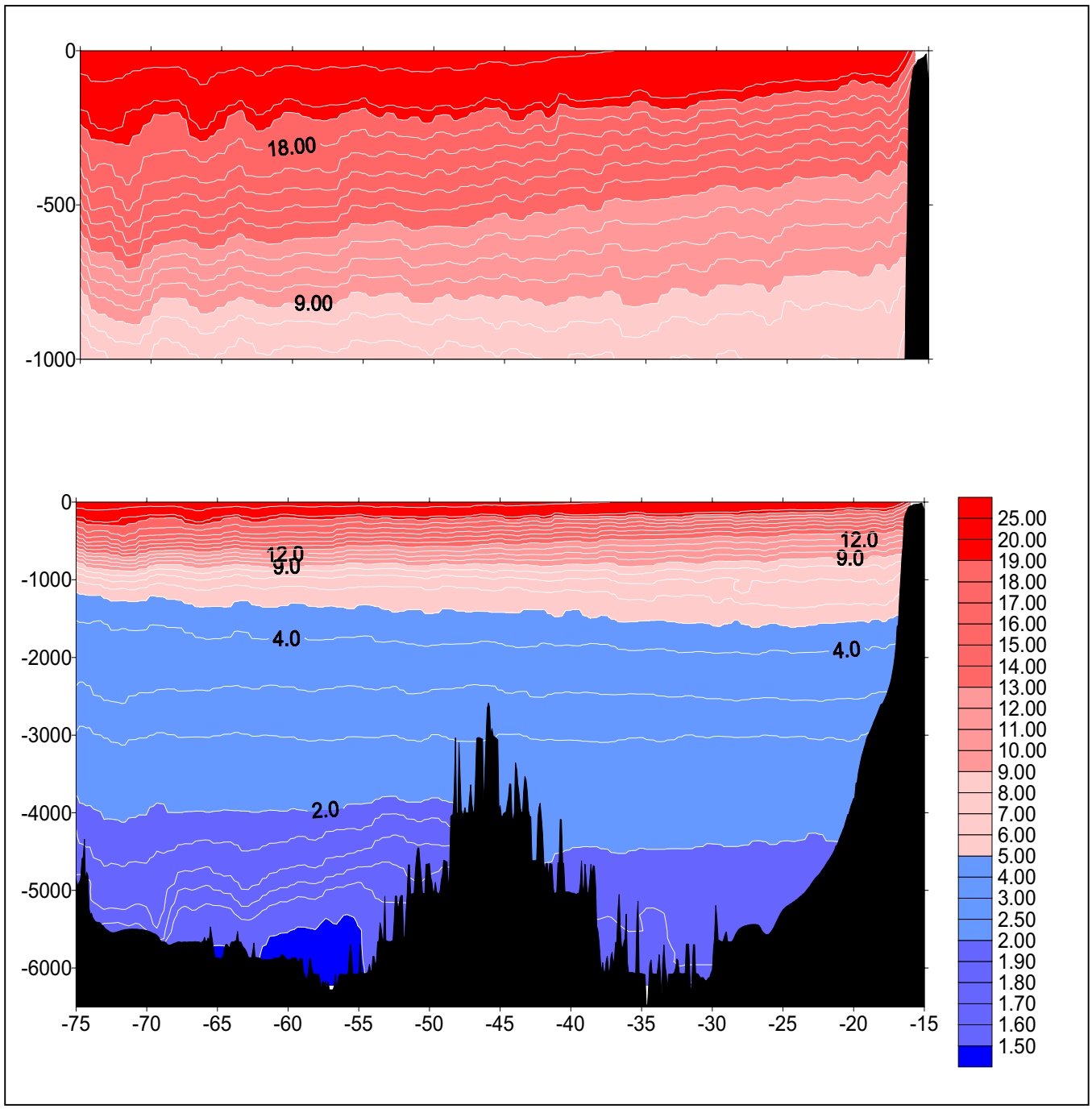

Figure 2.2: Zonal section of potential temperature (ºC) across 24.5ºN from the hydrographic stations taken aboard *Hespérides* in July-August 1992. The upper plot has expanded vertical scale.

2.4.2 Salinity

High salinity waters (>37) created by the excess of evaporation over the subtropical gyre are found in the upper 150 m of the water column from 25ºW to 55ºW (Fig. 2.3). In the thermocline waters, salinity decreases, the 36 isohaline reaching nearly 300 m in the African margin and 600 m near the western boundary, rising to 500 m on the American

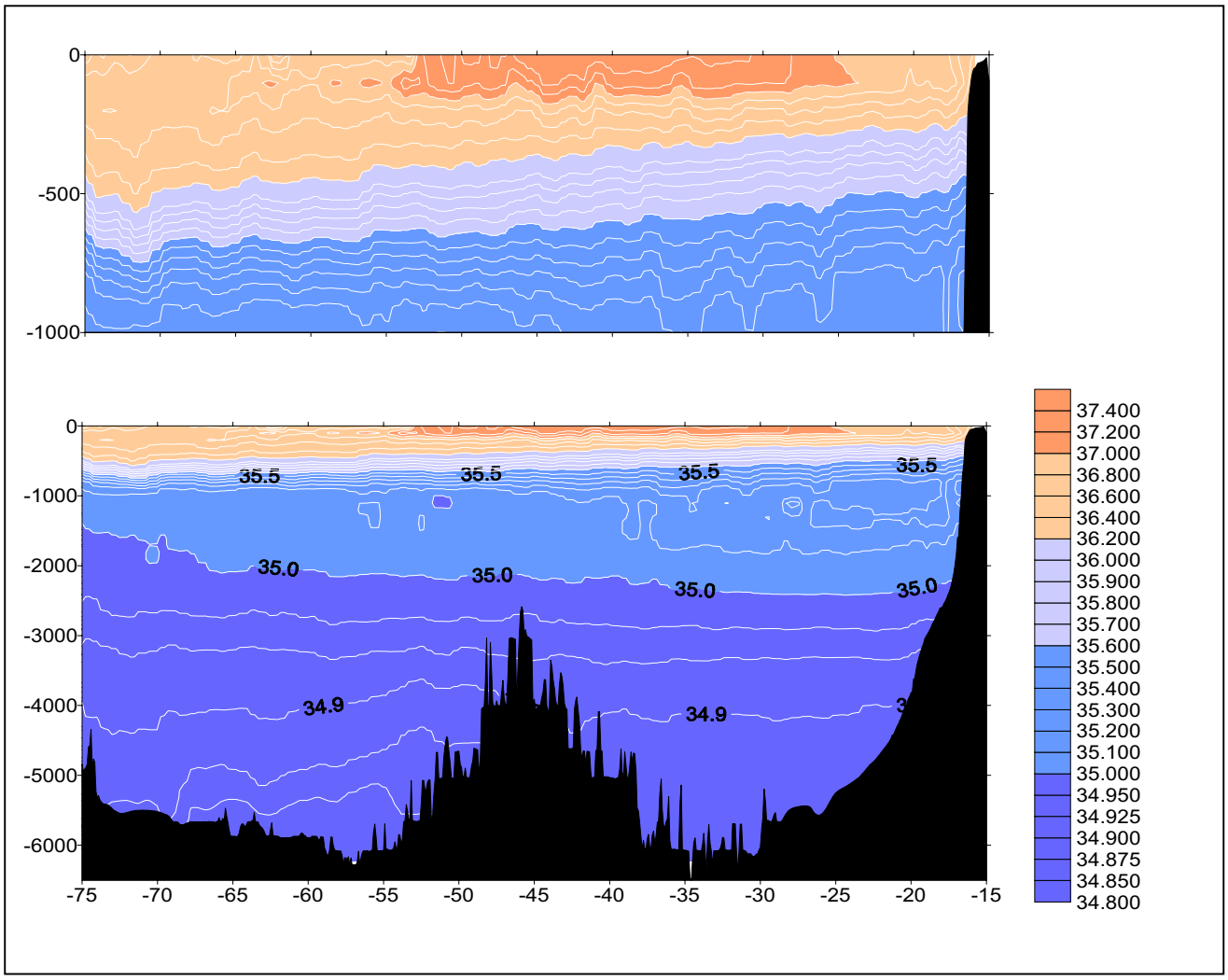

Figure 2.3: Zonal section of salinity across 24.5ºN from de hydrographic stations taken aboard *Hespérides* in July-August 1992. The upper plot has expanded vertical scale.

slope. This structure persists down to the intermediate waters where the two influences mentioned in the previous chapter: in the Eastern basin, the influence of MW from the Strait of Gibraltar, and in the North American basin the AAIW influence towards low salinity. 24ºN is the northern limit of the influence of AAIW, thus the influence is shown to be parcelled in small portions. The largest parcel is located in the western part of the

MAR between stations 60 and 62 (50º 29.7'W to 51º 40'W) between 1000 and 1100 m depth. In the MW influence region, an eddy of MW (MEDDY) is found at station 24 (24º 30.00'N, 27º 59.83'W) with maximum salinity anomaly at 1100 m. In the deep water, the influence of AABW is shown in the eastern part of the North American basin, near the MAR, with values of 34.86, values that are never reached in the Canary basin.

2.4.3 Oxygen

Oxygen distribution (Fig. 2.4) presents values at sea surface determined by the solubility of the gas when in equilibrium with the atmosphere. The solubility is influenced greatly by temperature and to a lesser degree by salinity. At 24.5ºN surface values correspond to temperature saturation (around 200-225 µmol kg^{-1}) with a maximum at the eastern boundary due to lower temperatures. In water which has sunk below the euphotic zone, the dissolved oxygen is removed by oxidation of organic matter. This effect is important at intermediate depths and contributes to the formation of the minimum oxygen layer. This layer is located in the thermocline with a deep minimum around 142 µmol kg^{-1} at 900 m in the zonal mean. The lowest values (less than 120 µmol kg^{-1}) are found near the eastern boundary between 500 and 1000 m depth. In this layer effects of the influence of MW and AAIW also contribute to this minimum. Recently ventilated NADW with a large concentration of dissolved oxygen leads to a large increase from 900 m depth in the western part, to 2000 m in the eastern part, reaching values greater than 240 µmol kg^{-1} from this depth to the bottom. Averaged over the section, the maximum is located around 4500 m with values of 255 µmol kg^{-1}, after which concentrations reduce to a relative minimum at 5800 m (248 µmol kg^{-1}) due to the AABW influence. At the western boundary the effect of water recently ventilated is clear. Maximum values are found at the boundary between 3000 and 4000 m where the DSOW (Denmark Straits Overflow Water) is located and spreads further east to achieve values of 260 µmol kg^{-1} even at 55ºW at these depths. In the upper lobe of the NADW, the LSW high oxygen levels spread much less and only reach 69ºW between 1800 and 3000 m. 1992 oxygen data in ml l^{-1} were converted to µmol kg^{-1} using Millard's formula (Millard, per. comm.), for comparison old units were kept.

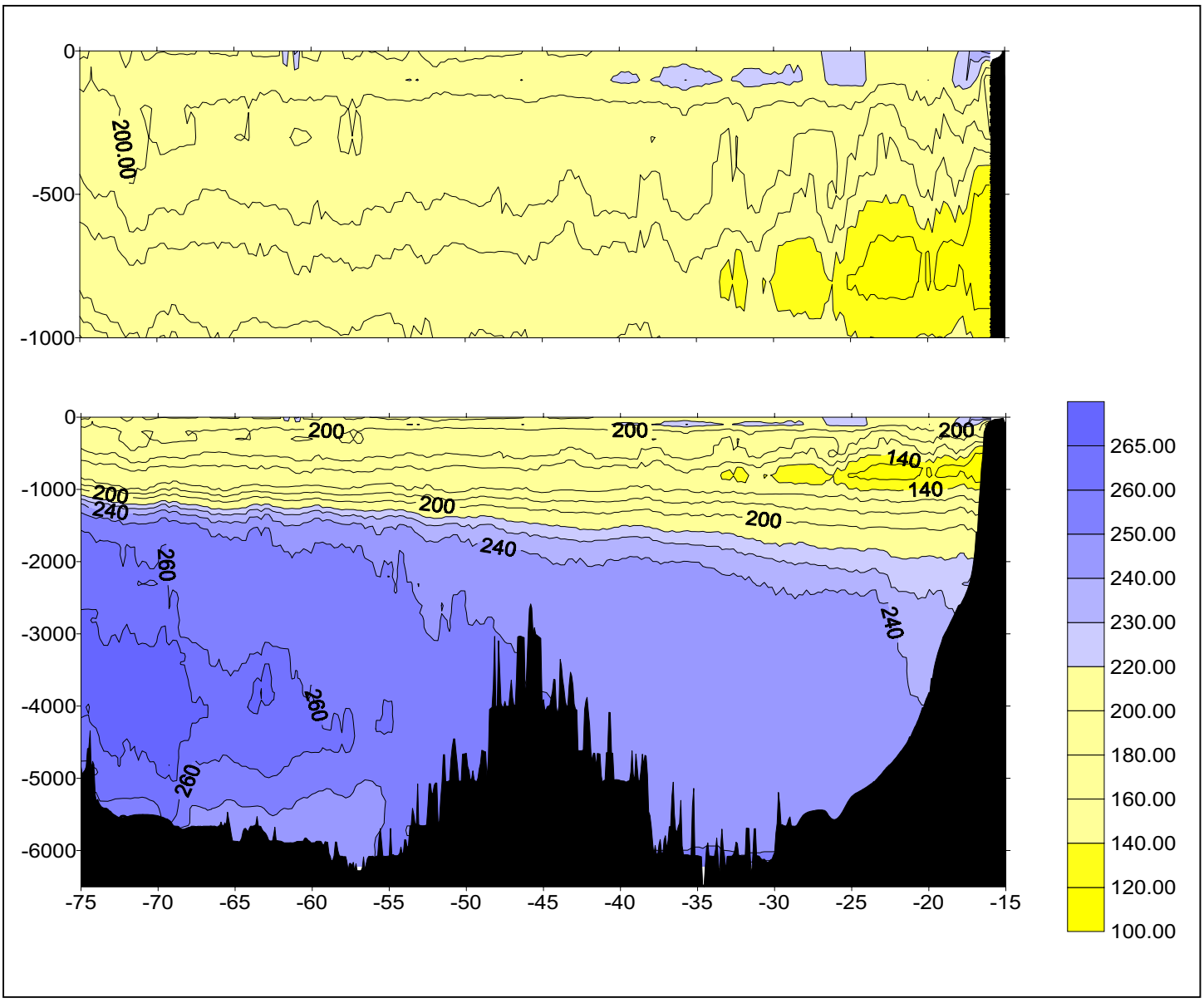

Figure 2.4: Zonal section of oxygen (µmol kg^{-1}) across 24.5ºN from the hydrographic stations taken aboard *Hespérides* in July-August 1992. The upper plot has expanded vertical scale.

2.4.4 Silicate

Silicate distribution (Fig. 2.5) has its minimum concentration at the surface and generally increases monotonically with depth, except for the AAIW influence between 600 and 1600 m depth where values higher than 20 µmol kg^{-1} are found over the MAR and Canary basin. Waters of southern origin have higher silica concentrations than those of northern origin. AAIW, Eastern Boundary Current and AABW have higher concentrations. Lower silica concentrations of LSW appear at around 1500 m in the North American basin.

Silica is mainly constant between 1000 and 1500 m at about 20 µmol kg^{-1} and thereafter increases at greater depth, reaching about 50 µmol kg^{-1}. The North American basin has lower concentrations of silica throughout the water column except for the AABW banked against the Mid-Atlantic ridge where concentrations are higher (reaching 60 µmol kg^{-1}) than in the Canary basin. Variability is large in LNADW where concentrations are between 20 and 40 µmol kg^{-1} in the North American basin and between 40 and 50 µmol kg^{-1} in the Canary basin.

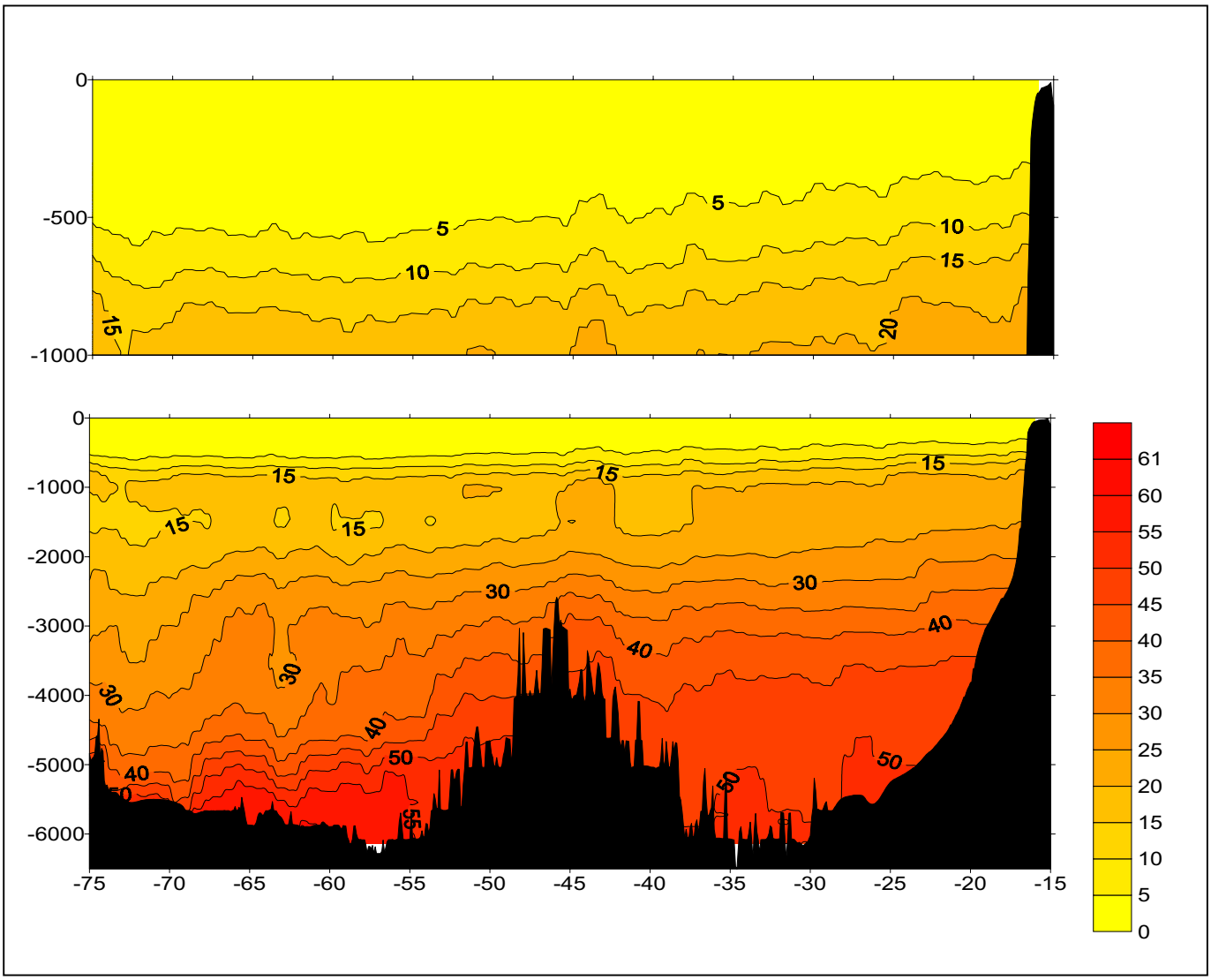

Figure 2.5: Zonal section of silicate (µmol kg^{-1}) across 24.5ºN from the hydrographic stations taken aboard *Hespérides* in July-August 1992. The upper plot has expanded vertical scale.

2.4.5 Nitrate + nitrite

The distribution of nitrate + nitrite (Fig. 2.6) increases from near zero values at the ocean surface to maxima between 900 and 1000 m depth with values over 30 µmol kg^{-1} in the eastern part of the section; this is where minimum oxygen is found. Below this concentrations for the UNADW reduce, and they increase for the LNADW as well as for the AABW, but values are lower than at the thermocline maximum. The distribution shows that concentrations are higher in the Canary basin than in the North American

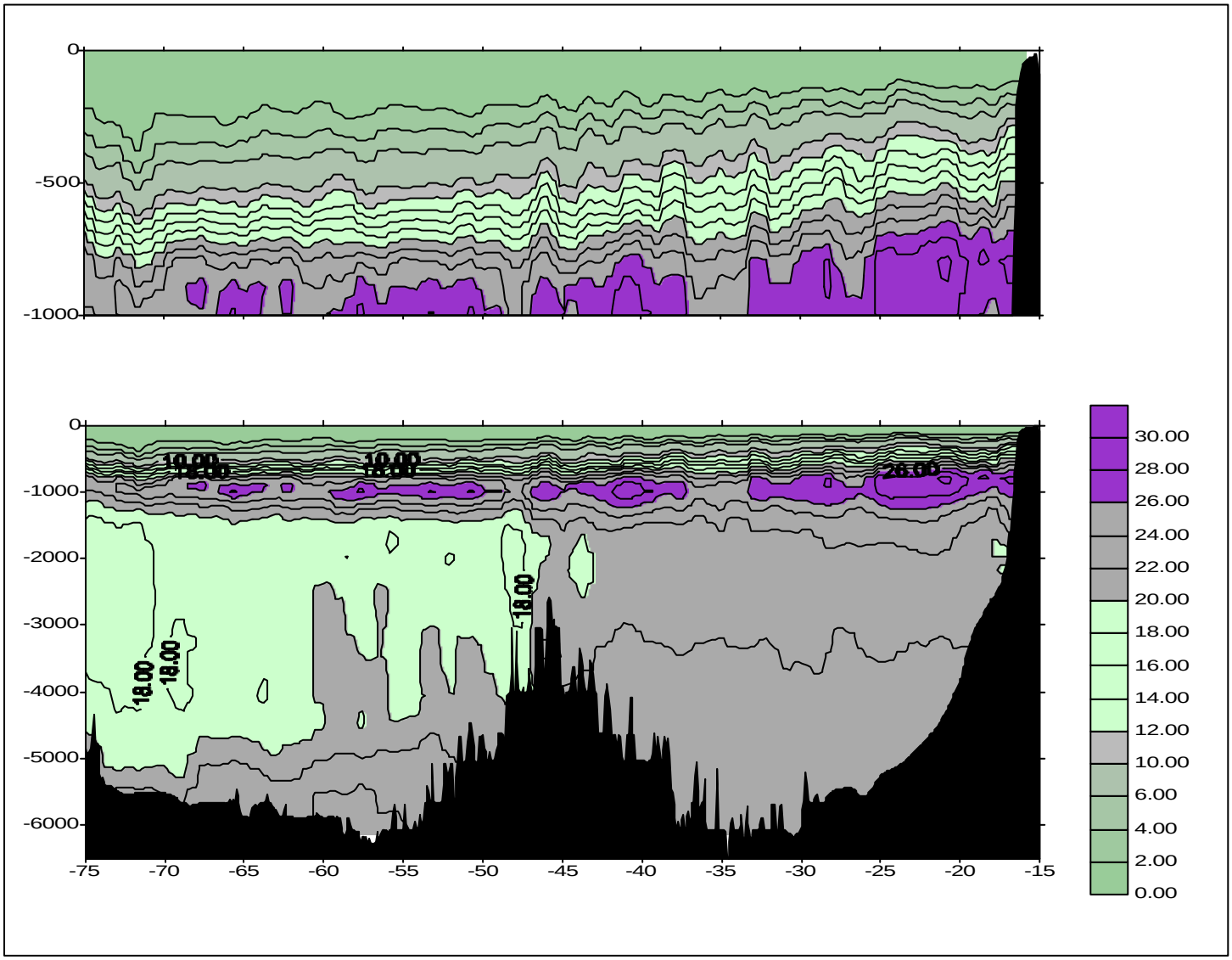

Figure 2.6: Zonal section of nitrate+nitrite (µmol kg^{-1}) across 24.5ºN from the hydrographic stations taken aboard *Hespérides* in July-August 1992. The upper plot has expanded vertical scale.

basin, except for AABW. Relatively smaller values are found in the western boundary current where recently ventilated water flows southward. These waters of northern origin

(LSW and DSOW) have lower concentrations of nitrates and the signal is presented in a manner similar to high oxygen concentrations. There is a region of low nitrate concentration over the Mid Atlantic Ridge, showing the flow of Labrador Sea Water as part of the NADW.

2.4.6 Phosphate

Phosphate distribution (Fig. 2.7) is similar to those of nitrate, as the well known Redfield ratio NO_3/PO_4, around 15 would suggest; nevertheless, since data are available

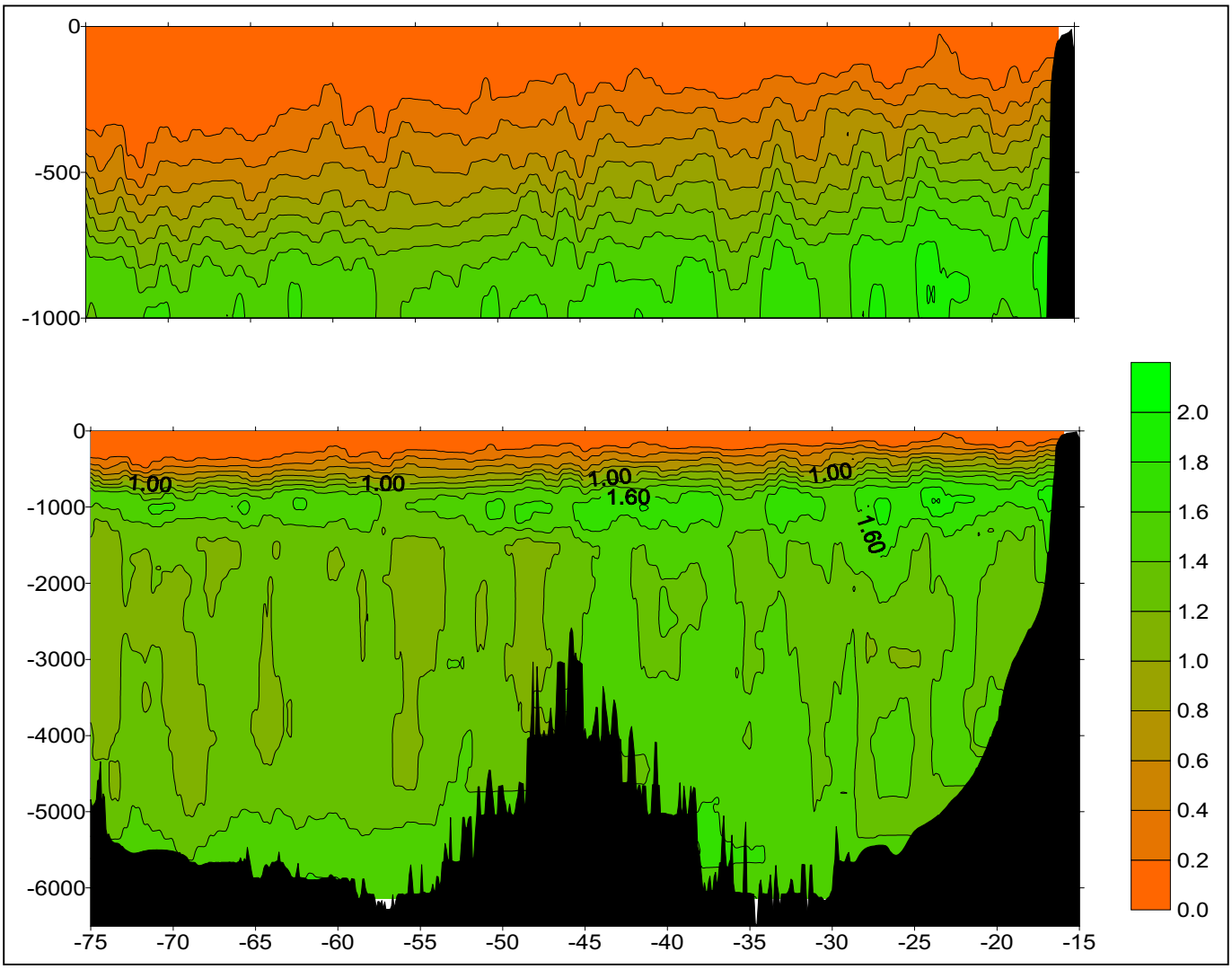

Figure 2.7: Zonal section of phosphate (µmol kg^{-1}) across 24.5ºN from the hydrographic stations taken aboard *Hespérides* in July-August 1992. The upper plot has expanded vertical scale.

we will try the data as a new source of constraints. Maximum phosphate values are located in the lower thermocline of the eastern boundary where values reach 2 μmol kg^{-1}. Phosphate is effectively zero at the surface and increases linearly toward the maximum values in the lower thermocline, NADW presents low phosphate concentration in its source regions but slightly higher in the Canary basin. Finally, a second relative maximum is found in the AABW influence.

Chapter 3

Comparison over time of temperature and salinity

3.1 Introduction

In this chapter the climatic variations of temperature and salinity over the subtropical Atlantic Ocean from the surface to 6000 m depth from 1957 to 1992 are investigated. Three available cruises have been compared at the nominal latitude of 24.5ºN. However, the 1981 cruise started on the African Continental shelf at 27.9ºN and angled southwestward to joint 24.5ºN at 24.3ºW (Fig. 2.1) due to the Sahara war which was close to the coast at 24.5ºN. The *nominal* station spacing in the IGY survey was 185 km. On the *Atlantis II*, the spacing varied between 50 and 80 km with shorter spacing when the stations were over the continental slopes and the Mid-Atlantic Ridge. The same criteria were used for the *Hespérides* survey, but the spacing was more regular, between 58 and 67 km. Therefore, in order to compare directly the variables from the different cruises it is necessary to interpolate all the data onto a set of common geographic locations. The data were interpolated onto a two dimensional grid at 24.5ºN. The horizontal spacing chosen was 0.5º of longitude. This corresponds approximately to 50 km at this latitude (0.5 x 60 x 1.85 x cos(24.5) = 50.5 km). The data were placed vertically onto a set of 35 standard depths defined in Table 2.1

3.2 Methodology

In order to choose a scheme of interpolation, we compared spline interpolation and objective mapping, two methods which could reasonably be used. Here we describe how their advantages and disadvantages led to the decision to use one of them for this work. Between the results of the two methods, discrepancies are within the expected error in all regions except the boundaries. Cubic spline is simpler to use but the advantage of calculating expected errors made objective mapping the most suitable method of interpolation for this analysis.

3.2.1 Spline interpolation

The spline interpolation (Ahlberg *et al.,* 1967) assumes the existence of a function $y = f(x_i)$ whose value is known at a set of x_i points, $a = x_0<x_1<...<x_n = b$, regularly or irregularly spaced. The cubic spline is the cubic polynomial $f(x)$ that is continuous in the interval [a,b], has continuous first and second derivatives, and passes through the points $f(x_i)$ (i=0,n). The interpolating cubic spline defines a separate cubic polynomial for each interval $x_{i-1}< x < x_i$, or a total of n polynomials for the n+1 points. We can write the polynomial equation, take derivatives and, at each data point, equate the first and second derivative of the left-side polynomial to those of the right-side. Following Thompson (1984), writing the Taylor series for the cubic polynomial for interval i, expanded about the point x_i be

$$y(x) = y_i + (x - x_i)\, y'_i + (x - x_i)^2\, y''_i / 2 + (x - x_i)^3 (y''_{i+1} - y''_i)/6h \quad (3.1)$$

where y'_i e y''_i stand for the first and second derivatives evaluated at $x = x_i$, and the third derivative has been replaced by its divided difference form, which is exact for a cubic function (Bevington and Robinson, 1992). At $x = x_i$, we have $y = y_i$ as required. Setting $x = x_{i+1} = x_i + h$, it is possible to solve the equation

$$y(x_{i+1}) = y_i + (x_{i+1} - x_i)\, y'_i + (x_{i+1} - x_i)^2\, y''_i /2 + (x_{i+1} - x_i)^3 (y''_{i+1} - y''_i)/6h \quad (3.2)$$

to obtain

$$(y_{i+1} - y_i) = h\, y'_i + h^2 [2\, y''_i + y''_{i+1}]/6 \quad (3.3)$$

Repeating the calculation, using the equation for $y(x)$ in the interval $i-1$ and requiring that $y(x) = y(x_i)$ at the i data point we obtain

$$(y_i - y_{i-1}) = h\, y'_{i-1} + h^2 [\, 2\, y''_{i-1} + y''_i]/6 \quad (3.4)$$

To establish continuity conditions at the data point, we equate first and second derivatives at the boundaries $x = x_i$ and $x = x_{i-1}$. The use of the divided difference form for

the third derivative assures continuity of the second derivative across the boundaries and gives the spline equation

$$y''_{i-1} + 4\, y''_i + y''_{i+1} = D_i \qquad (3.5)$$

with

$$D_i = y\,[\, y_{i+1} + 2\, y_i + y_{i-1}]/\, h^2 \qquad (3.6)$$

These equations can be solved for the second derivatives y_i'', as long as the values of y_1'' and y_n'' at the boundaries are known. If those boundary values are set to 0 the *natural splines* are obtained.

In our case we have used *natural splines* for the interpolation. The fitting by cubic splines was done from the longitude of the western-most to the eastern-most station, for each of the 35 standard depths. After fitting, the function was evaluated every 0.5º of longitude. Below 2750 m (standard depth number 24), the North Atlantic is separated by the Mid-Atlantic Ridge in two basins, the North American basin and the Canary basin. Since the behaviour of the basins is different, the fitting was done separately for each of them below 2750 m.

The set of data obtained after the gridding is for *Hespérides* 1992 from 75.5ºW to 16ºW, for *Atlantis II* 1981 from 75.5ºW to 13.5ºW and IGY 1957 from 75.5ºW to 16.5ºW. *Atlantis II* data, due to the deviation of the track from 24.5ºN east of 24.5ºW, is only compared with the other sections west of 24.5ºW. After gridding for the three cruises, the differences on the common area were calculated:

- 1981-1957: Subtracting 1957 data from 1981 between 75.5ºW and 24.5ºW. This comparison was also done by Roemmich and Wunsch (1984) using objective mapping.
- 1992-1981: Subtracting 1981 data from 1992 between 75.5ºW and 24.5ºW.
- 1992-1957: Subtracting 1957 data from 1992 between 75.5 and 16.5ºW.

Because the grid-point temperature differences exhibit large variations due to the presence or absence of eddies during the different surveys, a horizontal gaussian filter of e-folding scale of 300 km has been applied to the temperature differences at each depth.

Behaviour of the boundaries

When the gaussian filter was applied at the boundaries, we extend the temperature difference matrices in an unbiased way with zeros past the boundaries so that smoothed temperature differences are obtained up to the western and eastern boundaries as well as in the Mid-Atlantic Ridge.

Figure 3.1A, B and C present temperature differences for 1981-1957, 1992-1981 and 1992-1957 obtained with this methodology.

For salinity calculation similar to those for temperature have been done, fitting by cubic splines at each standard depth and using a gaussian filter of the differences. Figure 3.2 A, B and C present salinity differences for 1981-1957, 1992-1981 and finally 1992-1957.

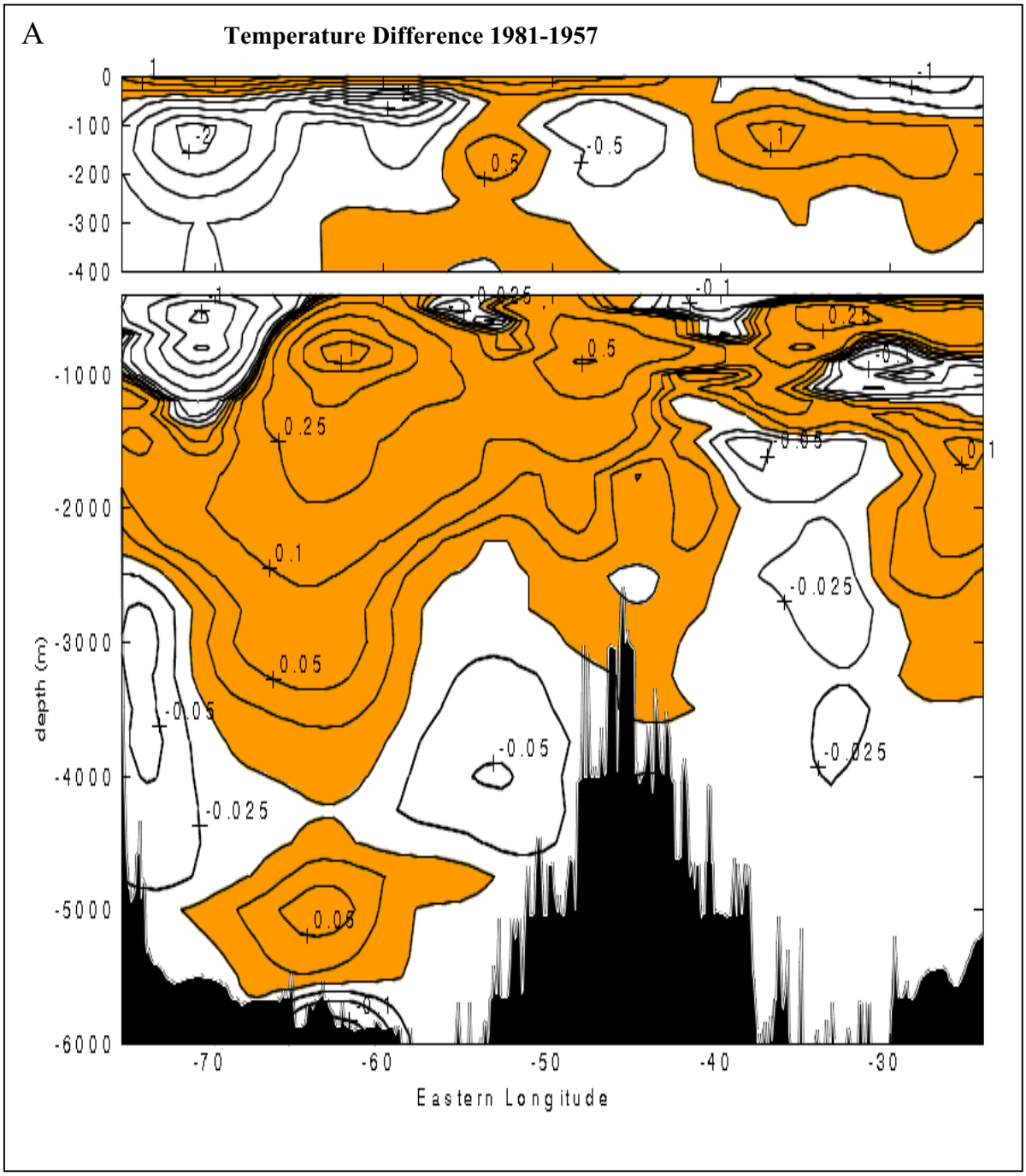

Figure 3.1: Difference of temperature at 24.5ºN using spline fitting and interpolating values each 0.5º of longitude. Differences were smoothed using a gaussian filter with e-folding scale of 300 km. Differences were calculated for A) 1981-1957 B) 1992-1981, and C) 1992-1957. Values are in ºC. Shading in colour indicates positive difference. The top plot has expanded vertical scale.

B

Temperature Difference 1992-1981

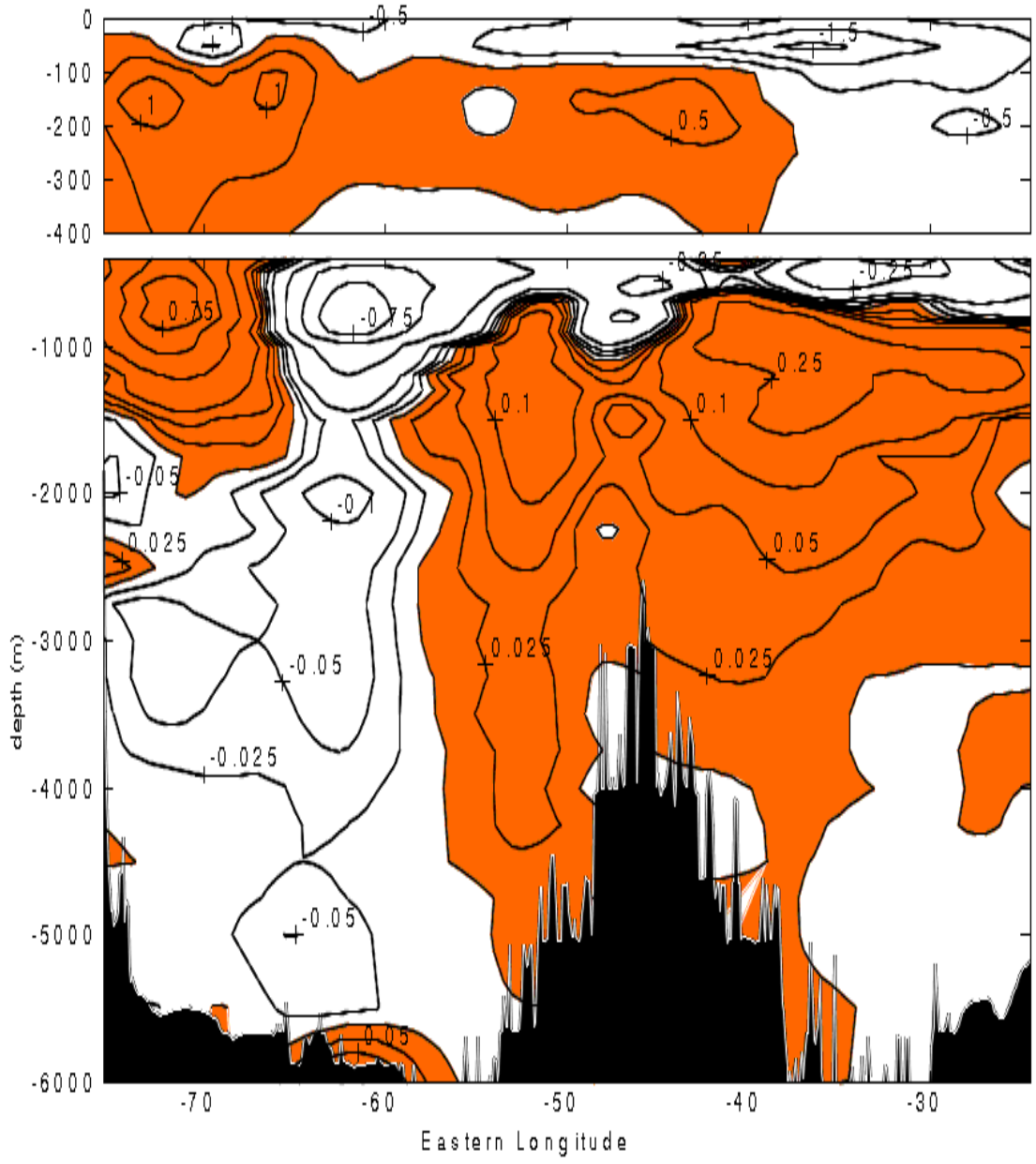

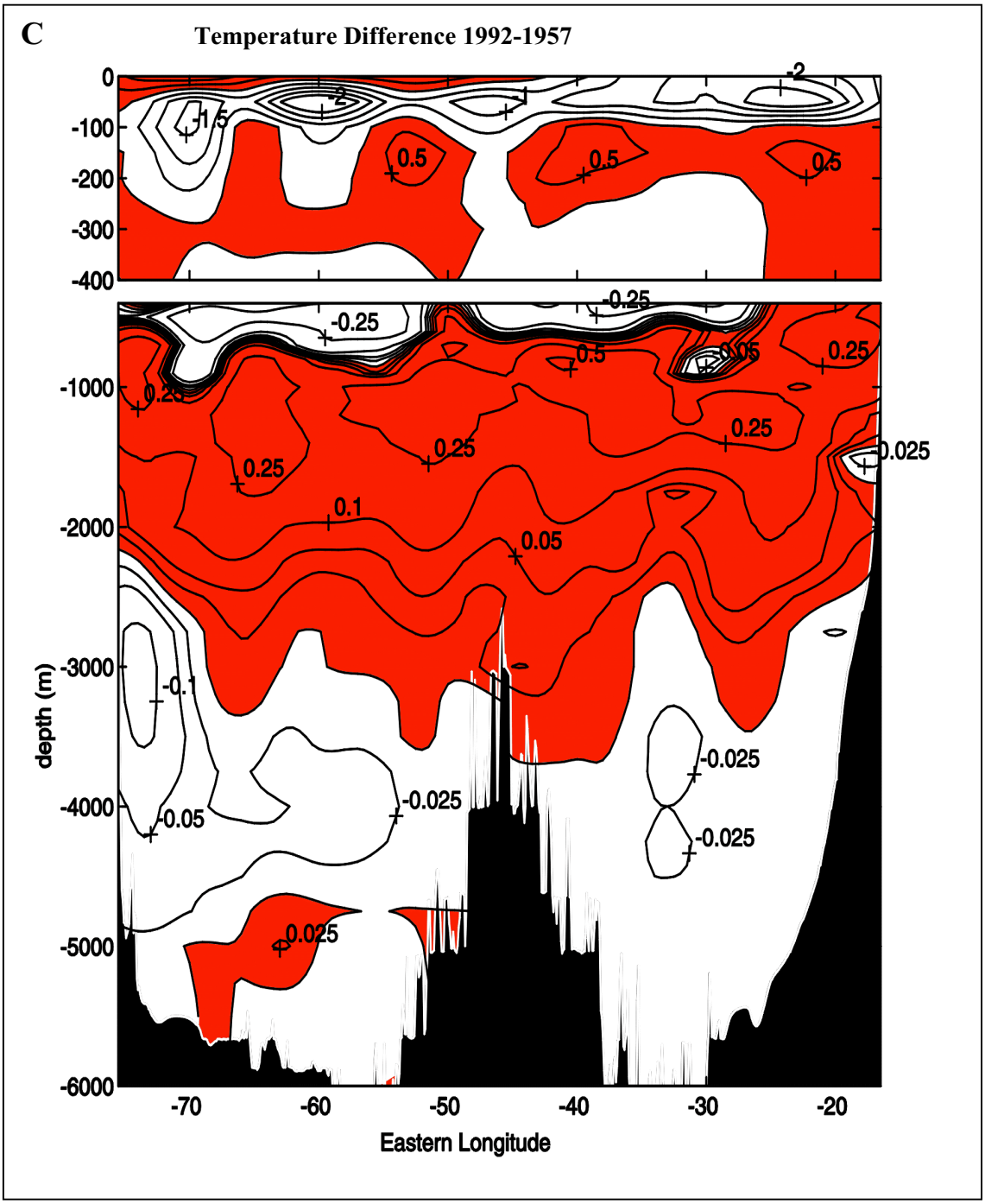
C
Temperature Difference 1992-1957
depth (m)
Eastern Longitude
0
-100
-200
-300
-400
-1000
-2000
-3000
-4000
-5000
-6000
-70
-60
-50
-40
-30
-20
-2
-1.5
-1
0.5
-0.25
0.25
0.1
0.05
0.025
-0.1
-0.05
-0.025

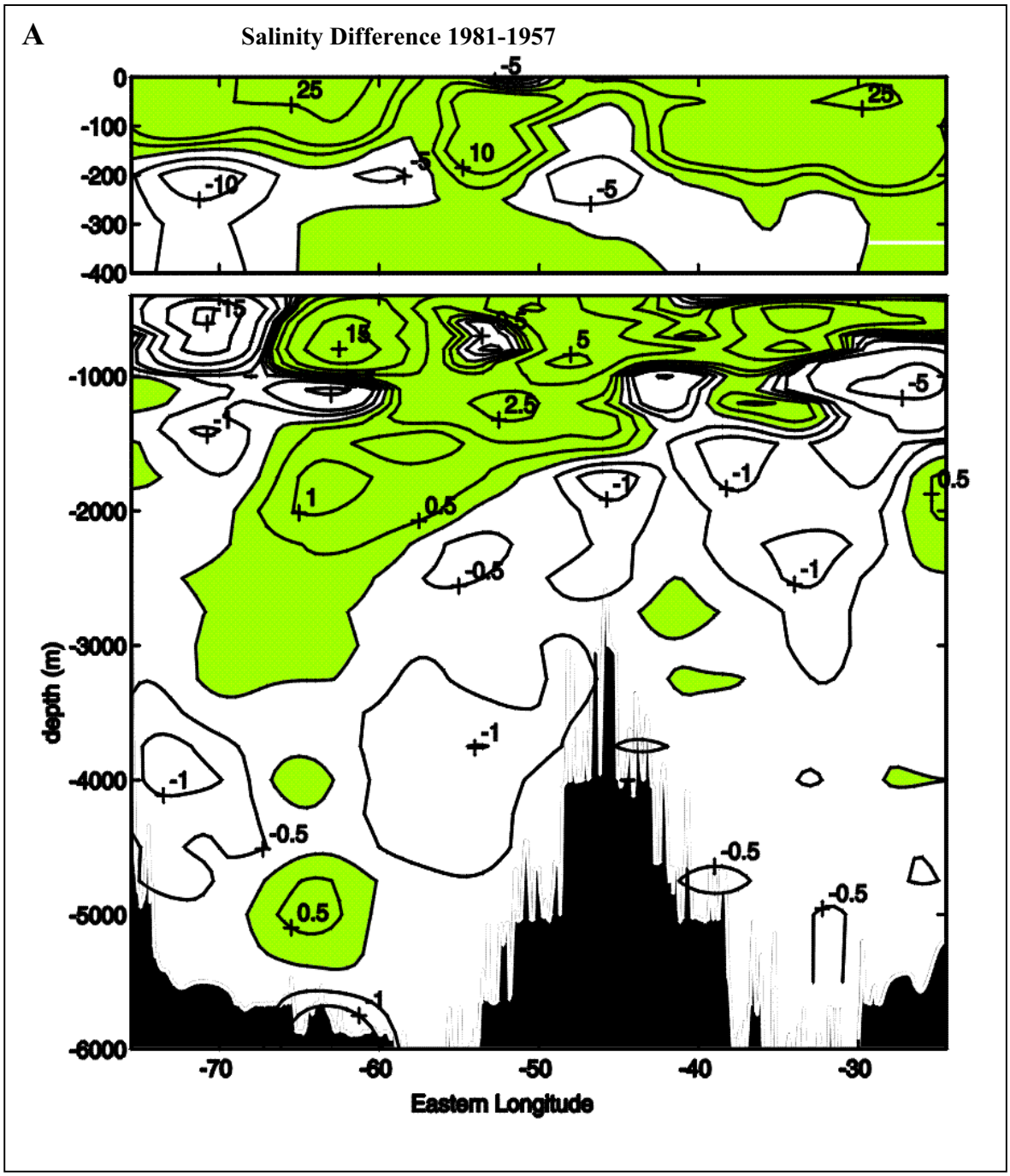

Figure 3.2: Difference of salinity (multiplied by 100) at 24.5ºN using spline fitting and interpolating values each 0.5º of longitude. Differences were smoothed using a gaussian filter with e-folding scale of 300 km. Differences were calculated for A) 1981-1957 B) 1992-1981, and C) 1992-1957. Shading in colour indicates positive difference. The top plot has expanded vertical scale.

B **Salinity Difference 1992-1981**

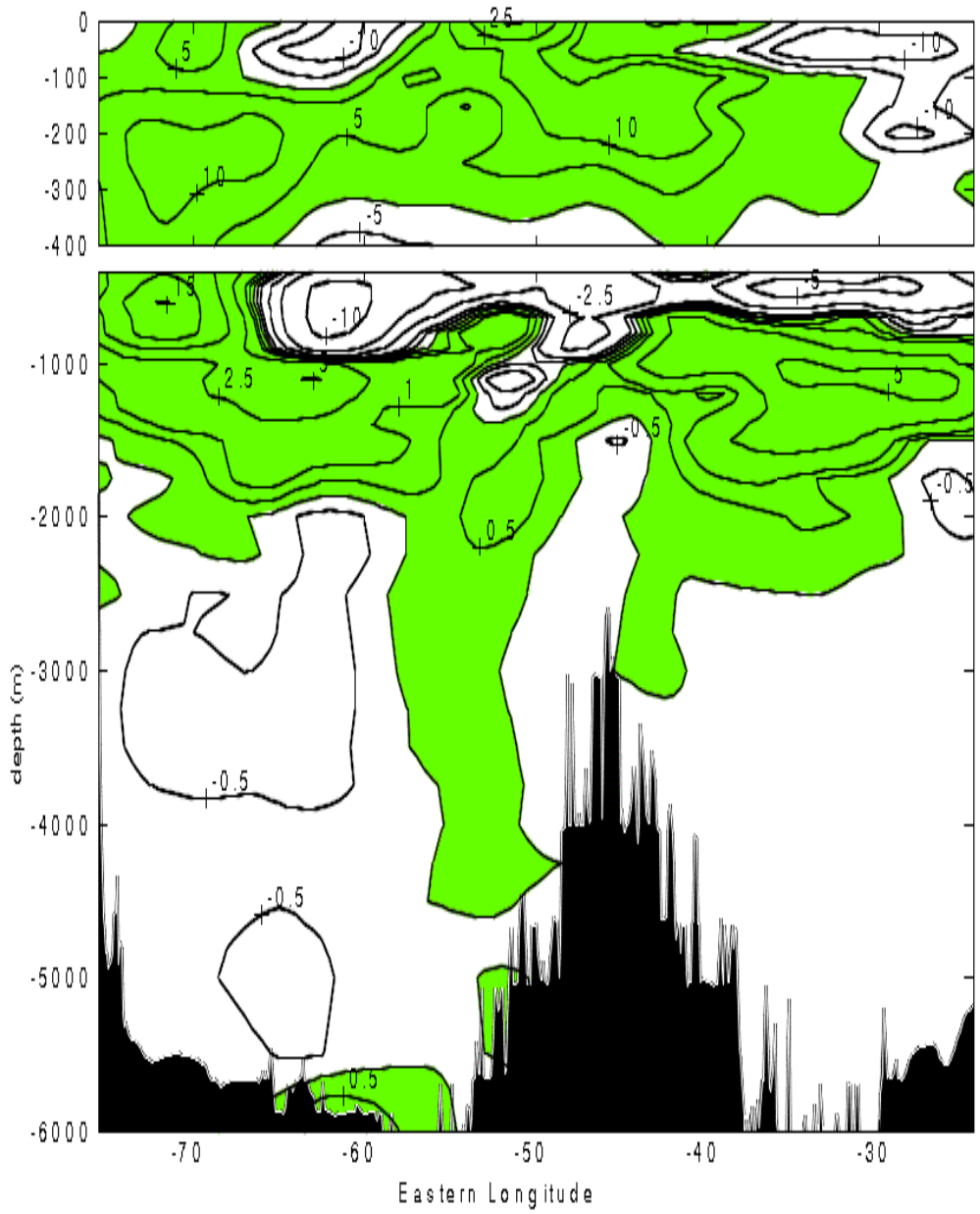

C **Salinity Difference 1992-1957**

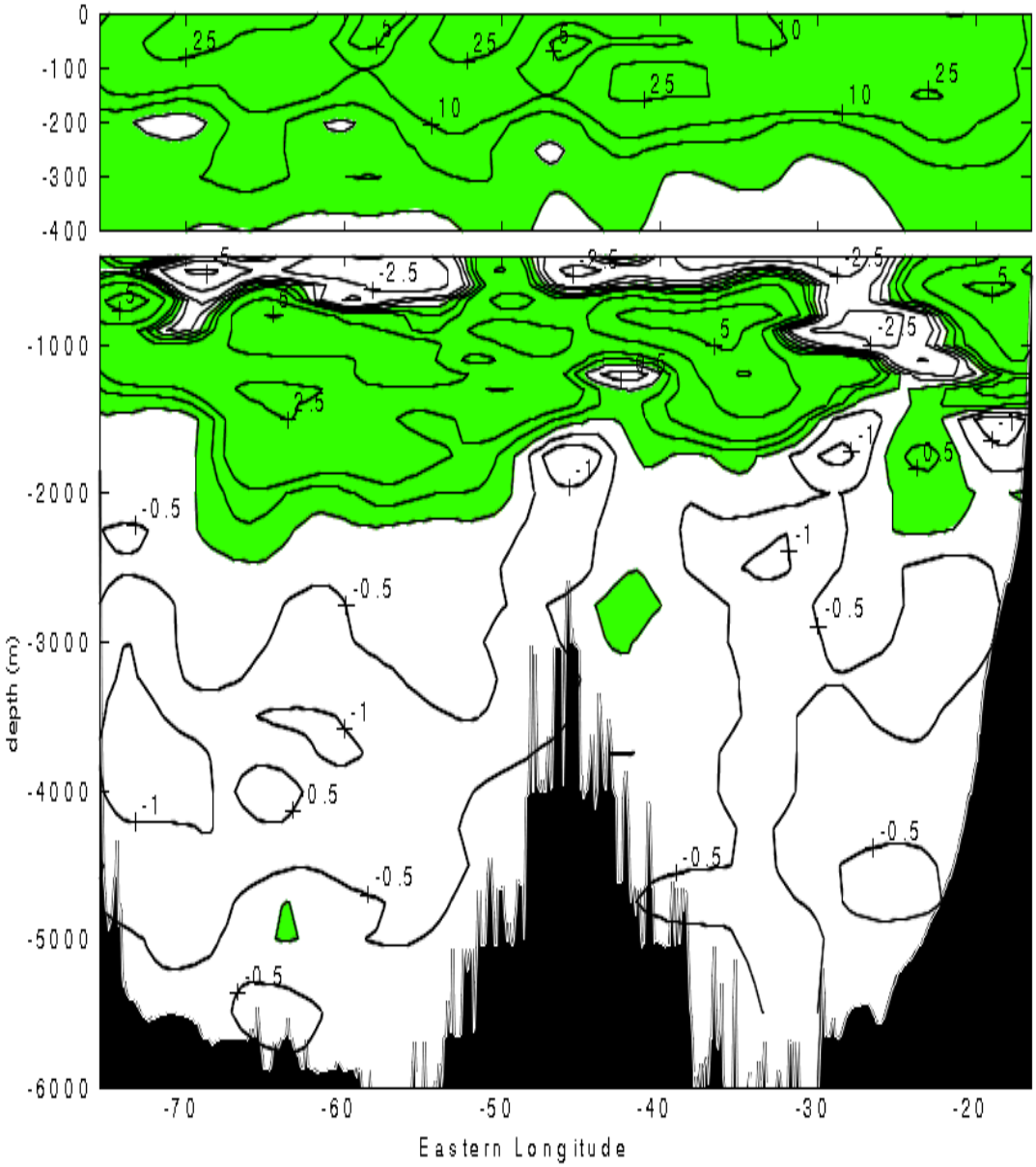

3.2.2 Objective mapping

The technique for the objective mapping is based on a standard statistical result, the Gauss-Markov Theorem, which gives an expression for the minimum variance linear estimate of some physical variable given measurements at a limited number of data points (Bretherton *et al*., 1976). Objective mapping has been used by a number of physical oceanographers, (e.g., Roemmich (1983), Wunsch (1985) and (1989), Fukumori *et al*. (1991)); the basic derivation applied to a hydrographic section will be given. We are dealing with a section of hydrographic stations, in the case of the *Hespérides* cruise 101 stations, located in a set of longitudes $r = r_i$. For each standard depth we have a data series of variables such as temperature, salinity, etc. Let us call them $\{T_i\} = T(r_i)$ where i goes from 1 to the number of stations sampled at that depth.

Because of sloping topography at the boundaries and the Mid-Atlantic Ridge, not all the depths will have 101 values. Below 3000 m, we will have two data series, one for the North American basin and another for the Canary basin. The total number of stations is denoted by N.

In the case that the mean, $<T_i> = 0$, (usually approximation is obtained by removing the sample mean value at each standard depth), the covariance matrix of T at the data point is given by:

$$\{ R_{ij} \} = R(r_i, r_j) = \{< T_i T_j >\} \quad (3.7)$$

where i and j go from 1 to N. The size of this data covariance matrix is an N x N. If T is *spatially stationary* or homogeneous, its second moments depend only on the separation of the evaluation points

$$R_{ij} = R(r_i - r_j) \quad (3.8)$$

The set $\hat{r} = \{\hat{r}_i\}$ contains the points where the values of T_i are required. In this case the points will be from the western coastline (75.5ºW) to the eastern coastline (16ºW) with an interval of 0.5º. The number of interpolated values, M, is 120. The aim is to

estimate the variable value $\hat{T}(\hat{r})$ from observations $S(r_j) = T(r_j) + n(r_j)$ where n is the observational noise, with zero mean and known covariance.

$$< n(r_i) n(r_j) > = N(r_i - r_j) \quad (3.9)$$

Then $R(\hat{r}_k, \hat{r}_i)$ is the covariance matrix of T at the interpolation points with its value at any data point. The field we seek to map has the statistics given by R. Suppose the noise is uncorrelated with the value of T:

$$< T(r_i)\, n(r_j) > = 0 \ \forall \ i, j \quad (3.10)$$

Suppose further, that the interpolated value is a weighted average of the observations:

$$\hat{T}(\hat{r}_k) = \sum_j B(\hat{r}_k, r_j)\, S(r_j) = B(\hat{r}_k)\, S \quad (3.11)$$

where B is an M x N matrix. We then evaluate the variance of the difference between the correct value at $\hat{r}_k$ and the interpolated value

$$P = < (\hat{T}(\hat{r}_k) - T(\hat{r}_k))^2 > = < (B\,S - T(\hat{r}))^2 > \quad (3.12)$$

The Gauss-Markov theorem states that the minimum of this difference is reached when B is chosen as

$$B = R(\hat{r}_k, r_i)[\, R(r_i, r_j) + N(r_i, r_j)\,]^{-1} \quad (3.13)$$

and the minimum possible expected error is,

$$P_{min} = R(\hat{r}_k, \hat{r}_k) - R(\hat{r}_k, r_i)\ [\, R(r_i, r_j) + N(r_i, r_j)\,]^{-1} R^T(r_j, \hat{r}_k) \quad (3.14)$$

where R is the covariance matrix and N the noise matrix.

One of the important uses of the mapping is the determination of a mean value. Let the measurements of a variable, temperature for example, be denoted by y_i and suppose that each is made up of a large-scale mean, m, plus a deviation from that mean of θ_i (Wunsch, 1989), so that we can write

$$m + \theta_i = y_i, i = 1...N \quad (3.15)$$

or

$$\mathrm{D}\,\mathrm{m} + \theta = \mathrm{y}, \mathrm{D}^{\mathrm{T}} = [1,1,..1] \quad (3.16)$$

We seek a best estimate, $\hat{m}$, of m. Suppose an *a priori* estimate of the size of m exists, and is called m_0, i.e. $< m^2 >= m_0^2$. If **R** is the spatial covariance of the measured field about its true mean, the best estimate of the mean (Liebelt, 1967, Eq. 5-26) can be written

$$\begin{aligned} \hat{m} &= [\frac{1}{\mathrm{m}_0^2} + \mathrm{D}^{\mathrm{T}}\,\mathrm{R}^{-1}\,\mathrm{D}]^{-1}\,\mathrm{D}^{\mathrm{T}}\,\mathrm{R}^{-1}\,\mathrm{y} \\ &= \frac{1}{\frac{1}{\mathrm{m}_0^2} + \mathrm{D}^{\mathrm{T}}\,\mathrm{R}^{-1}\,\mathrm{D}}\,\mathrm{D}^{\mathrm{T}}\,\mathrm{R}^{-1}\,\mathrm{y} \end{aligned} \quad (3.17)$$

(**D**$^{\mathrm{T}}$**R**$^{-1}$**D** is a scalar). The expected error of the estimate is

$$\begin{aligned} \mathrm{E} &= (\frac{1}{\mathrm{m}_0^2} + \mathrm{D}^{\mathrm{T}}\,\mathrm{R}^{-1}\,\mathrm{D})^{-1} \\ &= \frac{1}{\frac{1}{\mathrm{m}_0^2} + \mathrm{D}^{\mathrm{T}}\,\mathrm{R}^{-1}\,\mathrm{D}} \end{aligned} \quad (3.18)$$

the goal of the analysis is to retain and separate the large-scale time-averaged features from the time-dependent features and errors.

Objective mapping requires a statement of the expected *a priori* measurement error, and mapped field covariances (Bretherton *et al*., 1976). We must define what is signal and what is noise because the variance of the data contains the signal variance as well as the noise variance. We assume that the noise includes two components: the first component, that we defined n_e is the variation caused by mesoscale eddies; the second one n_i is the variance caused by the local measurement error (including errors due to navigation, interpolation, instrumentation, etc) (Wunsch, 1989). Assuming the component are independent of one another, the total variance $<T_i^2>$, can be written,

$$< T_i^2 > = < s_i^2 > + < n_e^2 > + < n_i^2 > \quad (3.19)$$

where the total variance of the data is given by the sum of the signal variance $<s_i^2>$, the eddy noise variance $<n_e^2>$, and the intrinsic noise variance $<n_i^2>$.

Signal and eddy noise covariances will be modeled by a gaussian covariance function, n_i is modeled by a delta function, n_e, on the other hand, has a finite correlation distance but this distance may be smaller than the correlation distance of the signal we are trying to map.

To estimate the e-folding scale of these distributions, the correlation function R in eq. 3.7 has been calculated. The calculations done for the 1992 cruise are been described. Because of the different station spacing, we have used 3 sets of data: the Canary basin between station 11 and 41; the Mid-Atlantic Ridge between stations 42 and 64 and the North American basin between stations 65 and 96. The distance between stations was 58 km for the Mid-Atlantic Ridge region and 67 km on the other two regions. To estimate the dominant length scales of the eddies we compute the spatial correlation function

$$P(\Delta x) = \frac{< T'(x)\, T'(x+\Delta x) >}{\sqrt{< (T'(x))^2 >< (T'(x+\Delta x))^2 >}} \quad (3.20)$$

where T' are the data values once we have subtracted the linear trend.

We have computed the function for Δx = 0, 58, 67, 116, 134,... km. Figure 3.3A, B and C present the values for depths of 100, 900 and 5000 m. For these plots we can see short scale correlations over the Mid-Atlantic Ridge for the shallower depths (there are no 5000 m depths over the Mid-Atlantic Ridge). The zero-crossing distance is between 75 and 100 km. In deep water, for the eastern basin, this distance is around 150 km, and between 150 and 200 km for the western basin. We have taken a value of 175 km for e-folding distance of the gaussian noise covariance. The scale is perhaps somewhat too large, but it has been chosen to make the plots smoother.

To remove eddies, temperature were filtered with a Gaussian filter with 175 km of e-folding distance. Same as figure 3.3 but with eddy motion filtered out was done for the signal correlation function. Figure 3.4 A, B and C show the signal correlation function for depths of 0, 1200 and 4250 m. We have taken an e-folding scale of 400 km for the signal covariance at all depths.

The zero-lag covariances have been estimated following the method described by Fukumori and Wunsch (1991). Let T_j the data at station j, at a certain depth, with signal s_j, eddy noise n_{ej} and intrinsic noise n_{ij}

$$T_j = s_j + n_{ej} + n_{ij} \quad (3.21)$$

The mean square difference from a neighbouring station *(j+1)* is,

$$\begin{aligned} <(T_j - T_{j+1})^2> &= <(s_j - s_{j+1} + n_{ej} - n_{ej+1} + n_{ij} - n_{ij+1})^2> \\ &= <(s_j - s_{j+1} + n_{ej} - n_{ej+1})^2> + 2<n_i^2> \end{aligned} \quad (3.22)$$

where we have assumed the intrinsic noise is uncorrelated over the distance and has uniform variance. If the signal and the eddy noise have much longer correlation distances than the station separation, it is possible to neglect the first term on the right hand side of eq. (3.22) with respect to the second term which yields

$$<(T_j - T_{j+1})^2> \approx 2<n_i^2> \quad (3.23)$$

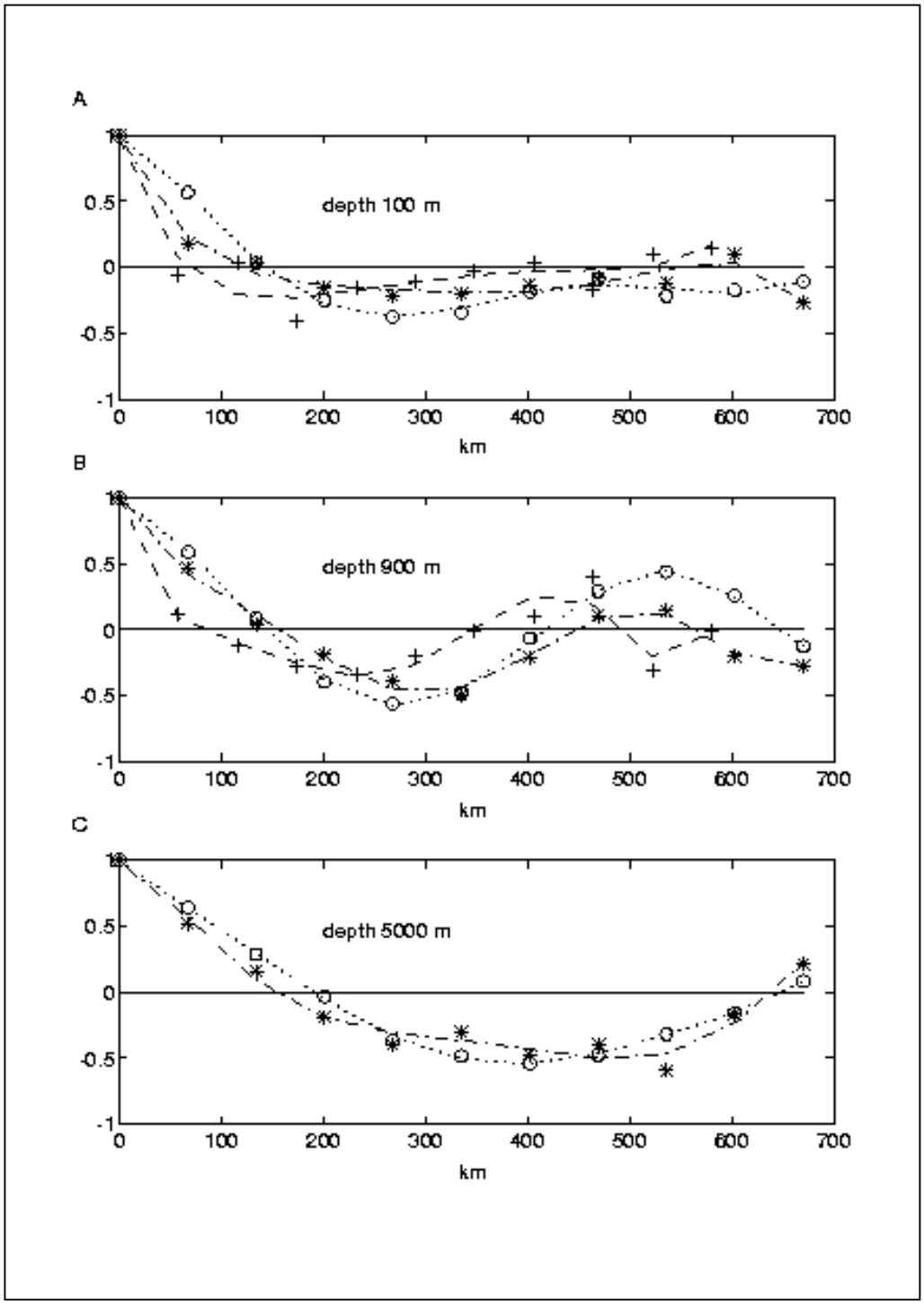

Figure 3.3: Correlation function (equation 3.20) for the North American basin (o), Mid-Atlantic Ridge (+) and Canary basin (✶) for depths A) 100 m, B) 900 m and C) 5000 m.

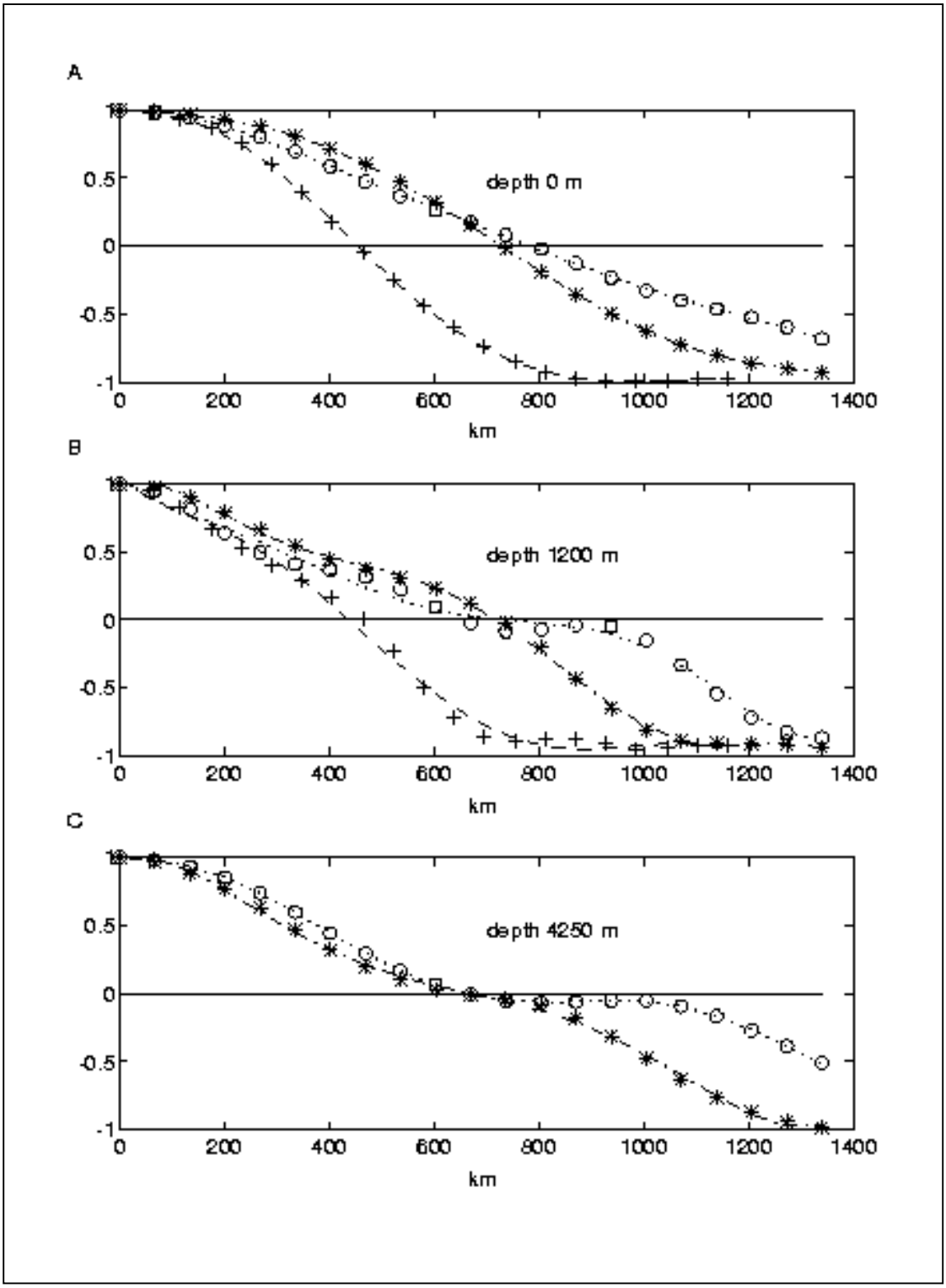

Figure 3.4: Signal correlation function (same as Fig 3.3, but with eddy motion filtered out) for the North American basin (o), Mid-Atlantic Ridge (+) and Canary basin (✶) for depths A) surface, B) 1200 m and C) 4250 m.

In the same way, let $<(T_j-T_k)^2>_L$ denote the mean square difference of data between two points, j and k, separated by L km, then

$$<(T_j - T_k)^2>_L = <(s_j - s_k + n_{ej} - n_{ek} + n_{ij} - n_{ik})^2> \quad (3.24)$$
$$= 2<s^2> -2<s_j\, s_k>_L + 2<n_e^2> -2<n_{ej}\, n_{ek}>_L + 2<n_i^2>$$

If the signal s, has a length scale much longer than L, the second term will be similar to the first and they will partially cancel. Using a distance of 400 km, these two terms cancel. If the eddy noise covariance has a length scale smaller than that distance, then eq. (3.24) will be approximated by

$$<(T_j - T_k)^2>_{400km} = 2<n_e^2> + 2<n_i^2> \quad (3.25)$$

Signal variances have then been calculated then using eq. (3.19)

For computing the expected difference for a spatial separation, we have taken the data set between station 11 and station 96, where the spacing is homogeneous, a separation of 6 stations was used for 400 km. The distance between a station and the neighbouring one is less than 70 km. Due to the different behaviour of the deeper part of the North American and the Canary basins the variance calculations for depths below 2750 m (the depth of the shallowest station in the Mid-Atlantic Ridge) have been computed separately for each basin.

At 900 m the signal variance is smaller than the noise variance. The mapping is practically using the mean temperature value for most of the section. In the Canary basin, values below 4750 are scarce. For the computations of the eddy noise variance we have used a distance of 200 km, and for the intrinsic noise a value of 0.004ºC at 4750 m and 6000 m. On the western basin at 6000 m we have used a value 0.002ºC. These values are slightly higher than the value for instrumental noise of a Mark III CTD given by Millard *et al.* (1990).

The variances used are:

$$<s_i^2> = <T_i^2> - \frac{1}{2}<(T_i - T_j)^2>_{400Km} \quad (3.26)$$

$$< n_e^2 > = \frac{1}{2} < (T_i - T_j)^2 >_{400Km} - < n_i^2 > \quad (3.27)$$

$$< n_i^2 > = \frac{1}{2} < (T_i - T_{i+1})^2 >_{70Km} \quad (3.28)$$

The variance of the temperature signal (s_i^2), eddy noise (n_e^2) and measurement noise (n_i^2) are summarised in Table 3.1 at the standard depths for all the North Atlantic basin shallower than 2750 m, Table 3.2 below 3000 m for the North American basin and Table 3.3 below 3000 m for the Canary basin.

The variance of the salinity signal (s_i^2), eddy noise (n_e^2) and measurement noise (n_i^2) are summarised in Table 3.4 at the standard depths for all the North Atlantic basin shallower than 2750 m., Table 3.5 below 3000 m for the North American basin and Table 3.6 below 3000 m for the Canary basin.

Since the distance (r_i - r_j) in our covariance functions is given in longitude, we have used 4º and 1.75º, which is equivalent to 400 and 175 km (at this latitude 1º x 60' x cos(24.5) = 101 km). Then the covariances are:

$$R(r_i - r_j) = < s_i^2 > \exp(-(r_i - r_j)^2 / 4^2) \quad (3.29)$$

$$N_e(r_i - r_j) = < n_e^2 > \exp(-(r_i - r_j)^2 / 1.75^2) \quad (3.30)$$

$$N_i(r_i - r_j) = < n_i^2 > \delta(r_i - r_j) \quad (3.31)$$

Behaviour of the mapping function on the boundaries

As one approaches the boundaries, not all data point are available and the mapping function weighted interpolant (**B**), given by eq. (3.13), becomes one sided. The mapping function reduces the variability of the data, errors increase and the expected value tends to the mean.

depth	s_i	n_e	n_i
0	2.41	0.33	0.17
50	1.94	0.81	0.64
100	1.54	0.73	0.65
150	1.10	0.69	0.71
200	1.04	0.44	0.47
250	1.15	0.29	0.30
300	1.34	0.23	0.25
400	1.59	0.29	0.24
500	1.50	0.35	0.24
600	1.17	0.33	0.24
700	0.85	0.33	0.24
800	0.50	0.28	0.23
900	0.19	0.24	0.19
1000	0.22	0.15	0.16
1100	0.36	0.10	0.23
1200	0.45	0.10	0.21
1300	0.46	0.11	0.14
1400	0.43	0.10	0.12
1500	0.37	0.08	0.11
1750	0.22	0.06	0.06
2000	0.13	0.05	0.05
2250	0.09	0.04	0.04
2500	0.06	0.03	0.03
2750	0.03	0.02	0.03

Table 3.1: Signal (s_i^2), eddy noise (n_e^2) and measurement noise (n_i^2) square root variances for mapping temperature data at the indicated depth at 24.5ºN for all the North Atlantic basin shallow than 2750 m. Data are given in ºC.

depth	s_i	n_e	n_i
3000	2.57	1.31	2.97
3250	3.42	1.55	2.62
3500	3.59	1.90	2.68
3750	1.56	1.53	1.96
4000	2.70	1.70	1.56
4250	3.65	2.39	1.74
4500	4.92	3.31	1.69
4750	5.48	4.48	1.87
5000	6.15	7.15	2.96
5500	5.62	6.20	3.75
6000	1.17	0.11	0.20

Table 3.2: Signal (s_i^2), eddy noise (n_e^2) and measurement noise (n_i^2) square root variances for mapping temperature data below 3000 m at 24.5ºN for the North American basin. Data are given in ºC x $10^{-2.}$

depth	s_i	n_e	n_i
3000	1.24	1.55	1.57
3250	1.10	1.60	1.00
3500	2.31	0.96	0.99
3750	2.51	1.15	1.16
4000	2.22	0.96	1.04
4250	0.98	1.42	1.04
4500	1.70	0.27	0.59
4750	0.49	0.13	0.40
5000	1.17	0.72	0.53
5500	1.22	1.38	0.78
6000	0.67	0.37	0.40

Table 3.3: Signal (s_i^2), eddy noise (n_e^2) and measurement noise (n_i^2) square root variances for mapping temperature data below 3000 m at 24.5ºN for the Canary basin. Data are given in ºC x $10^{-2.}$

depth	s_i	n_e	n_i
0	4.21	1.93	1.24
50	3.36	1.18	0.99
100	2.10	0.90	1.11
150	1.12	0.73	1.31
200	0.93	0.46	0.81
250	1.47	0.39	0.56
300	1.96	0.33	0.44
400	2.40	0.43	0.38
500	2.09	0.49	0.36
600	1.42	0.42	0.35
700	0.91	0.42	0.34
800	0.49	0.34	0.34
900	0.36	0.29	0.25
1000	0.42	0.22	0.24
1100	0.50	0.20	0.50
1200	0.59	0.18	0.39
1300	0.60	0.19	0.25
1400	0.59	0.19	0.22
1500	0.51	0.17	0.19
1750	0.35	0.12	0.10
2000	0.22	0.07	0.06
2250	0.15	0.04	0.04
2500	0.10	0.03	0.03
2750	0.06	0.02	0.02

Table 3.4: Signal (s_i^2), eddy noise (n_e^2) and measurement noise (n_i^2) square root variances for mapping salinity data at the indicated depth at 24.5ºN for all the North Atlantic basin shallow than 2750 m. Data are given x 10^{-1}.

depth	s_i	n_e	n_i
3000	1.71	1.91	2.14
3250	1.32	1.93	1.89
3500	2.29	2.25	2.08
3750	3.21	2.42	1.98
4000	5.29	3.19	1.66
4250	6.19	4.06	2.41
4500	7.61	5.20	2.21
4750	8.35	5.72	2.45
5000	7.77	8.51	3.62
5500	6.76	7.50	4.79
6000	1.58	0.41	0.91

Table 3.5: Signal (s_i^2), eddy noise (n_e^2) and measurement noise (n_i^2) square root variances for mapping salinity data at the indicated depth at 24.5ºN below 3000 m for the North American basin. Data are given x 10^{-3}.

depth	s_i	n_e	n_i
3000	2.28	1.18	1.57
3250	0.70	1.57	1.08
3500	1.25	0.84	0.87
3750	1.73	1.23	1.30
4000	1.23	1.11	1.00
4250	0.49	1.28	0.99
4500	1.28	0.57	0.78
4750	0.47	0.34	0.57
5000	0.98	1.05	0.63
5500	1.22	1.61	0.76
6000	0.39	0.51	0.85

Table 3.6: Signal (s_i^2), eddy noise (n_e^2) and measurement noise (n_i^2) square root variances for mapping salinity data at the indicated depth at 24.5ºN below 3000 m for the Canary basin. Data are given x 10^{-3}

Figure 3.5 presents values of raw data and mapped data with its error at 5000 m depth in the North American and Canary basins. It is possible to see the different behaviour of the temperature in both basins and the associated error. The uncertainty is around 0.04ºC in the North American basin and only about 0.005ºC in the Canary basin. Errors are slightly increased near the boundaries. In this case the mapped values are practically within the sampled area. Near the boundaries of the basins where there are some gaps due to the irregular topography, we have mapped values outside the sampled area.

A

B

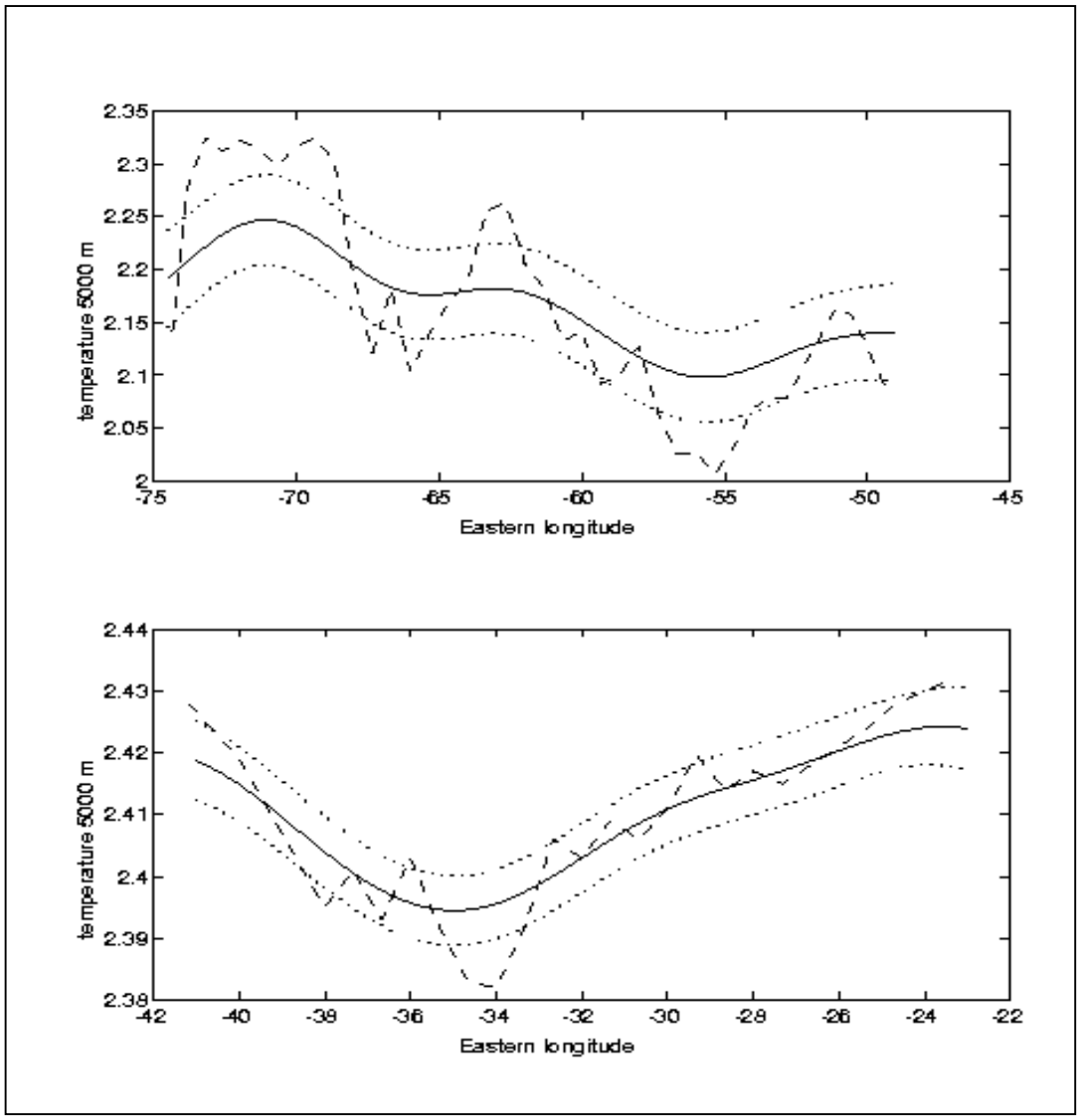

Figure 3.5: 1992 cruise Temperature (ºC) at 5000 m depth, raw data (dashed), mapping data (solid) plus/minus the error in the mapping (dotted) for A) North American basin and B) Canary basin.

The mapping values of temperature for the 1992 cruise are presented in figure 3.6. The expected error in the temperature mapping (Bretherton *et al*., 1976) as a function of depth is shown on the right side. Below 3000 m, the error is given separately for the North American and Canary basins. These errors have been computed by the square root of the diagonal of $\mathbf{P}_{\mathbf{min}}$ in eq. (3.14). The highest values appear at 50 m, where the highest eddy noise variance was found (Table 3.1). Between this depth and the middle of the thermocline (~850 m), the error decreases to 0.2ºC. Below 2000 m, the expected error is less than 0.05ºC, for all the cruises. Errors in the Canary basin are less than 0.02ºC while in the North American one they are between 0.01 and 0.04ºC with the highest values appearing between 5000 and 5500 m.

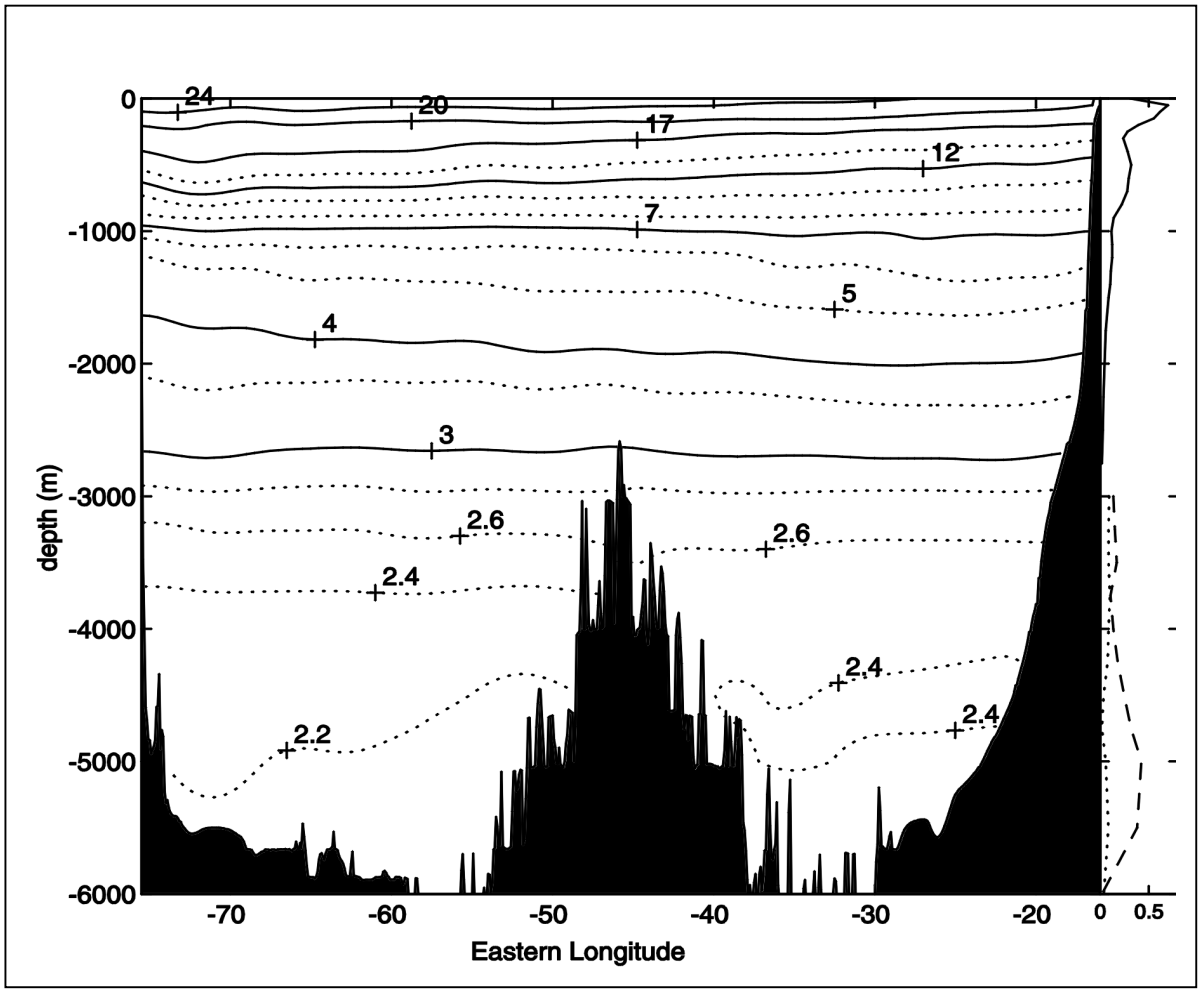

Figure 3.6: 1992 Temperature (ºC) section using objective mapping. The expected error in the temperature mapping in function of depth is shown on the right side. Below 3000 m, the error is given separately for the Canary (dotted) and North American (dashed) basins and values are multiplied by 10. Expected errors are inºC.

Salinity mapping has been done in the same way as the temperature mapping. Figure 3.7 presents salinity mapping for the 1992 cruise including the expected error for this mapping. Expected errors in salinity are largest at the surface and reduce with depth.

Calculations of covariances and mapping were performed for 1981 and 1957 datasets in a manner similar to that described for 1992 dataset. After interpolation to a common grid, the difference for the three cruises has been calculated for the same zonal extent as used for spline interpolation. Figure 3.8A presents the temperature difference between the 1981-1957 cruises. Figures 3.8B and 3.8C give the temperature differences from 1992-1981 and 1992 and 1957. The expected error of the differences is the sum of the expected errors of the mapping values for each map. The values of $\mathbf{P}_{\mathbf{min}}$ in eq. (3.14) has been added for each set of data and the square root of the diagonal has been calculated. On

the right side of the figures the expected error in function of depth is presented. Figure 3.9A, B and C present the difference in salinities for 1981-1957, 1992-1981 and 1992-1957. Expected errors were calculated in the same way as for temperature.

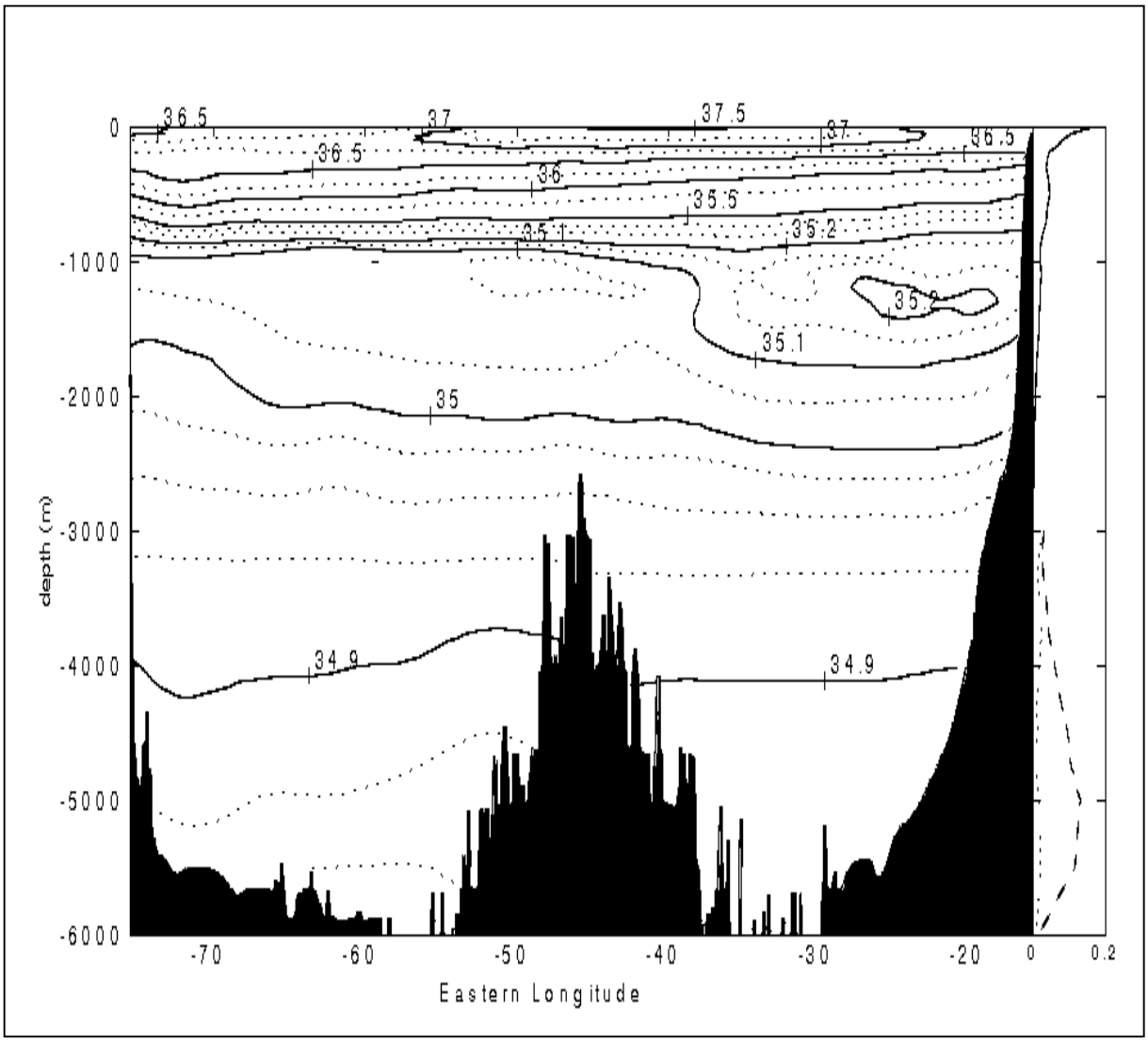

Figure 3.7: Salinity section for the 1992 cruise using objective mapping. The expected error in salinity mapping in function of depth is shown on the right side. Below 3000 m, the error is given separately for the Canary (dotted) and North American (dashed) basins. Values are multiplied by 25.

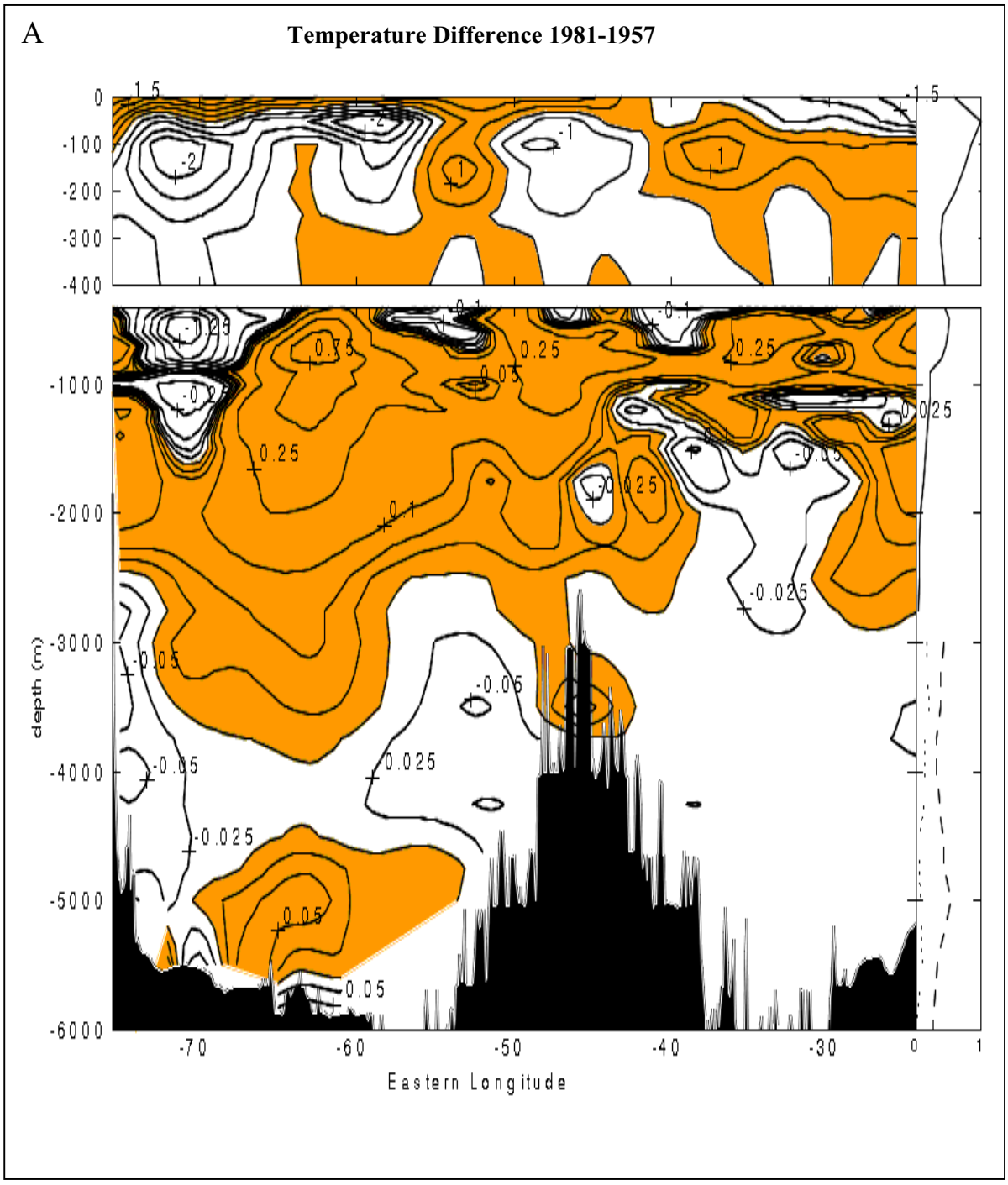

Figure 3.8: Difference of temperature (ºC) by objective mapping, A) 1981-1957, B) 1992-1981 and C) 1992-1957. The expected error in the temperature difference in function of depth is shown in the right side. Below 3000 m, the error is given separately for the Canary (dotted) and North American (dashed) basins. Values are multiplied by 10. Expected errors are in ºC. Shading in colour indicates positive difference. The top plot has expanded vertical scale.

B

Temperature Difference 1992-1981

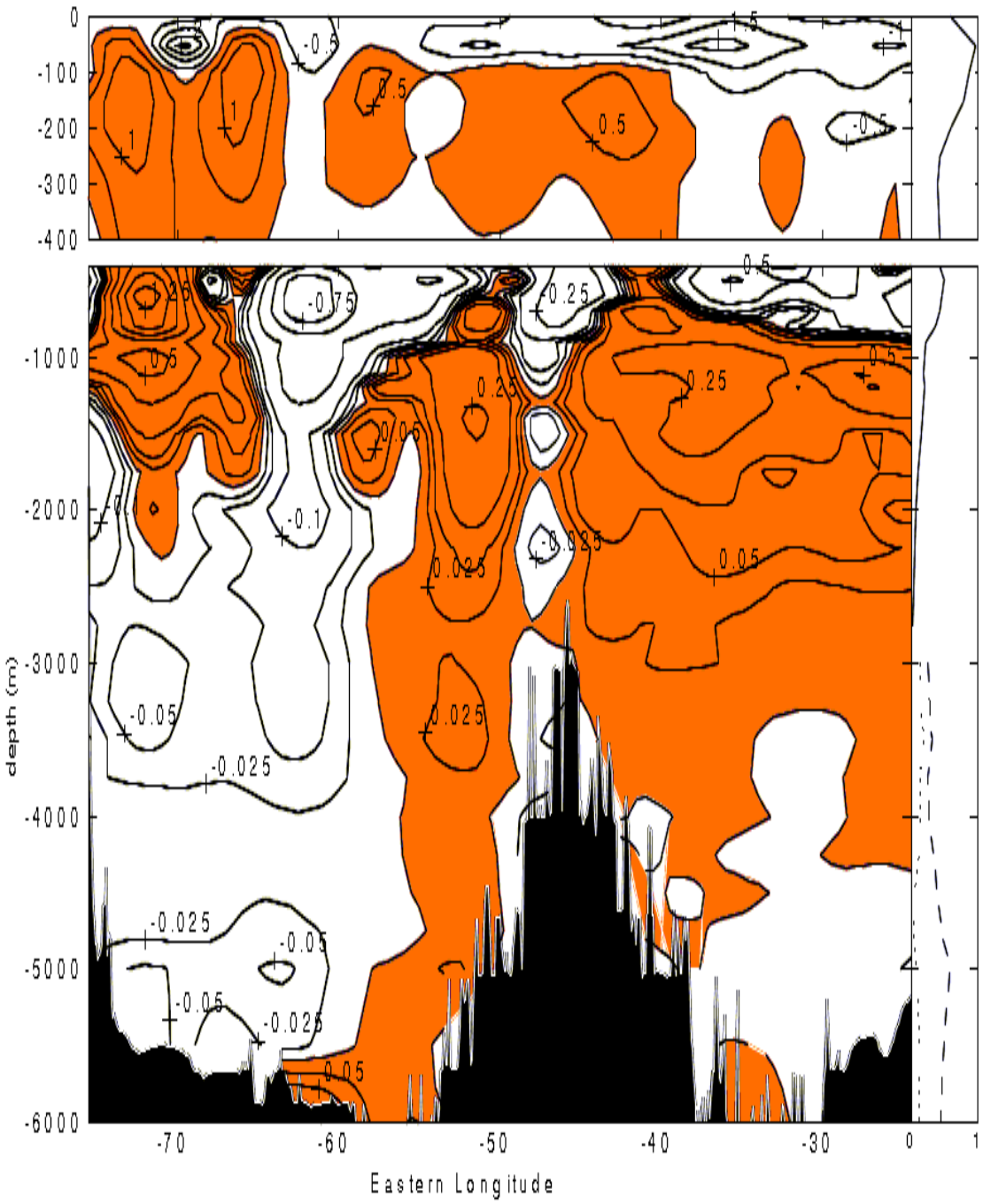

C

Temperature Difference 1992-1957

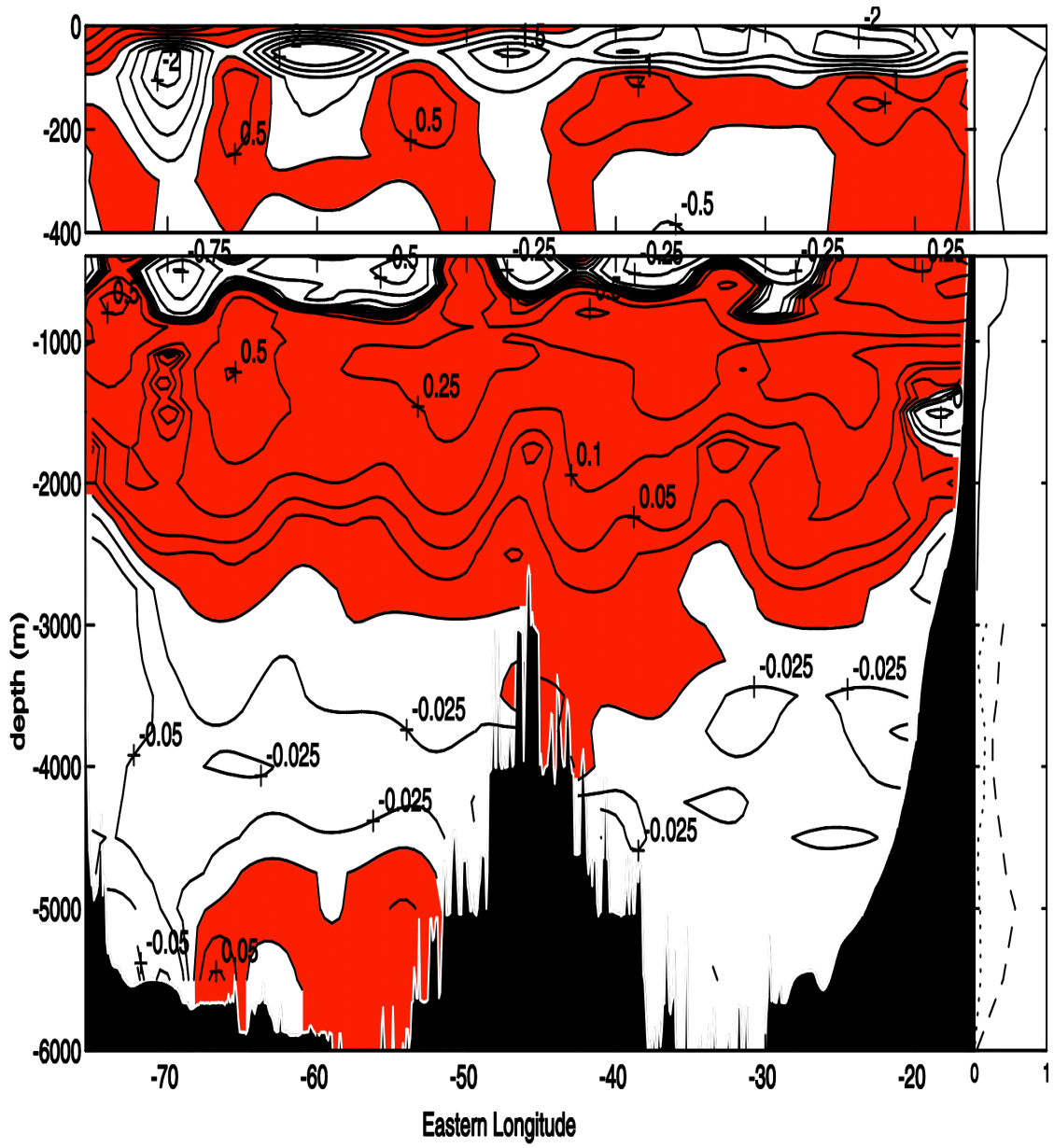

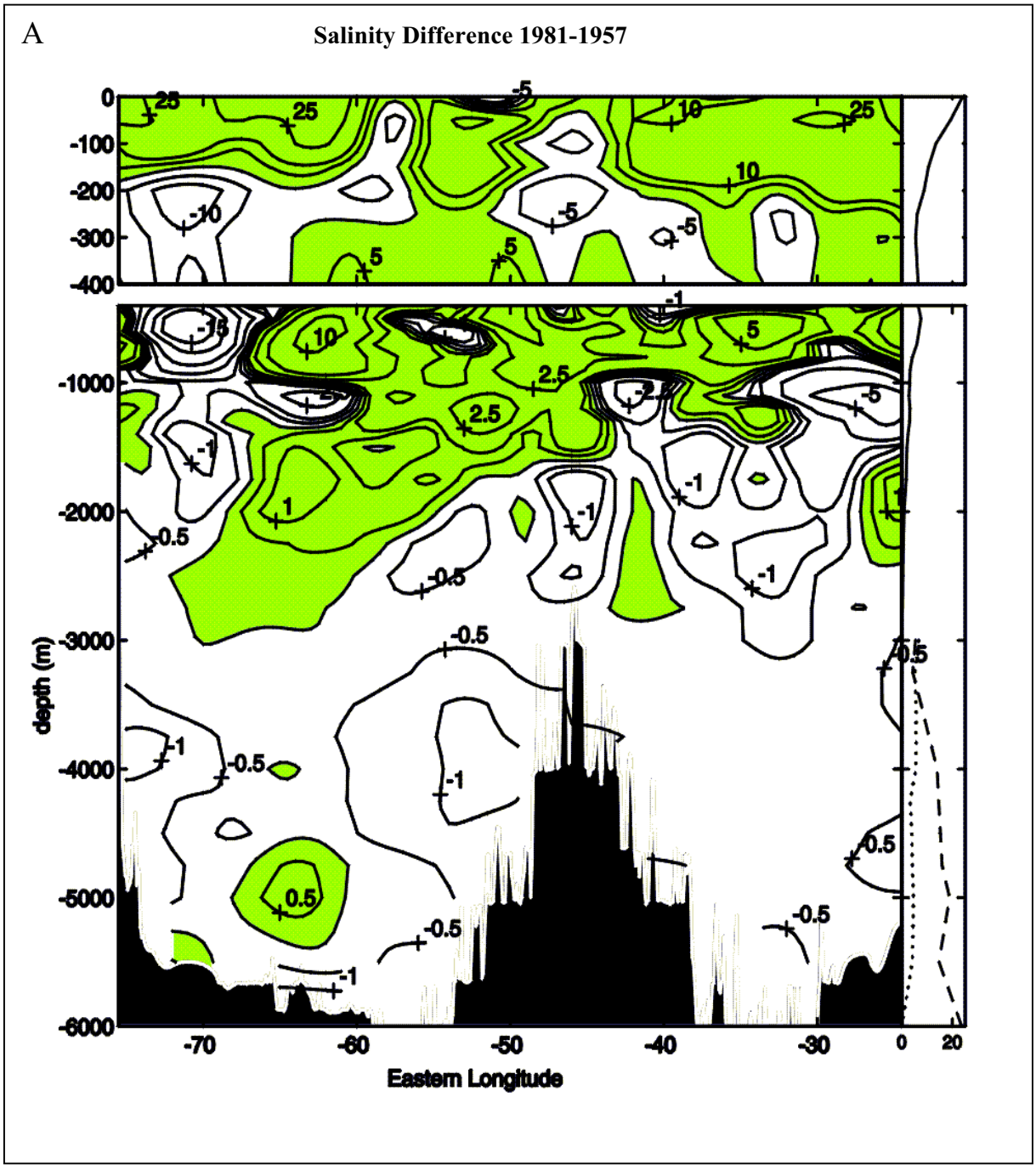

Figure 3.9: Difference of salinity (multiplied by 100) by objective mapping, A) 1981-1957, B) 1992-1981 and C) 1992-1957. The expected error in salinity difference in function of depth is shown in the right side. Below 3000 m, the error is given separated for the Canary (dotted) and North American (dashed) basins. Values are multiplied by 25. Shading in colour indicates positive differences. The top plot has expanded vertical scale.

B

Salinity Difference 1992-1981

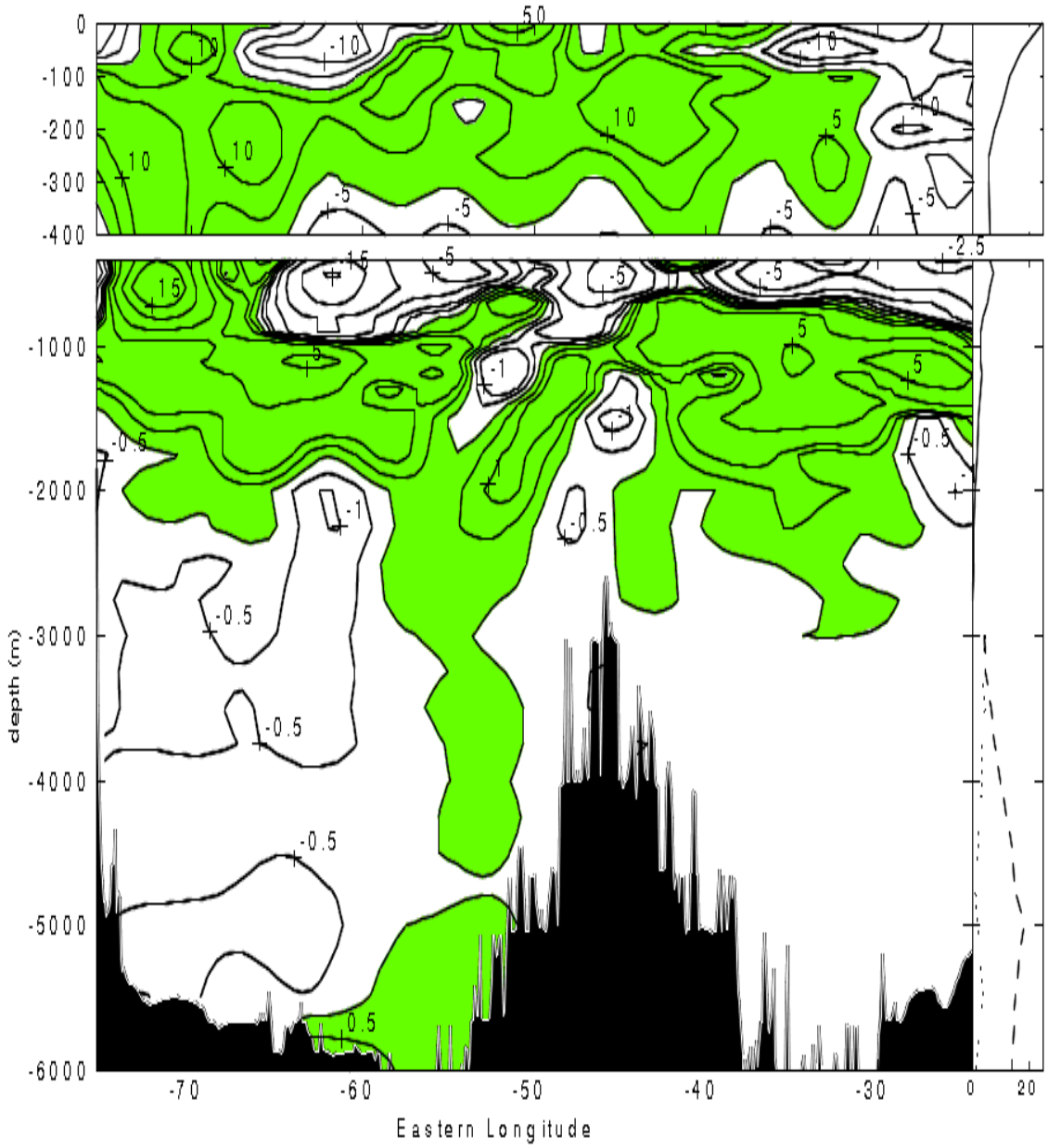

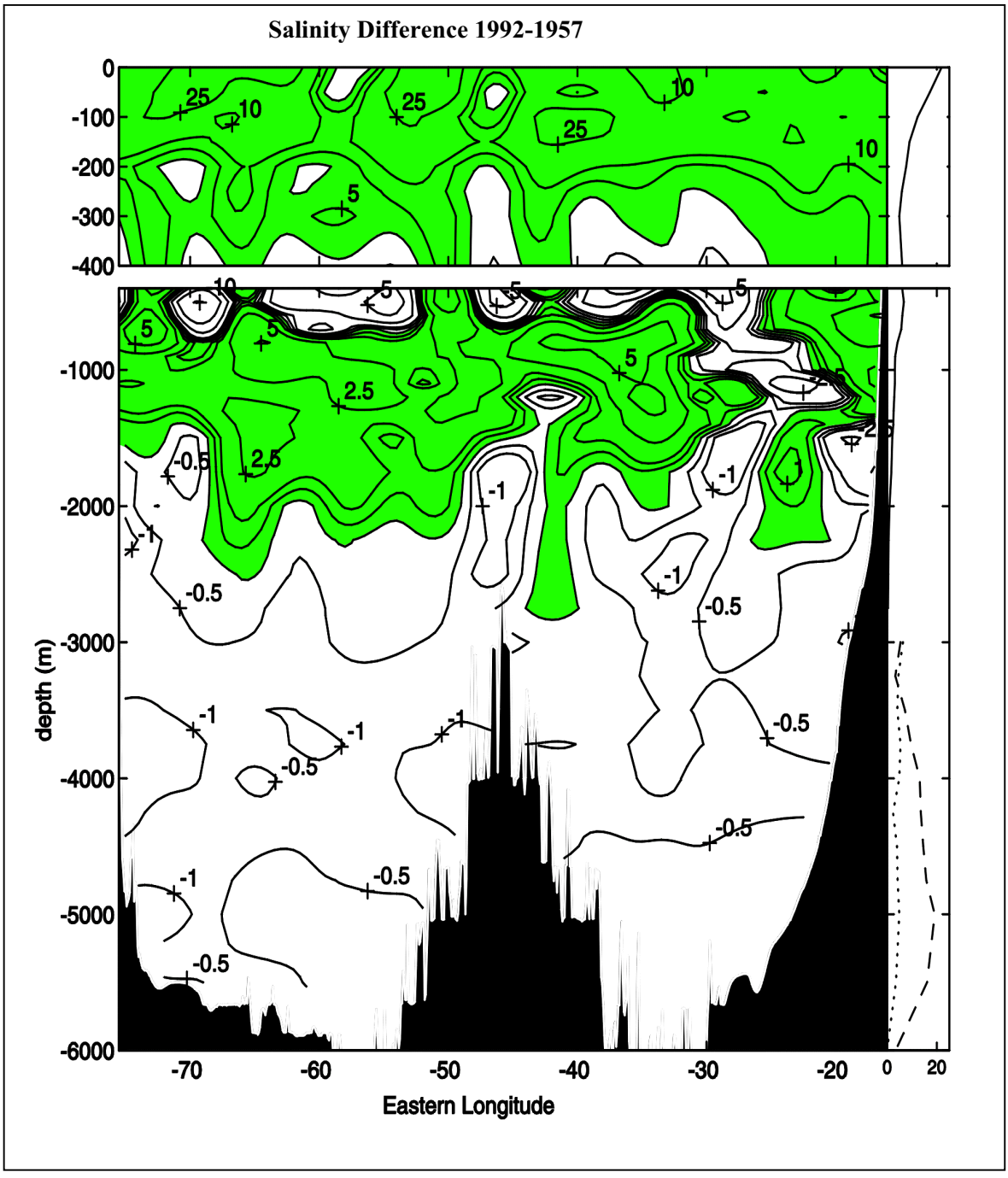
Salinity Difference 1992-1957
depth (m)
Eastern Longitude
0
-100
-200
-300
-400
-1000
-2000
-3000
-4000
-5000
-6000
-70
-60
-50
-40
-30
-20
0
20
25
10
5
2.5
-0.5
-1

3.2.3 Discussion

The use of cubic spline interpolation and objective mapping to interpolate the data to a regular grid has been compared. The most significant differences between the two methodologies are that the spline interpolation with the gaussian filter gives a large scale vision of the features, smoothes over the small scale features, and reduces the maximum values in most of the cases.

The behaviour of the gaussian filter on the boundary data is to smooth these values and tends to reduce the differences in this region. The objective mapping also smoothes the values and reduces the differences in the boundaries, but to a lesser extent; so that the objective mapping slightly increases differences relative to the gaussian filter. This effect can be seen in the eastern boundary 1992-1957 difference (Fig. 3.1C and Fig. 3.8C). In the North American basin, most of these effects are found on the two boundaries (Continental shelf and Mid-Atlantic Ridge) and at the bottom of the basin. Even when we are looking at the large scale effects, it is convenient to maintain these boundary differences.

Due to the behaviour of polynomial functions, when the fitting has to be extended outside the sampled area, values calculated by splines change very quickly. In these regions, values given by objective mapping are more realistic than values given by spline interpolation.

There is a high degree of similarity among cubic spline smoothing with a gaussian filter and objective mapping methods using the convenient parameters. The discrepancies are within the expected error in all regions except the boundaries.

Advantages of using cubic spline

- fast and easy to use, needing no complicated mathematical machinery, not much computer memory.
- there exist well-tested routines in software, i.e., in packaged form.
- not requirement for *a priori* knowledge about the data or the measurement error.
- gives the real value on the sampled locations

- the results are reasonable, discrepancies are within the expected error, in this application.

Disadvantages of using cubic spline

- there is no estimate of uncertainties

Advantages of using objective mapping

- extrapolated values near the continental slopes or the bottom topography are better determined.
- the expected error is explicitly given by the method in the form of an error map.

In this case, when we are attempting to perform data comparison, the error maps are a fundamental requirement. Without estimates of expected errors, we cannot recognise whether or not the differences are significant.

Disadvantages of using objective mapping

- It requires much work and computing time, matrices are usually big and inversion demands large computer memory
- It requires previous knowledge of the covariance functions or assumptions for the correlation matrices.
- not available in packaged form. One must build it up from the start.

The possibility of calculating expected errors has made objective mapping the most suitable method of interpretation for this analysis.

3.3 Differences in temperature and salinity

In this section we will describe the features found in the comparison of data carried out by the objective mapping techniques shown previously

3.3.1 Temperature differences

- 1981-1957 (Fig. 3.8A)

This comparison was already done by Roemmich and Wunsch (1984). Their comparison had revealed that the ocean waters along 24.5ºN had warmed appreciably down to 3000 m depth and had cooled below it over the 24-yr period. Differences in temperature using the same dataset have been calculated here and obtained similar results. Small differences could be due to the selected parameters for the objective mapping as spacing and covariances.

The most notable feature has been a large warming mainly in the North American basin between 55ºW and 68ºW. Although this feature was the most relevant. All the main differences beginning with the surface water and continuing down through to the water column will be described.

At the surface, there are positive differences in a very thin layer west of 40ºW and negative differences east of that longitude. Between this layer and 500 m negative differences are found in the whole area except in the Canary basin. There is also an area of large cooling in the western part of the North American basin, centred around 70ºW, between 100 and 1500 m. Differences are as large as -2ºC at 150 m and -1.25ºC at 600 m. East of 60ºW there is a cooler layer between 200 and 600 m and a warmer one below it.

In the North American basin, there is a large warming between 55ºW and 68ºW. Warming penetrates deeply down to 4000 m and dominates the zonal average temperature change. Maximum positive difference is centred at 62ºW, with values of 0.75ºC between 700 and 800 m. Warming also affects the Canary basin between 700 and 2500 m. The highest positive differences in this area are about 0.5ºC between 800 and 900 m. Below

2500 m on both sides of the North American basin, and below 4000 m on the central portion, water has cooled, with slightly larger cooling along the western boundary. In the central part of the Canary basin negative differences are found below 1500 m.

The values of the differences are of the same order of magnitude as the uncertainty in the measurements. Trying to justify that the differences are statistically significant, we have plotted (Fig. 3.10) the temperature correlation, function B in eq. (3.13) for a point situated at 50ºW for 500, 1200 and 5000 m depth (the last one in both basins). The horizontal correlation scale is around 5 longitude degrees. The scale of most of the features discussed above is larger than this value. Since the calculations have been done independently for each standard depth, features are not artificially correlated at each depth. These two factors increase the reliability of the calculated differences.

- 1992-1981 (Fig 3.8B)

The substantial area of warming in the central North American basin during 1981-1957 cooled between 1981 and 1992. So that the area of Roemmich and Wunsch (1984) of large warming is now a large cooling region. Similarly, the area of substantial cooling during 1981-1957 centred at about 70ºW, has now warmed. Thus, there appears to be an oscillation in temperature with a zonal half-wavelength of about 1000 km. The Canary basin warmed considerably down to 4000 m.

The surface layer down to 50 m cooled. Below this layer, the differences are positive down to 300 m west of 40ºW; this warming trend reaches 2000 m in the western part of the North American basin.

Colder water appears between 400 and 800 m across the entire section. Differences achieve a peak value of -0.75ºC at 61ºW. This is where Roemmich and Wunsch (1984) found warming. Below 800 m, there is generally a warming trend with differences larger than 0.5ºC around 1000 m. The warmer water reaches 4000 m in the Canary basin and the bottom on the eastern part of the North American basin. In the rest of the North American basin differences are negative below 2000 m and below 4000 m in the eastern part. In the western boundary, cooling occurs between 1500 and 2000 m. Below that depth, the cooling presented in the previous period reduce in a large extent.

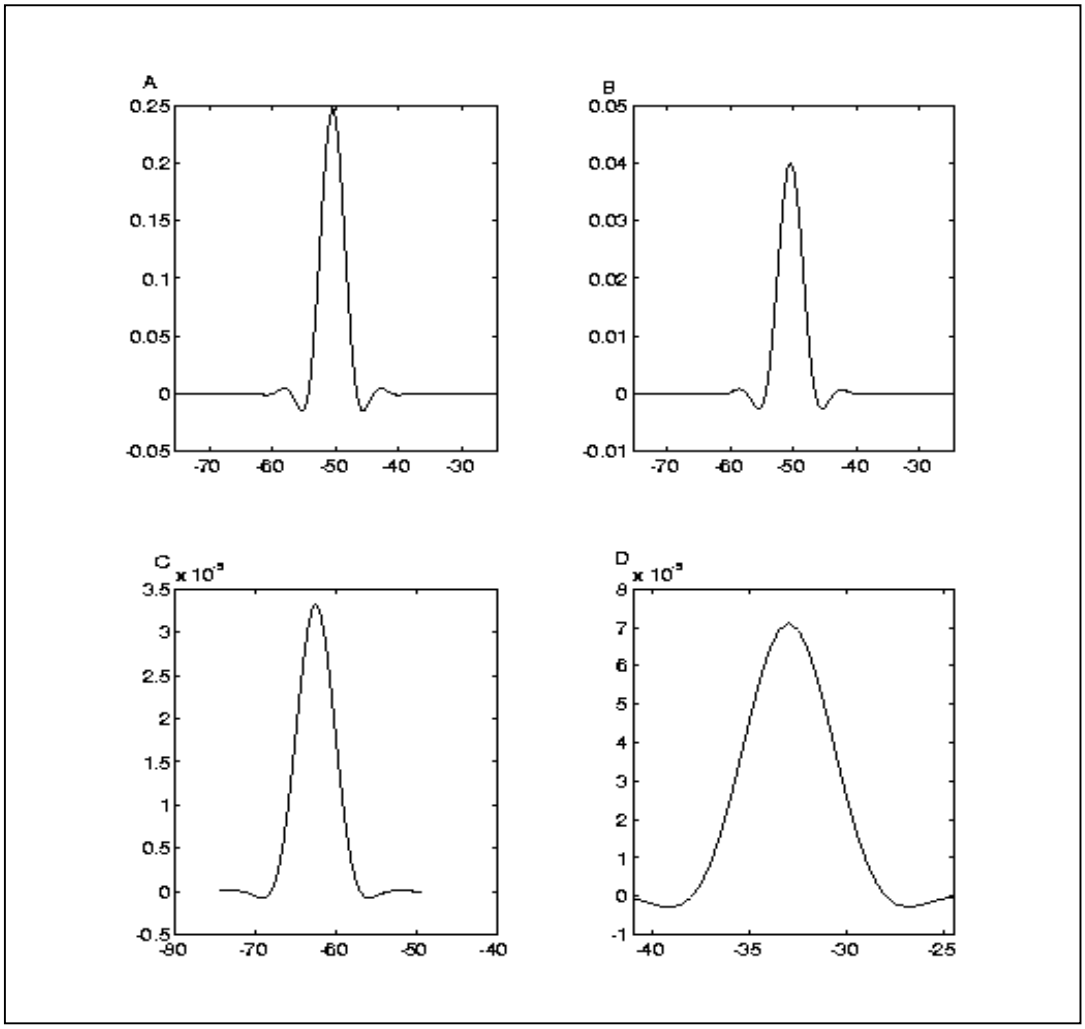

Figure 3.10: Correlation function versus longitude for temperature (ºC) of a point situated at 50ºW for A) 500 m, B) 1200 m, C) 5000 m in the North American basin and D) 5000 m in the Canary basin.

- 1992-1957 (Fig 3.8 C)

A remarkable regular warming occurred between 700 and 3000 m from 1957 to 1992. The contours of temperature differences are nearly horizontal across most of the section. Both the North American and Canary basins have warmed by about the same amount. Peak values are larger than 0.5ºC at around 1000 m.

The surface layer is warmer between 0 and 50 m in the North American basin. Negative differences occur above 100 m, in the North American basin below the warmer

surface layer. This feature may result from seasonal variability, (measurements were done in July-August 1992 and during October 1957). Seasonal variations in this area principally affect depths shallower than 100 m. Negative differences are deepening to 900 m in the western part of the North American basin. While the Canary basin presents two well defined layers one colder and one warmer above 200 m, the North American basin has alternating cold and warm rings in longitude. The negative ones are located at 46º, 60º and 70ºW.

There is a large area of negative temperature difference centred around 500 m. Peak values are between -0.75ºC and -0.5ºC in the North American basin and -0.5ºC in the Canary basin. Those values are significantly higher than the uncertainty at this depth.

Near the western boundary region, below 2000 m, negative differences greater than -0.05ºC appear west of 70ºW. The negative differences extend all over the North American basin between 3000 and 5000 m. Most of these values are statistically significant. (Note that the error values on the temperature plots are multiplied by 10 below 3000 m.)

The deep Canary basin also has cooled from 1957 to 1992. The cooling is stronger around 4000 m, and at the eastern boundary. The uncertainty is less than 0.01ºC for most of the values in this basin. The differences are statistically significant. At the eastern boundary, between 1300 and 1800 m an area of cooling appears. This area is situated just below the northward eastern boundary current cited by Roemmich and Wunsch (1985). They interpreted this current as the eastern flow of Antarctic Intermediate Water in the tropics, which feeds an eastern boundary current flowing into the Mediterranean salt tongue.

3.3.2 Salinity differences

Salinity in the 1957 cruise was measured by water samples, and data have been interpolated to standard depths throughout the water column. All values are in the Practical Salinity Scale.

- 1981-1957 (Fig. 3.9A)

Saltier water was found on the area of warming noticed by Roemmich and Wunsch (1984). Salinity differences are positive all over the section from the surface to 200 m depth, and generally negative in a band between 200 and 500 m. Deeper than 500 m, as for temperature, there is substantial zonal variability. The western part of the section shows negative values to the bottom, with differences as large as -0.15 between 500 and 700 m. Positive differences are found between 300 and 3000 m in the central part but only down to 2000 m in the eastern part of the North American basin. In the Canary basin, freshening is found between 1000 and 1500 m and near the bottom. At 4000 m depth, water becomes fresher at both boundaries of the North American basin. Around 5000 m in the central part of the North American basin, water appears saltier than in the previous cruise. Differences are significant over most of the basin, except for the deep water in the North American basin. Even when the uncertainty given by the mapping is very small, as in the Canary basin, problems with the salinity determination from the batches of Standard Sea Water prevent the plotting of smaller salinity differences.

- 1992-1981 (Fig. 3.9B)

Salinity differences present a zonal distribution similar to that of temperature except near the surface where the difference is positive. Positive differences are found between 50 and 350 m, and negative (fresher water) from 350 m until 800 m. The water is saltier between 800 m and about 2500 m for all of the section. This saltier water reaches the bottom over the western part of the Mid-Atlantic Ridge with an interruption around 5000 m. The rest of the deep regions appears to be fresher. This freshening is strongest around 3000 and 5000 m in the central and western parts of the North American basin.

- 1992-1957 (Fig. 3.9 C)

The most important feature is the increase in salinity occurring between 600 and 2500 m, with maximum values of 0.05. The salinity gives generally positive differences above 300 m. Differences are predominantly negative between 300 and 600 m with values as high as -0.1 in the western part and -0.05 for the remainder except near the eastern boundary where the differences are positive down to 1400 m depth.

Below 2000 m the differences are negative, peak values are found at 4000 m, at the western boundary and over the Mid-Atlantic Ridge. In those areas the freshening is shallower than in other locations. In the Canary basin the least freshening occurs around 4000 m. Below 4250 m there is a significant freshening to the bottom, with differences larger than 0.005. Note again possible problems with biases due to standard water.

3.3.3 Zonal averages

The technique for determination of a mean value by objective mapping was used to determine the average of the temperature and salinity differences at each standard depth. For this calculation we assume that the error in the mapping of two different cruises is uncorrelated one with the other. The covariance functions of the cruises are $\mathbf{R_{\theta\theta}}$ and $\mathbf{R_{rr}}$ respectively. These covariance was calculated using eq. (3.7). The spatial covariance function, **R**, of the difference of the two mapping will be the sum of the covariance functions of each of them,

$$R = R_{\theta\theta} + R_{rr} \qquad (3.32)$$

We have estimated the zonal average of the differences by $\hat{m}$ in eq. (3.17) and the expected error of the mean by taking the square root of **E** in eq. (3.18) for each standard depth.

Since we have no previous hypothesis about the mean difference, we take the limit $m_o \to \infty$ in equations (3.17) and (3.18). The calculated values are presented in the next section

3.3.3.1 Temperature

In figure 3.11 the zonal average temperature ± error estimate is presented for the three differences A) 1981-1957, B) 1992-1981 and C) 1992-1957 from surface down to 3000 m (upper plot), and for the North American and Canary basins deeper than that depth (down right and left plots).

- 1981-1957 (Fig. 3.11A)

As noted by Roemmich and Wunsch (1984) the average warming begins at 400 m, and all values are significantly warmer between 600 and 2500 m, with a peak value of 0.22±0.11ºC at 800 m. In the North American basin waters were significantly cooler between 3750 and 4500 m, with values around -0.025ºC. In the Canary basin, cooling occurred all over the deep basin. Values are statistically significant below 3750 m. At 6000 m values in the 1957 dataset were scarce, particularly in the Canary basin.

- 1992-1981 (Fig. 3.11B)

The zonal average values above 800 m have opposite signs from the results obtained from the previous period. Significant cooling occurs between 500 and 600 m with values around -0.20ºC. Continuous warming between 900 and 2750 m is statistically significant between 1000 m and 1750 m with a peak value of 0.16±0.05 between 1000 and 1100 m depth. Below 3000 m, in the North American basin there is cooling above 5500 m, which is statistically significant between 3000 and 4250 m, with values ranging from -0.025ºC to -0.013ºC. At 6000 m there appears to be a significant warming, but at this depth values are scarce and calculation of variances for the mapping are also problematic producing poor statistics. In the Canary basin, warming occurred above 3250 m. Very small and statistically insignificant changes appear below this depth.

- 1992-1957 (Fig. 3.11C)

Positive values are found for zonal averages between 600 and 2750 m and between 200 and 400 m. Cooling occurred between 400 and 500 m and below 2750 m. The warming is significant between 700 m and 2500 m depths. Values are greater than 0.2ºC between 800 and 1400 m. The peak value is 0.28±0.05ºC at 1000 m. In the North American basin significant cooling occurs between 3250 and 5500 m, with a maximum difference of -0.03ºC at 4250 m. In the Canary basin, cooling is significant in waters below 3500 m, with a peak difference of -0.02ºC at 4250 m.

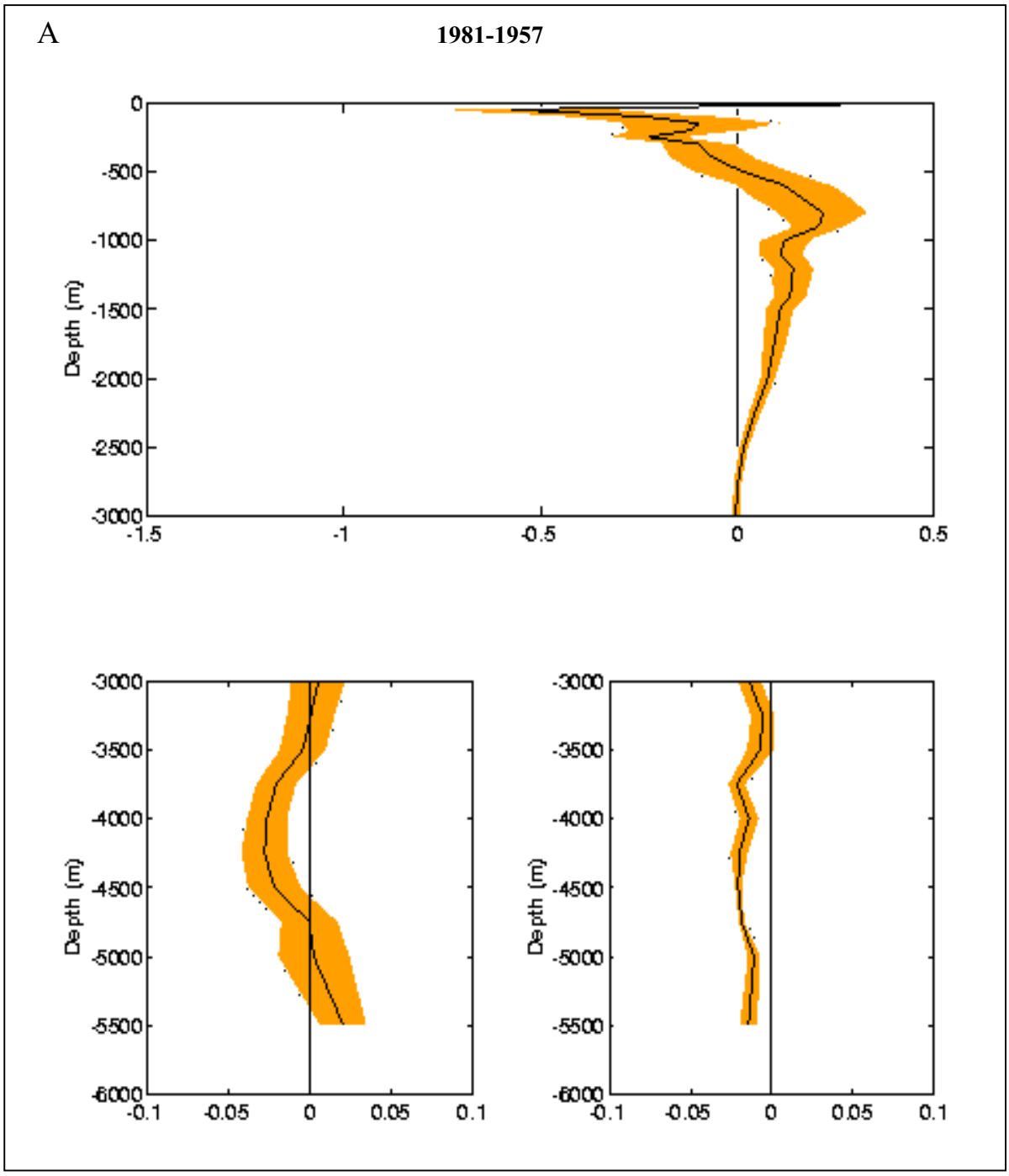

Figure 3.11: Zonal average temperature differences (ºC) plotted ± the error estimate (colour shading) for A) 1981-1957, B) 1992-1981 and C) 1992-1957 from surface to 3000 m for all the Atlantic basin (upper plot) and deeper for the North American basin in the bottom left figure and for the Canary basin, bottom right.

B

1992-1981

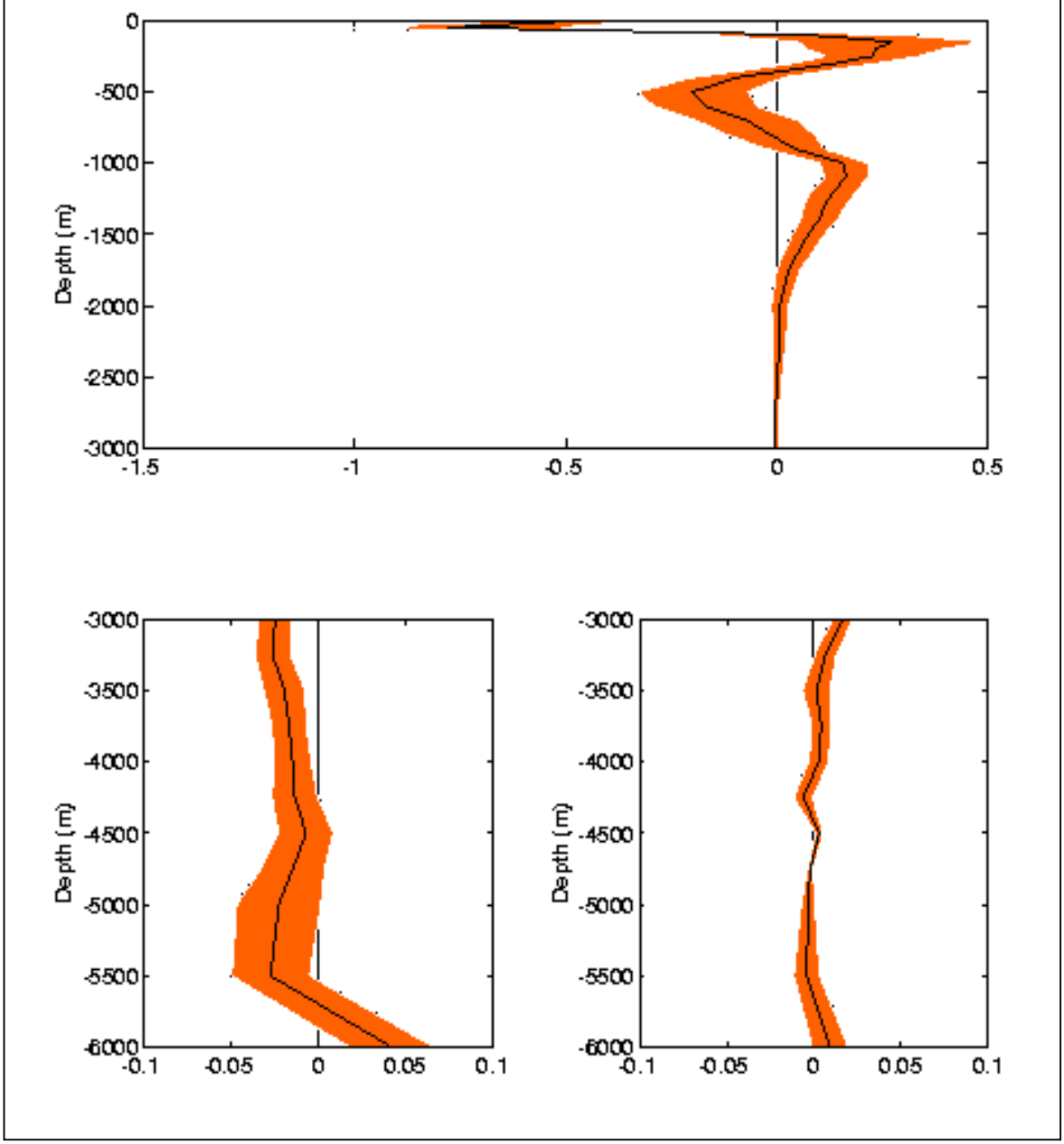
Depth (m)
0
-500
-1000
-1500
-2000
-2500
-3000
-1.5
-1
-0.5
0
0.5
Depth (m)
-3000
-3500
-4000
-4500
-5000
-5500
-6000
-0.1
-0.05
0
0.05
0.1
Depth (m)
-3000
-3500
-4000
-4500
-5000
-5500
-6000
-0.1
-0.05
0
0.05
0.1

C

1992-1957

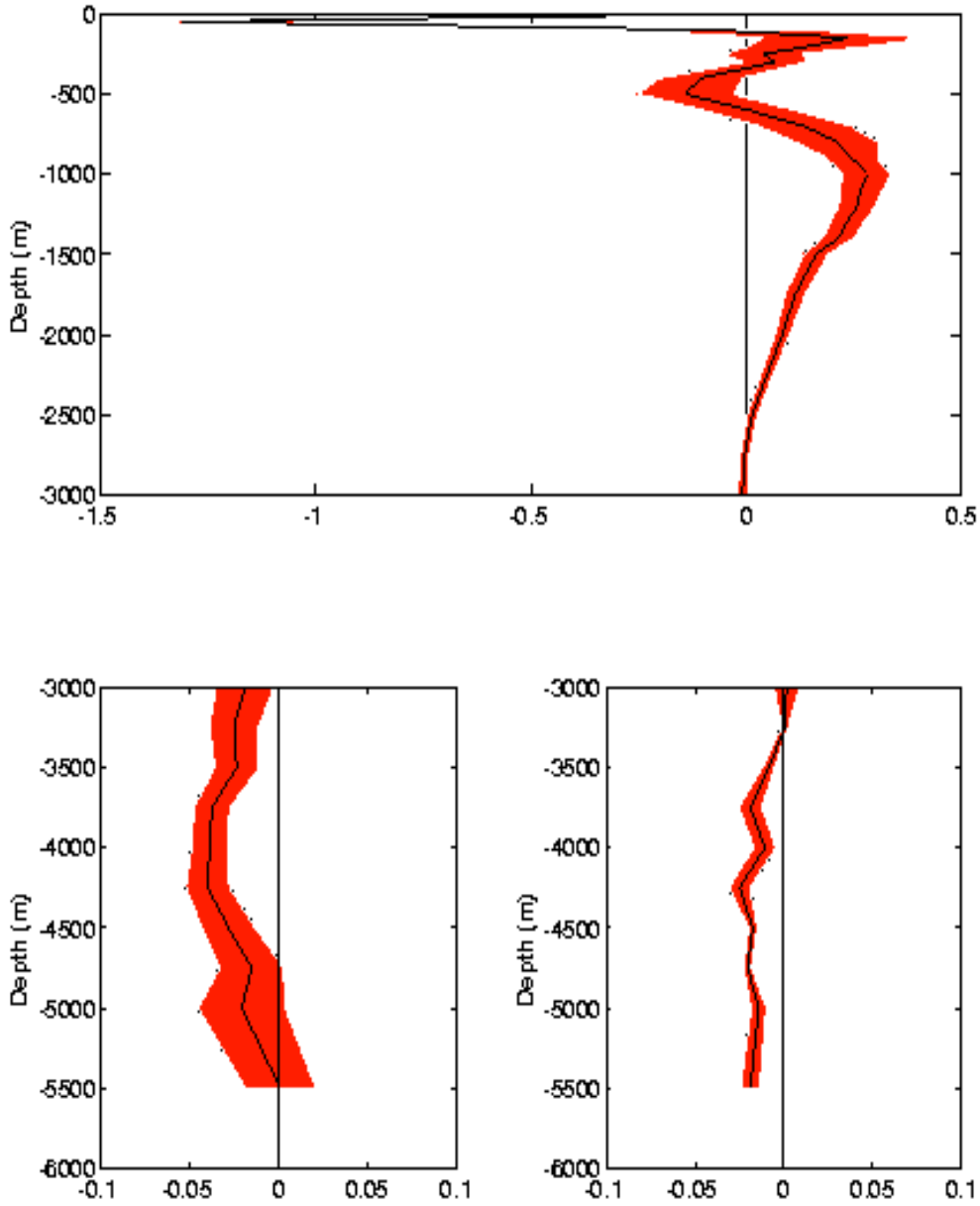
Depth (m)
0
-500
-1000
-1500
-2000
-2500
-3000
-1.5
-1
-0.5
0
0.5
Depth (m)
-3000
-3500
-4000
-4500
-5000
-5500
-6000
-0.1
-0.05
0
0.05
0.1
Depth (m)
-3000
-3500
-4000
-4500
-5000
-5500
-6000
-0.1
-0.05
0
0.05
0.1

3.3.3.2 Salinity

In Figure 3.12 the zonally averaged change in salinity ± the error estimate is shown for the three differences A) 1981-1957, B) 1992-1981 and C) 1992-1957 from surface down to 3000 m, and for the North American and Canary basins separately deeper than 3000 m. The more notable features are:

- 1981-1957 (Fig. 3.12A)

Saltier water is found between 400 and 900 m. Deeper than 1000 m differences are not significant until 2000 m, where water is fresher by -0.003. The freshening continues in the North American basin down to 5000 m where significant values are around 0.006. In the Canary basin freshening occurs until the bottom, with zonal average values around -0.004.

- 1992-1981 (Fig. 3.12B)

The most significant part is the saltier water between 800 and 1750 m. The maximum increase in salinity was 0.026±0.007 at 1100 m. Saltier water is also found between 100 and 300 m, while below that appears fresher water. Most of the differences are not significant in this layer. Below 2500 m, water is significantly fresher until 5500 m in the North American basin. At 6000 m the zonally averaged difference is significantly positive with a value of 0.005. In the Canary basin the water become fresher but the values are smaller than in the North American basin.

- 1992-1957 (Fig. 3.12 C)

Saltier water occurs between 600 and 1750 m. The maximum value was 0.031±0.012 at 800 m. Water is also saltier at depths shallower than 300 m. Differences are significantly negative below 2000 m, where the differences are around -0.004. In the deep North America basin differences are between -0.011 and -0.005 and in the deep Canary basin between -0.007 and -0.003.

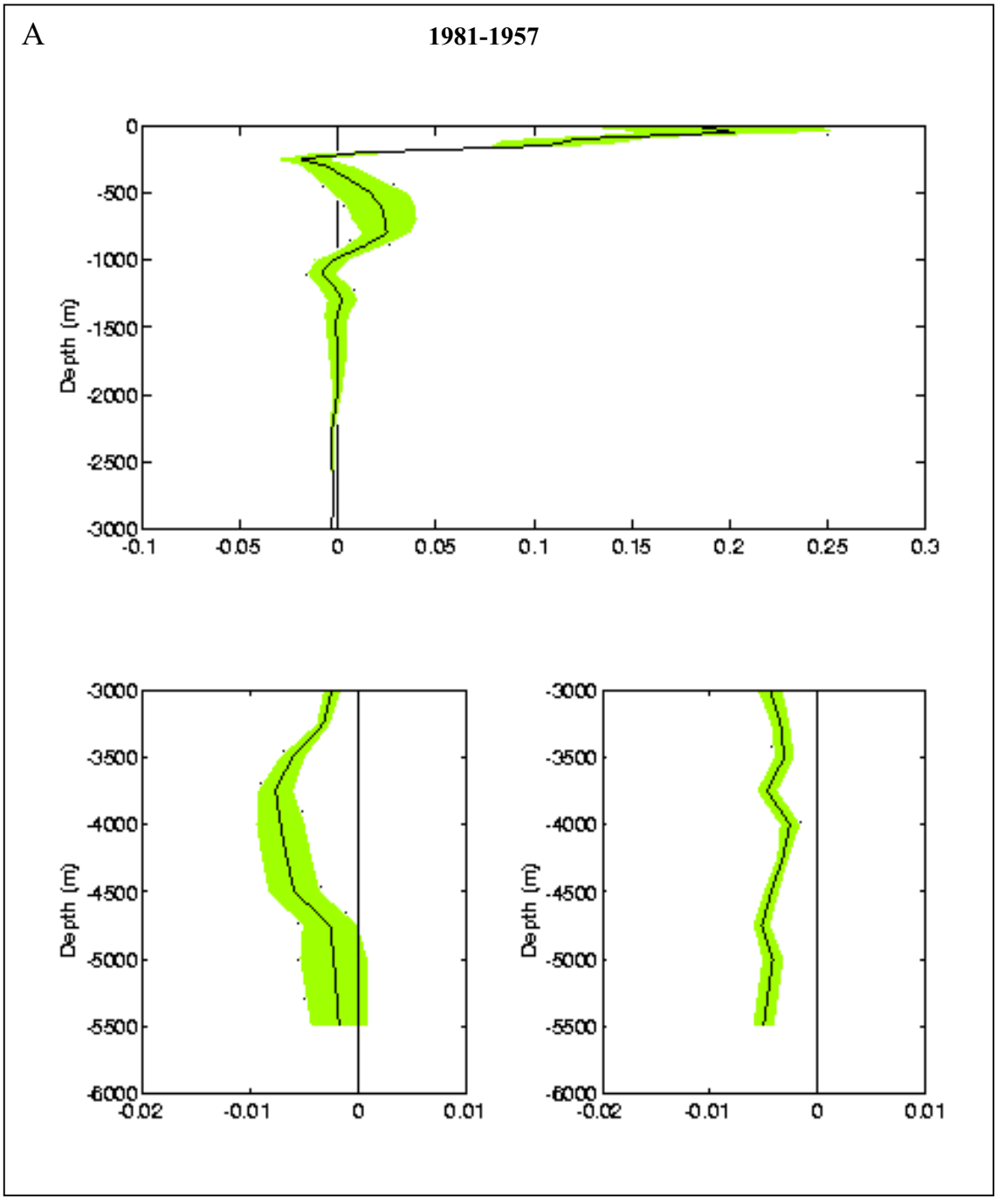

Figure 3.12: Zonal average salinity differences plotted ± the error estimate (colour shading) for A) 1981-1957, B) 1992-1981 and C) 1992-1957 from surface to 3000 m for all the Atlantic basin (upper plot) and deeper for the North American basin in the bottom left figure and for the Canary basin, bottom right.

B

1992-1981

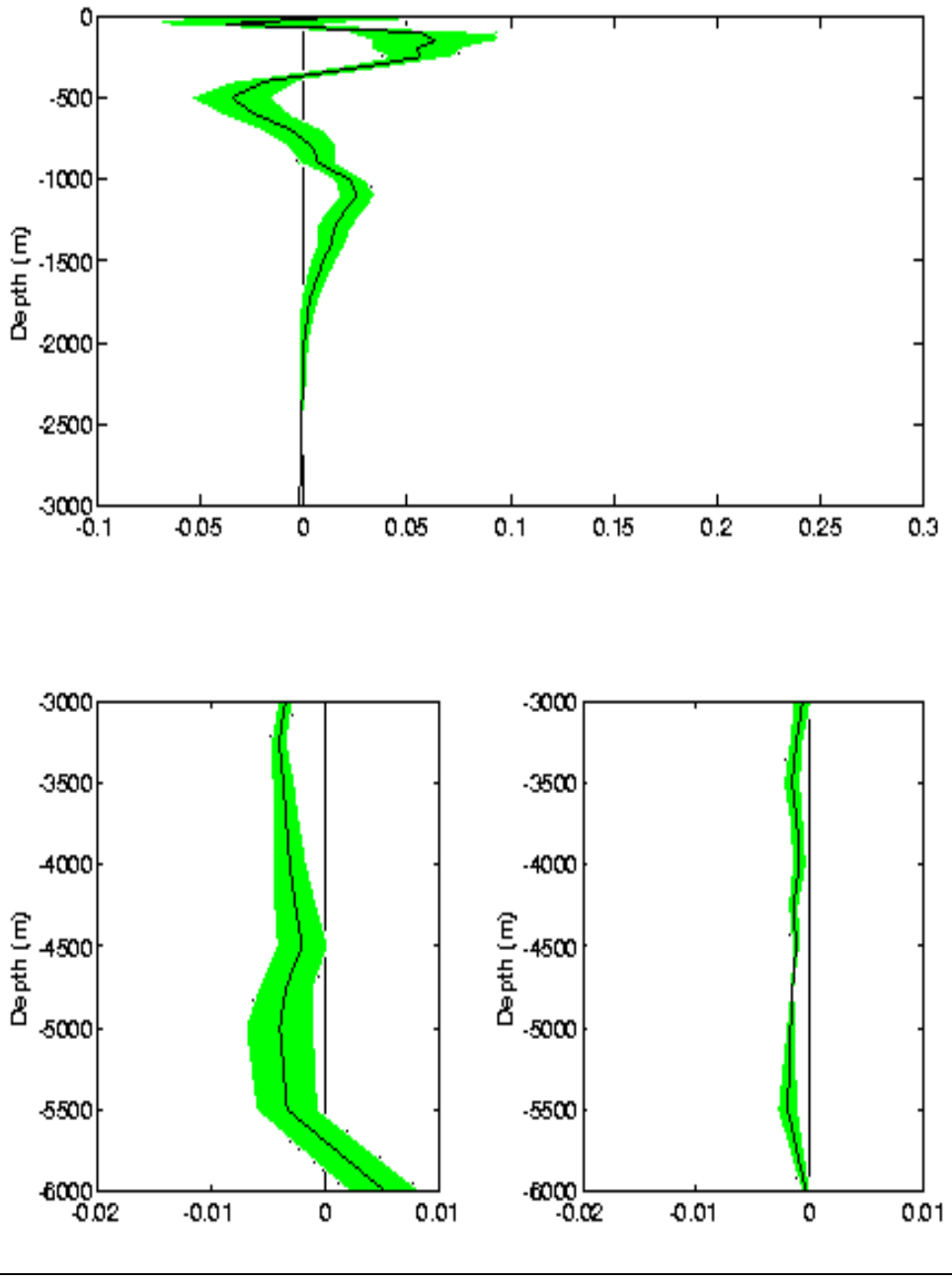
Depth (m)
0
-500
-1000
-1500
-2000
-2500
-3000
-0.1
-0.05
0
0.05
0.1
0.15
0.2
0.25
0.3
Depth (m)
-3000
-3500
-4000
-4500
-5000
-5500
-6000
-0.02
-0.01
0
0.01
Depth (m)
-3000
-3500
-4000
-4500
-5000
-5500
-6000
-0.02
-0.01
0
0.01

C

1992-1957

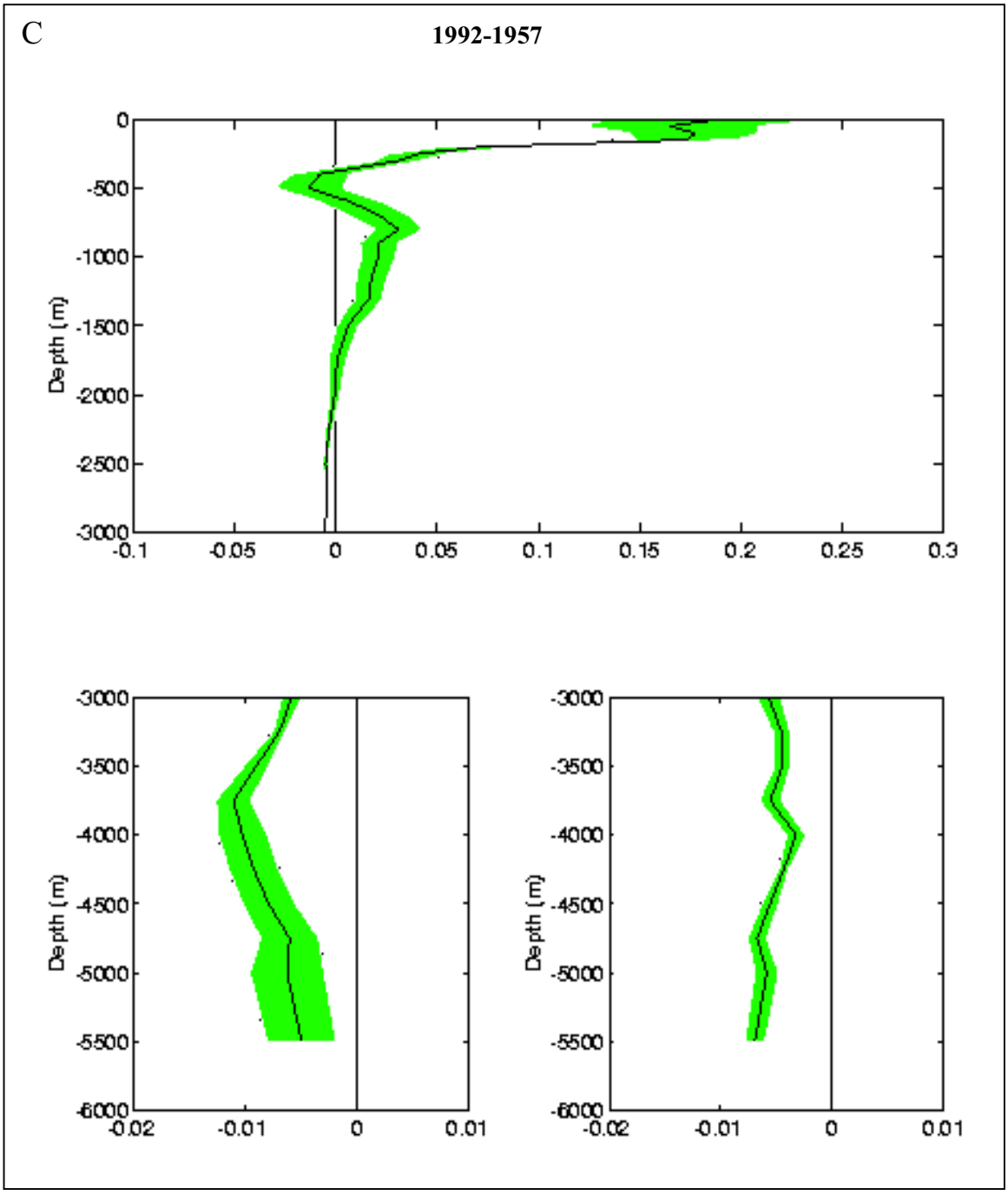
Depth (m)
0
-500
-1000
-1500
-2000
-2500
-3000
-0.1
-0.05
0
0.05
0.1
0.15
0.2
0.25
0.3
Depth (m)
-3000
-3500
-4000
-4500
-5000
-5500
-6000
-0.02
-0.01
0
0.01
Depth (m)
-3000
-3500
-4000
-4500
-5000
-5500
-6000
-0.02
-0.01
0
0.01

3.3.4 Discussion

In the western part of the North American basin, the horizontal temperature variation reverses sign between the two periods 1981-1957 and 1992-1981. In the area east and north of the Bahamas, the flow seems to have a C-shaped circulation (Schmitz *et al*., 1992), the recirculation is described by Schmitz and McCartney (1993) (their figure 8 for water above 7ºC and figure 10 below 7ºC). Schmitz and Richardson, (1991) found that 45% of the transport of the Florida Current is of South Atlantic origin. This water is fresher and warmer than the water of North Atlantic origin. Variations in the origin of the water carried by the recirculation may be responsible for the varying behaviour found in this area in the sampled periods.

Joyce and Robbins (1996), in a study of a long-term hydrographic record at Bermuda (32.17ºN, 64.50ºW), showed that the variations in temperature and salinity on interannual time-scales are largely independent of each other in the surface layer (0-500 m depth), and highly correlated in the thermocline. Between 500 and 1500 m, correlation between temperature and salinity changes is due to vertical oscillations of the thermocline with amplitudes of ±50 m. Within their records (1955-1988), they found a long-term negative trend in temperature for the layer between 500 and 1000 m, and a positive trend between 1500 and 2500 m. This result is consistent with the trend found in this study for the zonal average of the 24.5ºN with negative differences around 500 m and significant warming found below 700 m. They extended the time series back to at least 1922 and found that the long-term trend in the shallow layer disappears, while the one in the deep layer persists. The long-term trend is about 0.5ºC per century, with oscillations on the deep layer of approximately 0.05ºC over decadal time scales.

In the Roemmich and Wunsch (1984) comparison of 36ºN and 24.5ºN sections, the cooling of the upper layers from 1957 to 1981 penetrates to 700 m at 36ºN but only to 500 m at 24.5ºN. The Bermuda station is situated between them and the cooling there is found between 500 and 1000 m.

Vertical profiles of the zonally averaged warming for the three periods indicate both warming and cooling in the upper few hundred metres of the water column, which

may be due to the different sampling times within the annual cycle of the three sections. For all three time periods there is consistent and significant warming between 700 and 2500 m depths. The maximum warming occurs at about 1000 m depth and reaches as high as 0.28±0.05ºC over 35 years, or ~0.008 ºC yr^{-1}. Below 3000 m depth, there is consistent and significant cooling of the deep waters for all the three time periods but the maximum cooling is only 0.04±0.01ºC over the 35 year at 3750 m depth in the North American basin and half of that value in the Canary basin, an order of magnitude less than the warming at 1000 m.

Over the depth range from 700 to 2500 m, the vertically integrated heat content has increased by 1 x 10^9 J m^{-2}, or at an average rate of 1 W m^{-2} over the 35 yr between 1957 and 1992 surveys. The change in dynamic height over this depth interval, which is the effective sea level rise due to warming, is 3 dynamic centimetres.

Changes in salinity are principally to maintain the temperature-salinity relationship of the various water masses. Salinity increases significantly between 700 and 1500 m. The maximum values occur at 800 m with an increase of 0.031±0.012. The rate of increase in salinity is around 0.001 yr^{-1} over the complete period. In the deep water reduction on salinity is of 0.005±0.003 in the North American basin and smaller in the Canary basin. Freshening in both basins is significant. We will study the main variations in deep water in the following chapter in changes in water mass characteristics.

Recent research on oceanic climate variability has centred on changes observed at 24.5ºN in the Atlantic Ocean, for which the thesis has made substantial contributions. The following paragraph summarise this recent research including the contribution of the author in documenting ocean climate change.

Roemmich and Wunsch (1984) first estimated the temperature change along 24°N by differencing the 1981 and 1957 sections. They found considerable warming between 600 m and 3000 m depths reaching a maximum zonally averaged value of 0.2°C between 1000 to 1500 m depths. Levitus (1989a) reviewed earlier attempts at estimating decadal scale variations in ocean temperature and explored the pattern of decadal scale changes over the North Atlantic by differencing 5-year averaged data sets between 1970-74 and 1955-59. In fact, these averages were dominated by measurements made during 1957-58

(IGY years) and 1970-72. He emphasised a large-scale cooling over much of the North Atlantic at intermediate depths between 500 and 1500 m (Levitus, 1989a), but in the deep waters at 1750 m and below, he found a general warming over nearly all of the North Atlantic. Antonov (1993) examined trends of temperature over the period from 1957 to 1981 in the North Atlantic and North Pacific from additional extensive Russian data sources. He confirmed that in the depth range from 800 to 2500 m the waters were warming by order 0.1°C over 25 years over almost the entire North Atlantic, but that there was no significant trends in temperature in the North Pacific over this depth range.

Read and Gould (1992) observed a marked cooling and freshening from 1962 to 1991 in the subpolar gyre of the North Atlantic. Parrilla, Lavín, Bryden, Millard and García (1994) analysed the 1957, 1981 and 1992 sections across 24.5°N to find that the remarkable warming in the subtropical gyre over the depth range from 800 to 2500 m depths had persisted through 1992, that the warming from 1957 to 1992 was zonally uniform all the way across the 24.5°N section and that the maximum warming at 1100 m depth was occurring at a rate of almost 1°C per century (Fig. 3A and 4A). There were corresponding changes in salinity (Fig. 3b and 4b), first determined by Lavín (1993). From the long time series of hydrographic stations near Bermuda, Roemmich (1990) showed statistically significant warming of the deep waters from 1954 to 1981; Levitus and Antonov (1995) confirmed the remarkable linear warming trend from 1960 to 1990; and Joyce and Robbins (1996) have recently demonstrated that the general warming trend between 1500 to 2500 dbar extends back to at least 1922, although there are considerable decadal-scale oscillations in temperature at fixed depth (Levitus *et al.,* 1996) which can obscure the trend for observational periods of order 10 years. Joyce and Robbins (1996) also showed that the warming in the deeper waters extended meridionally over the entire subtropical gyre along 66°W in the western basin from 20°N to 35°N.

Chapter 4

Decadal changes in water mass characteristics at 24.5°N

4.1 Introduction

The purpose of this chapter is to use the three occupations of the 24.5°N transatlantic section to estimate the decadal changes in water mass characteristics at the centre of the subtropical gyre. The subtropical gyre in the North Atlantic is quite rich in water masses (Fig. 2.2A and B) as was described in chapter 2. It is our intention here to examine the decadal changes in potential temperature (θ) - salinity (S) characteristics of these water masses across 24.5°N from the three occupations of the 24.5°N section over the past 35 years. Because the Antarctic Intermediate and Bottom Waters and the North Atlantic Deep Waters are quite far from their sources, changes in their characteristics may reflect longer term trends in their source strengths or in the conditions under which they are formed or in conditions along their pathways. Surface and thermocline water types as well as the Mediterranean Water signal are generated closer to the 24.5°N section and hence changes in their characteristics may reflect more recent trends. To examine changes in water mass characteristics, vertically continuous CTD data are available on closely spaced stations in 1992 and 1981 but only discrete water sample data on more distantly spaced stations in 1957. The sparseness of the 1957 data will limit in some cases our ability to examine the longer term changes.

For the 1981-1957 differences, Roemmich and Wunsch (1984) noted that to first order the temperature and salinity changes were such as to preserve the classic temperature-salinity relationship; that is, to first order the warming is due to a deepening of the isotherms. Levitus (1989a, 1989b) also emphasised that the interpentadal cooling at intermediate depths from 1955-59 to 1970-74 was due to an upward displacement of isopycnal surfaces and that the general warming in the deeper layers was accompanied by nearly compensating increases in salinity so that the warming appeared to be related primarily to a downward displacement of the isopycnals. Because temperature decreases monotonically with increasing pressure, we first examined the vertical displacement of isotherms from 1957 to 1992. Differences in isotherm depths using the zonally averaged

temperature profiles across 24.5°N in 1957 and 1992 indicate that the maximum deepening of the isotherms from 1957 to 1992 is about 65 db for waters between 5°C and 3.8°C, between 1350 and 1900 db (Fig. 4.1). Because warmer temperatures are generally related to higher salinities in the subtropical North Atlantic θ-S relationship, salinities would also typically increase as the isotherms deepen if the water mass characteristics remain constant. But how much have the actual water mass properties changed? The primary objective of this chapter is to quantify how much of the changes in temperature and salinity at 24.5°N in the centre of the North Atlantic subtropical gyre is due to the deepening or shallowing of a constant water mass structure and how much is due to changes in the water mass structure itself. The 24.5°N transatlantic section one of the few large-scale oceanographic sections that has been repeated before WOCE, and it has been repeated twice including two occupations with modern CTD measurements. Thus, these repeated sections offer the opportunity for examining changes in water mass characteristics, changes which are expected to be relatively small so that highly accurate and precise measurements are required.

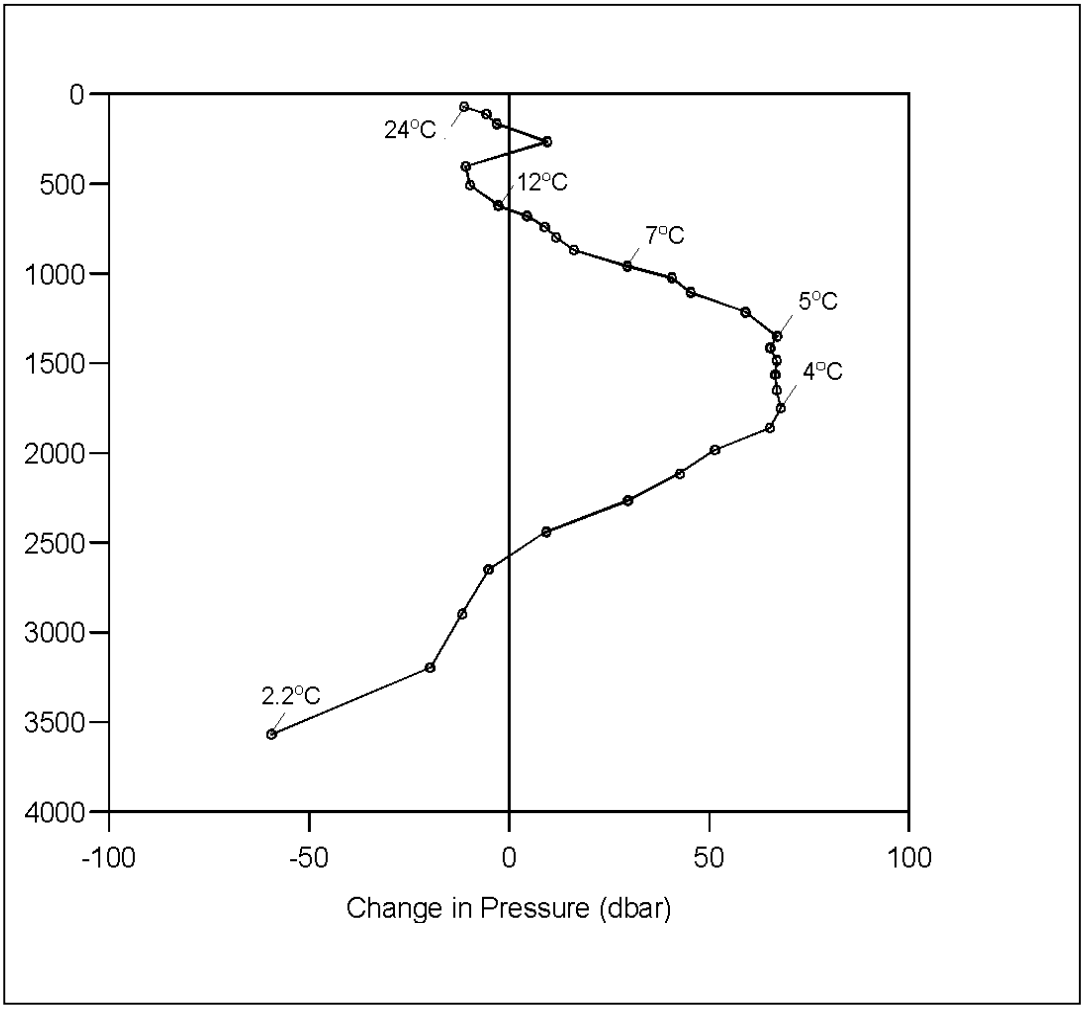

Figure 4.1 Change in pressure of isotherms from 1957 to 1992 at 24.5ºN. Zonally averaged temperature differences from 1957 to 1992 are divided by the average vertical potential temperature gradient to determine the zonally averaged change in pressure of the isotherms

4.2 Changes in water mass characteristics

There are two natural ways in which temperature and salinity at constant pressure in the ocean might change: first, the changes might be along the θ-S relationship defined by the historic water mass characteristics due to vertical movement upward or downward of a constant water mass structure; secondly, the changes might be along constant, locally defined, density surfaces (Pingree, 1972). In the first case, the temperature and salinity changes are related by the slope of the θ-S relationship. In the second case, the temperature and salinity changes are density-compensating and hence are related by the equation of state for seawater. Many analyses of observed fluctuations in temperature and salinity (including the interpentadal changes reported by Levitus, 1989a) have separated the changes into these two components.

Recently, Bindoff and McDougall (1994) repeated the argument for a natural separation into the two components, called the vertical displacement process "heaving", and analysed decadal changes in South Pacific water mass characteristics in terms of a new set of density surfaces called "neutral surfaces" (the same phrase used by Pingree, 1972). Bindoff and McDougall go on to distribute any changes in water mass characteristics into a component due to warming and a component due to freshening at the sea surface. To make this distribution, they implicitly use a model of ventilation that preserves the heat content and the salinity of the surface waters as they subduct into the interior ocean. Viewing the changes from the interior ocean, we argue that the new surface properties would intermix with existing waters at the same density as they subduct into the interior and hence blur the surface temperature or salinity anomaly into compensating temperature and salinity anomalies on a density surface. Thus, we choose to analyse the changes in the interior ocean along 24.5°N into only two components: a vertical heaving of isopycnal surfaces (which may or may not have constant water mass structure) and changes in the temperature and salinity characteristics on the isopycnal surfaces.

Because the changes in temperature and salinity at 24.5°N appear to be zonally uniform (Fig. 3.8C and 3.9C), we initially examined the zonally averaged (at constant depth) temperature and salinity profiles to generate the θ-S relationships for 1957 and 1992. Above 17°C, the changes are principally toward a saltier θ-S relationship and the

changes roughly parallel constant density surfaces. In contrast, in the main thermocline between 9° and 17°C, the changes appear to be mostly parallel to a constant θ-S relationship (Fig. 4.2A). In the intermediate waters between 4°C and 8°C, however, there is a striking change in the zonally averaged θ-S relationship towards higher salinities and the changes roughly parallel density surfaces (Fig. 4.2B). Thus, it appears that the temperature and salinity changes from 1957 to 1992 along 24.5°N do involve changes in the θ-S relationship and they are not principally due to the heaving of a stable θ-S relationship.

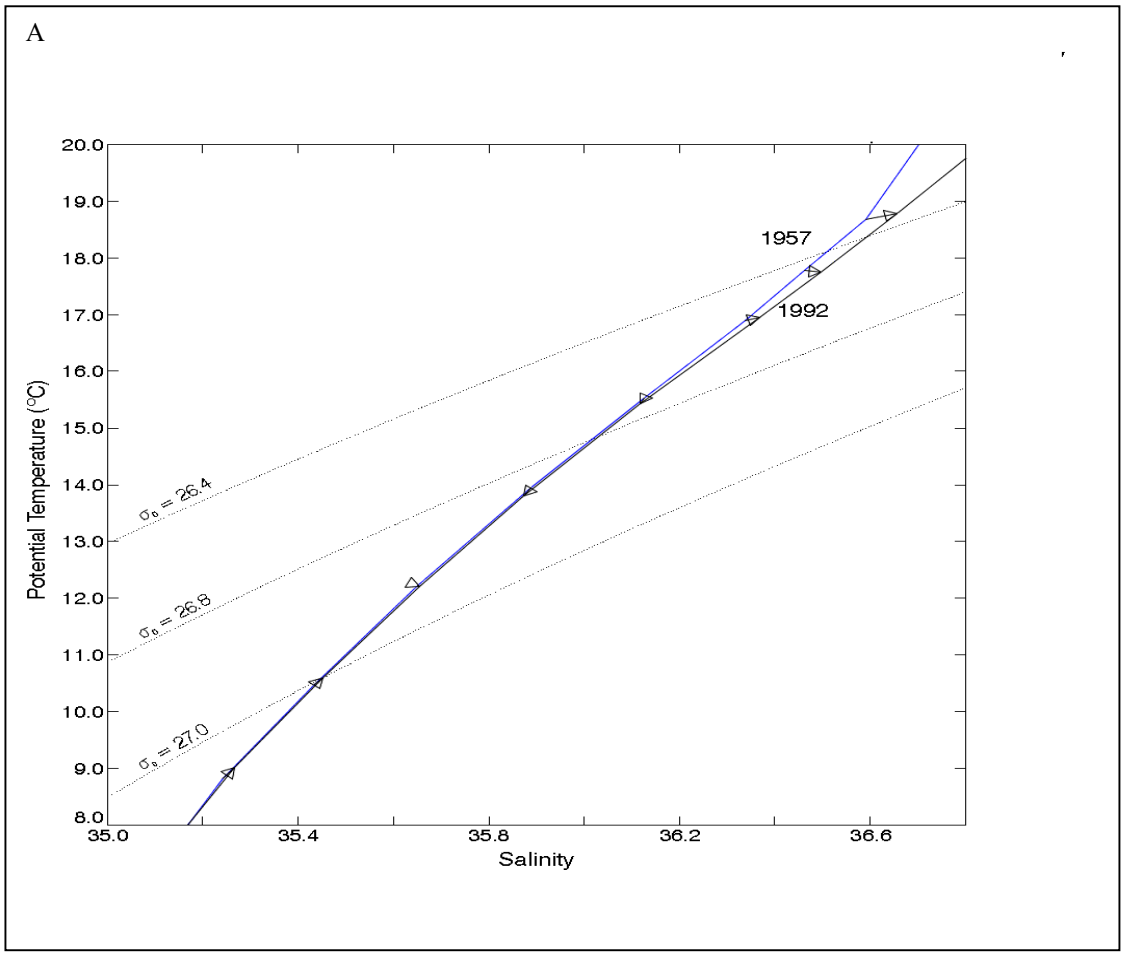

Figure 4.2 Direction of the zonally averaged changes in potential temperature and salinity at fixed pressure from 1957 to 1992 for A) warm and thermocline waters between 8 and 20ºC and B) intermediate and upper deep waters between 3 and 8ºC. Potential density anomaly surfaces relative to 1000 dbar are indicated so the changes relative both to the zonally averaged potential temperature-salinity θ-S relationship and to the density surfaces at 24.5ºN can be assessed. The direction of the arrows is from the 1957 θ-S relationship towards the 1992 θ-S relationship.

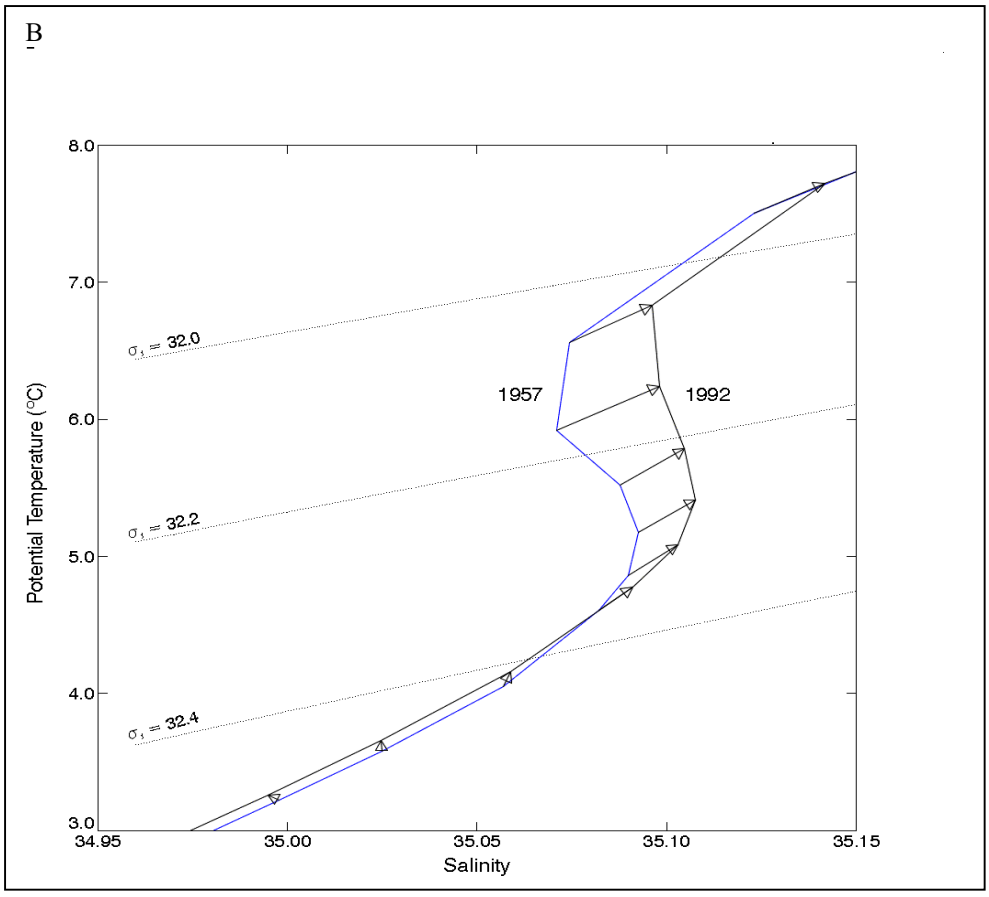

In order to examine the questions of how the θ-S relationship has changed since 1957 for the various water masses along 24.5°N and what is the spatial structure of the changes, we prefer to use the individual water sample measurements of temperature, salinity and pressure in 1957 to avoid any vertical interpolation procedure degrading the tightness of the θ-S relationship from the water samples. In the deep water and in the thermocline where there are strong θ-S relationships that can be defined by the 1957 water samples, we are able to use the 1957 measurements to assess the long-term changes in water mass characteristics.

In the intermediate waters, however, where there are substantial vertical and horizontal variations associated with the Mediterranean Water influence, the 1957 water sample data set is not sufficient to determine definitely whether water mass characteristics changed from 1957 to 1981. The vertically continuous CTD data from 1981 and 1992 can be used to examine the changes in the θ-S relationship throughout the water column and hence they provide reliable estimates of the changes over the last decade, especially for the intermediate waters. In the end, we do assess the changes in θ-S characteristics on density

surfaces throughout the water column for both the 1957-1981 and 1981-1992 periods. But the 1957 data set proves most reliable for defining the long-term changes in characteristics of surface and thermocline waters.

4.2.1 Eastern basin deep water

Because subtle long-term changes in the θ-S relationship ultimately depend on the quality of salinity determinations, we begin with an analysis of the characteristics of the deep water in the eastern basin. Saunders (1986) and Mantyla (1994) argued that the eastern deep water is the oldest water in the North Atlantic, it has no direct source, and it represents a blending of NADW and AABW over a long period. Therefore, Mantyla argued that this water might be expected to maintain constant characteristics over decadal time scales, so that any differences in θ-S characteristics would be attributable to differences in measurement accuracy.

The potential temperature-salinity values for each water sample in the eastern basin with a potential temperature between 2.0°C and 2.5°C are plotted and a least-squares fit line for each of the 1957, 1981 and 1992 water sample sets calculated (Fig. 4.3). For comparison, the relationships defined by Mantyla (1994) for 24°N and by Saunders (1986) for the eastern basin deep water are also shown. The 1992 and 1981 relationships are essentially identical (within 0.001 in salinity[1]) and both are close to Saunders' relationship. From this figure, it appears that the 1957 salinities along 24°N are too high by about 0.006, a conclusion shared by Mantyla who also cited an independent set of salinities drawn during the 24.5°N section on *Discovery* in 1957 that were systematically lower by 0.0045 than the salinity values finally reported for the section. The relationship given by Mantyla for that independent set of salinity determinations is effectively the same (within 0.001) as the 1992 and 1981 relationships shown in Table 4.1. Thus, the 1957 salinities along 24.5°N appear to be biased high by as much as 0.006 in the deep water and this bias may persist throughout the 1957 data set. We do not, however, make any correction for this bias in the

[1] All salinities are according to the practical salinity scale (UNESCO, 1981). On this scale a salinity of 35 has approximately 35 grams of dissolved salts per kilogram of seawater; and a salinity difference of 0.001 is effectively a difference of 1 part per million. Because the difference between the older and newer definitions of salinity is negligible in the oceanic range of salinity (UNESCO, 1991), no adjustments are made to the 1957 salinities due to the revised definition of salinity

1957 data set, as there are arguments that it may be restricted to salinities close to 35.0 because the salinometer used may have had a discontinuity for scales higher and lower than 35.0 (Mantyla, 1994). But our conclusions regarding changes in the θ-S characteristics of intermediate and deep waters since 1957 will be limited by this question of the accuracy of 1957 salinities. Overall, there appears to be no significant difference between the 1981 and 1992 water sample data sets in the eastern deep water; and taking account of the probable measurement error in 1957 salinities of 0.004 to 0.006, we see no differences among the three 24.5°N sections in the θ-S characteristics of the deep water in the eastern basin.

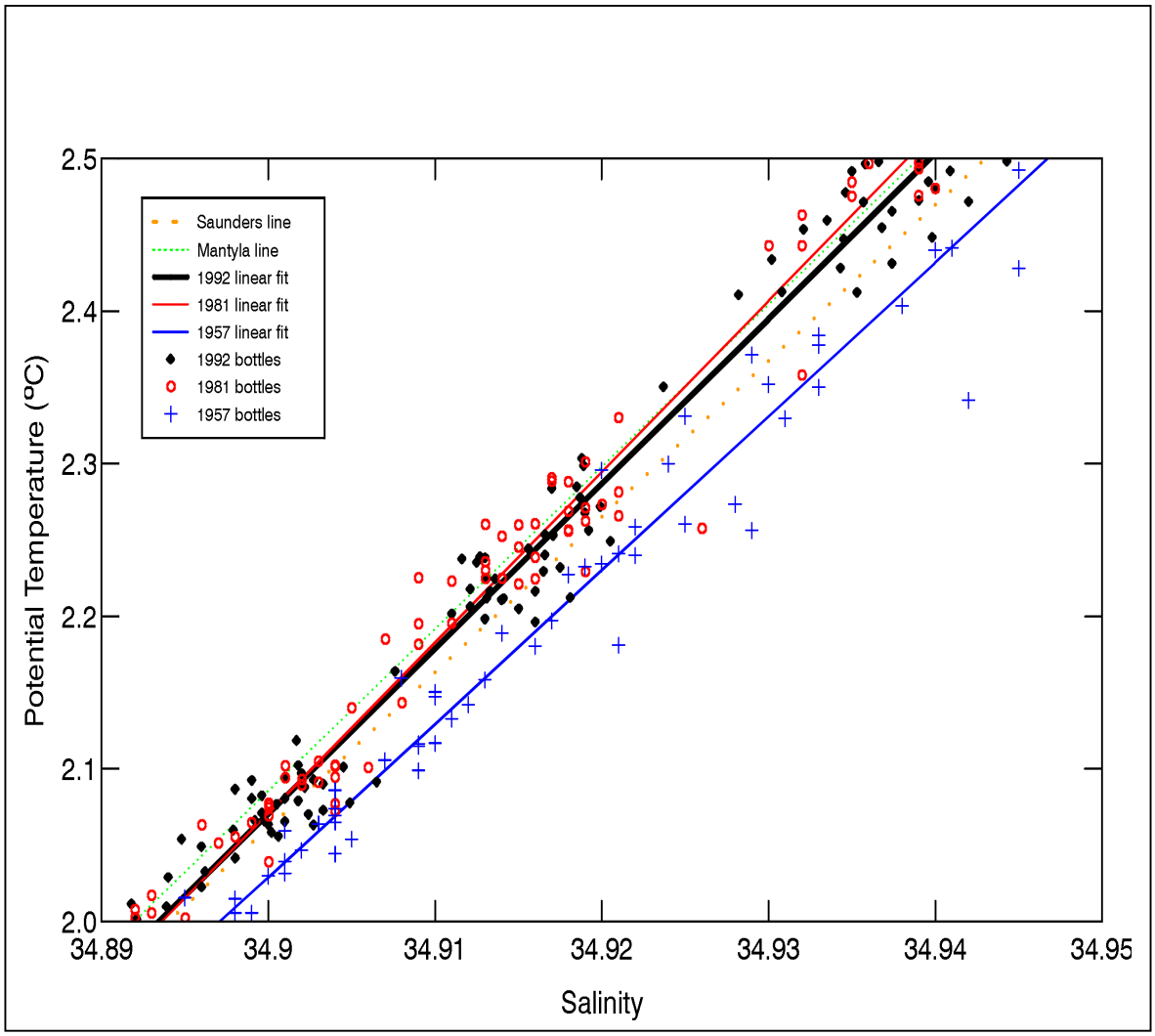

Figure 4.3 Water mass characteristics of deep water in the eastern basin at 24.5ºN in the Atlantic. Salinity is plotted against potential temperature for all water masses in the eastern basin with potential temperature between 2 and 2.5ºC for the 1957 (+), 1981 (o) and 1992 (•) sections across 24.5ºN. Regressions lines are plotted for each section, as well as for Mantyla's (1994) recommended line for 24ºN and Saunders' (1986) suggested relationship for the eastern basin deep water. Details for the five lines are given in table 4.1.

$S=S_{2.25ºC} + B\ (\theta - 2.25ºC)$	$S_{2.25ºC}$	B
1957	34.9220	0.09928
1981	34.9169	0.08943
1992	34.9166	0.09254
Saunders (1986)	34.9185	0.09800
Mantyla (1994)	34.9155	0.09414

Table 4.1. Deep water θ-S relationship regressions at 24.5ºN in the eastern basin of the subtropical Atlantic Ocean

4.2.2 Main thermocline

Considering now the main thermocline where there is a relatively tight θ-S relationship throughout the subtropical North Atlantic (Wright and Worthington, 1970), we plot all water sample values with potential temperatures between 12°C and 17°C for each of the three 24.5°N sections west of 24.5°W (Fig. 4.4) and determine a least-squares fit line of the form $S= S_{14.5} + B\ (\theta - 14.5°C)$. For each cruise, the standard deviation of individual salinities about the regression line is about 0.025, most likely reflecting real spatial variability (Table 4.2). The slopes, B, are not statistically different for the 1957, 1981, and 1992 regressions, but they appear to be increasing with time as the salinities for temperatures above 16°C become higher. The lines are clearly offset with time, however, as indicated by the median salinities, $S_{14.5}$, which increase by 0.018 from 1957 to 1981 and a further 0.012 from 1981 to 1992. Since the estimates of standard errors in these differences are only of order 0.003, these changes are significantly different from zero. Thus the salinities at constant potential temperature in the main thermocline have increased by 0.030 from 1957 to 1992. It is worth noting that, if the 1957 salinity offset of 0.006 found in the deep water were also present in the main thermocline, the salinity increase from 1957 to 1981 would have been larger, 0.024 rather than 0.018. In summary, the θ-S relationship in the main thermocline is changing so that the salinity at a given θ is increased at a nearly constant rate of 0.010 per decade from 1957 to 1981 to 1992.

Such changes in water mass characteristics are independent of the vertical movement of the isotherms and isohalines. As shown above, the thermocline has moved upward from 1957 to 1992 by about 20 db (Fig. 4.1). In the main thermocline at 24.5°N (12°C to 17°C, 340 db to 620 db) slight cooling over time at constant pressure

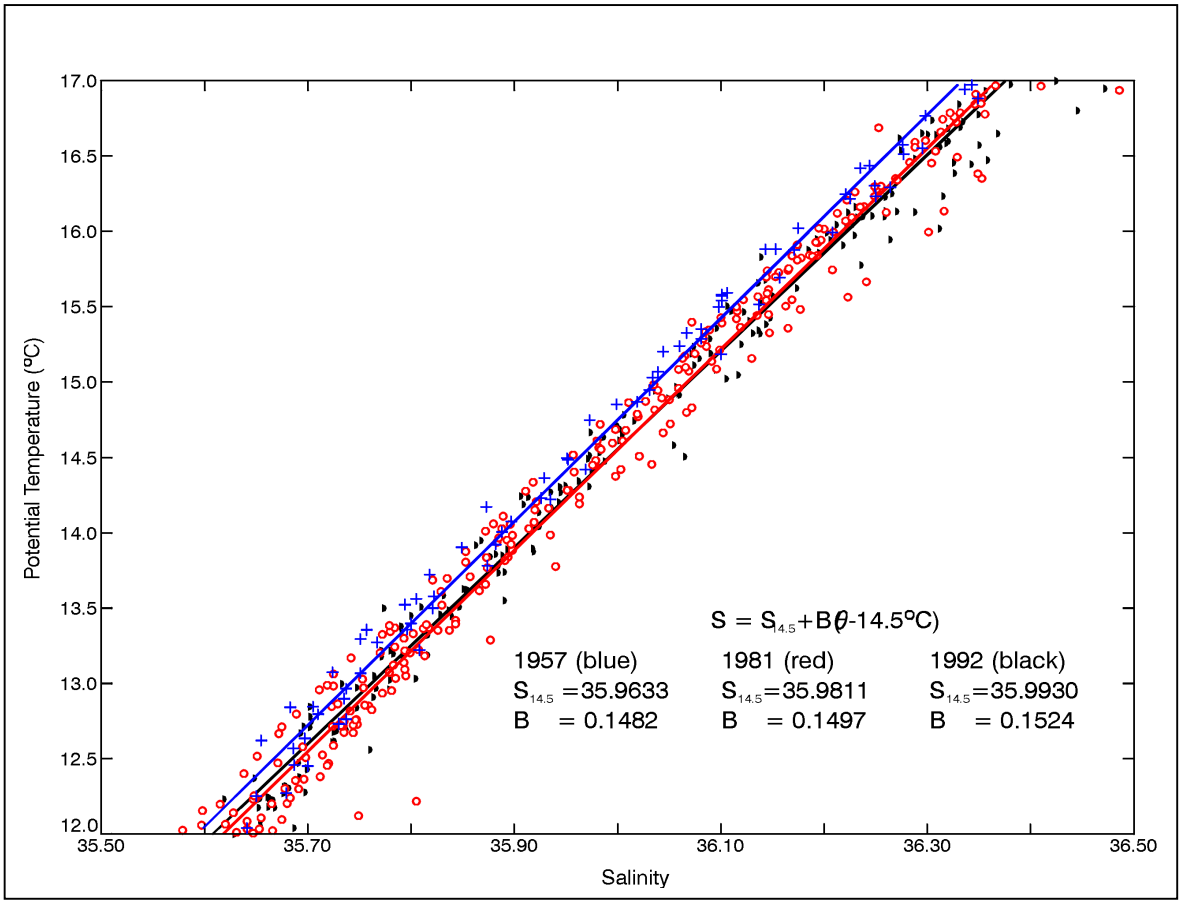

Figure 4.4 Water mass characteristics of the thermocline waters at 24.5ºN in the Atlantic. Salinity is plotted against potential temperature for all water samples with θ between 12 and 17ºC for 1957 (+), 1981 (o) and 1992 (•) sections. A lineal least squares regression line is plotted for each section, and the details for each line are given in table 4.2.

	Samples	$S_{14.5ºC}$	B	Residual std. dev.	$S_{12ºC}$	$S_{17ºC}$
1957	78	35.9633	0.1482	0.0210	35.593	36.334
1981	204	35.9811	0.1497	0.0225	35.602	36.350
1992	207	35.9930	0.1524	0.0274	35.612	36.374

Table 4.2. Thermocline θ-S regressions along 24.5ºN in the subtropical Atlantic Ocean. For each of the 1957, 1981 and 1992 hydrographic sections across 24.5ºN west of 24.5ºW, all samples with potential temperatures between 12 and 17ºC were least squares fitted to a line of the form

$$S=S_{14.5ºC} + B\ (\theta - 14.5ºC),$$

where $S_{14.5ºC}$ is the salinity at θ = 14.5ºC and B is the slope. The resulting regressions coefficients for $S_{14.5ºC}$ and B as well as the standard deviations of the samples from the fitted line are presented. In addition, the fitted values for salinity at 12ºC ($S_{12.5ºC}$) and 17ºC ($S_{17ºC}$) are given

was showed in the previous chapter. This cooling has been primarily due to the heaving upward of the isotherms resulting in a cooling at constant pressure. At the same time, as shown by this regression analysis, the θ-S relationship itself is changing towards higher salinity at constant potential temperature. While these subtle changes in water mass characteristics in the thermocline represent smaller, supplemental changes to those due to vertical movement of a nearly constant water mass structure, they do demonstrate that the thermocline θ-S relationship itself is changing at a measurable rate.

In order to assess whether the temporal change in the thermocline θ-S relationship might be due to a horizontal shift in the large-scale distribution of water masses, the zonal and meridional gradients of salinity at the 14.5°C isotherm are estimated from hydrographic sections taken during the 1980's: the 1981 *Atlantis II* section along 24.5°N, the 1983 *Knorr* section along 35°W, the 1983 *Oceanus* section along 52°W and the 1984 *Endeavour* section along 66°W (Table 4.3). For the zonal 1981 section, 10°-longitude averages of the potential temperature and salinity on the set of potential density anomaly surfaces at intervals of 0.05 from 25.50 to 26.85 kg m^{-3} are estimated and then the salinity on the 14.5°C isotherm is determined. For the meridional sections, overlapping 5°-latitude averages are estimated in the same way around 24.5°N and the salinity at 14.5°C determined. There are no consistent or significant meridional gradients in the salinity on the 14.5°C isotherm from the 3 meridional sections, but there is a zonal gradient such that salinity increases eastward by 0.040 over 40° of longitude from 70°W to 30°W. Thus, the temporal increase in salinity of 0.030 in the thermocline θ-S relationship from 1957 to 1992 might be explained by a 3,000 km westward shift in water masses, although that is half of the total zonal width at 24.5°N and leaves open the question as to where the higher salinities in the eastern half of the section during 1992 would have originated. We prefer to think that the θ-S changes are due to higher evaporation or less precipitation in the surface formation regions which would then lead to higher salinities in the thermocline after the water subducts. For a mixed layer with a salinity of 36.0 over 50 m depth in the formation region for the thermocline water masses, an increase in salinity of 0.030 could be attributed to an increase in evaporation minus precipitation of 4 cm, clearly not a large change in the E-P values which are of order 60 cm yr^{-1} over the subtropical North Atlantic (Schmitt, *et al.,* 1989). But the persistence of even such small changes over long time periods and large

spatial scales can clearly lead to measurable changes in the water mass structure of the thermocline.

		1984 Endeavour 66°W		*1983 Oceanus 52°W*				*1983 Knorr 35°W*			
	70°W		60°W		50°W		40°W		30°W		
27°N		35.955		35.965				35.979			
24.5°N	35.940	35.961	35.959	35.968	35.969		35.975	35.984	35.980		1981 AtlantisII 24.5°N
22°N		35.945		35.967				35.978			

Table 4.3 Spatial distribution of salinity at θ = 14.5ºC in the subtropical North Atlantic. Along 24.5ºN 10º-longitude averages on potential density surfaces were made for the 1981 *Atlantis II* cruise to determine the salinity at θ = 14.5ºC. For the meridional sections, overlaping 5º-latitude averages were made on potential density surfaces to determine the salinity at θ = 14.5ºC at 27, 24.5 and 22ºN from the 1984 *Endeavour* section along 66°W, the 1983 *Oceanus* section along 52°W and the 1983 *Knorr* section along 35°W.

Since the primary processes of subduction and mixing that lead to the water mass structure of the thermocline occur along density surfaces, these temporal changes should also be assessed on density surfaces. As temperature and salinity jointly determine density at a given pressure, any change in salinity on a density surface is accompanied by a change in temperature. Thus, the increase in salinity in the thermocline along 24.5°N implies an increase in temperature on constant potential density surfaces (Fig. 4.5). In fact, on density surfaces the temporal increases in salinity become more dramatic because of the strong correlation between higher salinity and temperature in the thermocline θ-S relationship: higher salinity implies higher temperature according to the θ-S relationship and the temperature and salinity changes along the θ-S curve partially compensate in density. In a density analysis, both the temperature and salinity in the thermocline are increasing with time: the salinity increases by 0.064 from 1957 to 1992, that is at a rate 0.018 per decade, and the temperature also increases by 0.228°C over 35 years, at a rate 0.065°C per decade.

In summary, the θ-S relationship in the main thermocline of the subtropical North Atlantic has become saltier from 1957 to 1981 to 1992. At constant potential temperature, salinity in the main thermocline has increased by 0.010 per decade, while at constant potential density salinity has increased by nearly twice as much, 0.018 per decade, and the temperature has warmed at a rate of 0.065°C per decade. It is unlikely that such changes in the θ-S relationship can be explained by lateral movements in water mass structure as there is little meridional variation in θ-S characteristics around 24.5°N and the small zonal

gradient in characteristics would require a westward shift of 3,000 km, half the zonal extent of the 24.5°N section, to account for the observed changes from 1957 to 1992. Thus, it appears that the subtropical North Atlantic thermocline is becoming saltier.

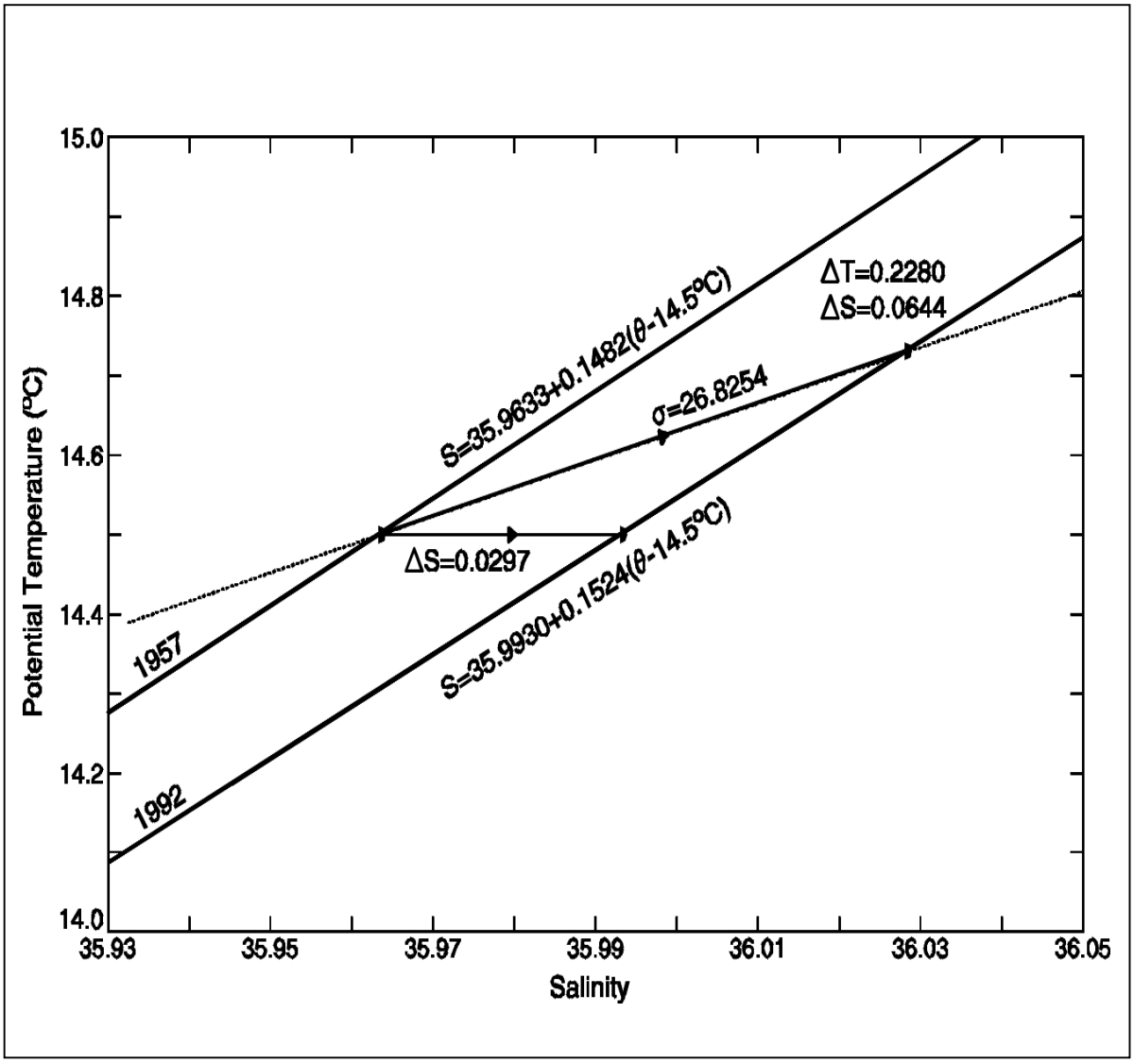

Figure 4.5 Changes in the thermocline water mass characteristics along 24.5ºN from 1957 to 1992. The regression lines expressing the θ-S relationship in the thermocline for the 1957 and 1992 sections are drawn between 14ºC and 15ºC. The potential density surface passing through the median value for the 1957 regression at θ = 14.5ºC, S=35.9633 is drown and this surface intersects the θ-S regression at θ = 14.728ºC, S=36.0277. The change in water mass characteristics over time can be interpreted as a change in salinity at constant potential temperature of 0.0297, or as a combined change along a constant potential density surface of 0.064 in salinity and of 0.228ºC in temperature, and these alternatives are shown by arrows.

4.2.3 Intermediate waters

In the intermediate waters of the lower thermocline, roughly defined by potential temperatures between 4°C and 9°C, there are two principal influences: higher salinity Mediterranean Water (MW) and lower salinity Antarctic Intermediate Water (AAIW). The Mediterranean Water signal is stronger in the eastern basin, of course. The Antarctic Intermediate Water, as evidenced by lowest salinity in 10°-longitude averaged θ-S plots (Fig. 4.6), appears to be strongest over the Mid Atlantic Ridge between 45°W and 55°W in both the 1981 and 1992 sections.

To examine the spatial structure of the changes in water mass characteristics in the lower thermocline, it is necessary to concentrate on the 1981 and 1992 sections: for the 1957 section, there are just not enough water samples in the 4°C to 9°C range to reliably average out the vertical and horizontal variations in salinity associated with the Mediterranean Water. For the continuous CTD stations during 1981 and 1992, 10°-longitude averages of potential temperature and salinity on σ_1 surfaces (potential density anomaly referenced to 1000 db; the set of surfaces is listed in the caption for figure 4.6) are determined in order to illustrate the changes over time. In both the eastern and western basins, the salinity throughout the lower thermocline has markedly increased from 1981 to 1992 (Fig. 4.7).

In this region of the θ-S diagram, there is very little variation in average salinity with potential temperature (or with depth). This is the depth range of maximum warming found in chapter 3 and it is the depth range where isotherms descended dramatically from 1957 to 1992. The salinity increases, however, cannot be explained by vertical heaving, for there just was no water with high enough salinity in the 1981 lower thermocline to match the 1992 salinities. For the 65°W and 75°W averages in the range between σ_1=32.1 and 32.2 (6.4°C and 5.6°C), the salinity increased by 0.015 to 0.018 from 1981 to 1992 with a standard error in the difference of 0.002 to 0.005 (Fig. 4.7A).). In the east for similar averages between 25°W and 35°W, the situation is the same although the signal is increased. Again between σ_1=32.1 and 32.2 (about 6.8°C to 6.0°C) the salinity increased by 0.054 to 0.068 from 1981 to 1992 with a standard error in these differences due to variability among the stations of only 0.018 to 0.026 (Fig. 4.7B) .Thus, these increases in

intermediate water salinity are statistically significant. Zonally across the 24.5°N section, the increase in salinity in the lower thermocline from 1981 to 1992 is largest in the east, but is a minimum with virtually no increase over the Mid Atlantic Ridge between 45°W and 55°W, and then rises again in the western basin.

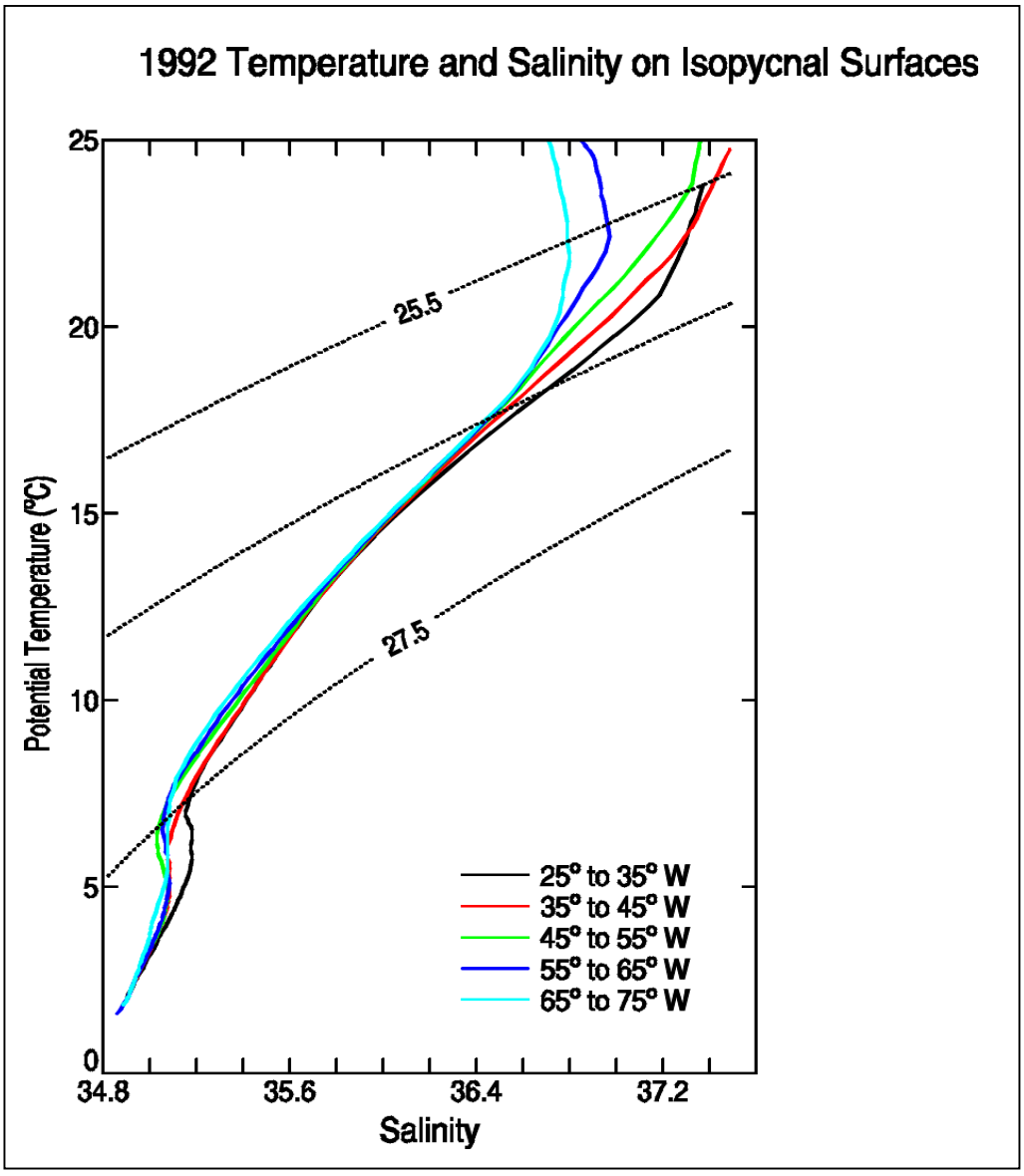

Figure 4.6. Potential temperature-salinity relationship by 10º-longitude bands across 24.5ºN for the 1992 hydrographic section. Potential temperature and salinity are determined at each station on a set of density anomalies surfaces. The density surfaces are taken to be potential density anomalies σ_0 referenced to sea surface pressure, at intervals of 0.05 from 25.50 to 26.85 kg m^{-3}, σ_1 (referenced to 1000 dbar) at intervals of 0.02 from 31.24 to 31.98, σ_2 (referenced to 2000 dbar) at intervals of 0.01 from 36.82 to 37.03; σ_4 to 4000 dbar) at intervals of 0.005 from 45.785 to 45.935. Averages of potential temperature and salinity on these density surfaces are made for all the stations within each 10º-longitude bands to create the θ-S curves. Several potential density anomaly surfaces (referenced to the surface) are also included to indicate the general slope of isopycnal surfaces.

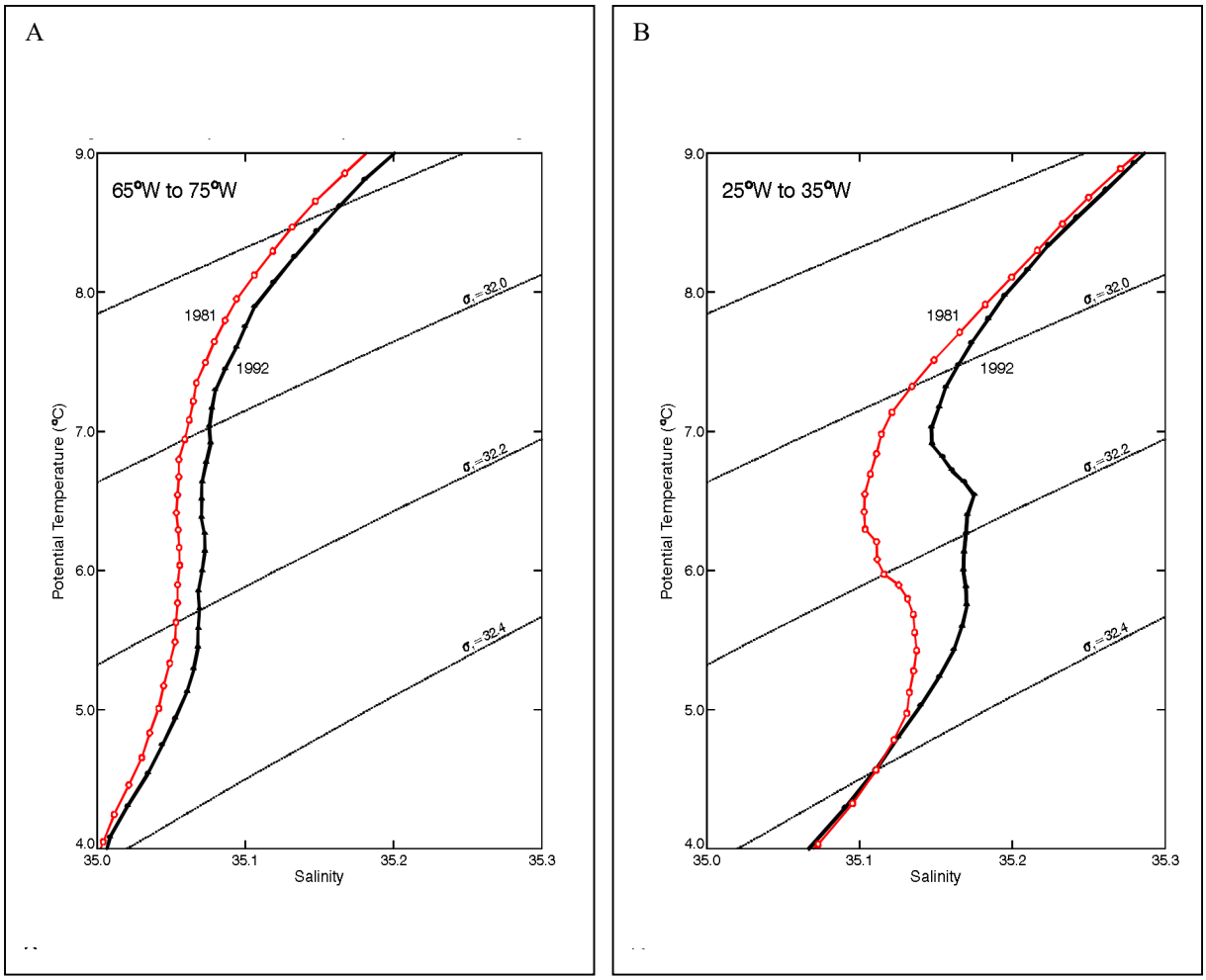

Figure 4.7 Changes in potential temperature salinity relationships from 1981 to 1992 for the intermediate waters between 4ºC and 9ºC for A) western (65ºW to 75ºW) and B) eastern (25ºW to 35ºW) regions of the 24.5ºN hydrographic section. Average of potential temperature and salinity on σ_1 surfaces listed in the caption of figure 4.6 are made for all the stations within the 10º-latitude band. The black line denotes the 1992 relationship and the red line denotes the 1981 relationship. Potential density anomaly surfaces referenced to 1000 dbar are also indicated.

Although the changes in the intermediate waters along 24.5°N cannot be attributed to vertical heaving of a constant water mass structure, there are horizontal variations in the properties of the intermediate waters, notably in the Mediterranean Water tongue (see Fig. 23 of Worthington, 1976), and lateral movements of this structure might account for the observed temporal changes in water masses along 24.5°N. Again using the sections from the early 1980's along 24.5°N (1981), 35°W (1983), 52°W (1983) and 66°W (1984) to determine the horizontal variations in salinity at the 6.5°C isotherm (Table 4.4), we note

that there is a substantial northward increase in salinity ranging from 0.21 over 5° of latitude (3.8 x 10^{-9} cm^{-1}) at 35°W to 0.09 over 5° of latitude (1.5 x10^{-9} cm^{-1}) at 66°W.

The temporal increase in salinity from 1981 to 1992 in the east between 25°W and 35°W could be due to a southward shift in the Mediterranean Water tongue of order 160 km; and the temporal increase in the west between 65°W and 75°W could have been due to a southward shift in water mass characteristics of order 110 km. Such southward shifts, however, are contrary to the meridional shifts implied by the observed oxygen changes from 1981 to 1992. Throughout the intermediate waters, oxygen decreases by about 0.1 ml l^{-1} from 1981 to 1992 (see Fig. 4.12B). As Lozier *et al.* (1995, Fig. 13 and 15) have shown that there is a northward increase in oxygen in the intermediate waters of the subtropical North Atlantic, such decrease in oxygen over time would suggest a northward shift of the spatial pattern in contrast to the southward shift suggested by the salinity increase.

		1984 Endeavour 66°W		***1983 Oceanus 52°W***				***1983 Knorr 35ºW***			
27ºN	70ºW	35.071	60ºW	35.103	50ºW		40ºW	35.231	30ºW		
24.5ºN	35.058	35.028	35.026	35.033	35.032		35.069	35.093	35.110		1981 AtlantisII 24.5ºN
22ºN		34.985		34.961				35.021			

Table 4.4 Spatial distribution of salinity at θ = 6.5ºC in the subtropical North Atlantic. Along 24.5ºN 10º-longitude averages on potential density surfaces were made for the 1981 *Atlantis II* cruise to determine the salinity at θ = 6.5ºC. For the meridional sections, overlaping 5º-latitude averages were made on potential density surfaces to determine the salinity at θ = 6.5ºC at 27ºN, 24.5ºN and 22ºN from the 1984 *Endeavour* section along 66°W, the 1983 *Oceanus* section along 52°W and the 1983 *Knorr* section along 35°W.

It is also possible for zonal shifts in the spatial distributions to have caused the temporal changes. Especially in the east, zonal shifts could explain the temporal increase in salinity as the salinity at 6.5°C increases eastward in the eastern basin by about 0.04 per 10° of longitude (0.39 x 10^{-9} cm^{-1}). The observed temporal increase from 1981 to 1992 between 25°W and 35°W then might be due to a westward shift in the Mediterranean Water tongue of order 1,600 km. As oxygen increases westward in the intermediate waters throughout the subtropical North Atlantic (Lozier *et al.*, 1995), a westward shift in the

spatial distribution would also lead to the observed decrease in oxygen from 1981 to 1992. Interestingly, however, the salinity at 6.5°C is a minimum over the Mid Atlantic Ridge (45°W-55°W) in both the 1981 and 1992 sections along 24.5°N so that salinity at 6.5°C increases westward in the western basin. As a result, explaining the temporal increase in salinity in the west becomes problematic to interpret in terms of zonal shifts in the water mass characteristics.

In summary, the increases in salinity from 1981 to 1992 in the intermediate waters across 24.5°N range from 0.06 in the east, to effectively zero over the Mid Atlantic Ridge, to 0.02 in the west. These increases cannot be explained by vertical heaving of a constant water mass structure. Because there is little variation in salinity versus pressure or potential temperature in the intermediate waters, the increase in salinity is effectively the same on constant temperature or constant density surfaces. The increases in salinity could be explained by a southward shift in the water mass characteristics generally associated with the Mediterranean Water tongue by about 150 km, but such southward shift would conflict with the observed temporal decrease in oxygen. Westward shifts of the large-scale spatial distributions could lead to the observed increase in salinity and decrease in oxygen in the eastern basin but not in the western basin where the zonal salinity gradient has opposite sign. Thus, the observed temporal changes in intermediate water characteristics are not the result of simple vertical or lateral movements of the large-scale distributions in the subtropical North Atlantic. The θ-S relationship in the intermediate waters has changed measurably toward higher salinities from 1981 to 1992.

4.2.4 North Atlantic Deep Water

The zonal sections of chlorofluorocarbons, or CFC's (Fig. 4.8A and B), indicate two regions of high CFC concentration in the deep waters and both are against the western boundary on the continental slope off the Bahamas, one at about 1500 db and one at about 3500 db. Because CFC's are man-made chemicals produced only in this century, they are generally absent in deep waters which have not had contact with the atmosphere in the past 50 years (Bryden *et al.,* 1996). Measurable concentrations of CFC's in the deep waters therefore are found in waters that have been recently formed by air-sea interaction

processes such as deep convection. The high CFC concentrations along the western boundary of the North Atlantic have been used to identify and trace recently formed North Atlantic Deep Water (Smethie, 1993). Here at 24.5°N, the core of high CFC concentration at about 1500 db tags LNADW that is thought to be formed at the surface in or near the Labrador Sea (Pickart, 1992) and the lower core at about 3500 db tags LNADW that originates in the Greenland-Iceland-Norwegian Sea (Smethie, 1993).

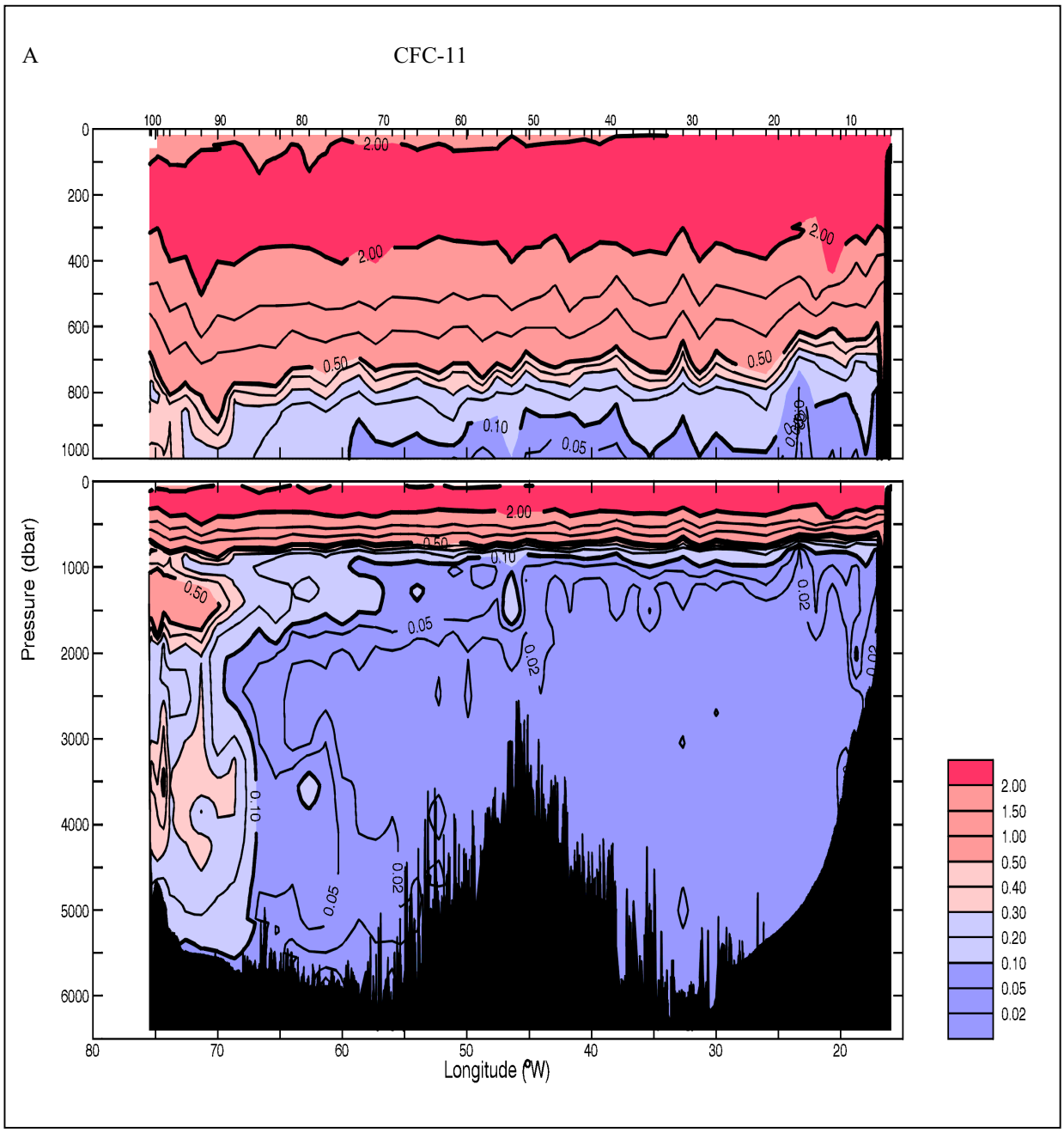

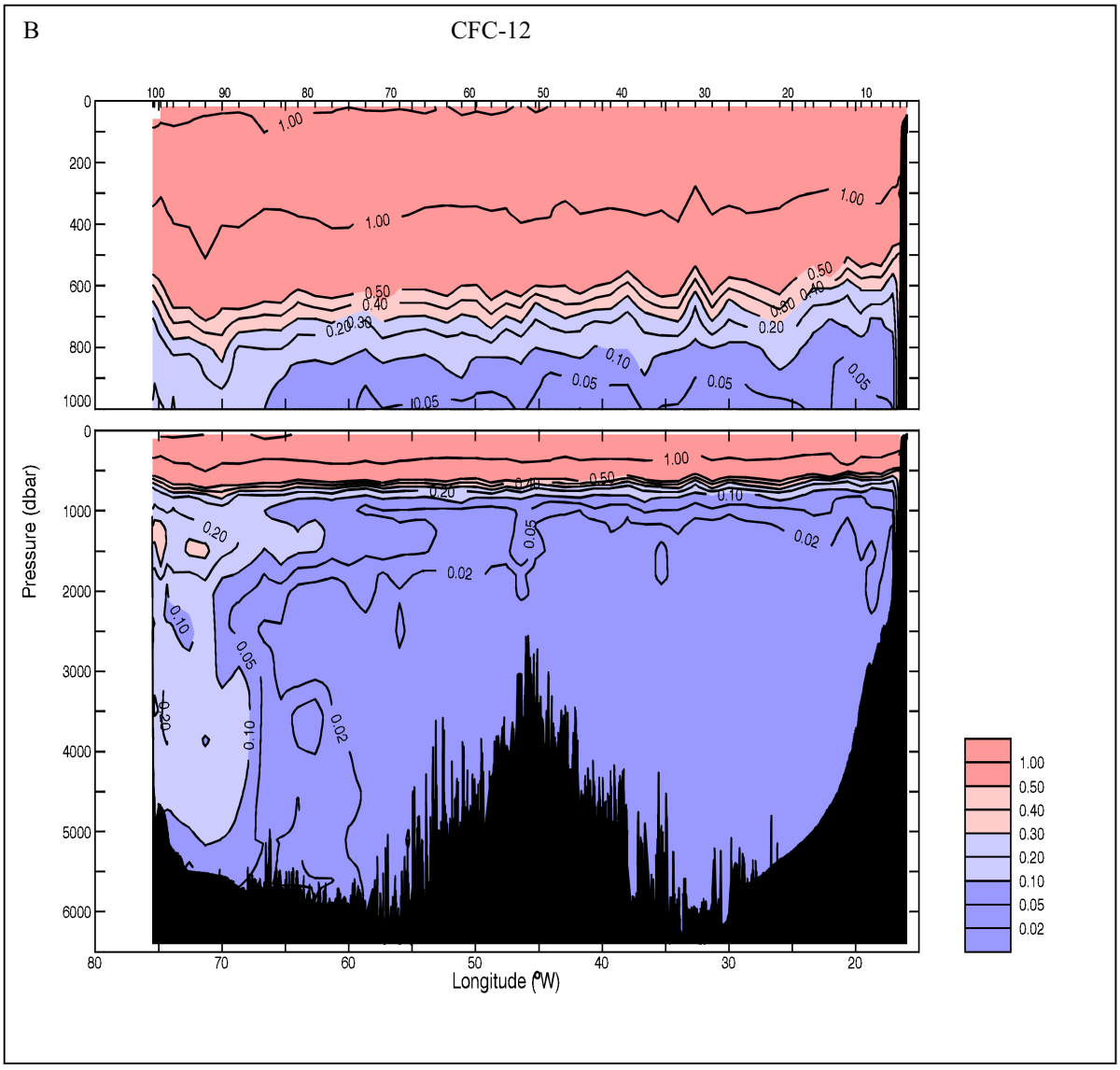

Figure 4.8. Zonal section of chlorofluorocarbon (A:CFC-11, and B:CFC-12) across 24.5ºN from the hydrographic stations taken aboard Hespérides in July-August 1992. Units are pmole kg^{-1}. The distribution of stations positions is indicated by tics along the top.

Because there is effectively no CFC signal in the eastern basin at 24.5°N, we searched for changes in deep water properties primarily in the western basin where the CFC signals suggest deep waters may have been in contact with the atmosphere over the recent past. The θ-S relationships in the deep water for the 10°-longitude averages on density surfaces for CTD stations between 65°W and 75°W in the western basin indicates an increase in salinity from 1981 to 1992 above about σ_2=37.00 (θ=3.0°C) but a decrease below (Fig. 4.9)

The 1957 water sample data set (shown as + signs on Fig. 4.9) appears saltier in the lower deep water than either the 1981 or 1992 averages, probably reflecting the high salinity bias in IGY salinities. It does appear that the 1957 measurements approach the 1981 and 1992 θ-S relationships where they cross at about 3.1°C. For the shallower core, the maximum increase in salinity from 1981 to 1992 of 0.009 occurs at about 3.8°C (σ_2=36.91, pressure=1790 db), but such increase is not twice as large as the standard error of 0.005. For the deeper core, the maximum decrease in salinity of 0.005 from 1981 to 1992 occurs near the 2.3°C isotherm (σ_4= 45.84, pressure= 3340 db) and again such difference is just about 2 standard errors and is at the level of our ability to measure salinity. The locations of maximum increase and maximum decrease in salinity are close to the positions of the upper and lower cores of NADW at the western boundary.

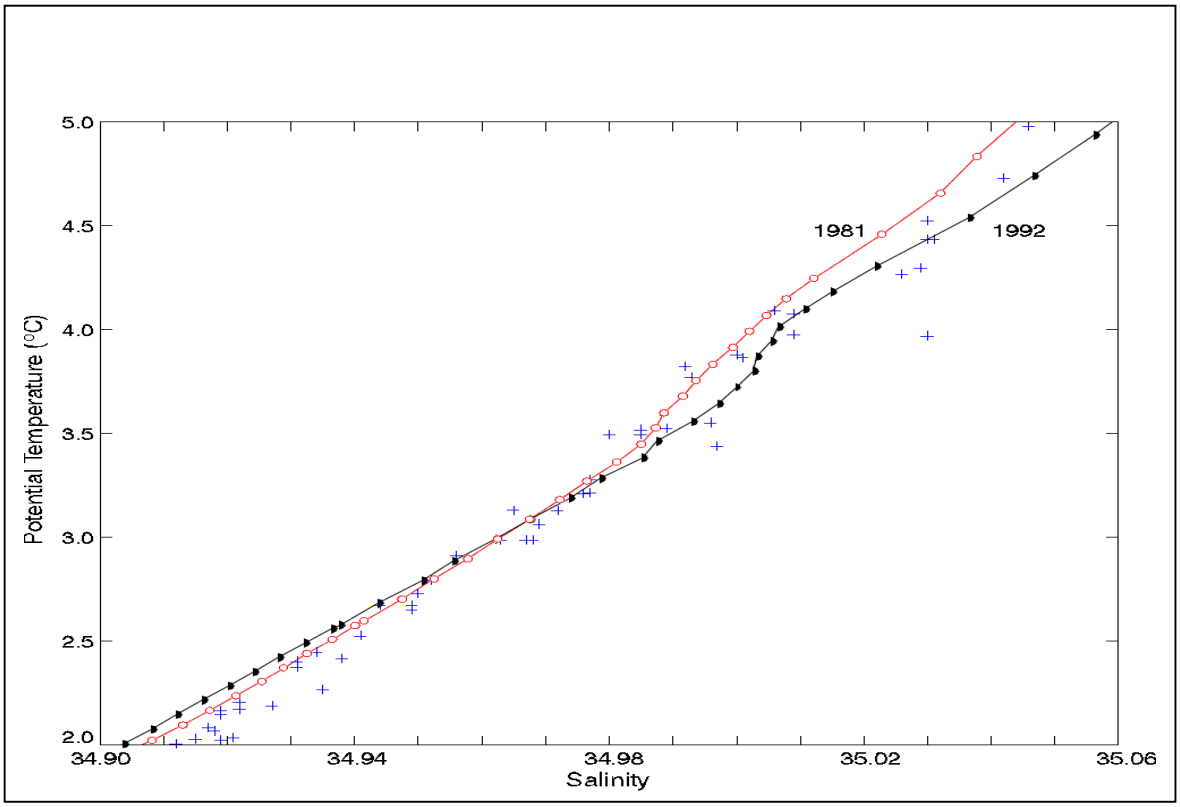

Figure 4.9 Potential temperature-salinity relationship for North Atlantic Deep Water between 65ºW and 75ºW near the western boundary. Continuous curves for 1992 (black line) and 1981 (red line) represent averages on density surfaces listed in the caption for figure 4.6 over all the stations within the 10º-longitude band. Isolated values are indicated for all 1957 water samples (+) with potential temperature between 2ºC and 5ºC between 65ºW and 75ºW.

In order to assess whether the changes might be larger right at the western boundary, where the strongest equatorward flows of NADW occur, averages over the stations within 200 km of the Bahamian continental slope were examined but they yielded essentially the same salinity values as found in the 10°-longitude averages between 65° and 75°W.

Thus, there appear to be small changes in the water mass characteristics of the North Atlantic Deep Water, with salinity increasing somewhat from 1981 to 1992 in the upper core but decreasing slightly in the deeper core. Both changes are close to the limits of detectability.

4.2.5 Antarctic Bottom Water

For the Antarctic Bottom Water banked up against the Mid Atlantic Ridge in the western basin, we compared 1981 and 1992 averages on σ_4 surfaces (potential density anomaly referenced to 4000 db) between 55°W and 65°W to find a very small freshening from 1981 to 1992 by 0.001. Such difference is clearly within the measurement uncertainty. The AABW salinities for 1957 bottle samples with potential temperature below 1.9°C are about 0.004 higher than either the 1981 or 1992 salinities, presumably reflecting the high salinity bias in reported *Discovery* salinities. Hence we cannot conclude that there are any measurable changes in the water mass (θ-S) properties of AABW in the subtropical North Atlantic over the 35-year period from 1957 to 1992. The temperatures of the coldest AABW did notably decrease from 1981 to 1992, however, as first shown by Parrilla *et al.* (1994a). While the bottom temperatures for 1957 and 1981 remained essentially the same, the 1992 bottom temperatures of the AABW banked against the Mid Atlantic Ridge (55°W to 65°W) are 0.025°C colder than either the 1957 or 1981 bottom temperatures. For example, the bottom potential temperatures are significantly colder than 1.5°C at 24.5°N for the first time in 1992. The area and flow of AABW do not seem to be correlated with these changes in the bottom temperature: the shape of the 1.8°C isotherm against the Mid Atlantic Ridge (Fig. 4.10) indicates that the area of AABW is smallest in 1981 with about equal areas in 1957 and 1992, while the strongest flow, as indicated by steepest isotherm slope, occurred in 1981. Thus, the coldest bottom temperatures in 1992 correspond neither to a larger area of AABW nor to a stronger flow of AABW.

4.2.6 Overall distribution of changes in water mass characteristics

To begin to appreciate the vertical and zonal changes in water mass characteristics, we average the 1981 and 1992 CTD station measurements over 10°-longitude bands on density surfaces using potential density anomaly (σ_θ) for water masses above 500 db, σ_1 for water masses between 500 and 1500 db, σ_2 for water masses between 1500 and 3000 db, and σ_4 for water masses below 3000 db. (The set of density surfaces used is listed in the caption for figure 4.6). For each CTD station, the potential temperature and salinity

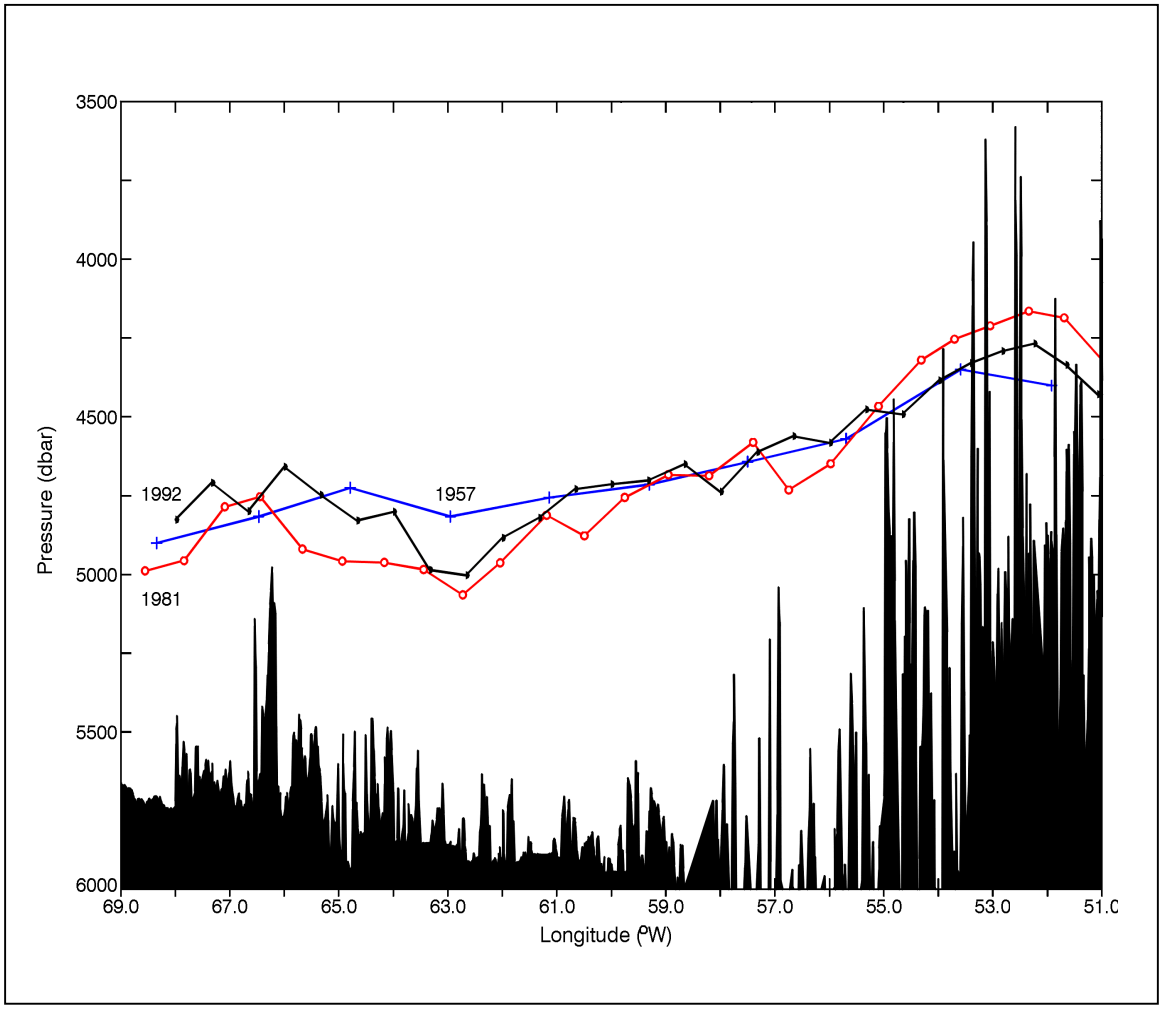

Figure 4.10. Distribution of Antarctic Bottom Water banked up against the western side of the Mid-Atlantic Ridge in 1957 (blue line, +), 1981 (red line, o) and 1992 (black line, •). The 1.8ºC isotherm is chosen here to represent the shape of the AABW layer.

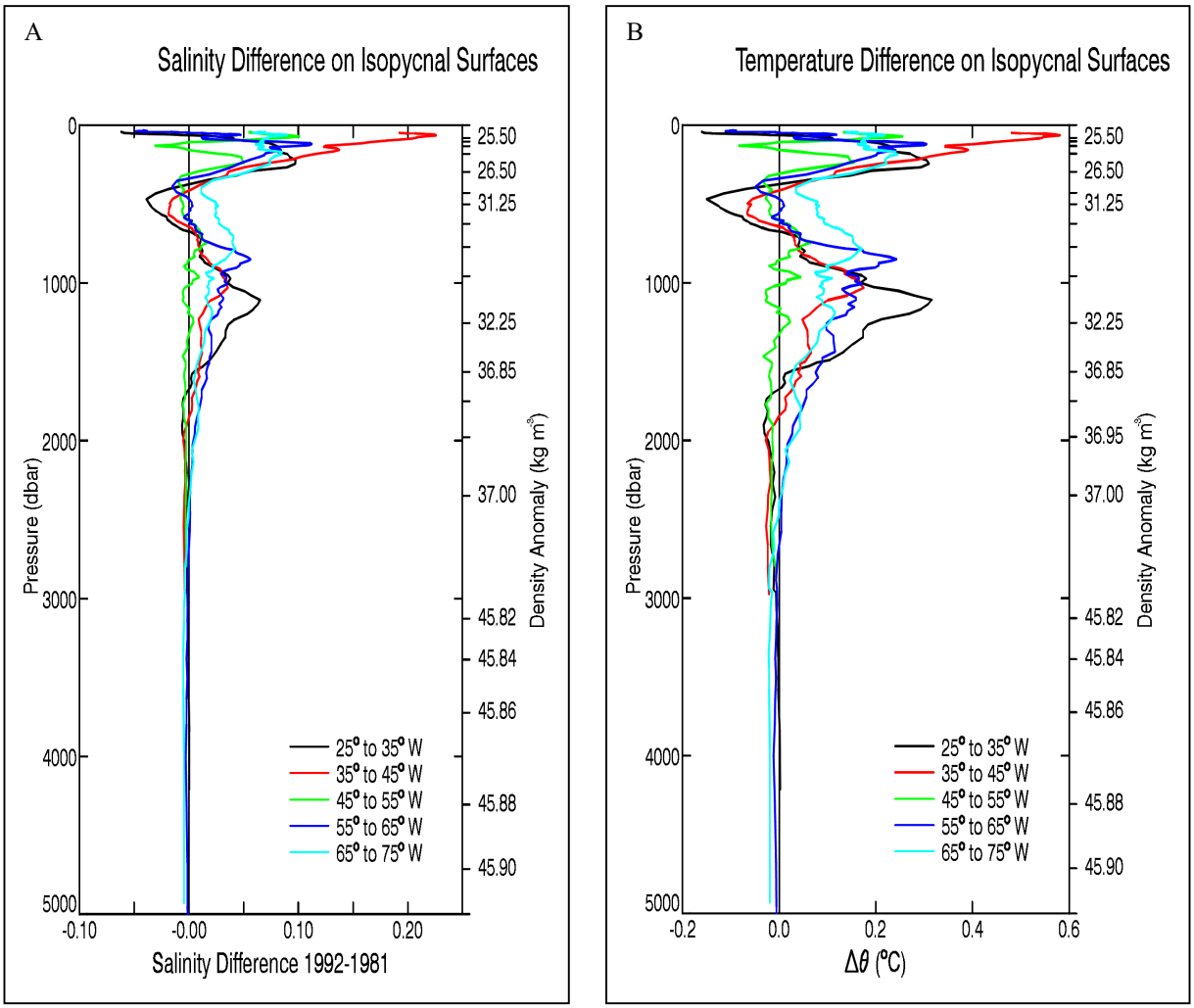

Figure 4.11. Average changes from 1981 to 1992 A) in salinity and B) in potential temperature (ºC) in isopycnal surfaces over 10º-longitude bands. The changes are calculated by finding the salinity, potential temperature and pressure for the set of isopycnals listed in the caption of figure 4.6 for each within the 10º-longitude band, and then averaging the salinities, potential temperature, and pressure over all stations within the band. The differences (1992-1981) in salinity and potential temperature are then plotted against the averaged pressure of the isopycnal surfaces. Thus, these profiles of changes in water mass characteristics on density surfaces are presented linearly versus pressure (left axis), but the corresponding density anomaly values are also indicated (right axis).

on each density surface is identified by interpolating between 10 db values. Then the potential temperatures and salinities are averaged for all stations within the 10°-longitude bin and the average pressures of the isopycnal surfaces are determined. The salinity differences (Fig. 4.11A) for the five 10°-longitude bands demonstrate the broad increase in salinity along 24.5°N over the past decade. From the surface down to nearly 2000 db, in virtually every longitude band there are higher salinities in 1992 than in 1981. The only exception is a small region of freshening between 400 and 600 db (11° to 14°C) in the eastern parts of the section. The upper waters above 400 db have become saltier by as

much as 0.2 and the intermediate waters below 600 db (from 10° down to 4°C) have become saltier by as much as 0.06 on isopycnal surfaces.

There are, of course, compensating increases in temperature (Fig 4.11B) corresponding to these increases in salinity on density surfaces of order 0.5°C in the upper waters and 0.2°C in the intermediate waters. Curiously, the minimum increase in salinity (or temperature) occurs in the central part of the 24.5°N section between 45°W and 55°W, where the salinity minimum associated with AAIW influence is strongest. In the deep waters below 2000 db or 3.5°C, there appears to be a general decrease in salinity (and temperature) on isopycnal surfaces, with the strongest signal in the western basin where, as noted above, lower NADW salinities are 0.005 fresher in 1992 than in 1981.

Contoured sections of the changes from 1981 to 1992 in potential temperature, salinity and oxygen on density surfaces (Fig. 4.12) indicate the same features showing that temperature and salinity have increased over the top 2000 db and decreased below. The changes in temperature and salinity on density surfaces exhibit similar zonal uniformity to the changes found at constant pressure shown in figures 3.8B and 3.9B. As exceptions to the zonal uniformity, there does appear to be a tongue of lower temperature and salinity penetrating westward from the eastern edge of the section at about 500 db and a small region of temperature and salinity decrease in the intermediate waters just west of the crest of the Mid Atlantic Ridge (Fig. 4.12A and B). The oxygen changes (Fig. 4.12C) appear more patchy in the thermocline, but there is a broad decrease in oxygen almost everywhere below about 900 db. Small regions of increased oxygen from 1981 to 1992 appear in the deep water on the eastern and western flanks of the Mid Atlantic Ridge and right next to the western boundary at 2000 and 3200 db, suggesting more rapid ventilation by the deep western boundary current.

Overall average profiles of the changes in salinity, potential temperature, pressure and oxygen from 1981 to 1992 on isopycnal surfaces (Fig. 4.13) are derived by averaging potential temperature, salinity, pressure, and oxygen on each isopycnal surface from 24.5°W to 75.5°W across the 1992 and 1981 sections. Differences of zonally averaged potential temperature, salinity, pressure and oxygen (1992-1981) are then plotted versus average pressure of the isopycnals for both sections. Potential temperature and salinity on isopycnal surfaces increased from 1981 to 1992 (Fig. 4.13A and B) from near surface

σ_θ=25.5 (average pressure 80 db) down to σ_2=36.93 (average pressure 1890 db) except for a small range between σ_1=31.24 and 31.48 (500 to 620 db). In the upper 250 db, the salinity increase is of order 0.06 to 0.08, while in the intermediate waters the increase is of order 0.025. In conjunction with the salinity increases, potential temperature on isopycnal surfaces also increased by order 0.2°C in the upper 250 db and by order 0.12°C in the intermediate waters. While the maximum salinity and temperature increases in the intermediate waters occurred at σ_1=32.14 (0.026 and 0.132°C), the increases are quite uniform between σ_1=31.7 and 32.3 (750 and 1350 db).

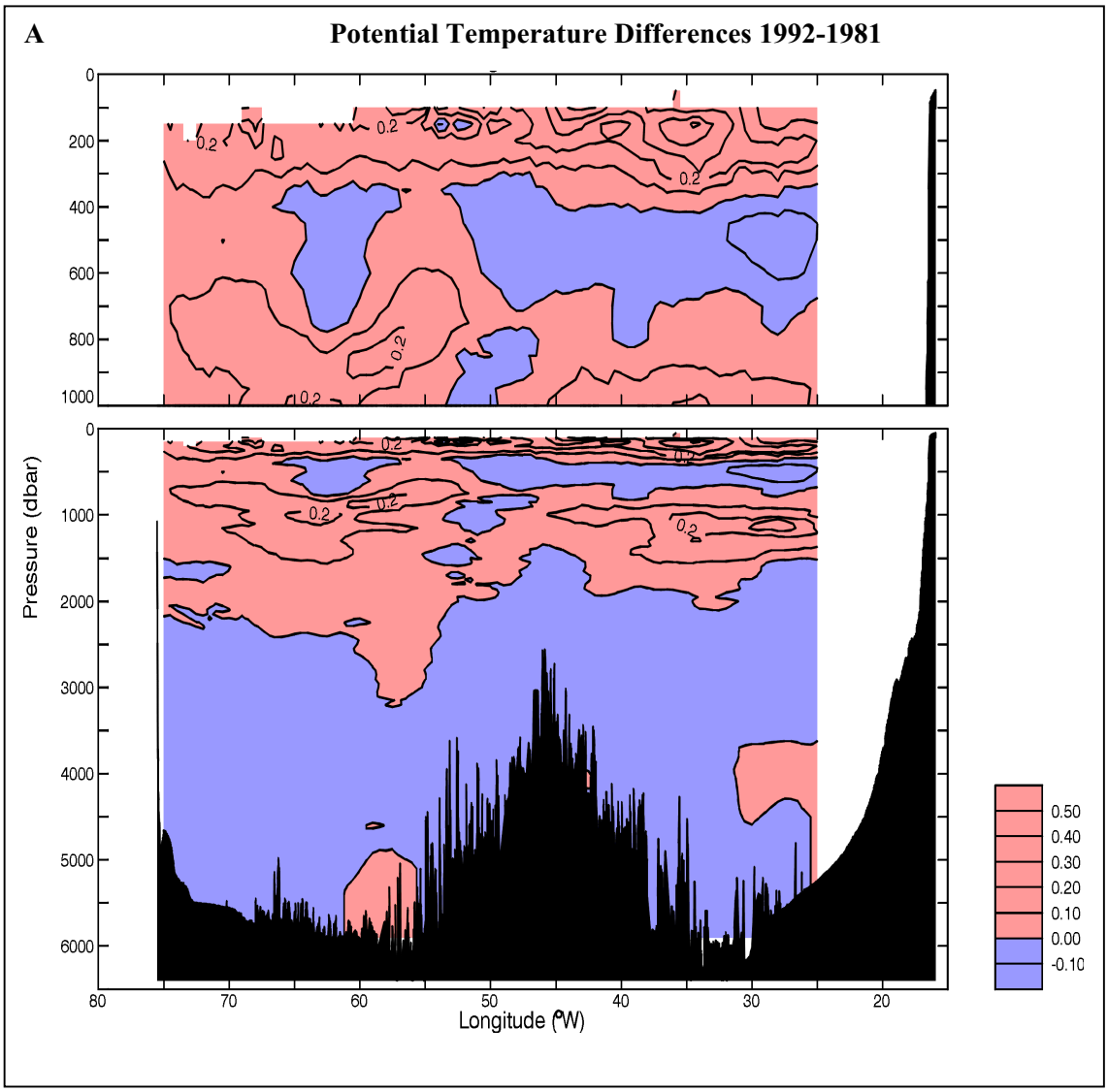

Figure 4.12. Zonal sections of the differences (1992-1981) in (A) potential temperature (ºC), (B) salinity and (C) oxygen (ml l^{-1}) on isopycnal surfaces across 24.5ºN in the subtropical Atlantic Ocean. For each station the salinity, potential temperature and pressure are found for the set of isopycnals surfaces listed in the caption of figure 4.6. Values from the individual stations are gridded at 0.5º-longitudeintervals from 24.5ºW to 75.5ºW. Differences are filtered zonally with a 300-km Gaussian filter. The gridded averaged pressure of the isopicnal surfaces for 1992 and 1981 are also filtered and used as vertical coordinate.

B **Salinity Differences 1992-1981**

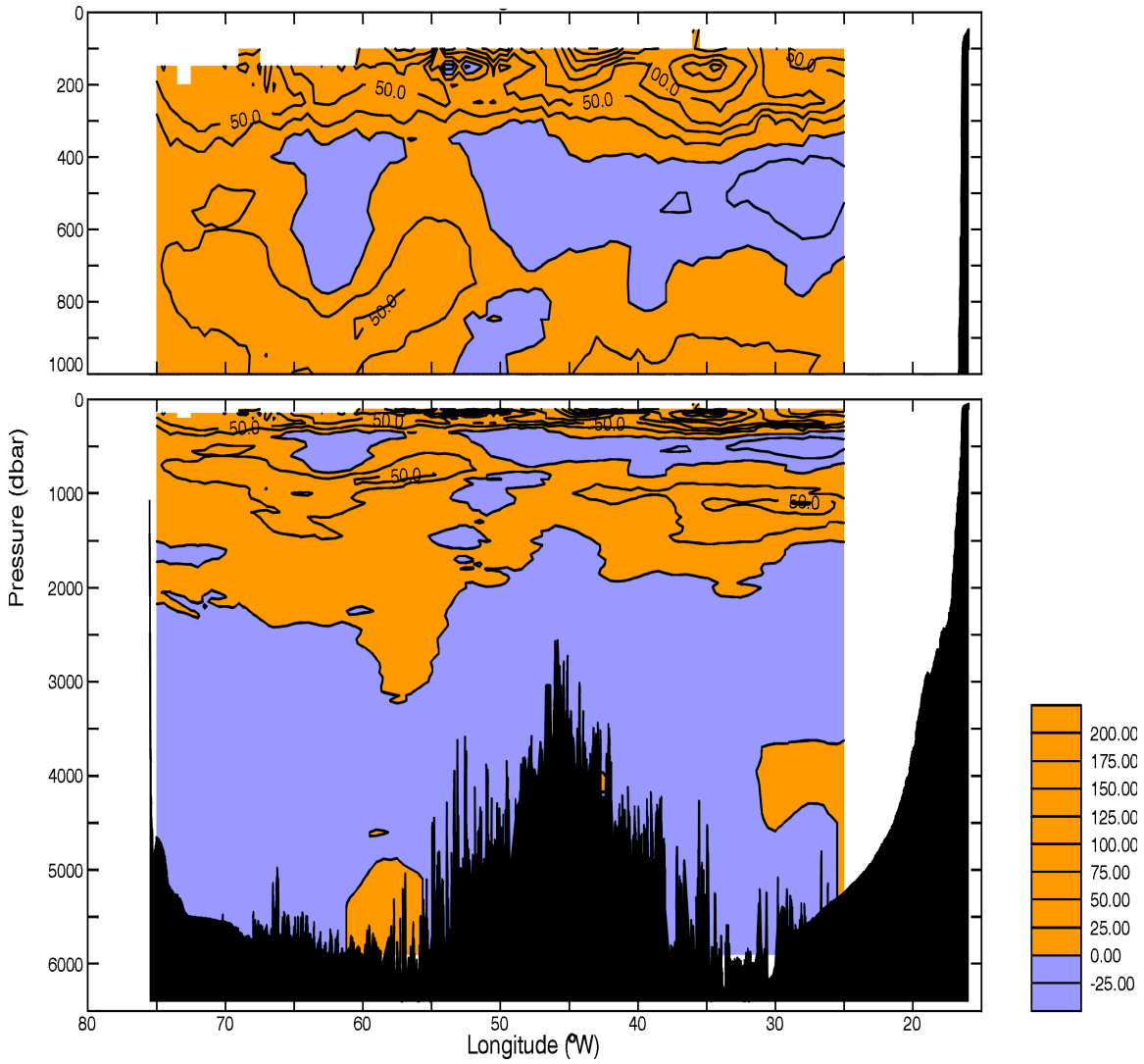

For isopycnals with average pressures greater than 1900 db, the salinity decreased from 1981 to 1992 but only by amounts less than 0.004, and the potential temperature decreased by less than 0.017°C. On average, the isopycnals shallowed from 1981 to 1992 (Fig. 4.13C) over the range from 300 to 930 db by amounts less than 11 db, which would yield a cooling at constant pressure. From 940 to 3260 db, the average isopycnals deepened from 1981 to 1992 with a maximum descent of 20 db at σ_2=36.82 (1470 db) and such deepening yields a warming at constant pressure throughout almost the entire water column, oxygen decreased from 1981 to 1992 (Fig. 4.13D). Only in the upper 220 dbar does oxygen increase by order 0.06 ml l^{-1}. There is a broad range of decreasing oxygen by as much as 0.15 ml l^{-1} from 660 to 3120 dbar in the range of the intermediate and upper deep waters. In the deep waters below 3700 dbar, oxygen has decreased by order 0.05 ml l^{-1}.

The combined effects from 940 to 1890 db of warming on isopycnal surfaces and deepening isopycnals yields the striking warming from 1981 to 1992 found by Parrilla *et al.* (1994a). For example, at σ_1=32.14 (1100 db) where the maximum warming of 0.132°C on isopycnals in the intermediate water occurs, the descent of that isopycnal by only 4.7 db gives rise to an added increase in temperature by 0.024 so that the warming at constant pressure from 1981 to 1992 is found to be 0.16°C (previous chapter). Thus, at the level of

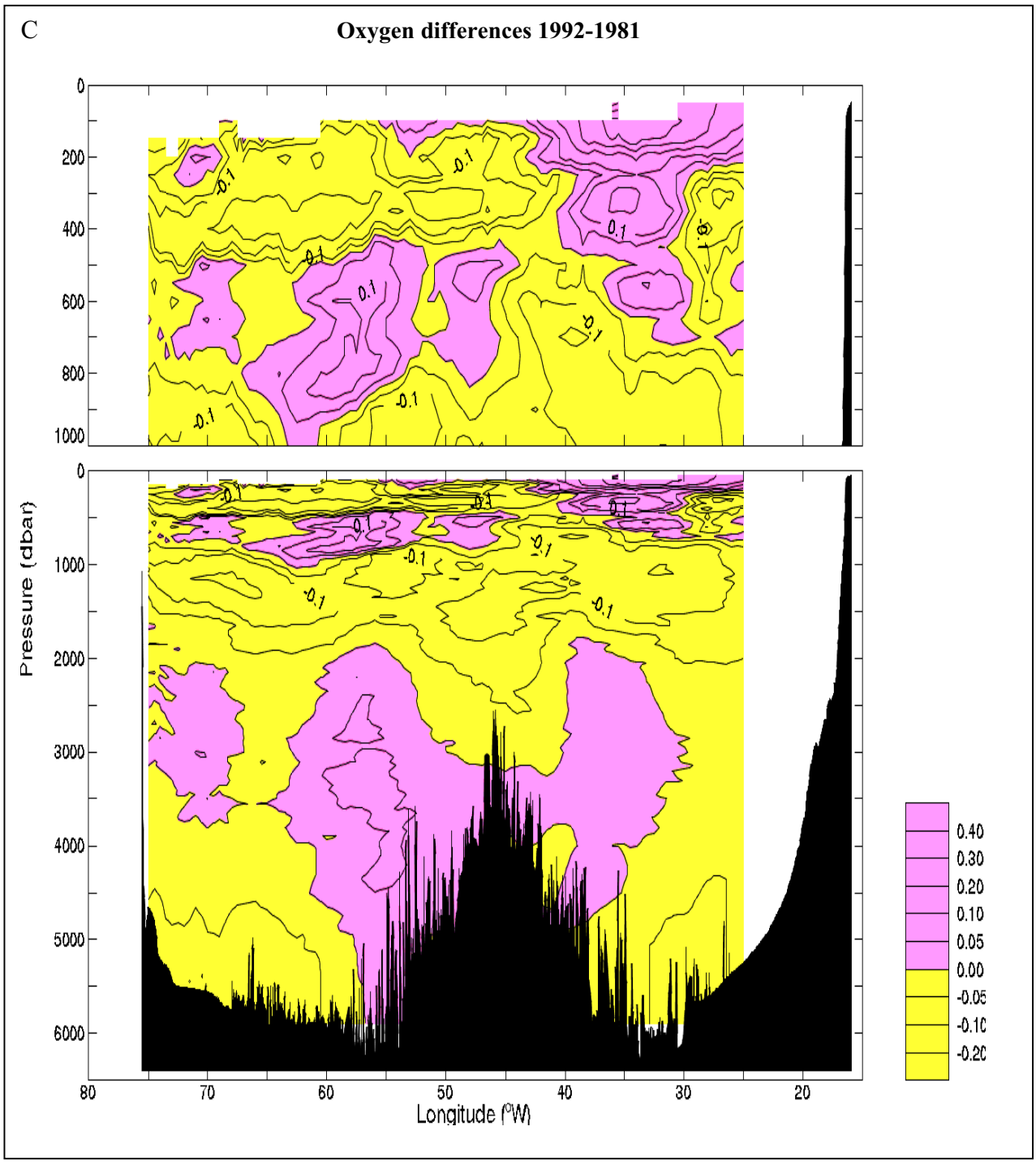

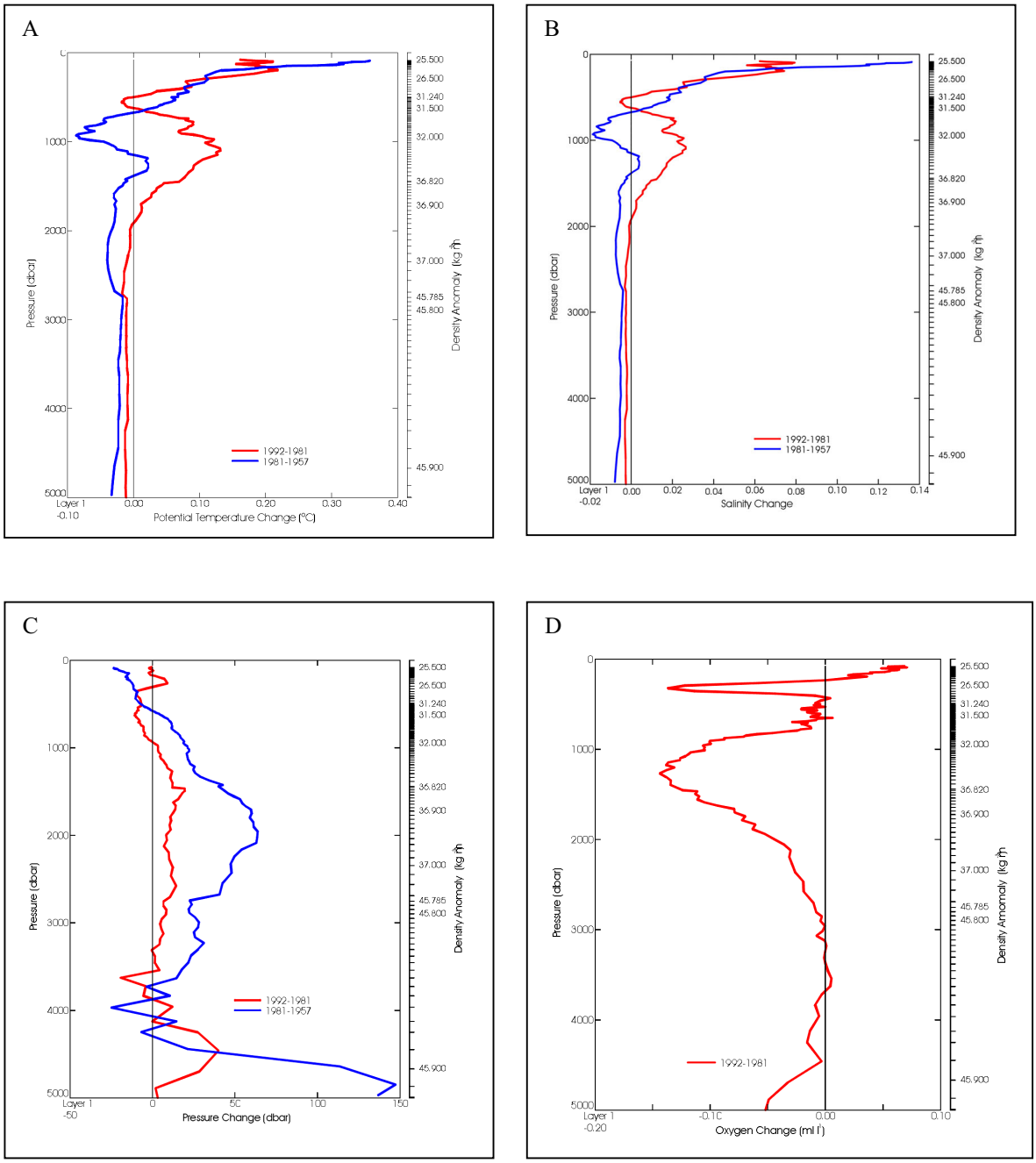

Figure 4.13. Profiles of zonally averaged differences in (A) potential temperature (ºC), (B) salinity, (C) pressure (db) and (D) oxygen (ml l^{-1}) on isopycnal surfaces across 24.5ºN in the subtropical Atlantic Ocean. For each station, the salinity, potential temperature, pressure and oxygen are found on the set of isopycnals surfaces listed in the caption of figure 4.6, and the values are then gridded at 0.5º-intervals from 24.5ºW to 75.5ºW for each of the 3 sections. The averaged differences, 1992-1981(red) and 1981-1957 (blue), are then calculated and plotted against the average 1992 and 1981 pressures. Thus, these profiles of change in water mass characteristics on isopycnal surfaces are presented linearly versus pressure (left axis), but the corresponding density anomaly values are also indicated (right axis).

maximum warming, the change is due principally to the change in water mass (θ-S) characteristics. Slightly deeper, however, the effects are comparable. At σ_2=36.82 (1470 db) where the downward displacement from 1981 to 1992 is a maximum in the intermediate waters, the deepening of the isopycnals by 20 db from 1981 to 1992 generates an increase in temperature of 0.056°C at constant pressure while the increase in potential temperature on the σ_2=36.82 surface contributes an additional temperature increase of 0.046°C.

In the deep water, the observed cooling at constant pressure appears to be dominated by the change in water mass characteristics because the isopycnal surfaces mostly deepened from 1981 to 1992. For example, at σ_4= 45.89 (4480 db) where the greatest decrease in temperature at constant density of 0.013°C occurs, the warming due to the deepening of this isopycnal by 27 db would cause a warming of 0.011°C. Thus, the overall decrease in temperature at constant depth found in the deep water from 1981 to 1992 is dominated by the cooling and freshening of the water mass characteristics on isopycnals but most of these changes in water mass characteristics are masked at constant pressure by the downward displacement of the isopycnals.

The average changes from 1981 to 1992 in salinity and temperature on isopycnal surfaces are integrated vertically from the sea surface down to 5000 db to determine an overall increase in salinity for the centre of the subtropical gyre of 0.005 and an overall average warming of 0.019°C from 1981 to 1992. For comparison, the vertical and zonal averages of the increases in salinity and temperature at constant depth previously reported for the period 1981 to 1992 amounted to 0.003 and 0.010°C. The changes on isopycnal surfaces are independent of the heaving up or down of the density surfaces. The density surfaces themselves have warmed and become saltier. If these changes were entirely due to local air-sea exchanges, these changes would represent a change in the net evaporation of 6.6 cm yr^{-1} and in the heating rate of 1.1 W m^{-2} over the 11-year period from 1981 to 1992.

In order to compare these changes with those from 1957 to 1981, similar averages on isopycnal surfaces were made for the 1957 section across 24.5°N from 24.5°W to 75.5°W. Because there is uncertainty as to whether or not a bias in salinity of 0.004 to

0.006 exists throughout the 1957 data set, we constructed two versions of the averages: one with no alteration made to the 1957 reported salinities and a second with 0.004 subtracted uniformly from all 1957 reported salinities. We show the decadal changes using the unadjusted 1957 salinities, but use the results from the adjusted salinities to qualify the reliability of the estimated changes from 1957 to 1981.

Isopycnals shallowed from 1957 to 1981 by order 20 db in the upper waters above 570 db and deepened by order 50 db in the intermediate and upper deep waters between 600 and 2600 db using either the unadjusted or adjusted 1957 data sets. In the intermediate waters, the downward displacement of the isopycnals from 1957 to 1981 is much more dramatic than the deepening by order 10 db from 1981 to 1992. The changes in water mass characteristics on isopycnal surfaces from 1957 to 1981 are more difficult to assess because there is a marked difference between the averages for the unadjusted and adjusted sets of 1957 salinities. Temperatures and salinities did clearly increase dramatically in the upper 660 db for either set. But in the intermediate waters between 670 and 1140 db, the unadjusted set yields a freshening and cooling by order 0.02 and 0.09°C while the adjusted set yields a more limited freshening and cooling of order 0.01 and 0.06°C over a smaller range between 720 and 1090 db. The adjusted set then yields a small region of higher temperatures and salinities between 1100 and 1500 db which is effectively absent in the unadjusted set. For the unadjusted set, there is nearly constant cooling and freshening on all isopycnal surfaces below 1500 db by order 0.004 to 0.007 and 0.02°C to 0.04°C, while for the adjusted set there is effectively no change in water mass characteristics on isopycnal surfaces below 1500 db.

For the 1957 to 1981 interval, we conclude that there was a dramatic deepening of isopycnal surfaces by order 50 db from 1957 to 1981 in the intermediate and upper deep waters between 600 and 2500 db; that there was a strong increase in salinity and temperature on isopycnal surfaces in the upper waters above 600 db; that there was at least a small decrease in salinity and temperature on isopycnal surfaces in the intermediate waters between 700 and 1100 db and a small increase in temperature and salinity between 1160 and 1370 db; but that it is not possible to determine whether the water mass properties in the deep waters changed from 1957 to 1981. The warming at constant depth from 1957 to 1981 between 800 and 2700 db across 24.5°N reported by Roemmich and Wunsch (1984) is clearly due to the downward displacement of isopycnal surfaces by order

50 db with only a minor contribution from changes in water mass characteristics on isopycnal surfaces. That such downward displacement is the mechanism for the warming from 1957 to 1981 is in striking contrast to the change in water mass characteristics which leads to the continued warming from 1981 to 1992.

4.3 Discussion

Levitus (1989a) first produced large-scale maps of the interpentadal changes in depths of isopycnals and changes in properties on the isopycnals for the North Atlantic and Bindoff and McDougall (1994) have emphasised that this separation is a natural one. Such separation of observed climate changes provides information on several different mechanisms by which the ocean climate could change. First, if more intermediate or deep water were formed, one would expect to see an increased thickness of a particular density layer due to the added water mass volume. Such changes could appear over relatively short time scales since variations in layer thickness can quickly propagate into the interior ocean. Second, isopycnals might move up or down in response to basin-scale changes in the wind forcing as the gyre circulation changes intensity. Again, the response to changing wind forcing would take place relatively rapidly. Both of the above types of changes could occur without any change in water mass characteristics. Third, if the buoyancy loss conditions under which water masses form change due to increased cooling or higher net evaporation, one would expect to observe changes in the θ-S characteristics of the water masses. Far from the source, these changes would likely occur only slowly as the new characteristics slowly advect and mix into the interior ocean. Thus, there are different time scales associated with these mechanisms for decadal change.

It is important not to lose sight of the fact that this separation into changes in isopycnal depth and changes in water mass properties is model dependent, relying on our understanding that mixing in the interior ocean happens primarily on density surfaces. One could have separated the observed changes at constant depth into any number of other model-derived components, and indeed we made some initial efforts to separate the

observed changes in the intermediate layers at 24.5°N into percentage changes in 3-component water types following Mamayev (1975).

In terms of the mechanisms for the observed changes along 24.5°N, it is clear that the changes from 1957 to 1981 principally involved downward displacement of isopycnals with little change in water mass properties below 500 db. Roemmich and Wunsch (1984), Levitus (1989a, 1989b) and Antonov (1993) reached the same conclusion for decadal changes from 1957 through 1981 in the subtropical North Atlantic. While Roemmich and Wunsch examined changes in volumes of various water masses, we would emphasise the overall large-scale nature of the downward displacement of the isopycnals from 1957 to 1981 with the maximum displacement of 60 db at 2000 db decaying to near zero at the surface and in the deep water. The continued descent of isopycnals from 1981 to 1992 has similar structure, though the maximum downward displacement is only 20 db at about 1500 db. The isopycnals in the middle of the water column (1500 to 2000 db) have descended at a rate of 1.5 to 2.5 db per year since 1957. As there is no apparent large-scale zonal structure to these displacements, we cannot associate this deepening with a spin-up of the subtropical gyre which might occur as the result of the increasing wind stress curl noted by Bunker (1980) from 1947 to 1972.

The striking increases in salinity and temperature on isopycnal surfaces in the main thermocline from 1957 to 1981 to 1992 suggest that the formation conditions of these recently ventilated waters must be changing. A model is, of course, needed to interpret these observed changes in terms of changing air-sea fluxes. In terms of Bindoff and McDougall's (1994) model, the observed changes in the thermocline are consistent with higher net evaporation at the sea surface in the formation region leading to higher salinity. The decrease in oxygen from 1981 to 1992 suggests perhaps less vigorous ventilation of the thermocline.

To explain the increases in salinity and temperature on isopycnal surfaces in the intermediate waters, the model needs to be more sophisticated for this is the depth region where waters of Mediterranean and Antarctic origin mix. Is the higher salinity due ultimately to stronger or saltier outflow of Mediterranean Water over the sill at Gibraltar, or to a lesser northward flow of relatively fresh Antarctic Intermediate Waters? While we would have preferred an explanation based on a westward and southward displacement of

the Mediterranean Water salt tongue, such lateral movement of the Mediterranean Water tongue is in conflict with the observed decrease in oxygen over time. The source strength or character of Mediterranean Water may be changing and, indeed, deep water in the western Mediterranean basin has exhibited increasing salinity and temperature by order 0.02 and 0.07°C over the period from 1955 to 1989 (Rohling and Bryden, 1992). The mixing of the Mediterranean Water as it cascades over the Gibraltar sill, however, would presumably dilute such anomalies by a factor of 10 so that in the intermediate waters of the eastern North Atlantic the salinity and temperature anomalies would then be too small to cause the changes observed along 24.5°N. We know of no information on long term changes in the strength of the Mediterranean outflow. From comparison of the geostrophic meridional circulation across 24.5°N from the 1957, 1981 and 1992 sections, a decrease in northward flow of Antarctic Intermediate Water over time was noted (see next chapter). Thus, the admixture of low salinity Antarctic Intermediate Water may be less which could lead to higher salinities in the intermediate waters. However, such interpretation has difficulty in explaining why the increased salinity is minimum over the crest of the Mid Atlantic Ridge where the most pronounced AAIW signature is generally found and, because AAIW has relatively low oxygen concentrations, a weaker source of low oxygen waters also fails to explain the observed decrease in oxygen on isopycnal surfaces from 1981 to 1992.

In the deep waters where the changes on isopycnal surfaces are smaller, we can explain the increasing salinities from 1981 to 1992 in the upper core of NADW as the result of a lesser source of low salinity waters formed in the Labrador Sea. The shutdown in production of Labrador Sea Water during the late 1960's and early 1970's is well documented (Lazier, 1980); estimated penetration speeds of order 0.8 cm s^{-1} for the upper core of NADW from CFC measurements (Smethie, 1993) suggest that the Labrador Sea anomalies would take of order 15 years to arrive at 24.5°N, that is after 1981 but before 1992; and the lower oxygens particularly in the upper core against the western boundary also suggest a reduced ventilation of this density surface. For the lower core of NADW, the decreasing salinities with time could be attributed to the freshening of deep waters formed in the Greenland-Iceland-Norwegian Sea, first observed by Brewer *et al.* (1983) in the northern North Atlantic.

Certainly more information is needed on the spatial structure of the changes over a basin like the North Atlantic to begin to determine the causes of decadal change. The 24.5°N changes, while intriguing, intrinsically suffer from a lack of information at other latitudes. Here, the use of only the highest quality data has been emphasised to determine the changes in water mass characteristics. But in this analysis of a single well-measured oceanographic section when we are ultimately confronted with the lack of information at other latitudes, we appreciate the large-scale maps that Levitus (1989a, 1989b) and Antonov (1993) have made using all globally available data. We do question, however, how much quality control must be exerted on the global data set before attempting to estimate such large-scale changes in water mass characteristics, especially after our struggle with the 1957 water sample data set, which is widely recognised as being of top quality for its era. Clearly, the changes in water mass characteristics are more readily determined using the horizontally dense and vertically continuous CTD stations which have been standardly taken since about 1980. In fact, there was quite a comprehensive hydrographic survey of the North Atlantic taken during the 1980's and many of these same sections has been repeated during the WOCE time period from 1990 to 1997. Comparison of these North Atlantic surveys a decade apart and then extension of the comparison back to the IGY survey of 1957-58 should establish the large-scale patterns in decadal scale changes of water mass characteristics as well as the changes in depths of the isopycnal surfaces throughout the North Atlantic. The spatial pattern of observed decadal changes could then be compared with realistic coupled ocean-atmosphere simulations with varying air-sea exchange conditions and wind forcing to understand the causes of the decadal changes. In many respects, a case study in which the magnitude and spatial pattern of decadal changes in ocean water mass characteristics in the North Atlantic are determined would provide a sensitive test-bed through which coupled ocean-atmosphere models could be assessed and developed. In this moment after the WOCE data acquisition phase (1990-1997), the AIMS is beginning. The 1992 data set is publicly available from the WOCE Hydrographic Program Office. After the WOCE Conference in May 1998, the use of these data for modelling has largely increased. Results from these simulations are coming.

Chapter 5

Meridional transport and heat flux variations

5.1 Introduction

The Atlantic Ocean, as was shown in previous chapters, has significant exchange of water masses, heat and salt with several marginal seas, regions in which important transformations of water masses take place. A complex thermohaline-driven circulation moves water masses both northward and southward mainly along its western boundary regions. The 24.5ºN transatlantic section provides a census of major intermediate, deep and bottom water masses whose sources are in the Antarctic and far northern Atlantic as well as estimates of the thermohaline circulation of these water masses and of the wind-driven circulation in the upper water column. The 24.5ºN transatlantic section has also provided important estimates of poleward ocean heat transport (Bryden and Hall, 1980; Roemmich, 1980; Wunsch, 1980; Hall and Bryden, 1982; Roemmich and Wunsch, 1985).

The relative importance of sea and air in transporting heat depends upon the latitude. Vonder Haar and Oort (1973) found that, in the region of maximum net northward energy transport by the ocean-atmosphere system (30-35ºN), the ocean carries 47% of the required energy. At 20ºN, the peak ocean flux accounts for 74%. Newell *et al*. (1974), Oort and Vonder Haar, (1976), Carissimo *et al*. (1985) and Hsiung and Houghtby (1989) have updated those values. Our section at 24.5ºN is located where the ocean likely transports poleward more of the absorbed solar energy than does the atmosphere to maintain the global heat balance (Bryden, 1993).

The direct method for calculating ocean heat transport is based on oceanographic data. The more problematic point is the determination of the reference level for geostrophic calculations of the velocities. Bryan (1962) used wind stress values to calculate Sverdrup transport. Bryden and Hall (1980) and Hall and Bryden (1982) required that the ocean interior transport balances the Gulf Stream transport through the Straits of Florida. Roemmich (1980), Wunsch (1980) and Roemmich and Wunsch (1985) used the inverse method for estimating reference level velocities (Wunsch, 1978) in two sections across

24ºN and 36ºN. In the inverse method, water masses, or layers, in which the transport out of the area between two sections must be equal to the transport into the area, are defined.

Hall and Bryden (1982) estimated the northward heat flux across 24.5ºN in the 1957 IGY section to be 1.2 x 10^{15}W. The same result was obtained by Roemmich (1980) using inverse calculations. Roemmich and Wunsch (1985) compared the 1957 data with the 1981 section and found the heat transport to be indistinguishable from computations of air-sea heat exchange. They attributed the steadiness of the heat transport to the invariance of the zonally averaged meridional circulation. Combining the Pacific heat transport with the established value of Atlantic heat transport across 24.5ºN, Bryden *et al*., (1991) estimated a total ocean heat transport of 2.0 x 10^{15}W, larger than the atmospheric heat transport of 1.7 x 10^{15}W.

In this chapter the data of the three sections (chapter 2 and figure 2.1) are used to examine the meridional fluxes of mass and heat in the subtropical North Atlantic and their possible changes from 1957 to 1992.

5.2 Components of Atlantic heat transport at 24.5ºN

The heat flux due to ocean currents across any latitude is well approximated by

$$T = \int\int \rho \; C_P \; \theta \; V \; dz \; dx \qquad (5.1)$$

where the integration is over depth and longitude and V is the north-south component of the absolute velocity of the water across the latitude circle in question (Bryan, 1962), in this case 24.5ºN. The variables ρ, C_p and θ are the density, the specific heat capacity and the potential temperature respectively. The mass of the system must be conserved. As we consider the North Atlantic to be essentially a closed basin north of 24.5ºN, the meridional heat transport in the North Atlantic alone can be calculated by integrating eq. (5.1), across a complete transatlantic section (Hall and Bryden, 1982).

Northward heat transport by ocean currents is the result of water flowing northward at one temperature and returning southward at a lower temperature. Temperature fluxes are considered to be the product of the estimated mass transport and a calculated averaged

temperature. This temperature, called velocity-weighted average temperature, is calculated by dividing temperature flux by volume transport:

$$t = \frac{\int_W^E \int_{-H(x)}^O \theta \; V \; dx \; dz}{\int_W^E \int_{-H(x)}^O V \; dx \; dz} \qquad (5.2)$$

where E and W represent the eastern and western limits of the zonal section and H(x) is the ocean depth.

Following the method of Hall and Bryden (1982), transport at 24.5ºN is separated into the Gulf Stream transport through the Florida Straits and the mid-ocean transport in the section between Africa and the Bahamas. In this mid-ocean section, transport is separated into geostrophic and Ekman transport components. Since conservation of mass is required, northward transport by the Gulf Stream flowing through the Straits of Florida and by the wind-driven Ekman transport in the surface layer must be balanced by the southward geostrophic transport in the interior of the section.

5.2.1 Florida Straits flow

During the 1981 and 1992 cruises, sections across the Florida Straits were made at 26ºN. However, to consider a mean flow across the Florida Straits section, long term values rather than the cruise data will be used. Larsen (1992) estimated the mean voltage-derived transport for the Florida Current at 27ºN to be 32.3 ± 3.2 Sv (1 Sv = 10^6 $m^3 s^{-1}$), and the velocity-weighted temperature to be 19.1 ± 0.6ºC. Using more than two years of PEGASUS ocean current measurements at 27ºN, Leaman *et al*. (1987) found a similar average northward volume flux for the Florida Current of 31.7 ± 3.0 Sv. They also gave a transport of 27.3 Sv between Key West and Havana (but this value may be less accurate because of meandering effects).

There appears to be little interannual variability in Florida Straits transport, as Larsen found the annual-averaged Florida Straits transport to range only from 31.2 Sv to 33.9 Sv over the years 1969-1974 and 1981-1990. Unfortunately, Larsen's electromagnetic cable measurements of Florida Straits transport are not available for the period of any of

the 1957, 1981 and 1992 hydrographic sections across 24.5ºN. Part of the variability is due to seasonal changes. Molinari *et al.* (1990) reported a standard deviation of 2.8 Sv for the Florida Straits flow mostly due to seasonal variability

According to Finlen (1966), approximately 2 Sv on average joins the Florida Current in the Straits of Florida through the Providence Channels located at roughly 26ºN, which is effectively north of the 24.5ºN section. Subtracting this amount to the values given previously we obtain the northward transport of the Florida Current across 24.5ºN to be 29.5 Sv. The velocity-weighted average temperature is taken to be 19.1º C. These values are consistent with the values given by Niiler and Richardson (1973).

5.2.2 Ekman layer flow

The zonally integrated meridional Ekman volume transport is computed from:

$$\int(\tau^x / f \quad \rho)\, dx \qquad (5.3)$$

where τ^x is the eastward wind stress, ρ is the density and f is the Coriolis parameter. The northward Ekman transport at 24.5ºN was estimated by Macdonald (1995) to be 5.4 Sv computed from the European Centre for Medium Range Weather Forecast (ECMWF) wind stress values (Trenberth *et al*., 1990) with a standard deviation in annual mean of 0.7 Sv. Hall and Bryden (1982) used Leetmaa and Bunker (1978) climatology which gives 5 Sv for the Ekman transport, Roemmich and Wunsch (1985) used Hellerman and Rosenstein (1983) climatology which result in an Ekman transport of 6 ± 2 Sv. Isemer and Hasse (1987) gave even higher values than Hellerman and Rosenstein (1983) (Böning *et al.*, 1991). Here the recent wind stress climatology by Trenberth *et al.* (1990) was used, which gives an intermediate value of 5.4 ± 0.7 Sv.

Taking into account new data obtained by satellite (ERS1) from August 1991 to March 1995 provided by IFREMER (1996), the mean and the standard deviation for this period were calculated. August mean zonal wind stress is -0.46 dyn cm^{-2} (which would result in an Ekman transport of 4.4 Sv), the annual mean is -0.42 (seasonal range from -0.32 to -0.46). Values are lower than Hellerman and Rosenstein (1983), but variability in

the Ekman transport is ± 0.7 Sv, which is the same as the value given by Trenberth *et al.,* (1990) and adopted in this thesis.

The temperature transport was determined by Hall and Bryden (1982) from

$$\int(\tau^x / f \ \rho)\theta C_p \, dx \qquad (5.4)$$

where the potential temperature θ was obtained by averaging the surface values with the 50 meter temperature values. Using eq. (5.3), they obtained a velocity-weighted average temperature of 26.0ºC for the Ekman flow in the mid-ocean section. Sea surface temperature varies by only ±0.3ºC over the three sections.

5.2.3 Mid-ocean geostrophic flow

Our objective is to compare the heat flux estimates made from the 1957, 1981 and 1992 sections. A zonally averaged profile of geostrophic velocities is calculated and then a uniform barotropic velocity is determined to achieve a mass balance for the complete zonal transect. Then the heat transport of the three different cruises is computed and compared. A mass conservation argument requires that the 29.5 Sv of northward transport in the Florida current and 5.4 Sv of northward Ekman transport be compensated by 34.9 Sv of southward transport within the mid-ocean section.

For the geostrophic calculations we need an initial reference level. No direct measures of velocity were available for any of the cruises. The general northward flow of AABW and Antarctic Intermediate Water (AAIW) below and above the southward flow of NADW respectively, suggest two possible reference levels, one at about 4000 m and the other at roughly 1000 m (Speer and McCartney, 1991). Roemmich (1980) used both 1000 and 4000 m, Roemmich and Wunsch (1985) used 1300 m. Saunders (1982) states that for the eastern North Atlantic, a deep level of no motion at 3200 db is satisfactory and cannot be distinguished from a shallower reference level at 1000 m given the errors in computing the geostrophic transport.

A comparison of deep water transport in the eastern basin shows a negligible transport in all the three cruises using 3200 dbar as a reference level. The eastern basin is essentially separated at 24.5ºN by the Mid Atlantic Ridge for waters deeper than 3000 m.

Thus we take our reference level at 3200 db from the eastern boundary (Africa) out to the beginning of the deep western boundary current at 69ºW. To identify the position for change in reference level, we relied on the oxygen distribution which has a sharp transition at 5.5 ml l^{-1} at about 69ºW in the 1957 cruise and at 6 ml l^{-1} in the last two cruises. [There was a problem with 1957 oxygens; Worthington (1976; page 54 footnote) suggested a scaling factor of 1.048 to force agreement with modern oxygen data.] Such distribution suggests that all of the high oxygen waters along the western boundary between 1000 and 4000 m depths out to 69ºW are flowing southward as part of the deep western boundary current. East of 69ºW, the high oxygen in the waters below 3400 m is indicative of the deep recirculation gyres of NADW that have been noted at many locations throughout the North Atlantic (Schmitz and McCartney, 1993). This frontal area is also shown by the CFC's distribution (see figures 4.8A and B). This oxygen front is situated between stations 3618 and 3619 in 1957 data (Fuglister, 1960), between stations 220 and 221 in 1981 data (Figure 3f on Roemmich and Wunsch, 1985) and between stations 87 and 88 in 1992 data (see the equivalent 260 μmol kg^{-1} isoline in Figure 2.4). Thus from stations 3619 (68º 20' W), 221 (69º 4' W) and 88 (68º 39' W) to the Bahamas we have used 1000 db as reference level for our geostrophic calculations for the three cruises so that all the flow deeper than 1000 db is southward along the boundary.

The 1981 *Atlantis II* section was further north than 24.5ºN at the eastern boundary. Transport from 25ºW to the African first station was calculated to be around 2 Sv, quite close to the result from the coast up to this longitude at 24.5ºN calculated for the *Hespérides* 1992 cruise. Thus we have made no extra adjustments for the 1981 section and have used the total section extent for the calculations.

CTD data from the 2 dbar station files for 1981 and 1992 cruises were smoothed to 20 dbar. IGY 1957 data were interpolated in depth to 20 dbar station files. Geostrophic velocity profiles for each station pair were calculated. Distances and areas between stations were calculated every 20 db, vertically integrated geostrophic transport was obtained for every pair of stations and then horizontally integrated for the total section. Zonally averaged geostrophic velocity, potential temperature and salinity were calculated every 20 db.

With the basic reference level of 3200 dbars from Africa out to the deep western boundary current and then 1000 db west of the oxygen transition, the mid-ocean geostrophic transport was calculated (Table 5.1). Geostrophic velocity profiles using this reference level are consistent with results presented by Hall and Bryden, (1982) and Roemmich and Wunsch, (1985) with generally southward flow in the thermocline, AAIW flowing north between 800 and 1100 m, NADW flowing southward and AABW flowing northward in the deep waters.

Reference level transport is very dependent on eddies located close to the area where the reference level changes from 3200 db to 1000 db. This behaviour affects 1981 and 1992 cruises when the spacing is eddy resolving. The same calculation was done just moving the change in reference level by one station for the 1992 data and the resulting reference level transport for 1992 becomes larger than that for 1981, but the mean circulation heat transport remained the same after the barotropic velocity was adding so that the mass is balanced.

A barotropic velocity of -0.1049 cm s^{-1} is added uniformly to the 1992 *Hespérides* section to make the southward mid-ocean geostrophic transport exactly equal to the combined northward Ekman and Florida Straits transport of 34.9 Sv (Table 5.1). This barotropic velocity equalled -0.0424 cms^{-1} for the *Atlantis* 1981 and -0.1366 cms^{-1} for the IGY 1957 data. Figure 5.1 presents the zonally-averaged geostrophic meridional transport per unit depth (equal to the zonal integral of the geostrophic velocity across the section) at 24.5ºN across the transatlantic section for the three cruises, 1992, 1981, and 1957.

A zonally-averaged potential temperature profile for each of the three sections was calculated (Fig. 5.2A). Using this temperature profile with its associated velocity, it was possible to estimate transport by temperature classes at this latitude. Zonally-averaged salinity profiles for each section were also calculated (Fig. 5.2B). In figure 5.3 differences between 1992-1957, 1992-1981 and 1981-1957 on zonal mean potential temperature and salinity are presented. Fluxes of temperature and salinity were both calculated.

	Ref. level transport (Sv)	Area ($10^8 m^2$)	Barotropic velocity (cm s^{-1})	Total transport (Sv)
IGY 1957	2.79	276	-0.1366	-34.9
Atlantis II 1981	-21.60	314	-0.0424	-34.9
Hespérides 1992	-4.59	290	-0.1049	-34.9

Table 5.1. Reference level transport (Sv), Area ($10^8 m^2$), Barotropic velocity (cm s^{-1}) and Total transport (Sv) for each of the cruises, 1957, 1981 and 1992.

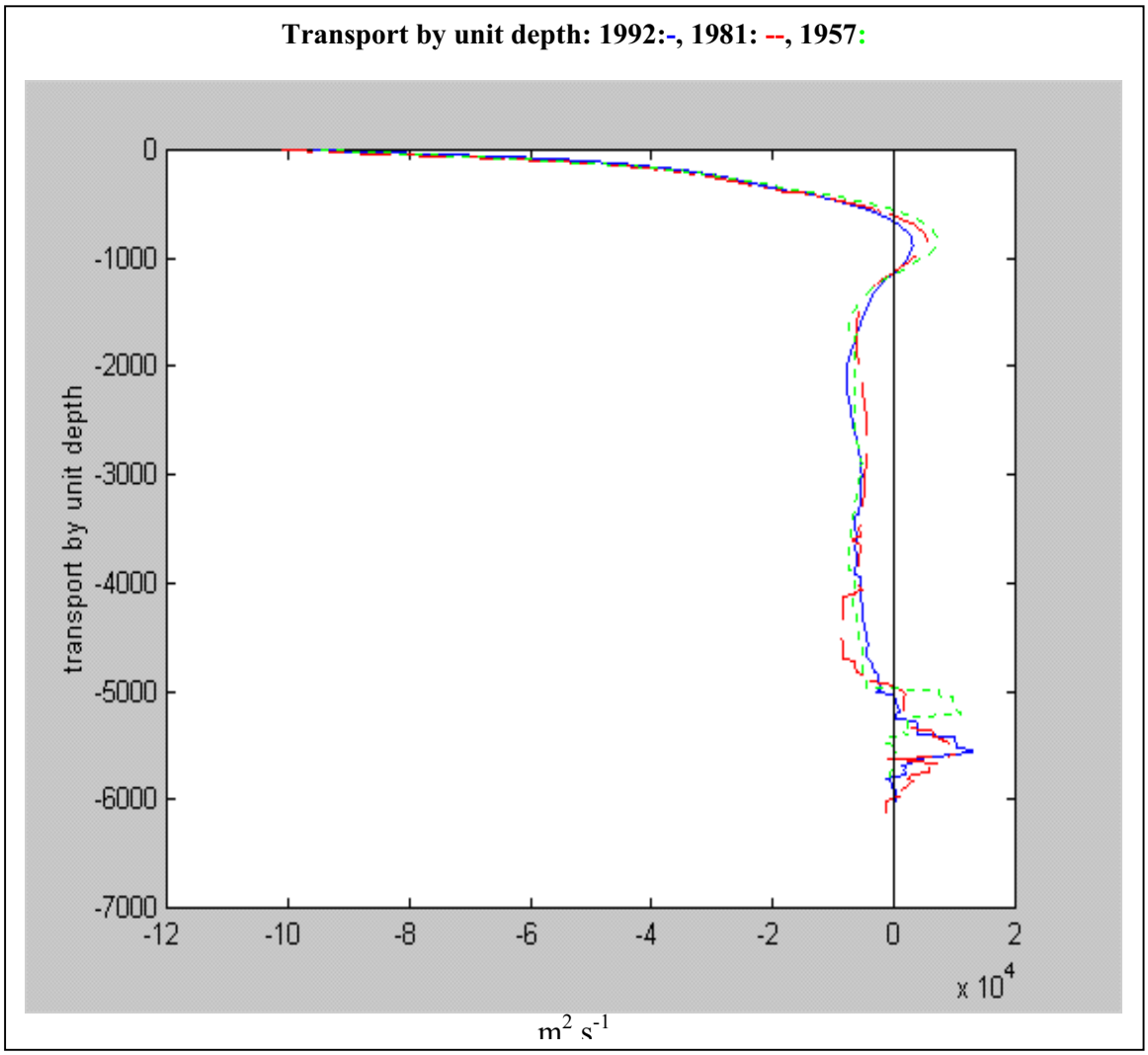

Figure 5.1. Zonally-averaged geostrophic meridional volume transport per unit depth at 24.5ºN across the transatlantic section for the three cruises, 1992 (solid blue), 1981 (dashed red) and 1957 (dotted green).

In table 5.2 transport for the three cruises for different depth intervals is presented. A comparison of these transport shows a quite similar scheme in overall vertical structure. The southward flow in the thermocline above 600 m, is quite similar for the three cruises:

the total transport varying from -17.1 in 1957, to -18.7 in 1981, to -17.4 Sv in 1992. A core of northward flow between 600 and 1200 m depths shows the influence of the AAIW. The transport over this depth interval reduces with time from 2.5 Sv in 1957 to 1.7 Sv in 1981, to only 0.7 Sv in 1992. These results are consistent with the increase in salinity at the intermediate salinity minimum with time at those depths from 35.074 at 1020 m in 1957, to 35.085 at 1060 m in 1981 and finally to 35.094 at 1050 m in 1992.

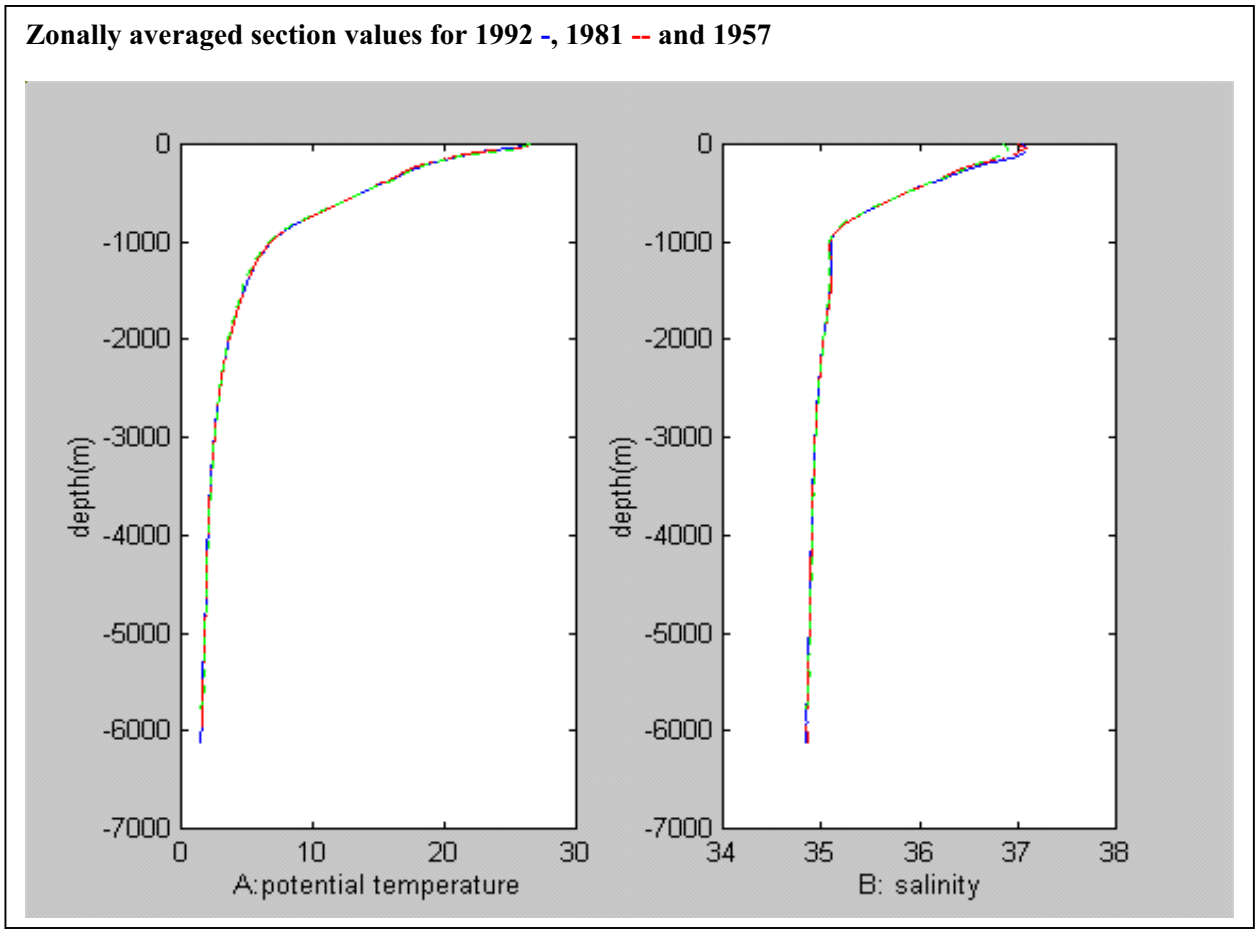

Figure 5.2. Zonally-averaged potential temperature (A) and salinity (B) profiles for the 24.5ºN transatlantic section for the three cruises, 1992 (solid blue), 1981 (dashed red) and 1957 (dotted green).

Transport (Sv) in depth clases	IGY 1957	Atlantis II 1981	Hespérides 1992
0-600m	-17.1	-18.7	-17.4
600-1200	+2.5	+1.7	+0.7
1200-3000	-10.8	-9.1	-10.9
3000-4900	-11.8	-12.0	-9.9
4900-5800	+2.3	+3.3	+2.7
4900-bottom	0	-0.1	-0.1

Table 5.2. Meridional northward volume transport in mid-ocean in depth classes. Transport units are Sv.

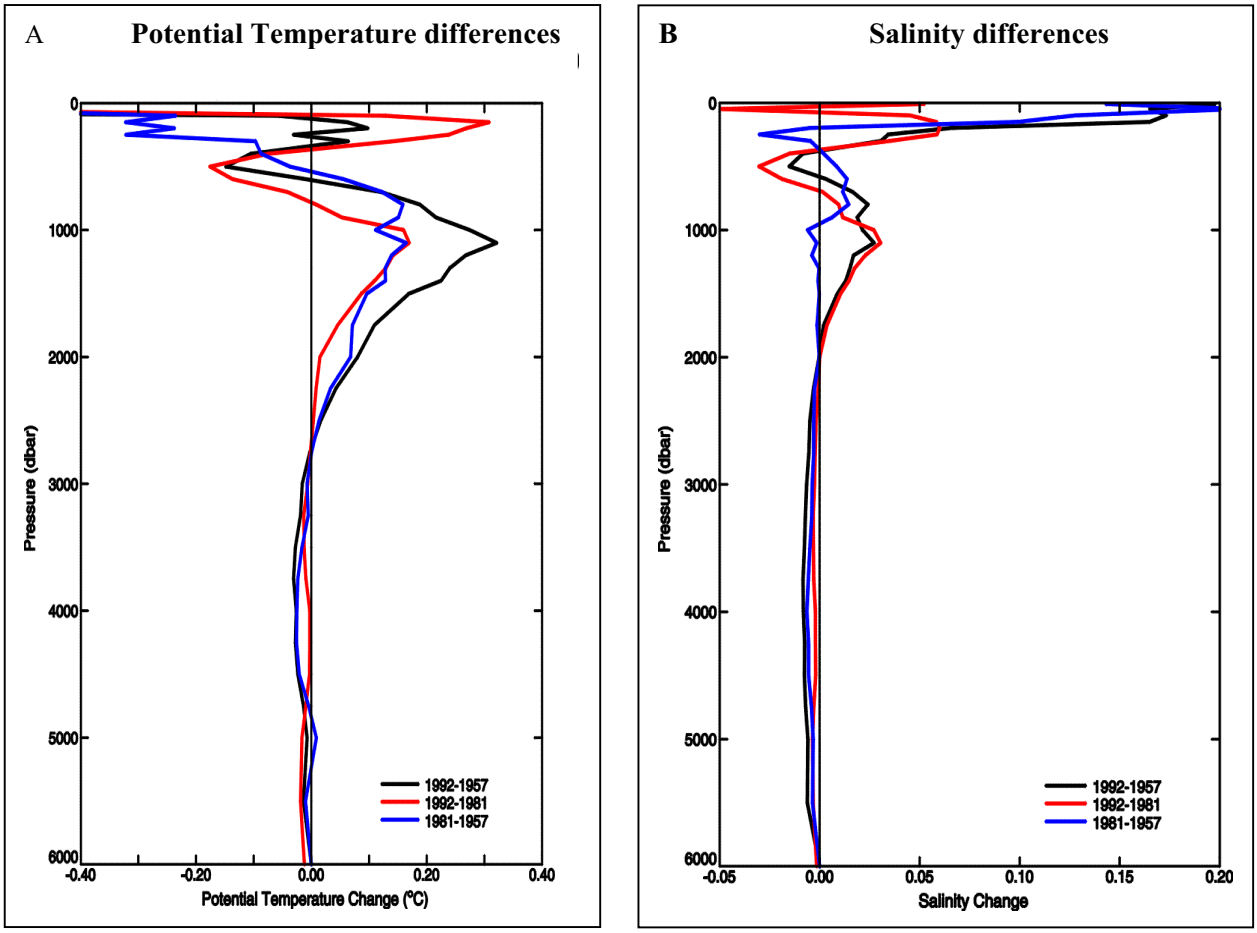

Figure 5.3 Vertical profiles of zonally-averaged potential temperature (A) and salinity (B) differences for the 24.5ºN transatlantic section for 1992-1957 (black), 1981-1957 (blue) and 1992-1981 (red).

The NADW appears clearly divided in two lobes, an upper lobe originating in the Labrador Sea and a deeper lobe from the Norwegian-Greenland Sea, as described by

Roemmich and Wunsch (1985). The upper lobe appears deeper and stronger in 1992 than in the previous cruises. CFC measurements (Smethie, 1993) suggest that it takes around 15 years for Labrador Sea Water to reach 24.5ºN (Bryden *et al.*, 1996), 1981 would correspond to the period of lack on deep water convection on the Labrador Sea during the late 1960's (Lazier, 1988) and 1992 would correspond to the following intensification period. The large increase in the transport of the lower lobe of NADW which occurred in 1981 has been reduced in 1992 to values lower than in 1957. This variation detected at 24.5ºN has been also shown at 36ºN by Dobroliubov *et al*. (1996). The total transport of NADW over the depth interval from 1200 to 4900 m was 22.6 Sv in 1957, 21.1 Sv in 1981 and 20.8 Sv in 1992. Thus, both the southward flow of NADW and the northward flow of AAIW are smallest in 1992, compared with 1981 and 1957.

Flow of AABW is about 3 Sv, the largest value of 3.3 was detected in 1981 and it was reduced in 1992 to 2.7. The water that was flowing between 5000 and 5200 m depth in 1957 has deepened to be flowing around 5500 m for both cruises 1981 and 1992. In contrast with 36ºN results (Dobroliubov *et al*., 1996), the AABW at 24.5ºN flows consistently northward over the complete period with some changes in the depth and volume of the transport.

5.3 Meridional transport into temperature classes

Meridional transports across the mid ocean section divided into temperature classes are qualitatively similar for the three cruises (Fig. 5.4), though they differ in detail. Surface Water (>22ºC) and thermocline water (22-9ºC) flow southward. Intermediate water (8-4ºC) flows mainly northward. The deeper segment of this layer is occupied by Subpolar Mode Water (SMW) and Labrador Sea Water (LSW), (McCartney and Talley, 1982) and they are flowing southward. NADW (4-2ºC) flows southward and AABW (<2ºC) flows northward.

The surface water shows a reduction over time in transport between 22 and 28ºC, and seasonal changes may be responsible for that. For waters between 17 and 22ºC, southward transport has slightly increased over time. Northward transport of intermediate water (AAIW) has decreased over time. This transport between 6 and 9ºC was 3.2 Sv in 1957, 2.1 Sv in 1981 and only 0.6 Sv in 1992. The reduction is largest in the 6º

temperature class, from 1 Sv in 1957 to 0.3 Sv in 1992. Northward transport reduction in temperature classes at 8º and 9ºC is small, but for the 7º temperature class the transport was 0.94 Sv in 1957 and -0.35 Sv (southward !) in 1992. Thus, the reduction in meridional transport in temperature classes of the AAIW is even larger than when the calculation is done over the fixed depth interval of 600 - 1200 db.

Upper NADW transport corresponds to the temperature classes 4.5 to 2.5ºC. In these temperature classes can be seen the same pattern as that in the transport shown in table 5.2 between 1200 and 3000 m: a reduction from 1957 to 1981 and slight recovery since then. For deep and bottom water a breakdown of meridional transport into finer temperature interval of 0.05ºC is helpful (Fig. 5.5). A southward transport maximum at 2ºC is shown in 1957 and a northward transport maximum at 1.8ºC. In 1981 the maximum southward transport appears to be between 1.8 and 1.95ºC and maximum northward transport occurs at 1.5ºC. In 1992 the maximum southward transport appear to be at 1.95ºC and maximum northward transport occurs at 1.75ºC. Clear deepening and cooling of both water mass transports are thus displayed.

Total NADW southward transport for temperature classes from 5 to 2ºC accounts for 22.4 Sv in 1957, 21.8 Sv in 1981 for temperature classes from 5 to 1.75ºC and 19.3 Sv in 1992 for temperature classes from 5 to 1.8ºC. AABW northward transport for temperature classes from 1.95 to 1.7ºC amounts to 2.3 Sv in 1957, 3.8 Sv in 1981 for temperature classes from 1.75 to 1.5ºC, and 1.9 Sv in 1992 for temperature classes from 1.8 to 1.45ºC.

5.4 Comparison on heat flux

Once we have determined the three components of the temperature transport, the heat flux across this latitude of the subtropical North Atlantic can be written by

$$T_{NA} = \int\int_{FS} \rho C_p \theta V_{FS}\, dz\, dx + \int\int_{MO} \rho C_p \theta V_{Ekman}\, dz\, dx + \int\int_{MO} \rho C_p \theta V_{geostrophic}\, dz\, dx \quad (5.5)$$

where NA denotes North Atlantic, FS denotes Florida Straits and MO denotes our mid-ocean 24.5ºN section.

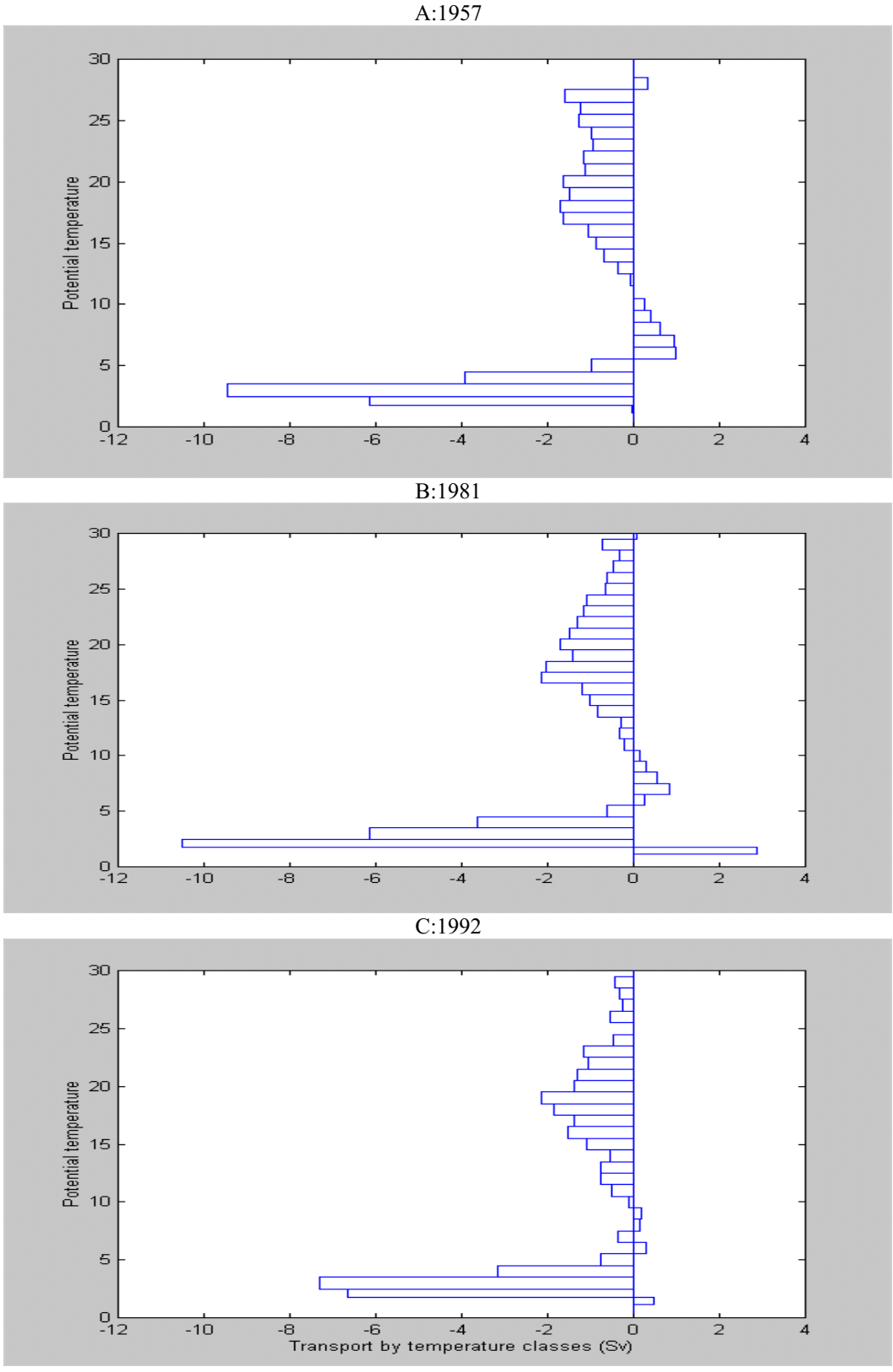

Figure 5.4. Northward transport (Sv) across 24.5ºN transatlantic section as a function of potential temperature for A:1957, B:1981 and C:1992. Transport are determined over temperature intervals of 1.0 ºC from 2.5ºC to 30ºC and 0.7ºC below 2.5ºC.

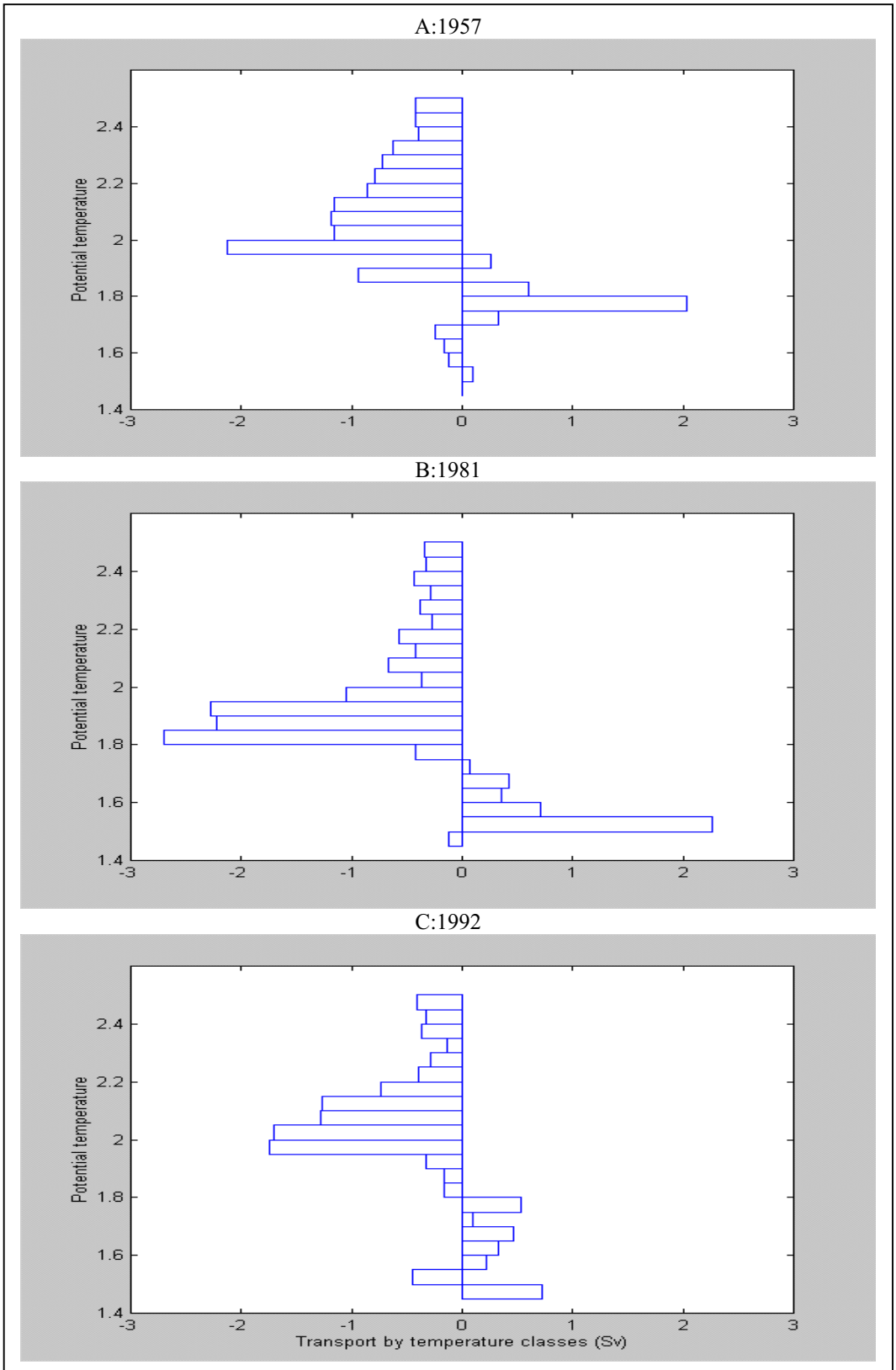

Figure 5.5. Northward transport (Sv) of deep and bottom waters across 24.5ºN transatlantic section as a function of potential temperature below 2.5ºC for A:1957, B:1981 and C:1992. Transports are determined over temperature intervals of 0.05ºC.

In the procedure used by Hall and Bryden (1982) total heat transport in the mid-ocean could be broken down into two parts: the mean field or vertical circulation cell and the eddy contribution. The eddy contribution is estimated by multiplying the difference between the zonally averaged meridional velocity at each depth, V - <V>, times the difference between the potential temperature at each station pair and its zonally averaged value, θ - <θ>, and integrating across the section. Then, the mid-ocean component of eq. 5.1 can be separated into:

$$\iint \rho\ C_P <\theta> <V>\ dz\ dx + \iint \rho\ C_P\ (\theta - <\theta>)\ (V - <V>)\ dz\ dx \quad (5.6)$$

because the zonal integral of V - <V> or θ - <θ> is zero by definition.Values for these contributions to the mid-ocean component of the total heat transport across the mid-ocean section are given in table 5.3 as well as the velocity-weighted average temperature given by (5.2) after dividing by ρ C_p (constant within the accuracy of the calculations) for the three cruises.

The eddy heat fluxes calculated had a small northward contribution in 1957 cruise (0.03 x 10^{15} W) when typical station spacing was 150 to 200 km, this contribution was slightly higher in 1981 (0.06 x 10^{15} W) when station spacing was between 50 and 80 km, and has doubled in 1992 (0.12 x 10^{15} W). The major contribution to his value in 1992 was an eddy located at 75ºW in the western boundary region of the western basin between station 94 and 95. For all 3 sections, it is notable that the eddy heat flux is small, of order 0.1 PW, a factor of 3 less than originally estimated in Bryden and Hall's (1980) error analysis.

Year	Mean Circulation heat transport x 10^{15} W	Eddy heat Transport x 10^{15} W	Total heat Transport x 10^{15} W	Velocity-weighted Average Temperature (ºC)
IGY 1957	-1.65	+0.033	-1.62	11.29
Atlantis II 1981	-1.74	+0.058	-1.68	11.77
Hespérides 1992	-1.67	+0.118	-1.55	10.86

Table 5.3. Geostrophic Mid-Ocean Circulation: Mean circulation, eddy and total heat transport across the mid ocean section. Units are 10^{15} W and velocity-weighted average temperature in ºC. In each case the total southward volume transport is 34.9 Sv.

The overall heat flux can be written as

$$T_{NA} = (FS_T\, t_{FS} + EK_T\, t_{EK} + MO_T\, t_{MO})\, \rho\, C_P \quad (5.7)$$

where FS_T stands for transport in the Florida Straits and t_{FS} is the velocity-weighted average temperature for this transport, and analogous terms are used for Ekman and geostrophic mid-ocean transport. Because the mid-ocean transport compensates the other transport MO_T=-FS_T-EK_T, the equation (5.7) can then be written as

$$T_{NA} = \{ FS_T (t_{FS} - t_{MO}) + EK_T (t_{EK} - t_{MO}) \}\ \rho\, C_P \quad (5.8)$$

Table 5.4 shows the values for the terms of equation (5.8) including transport through Florida Straits, wind-driven Ekman layer transport, their differences in temperature with mid-ocean section, and the total net heat transport for each cruise.

The variability in the Ekman transport of ± 0.7 Sv gives an uncertainty as much as ± 0.06 PW in the Ekman transport. The variability in the Florida Straits transport is around 3 Sv, such transport gives an uncertainty of ± 0.1 PW. Variability due to the Bering Strait and at different regions given by Hall and Bryden (1982) for an amount of ± 0.1 PW for the Mid-Atlantic Section was also added. The accumulated errors amount to ± 0.26 PW.

Differences between Roemmich and Wunsch (1985) and these results on deep water transport are mainly due to the different reference level we have used in the eastern basin. Roemmich and Wunsch's circulation actually has much of the deep southward transport in the eastern basin due to their use of the 1300 m as an initial reference level. We went to a 3200 dbar reference level to avoid such large southward transport in the eastern basin.

SECTION	COMPONENT	TRANSPORT (SV)	TEMPERATURE DIFFERENCE WITH MID- OCEAN (ºC)	NORTHWARD HEAT TRANSPORT (10^{15} W)	NET HEAT TRANSPORT W
1957	Ekman Layer	5.4	26.0-11.29=14.72	0.33	1.27 x 10^{15} W
	Florida Straits	29.5	19.1-11.29=7.81	0.94	
1981	Ekman Layer	5.4	26.0-11.77=14.23	0.32	1.20 x 10^{15} W
	Florida Straits	29.5	19.1-11.77=7.33	0.88	
1992	Ekman Layer	5.4	26.0-10.86=15.14	0.33	1.33 x 10^{15} W
	Florida Straits	29.5	19.1-10.86=8.24	1.00	

Table 5.4. Components of the heat fluxes, transport, difference of temperature, northward heat transport and net heat transport across 24.5ºN for 1957, 1981 and 1992.

5.5 Discussion

The values obtained for the net heat transport for each of the three cruises are the same within the range of the errors we estimate for the calculations. The heat transport is 1.27 x 10^{15}W with a variation of ± 0.06 x 10^{15}W. Even when the patterns of temperature and salinity have changed, it is found that the three cruises show similar features in their large-scale velocity and hence in their overall heat transport.

There is a small difference with Hall and Bryden's (1982) 1957 cruise calculations due to the different wind stress that it has been used here. Hall and Bryden used Leetmaa and Bunker's (1978) climatology for an Ekman transport of 5 Sv, while in this work an Ekman transport of 5.4 Sv has been used. Because of this change, an overall heat transport larger by 0.03 PW than that of Hall and Bryden was estimated. The northward heat transports for the 1957 and 1981 24.5ºN sections were estimated by Roemmich and Wunsch (1985) to be 1.1 and 1.2 x 10^{15} W using a variety of inverse model calculations. The higher eddy heat flux contribution in 1992 has produced a slight increase in the heat transport but also increases the error in the estimates.

One reason that the heat transports have not changed despite the overall warming along 24.5ºN is that temperature changes are observed to be effectively uniform zonally. Thus dynamic height (or pressure) rises uniformly hence there is little change in the zonal pressure gradient or geostrophic velocity fields so that the zonally averaged meridional

transports are similar, although there are some changes in the magnitudes of the flows. The highest velocity-weighted temperature is found in 1981 when the transport shallower than 600 m depth is largest. The principal warming has happened between 700 and 2500 m (see chapter 3), and at those depths the temperature increases have small influence on heat transport because the velocities are smaller. In the AAIW in the upper part of the warmed water, the transport has reduced over time so the increase in temperature is partially compensated by the reduction on transport. In the UNADW we observe a small increase in temperature transport mainly from 1981 to 1992, this increase is due both to the warming and to the increase in transport from 1981 to 1992.

The previous remarks are related to the zonally averaged circulation heat transport. The influence of the eddy heat transport in 1992 is twice as large as that in the 1981 and it is mainly due to a large eddy located at 75ºW (as noted earlier). Thus, the total overall heat transport from 1981 to 1992 is increased due both to the mean circulation and the eddy heat transport.

The fact that between 700 and 1100 m the northward flow seems to be reduced over time, could be related to the changes in salinity detected in the North Atlantic. Around these depths, the maximum increase of temperature and salinity over time has been reported. This is the depth range of the AAIW which is relatively fresher and a reduction in the northward flow of AAIW may result in an increase in the influence of the Mediterranean Water and a contribution to the increase in salinity over time that has been detected.

Changes of transport in temperature classes between 3 and 4ºC may be related to changes in the amount of deep water production over the convection areas (Lazier, 1995). Sy and Koltermann (1996) in an analysis of 48ºN and 36ºN sections suggest that for periods of low production of upper North Atlantic Deep Water the southward flow at intermediate depths is reduced and for periods of strong production, there is strong southward transport of intermediate waters. At 24.5ºN the decrease in flow of UNADW and increase of LNADW from 1957 to 1981 is opposite to the change from 1981 to 1992. This could be related with the long-term changes in the convective activity of the North Atlantic given by Dickson *et al*., (1996). Even though the distance from the formation regions is larger and the time for arrival of LSW to 24.5ºN would take 15 years (Bryden *et*

al., 1996) with presumably a few more years from the Arctic Seas, the periods of high production of LNADW (Greenland Sea) are during the 60's and decay later, while the LSW production is in opposite phase. Thus, the changes observed at 24ºN may be related to the changes in convective activity but with long phase lags.

Deepening by about 300 m of the AABW transport is associated with a cooling of order 0.25ºC from 1957 to 1981 and 1992. Maximum southward flow of LNADW in 1957 was at about 2ºC but was found to be at near 1.8ºC in 1981. For both AABW and NADW, deepening and cooling are associated with an increase of volume transport.

Chapter 6

Heat, freshwater, oxygen and nutrient fluxes and budgets in the North Atlantic Ocean

6.1 Introduction

We reconsider here the circulation of the subtropical North Atlantic, with a special focus on the distribution and transport of freshwater, oxygen and nutrients. The data used consist in the section at 24.5ºN occupied by *Discovery* in October 1957, by R.V. *Atlantis II* in 1981 and by the B.I.O *Hespérides* in July-August 1992 and described in chapter 3. Transport of heat and freshwater has been published by Hall and Bryden (1982) for the 1957 section and by Roemmich and Wunsch (1985) for the 1957 and 1981 sections. Brewer *et al.* (1989) using Hall and Bryden's transport of the 1957 cruise calculated oxygen flux. Rintoul and Wunsch, (1991) have published the oxygen and nutrients flux for the 1981 section. Roemmich and Wunsch (1985) used this section to construct a series of inverse models based on conservation of mass in density layers to estimate the meridional circulation and heat transport. Rintoul and Wunsch (1991) extended their analysis by including the oxygen and nutrient observations. The oxygen and nutrient information contains more constraints and helps to estimate the velocity field and then to determine nutrient fluxes themselves and increase the knowledge of the biogeochemical fluxes on the North Atlantic.

The observed distribution of oxygen and nutrients in the ocean are the result of the interplay of biological processes, such as nutrient uptake in the euphotic zone and remineralization of organic matter at depth, and the physical transport processes of advection and diffusion. Often it is assumed that advection is the dominant process below the upper layers of the ocean, and thus that the oxygen and nutrient distributions can be used to trace the spreading paths of the water masses (Wüst, 1935; Cooper, 1952; Rintoul and Wunsch, 1991).

Direct estimates of the advective transport of oxygen and nutrients provide an opportunity to investigate quantitatively the large-scale processes which contribute to the basin scale balance of those property fields. Basic models balance the effects of sinking the organic matter by vertical advection and diffusion, but the estimation of the downward flux of organic matter via the biological pump usually comes from local measurements from sediment traps and extrapolation to the broad ocean requires assumptions of large scale homogeneity. A section such as 24.5ºN provides us an estimate of the convergent or divergent transport of oxygen and nutrients for the Atlantic north of 24.5ºN and an alternative method to estimate the remineralization of organisms. Under steady state, the outward physical transport of inorganic nutrients from an isolated region of the ocean balances the net remineralization within that region. Integrating the product of velocity and a property concentration (i.e. a nutrient or oxygen) over a closed domain yields the net flux convergence-divergence within the domain north of the section.

Nutrient concentration is routinely measured with a great accuracy, but there are large uncertainties in the estimated flux divergence because of poorly determined velocity fields. An absolute velocity reference is required at some level as well as estimations of the ageostrophic portions of the flow such as at the frictional boundary layers. In the Atlantic Ocean there are a series of papers about chemical fluxes, the first one by Brewer *et al.* (1989). The estimations of Hall and Bryden (1982) of the net meridional transport across 24.5ºN were multiplied by the average property values in each depth to find the net flux across this latitude. The flux of both silicate and nitrate was found to be equatorward, with the transports roughly an order of magnitude larger than estimates of the rate at which these nutrients are supplied to the North Atlantic.

Roemmich and Wunsch, (1985) designed some inverse models with the 24.5º and 36ºN transatlantic sections and the Florida Straits section. Since the Atlantic is closed to the north except for a small inflow from the Pacific, the net (geostrophic and Ekman) flux across both latitudes must be approximately equal to zero. They included these mass conservation constraints to obtain a heat transport of 1.2 PW at 1981. Rintoul and Wunsch, (1991) found when doing the same calculations than Roemmich and Wunsch, (1985) that if mass is the only property conserved, the deep flow is sensitive to the choice of initial reference level. Because the concentrations of silicate and nitrate vary significantly in the deep water, the meridional nutrient transports also are sensitive to the initial model

assumed. A shallow reference level (1300 db) leads to large silicate residuals in the deep water layers. When they required both mass and silicate to be approximately conserved, the sensitivity of the flux results to the assumed initial reference level was removed. They concluded that a model that conserves mass and silicate produces a circulation consistent with what is known of nitrate, phosphate and oxygen behaviour as well, and is thus the simplest one consistent with the physical and chemical observations. Their adopted 'best estimate' of the circulation was a model with mass and silicate constraints imposed and with a reference level at 3000 db. They found a net nitrate divergence of 130 kmol s^{-1} in the Atlantic between 24.5º and 36ºN and attributed this to a counter-balancing advective transport of dissolved organic nitrate.

In this chapter, the divergence of the advective flux of oxygen and nutrients over the North Atlantic are estimated using the meridional velocity field constructed from the 24.5ºN section occupied in 1992 by the Hespérides and discussed in the last chapter. The transect cuts across the middle of the subtropical gyre along 24.5ºN latitude and across Florida Straits at 26ºN. The section encloses a large area of the North Atlantic, the mass flux through the Bering Straits is neglected since the associated nutrient fluxes are small compared with the uncertainty of the measurements. The Bering Straits throughflow will be only used to calculate freshwater flux. A total of 101 stations on the Mid-Atlantic transect and 11 across Florida Straits were performed. Each station consists of a full depth CTD cast with a 24 10 or 12 l Niskin bottles typically collected for ship board analysis for salinity, oxygen and nutrients.

Salinity and oxygen were measured by continuous $CTDO_2$ sampling calibrated with water samples (Millard and Yang, 1993), smoothed and linearly interpolated. Values were taken every 20 db. During the Hespérides 1992 cruise along 24.5ºN, dissolved inorganic nutrients (orthophosphate, nitrate+nitrite, and orthosilicate) were collected from the Nansen botles at each station (see chapter 2). Discrete nutrient values were checked again historical values and interpolated vertically and horizontally from neighbouring stations as necessary to complete a 20 dbar dataset. Due to the lack of Florida Straits nutrient data, Atlantis 1981 concentrations in the Florida Straits have been used.

Depth distributions of such chemical species as phosphate, nitrate and dissolved oxygen have proven especially valuable in understanding the major biochemical cycles in

the sea, the primary production of organic matter by photosyntesis in surface waters and its subsequent combustion by oxygen at greater depths. The dissolved components of sea water are transported from place to place by advection and move from one parcel of water to another by eddy diffusion. Biologically active constituents may move nutrients from one water layer to another in additional ways: namely, by sinking of organic matter under the force of gravity and by active vertical migration of organisms.

The nutrient and oxygen fluxes were calculated using

$$F = \rho\, c\, v \quad (6.1)$$

where ρ is the density of seawater (kg m^{-3}), v is the northward (cross track) velocity(m s^{-1}) and c the concentrations of the chemical variables (µmol kg^{-1}) at each depth measure.

The chemical transport (T_c, kmol s^{-1}) were calculated between station pairs each 20 db and by integration over all depth and the sampling area.

$$T_c = \int_x^{x0} \int_{z2}^{z1} F dx dz \qquad (6.2)$$

where x_o and x are the distance (m) between consecutive station pairs and z_1 and z_2 the depths of the integration. For simplicity, since we have made the calculation every 20 db, we are not including bottom triangular area deeper than the deepest common depth. Note that the velocity field has already been designed to conserve mass.

Diagnosis of the circulation field at 24.5ºN assumes the velocity geostrophically balances the observed density structure except for an ageostrophic surface boundary layer directly forced by the wind stress. The velocity shear at every station pair is computed using the thermal wind relation, since the thermal wind equations only give the vertical gradient of velocities, the absolute velocities field requires the determination of a reference level at an arbitrary level in each of the 100 pair of stations. The reference level velocities adopted and discussed in chapter 5 is used as an initial reference level and those initial reference levels will be adjusted to get a circulation more consistent with the constraints.

The previously adopted reference level can be summarised as follows. An initial level of no motion was located at 3200 db from the eastern boundary to about 69ºW where a oxygen front implied a transition to the western boundary region. From that point to the

western limit of the section 1000 db was chosen as reference level. The Ekman layer transport was calculated from the Trenberth *et al.* (1990) climatology as 5.4 Sv. A small barotropic correction of -0.0138 cm s^{-1} was added to balance the mass transport with the 29.5 Florida Straits transport.

6.2 Velocity and volume transport in the section

The velocity field at 24.5ºN throughout the water column from the adopted model is shown against longitude in figure 6.1A. The mid-ocean field is dominated by mesoscale features that are most energetic in the thermocline and above, in the western and eastern boundary regions and west of 60ºW. Upper layer velocities are stronger in the North American basin (larger than 40 cm s^{-1}) than in the eastern basin where only in the boundary velocities are about 25 cm s^{-1}. The WBUC is concentrated west of 70ºW (Fig. 6.1B),

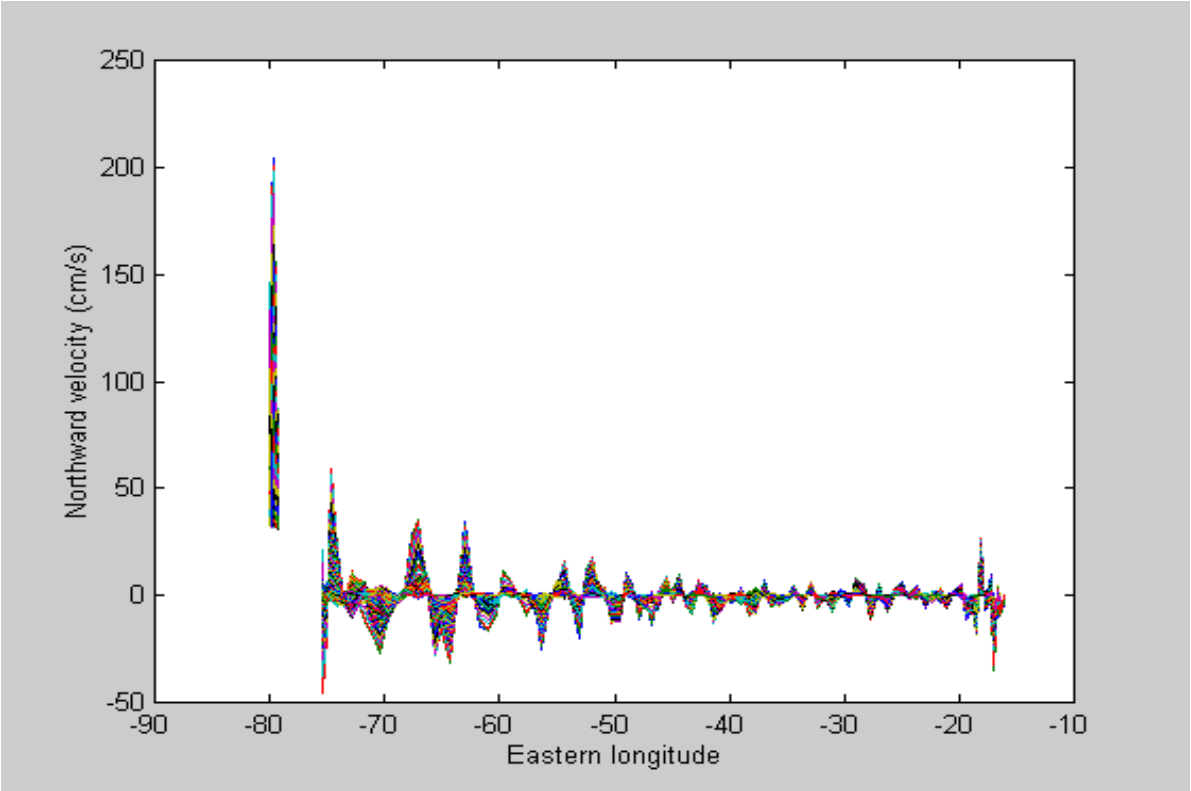

Figure 6.1A. Magnitude of northward (positive) and southward (negative) geostrophic velocities at each pair of stations all across the mid-ocean section and Florida Straits. Velocities are plotted every 20 m depth throughout the water column; for example velocities calculated between station 90 (70ºW) and 91 (70.67ºW) are plotted as dots at the mean longitude (70.345ºW). Note that there is a gap between the mid-ocean (16.19ºW to 75.49ºW) and the Florida Straits sections (79.23ºW to 80.06ºW).

with velocities larger than 10 cm s^{-1}. The total transport is calculated to be about 22 Sv (Table 6.1). The pattern of deep northward and southward flow is complicated, the banded structure may be due to topographic Rossby waves (Pickart and Watts, 1990; Pickart and Smethie, 1993) but the chemical components did not show this banded pattern in such an intensive way. Bands between 100 and 200 km wide in velocity are evident all across the section.

Maximum velocities are found in the Florida Straits (from 32.2 to 204 cm s^{-1}). Since zonal mean velocities are calculated as area averaged velocities, Florida Straits velocities weigh little in mean velocities, but they have a large influence in the horizontal transport of properties. Intensity of the circulation is stronger in the North American basin than in the Canary basin. Most of the higher velocities are restricted to the upper 1200 m, (compare magnitude of velocities plotted in figure 6.1A with figure 6.1B where only velocities below 1200 m have been plotted). Deeper than 1200 m maximum velocities are about 10 cm s^{-1}.

For the NADW range of depths in the western boundary region, southward velocities are between 8 cm s^{-1} and –10 cm s^{-1} (Fig. 6.1B). Larger contributions of northward transport are at the eastern boundary, around the Mid-Atlantic ridge and around 70ºW, where Schmitz and McCartney (1993) pointed out a recirculation of the Western Boundary Current with significant northward transport.

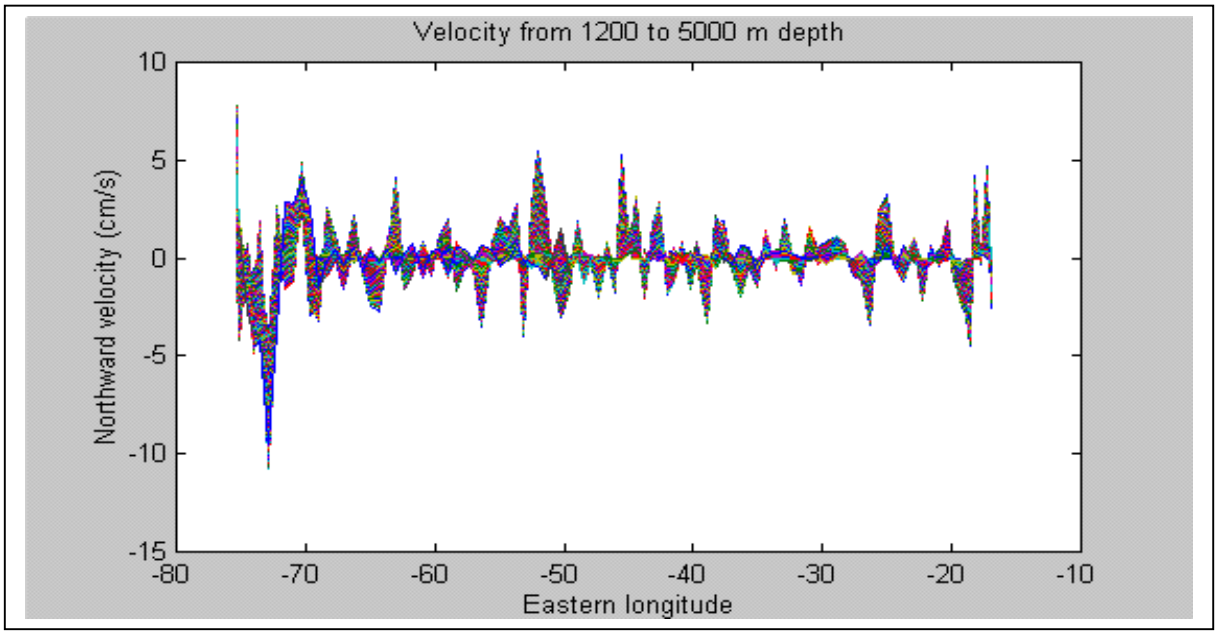

Figure 6.1B. Velocity from 1200 to 5000 m depth

In the deeper part of the water column (Fig 6.1C) at more than 5000 m depth, there is a small but intense (v = -10 cm s^{-1}) component of southern transport in the deep western boundary current and the previously marked northward recirculation around 70ºW also appears. In the Canary Basin current intensity is very low.

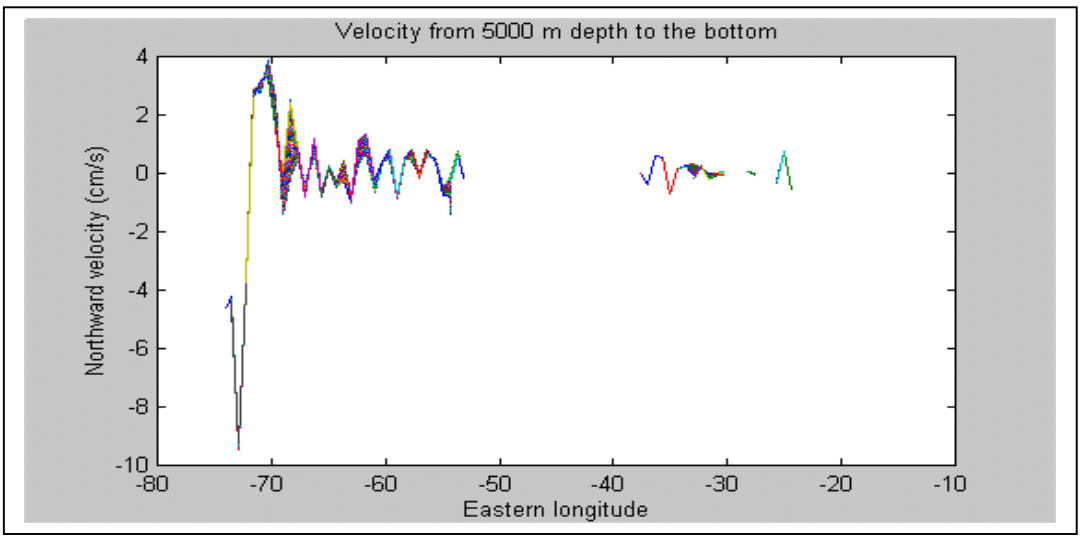

Figure 6.1C. Velocity from 5000 to the bottom. Most of the water deeper than 5000 m appears in the North American basin, with a small contribution from the Canary basin, mostly between 30ºW and 39ºW.

Deeper than 5600 m (Fig. 6.1D), below the deep western boundary influence, mostly northward flow was found around 70ºW and towards the Mid-Atlantic ridge signalling AABW northward transport. Lee *et al*. (1996) found a deep recirculation extending over a broad region at the DWBC in a section at 27ºN. Northward recirculation of water of northern origin is confirmed by the low concentration of silicate (Fig 6.2A) and nitrate (Fig. 6.2B) from 5600 m to the bottom, where to the east of 70ºW concentration increases greatly due to AABW flow.

The integrated transport (Florida Straits, mid-ocean section and Ekman layer) at 24.5ºN over depth is presented in figure 6.3. This volume transport is northwards from surface to 1200 m depth due to the northward flow of the Florida Straits and Ekman layer and the AAIW flow around 1000 m in the mid-ocean. Deeper than 1200m the well known two-lobe pattern of NADW southward transport is evident: the upper lobe presents a maximum transport at 2000 m corresponding to the Labrador Sea Water (LSW) source and the deeper lobe a maximum between 3500 and 4000 m corresponding to the Denmark

Strait Overflow Water (DSOW). The deepest transport corresponds to the AABW that flows northward from 5200 to 6000 m.

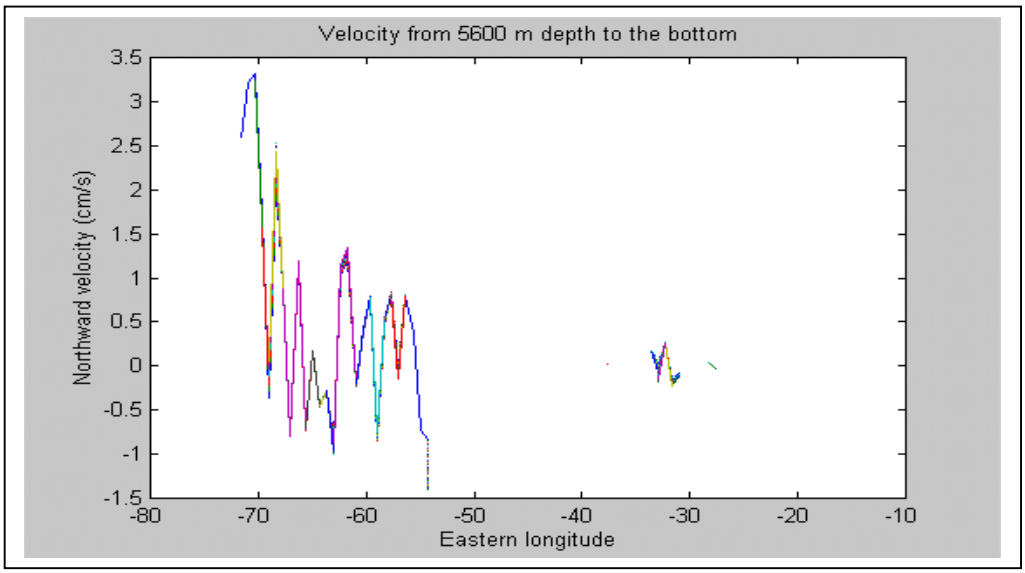

Figure 6.1D. Velocity from 5600 to the bottom. Most of the water deeper than 5600 m appears between 54ºW and 71ºW in the North American basin.

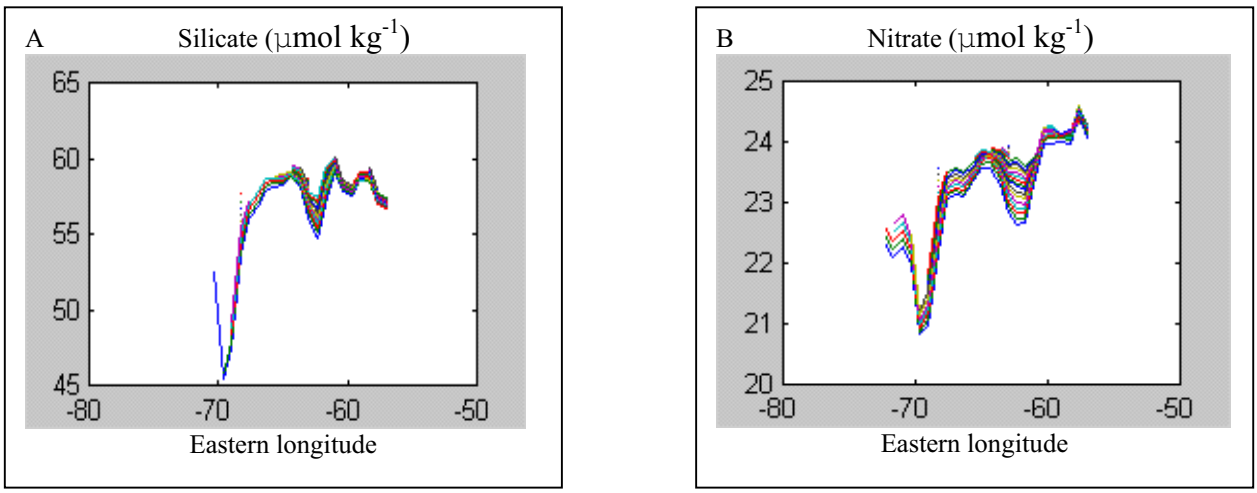

Fig 6.2. Silicate (A) and nitrate (B) concentration from 5600 m to the bottom.

Separating the mid-ocean section in 4 blocks: Eastern Canary basin (16ºW to 25ºW, stations 1-21), Canary basin (25ºW-45ºW, st 21-51), North American basin (45ºW-69ºW, st 51-88) and western boundary (69ºW-75ºW, st 89-101), it is possible to examine the zonal structure of the meridional circulation (Table 6.1). The most interesting feature is that the southward transport is principally due to the western boundary from 1200 to 4900 m, as result of the upper and lower NADW. There is also an important contribution from the upper waters of the Canary basin. The northward transport in the mid-ocean section is

due to the AAIW and to the AABW transport both mainly in the North American basin. Flow in the Florida Straits is mainly in the upper 600 m, only 0.3 Sv is calculated below that depth. Volume transport in the Canary basin below the Mid-Atlantic ridge (around 3000 m) is northward but very low.

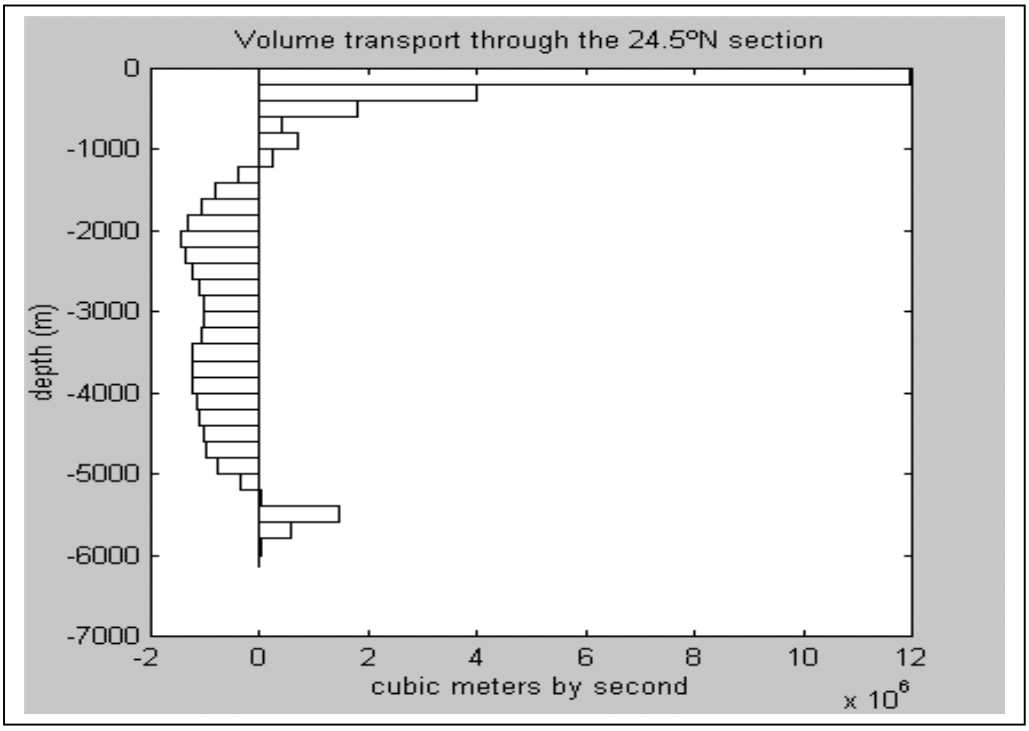

Figure 6.3. Overall volume transport through the 24.5ºN section by depth classes of 200 m, including Florida Straits, Ekman layer and mid-ocean section. Units are Sv (10^6 m^3s^{-1}).

Transport (Sv)	West Boundary (75ºW-69ºW)	N.American B (69ºW-45ºW)	Canary B. (45ºW-25ºW)	E. Canary B. (25ºW-16ºW)	Florida Straits	Ekman layer
Upper (0-600m)	-2.0	-1.9	-9.6	-3.5	29.2	5.4
Thermocl.(600-1200)	-2.3	5.4	-2	0	0.3	
UNADW(1200-3000)	-11.7	1.1	0.9	-0.1		
LNADW(3000-4900)	-10.3	-0.9	0.4	0.2		
AABW(4900-bottom)	-1.1	2.0	0.2	0.2		

Table 6.1: Transport (Sv) by classes of depth (0-600, 600-1200, 1200-3000, 3000-4900, 4900-bottom) for some parts of the section: Western Boundary (75ºW-69ºW), North American Basin (69ºW-45ºW), Canary Basin (45ºW-25ºW) East Canary Basin (25ºW-16ºW), Florida Straits and Ekman layer.

6.3 Mechanisms of heat, freshwater, oxygen and nutrients fluxes

6.3.1 Separation of components

Bryden and Hall (1980) and Hall and Bryden (1982) introduced the concept of barotropic, baroclinic and eddy or horizontal contribution to the total heat flux. For that purpose it is necessary a separation of the meridional velocity, v, into a section-averaged velocity $< \bar{v} >$, a baroclinic profile of zonally averaged velocities at each depth, $< v > (z)$ and deviations from zonal averages, v'(x, z) or anomalies for each pair of stations and depth:

$$v = \langle \bar{v} \rangle + \langle v \rangle (z) + v'(x,z) \quad (6.3)$$

We follow this separation for all the variables, in the case of potential temperature θ, the separation into a section depth-averaged $< \bar{\theta} >$, a profile of zonally averaged potential temperature and $< \theta > (z)$ and the anomalies θ'(x,z) are again given by:

$$\theta = \langle \bar{\theta} \rangle + \langle \theta \rangle (z) + \theta'(x,z) \quad (6.4)$$

In the following pages a description of the section mean values, zonally averaged profile, and spatial distribution of the anomalies over the Florida Straits and mid-ocean section of all the variables is given to diagnose the mechanism of the fluxes.

6.3.1.1 Velocity

Components of the velocity will be used for transport calculation of all the variables because of the flux formulation (eq. 6.1). Following the separation of components of eq. (6.3), figure 6.4 present the 3 components of the velocity.

The mean velocity $< \bar{v} >= -1.9\ 10^{-4}$ m s^{-1} corresponds to the southward flow that compensates the Ekman northward flow. The zonally averaged baroclinic velocity (Fig. 6.4A) presents a distribution of positive velocities in the upper 1200 m, negative from that depth to 5200 m and positive again to 6000 m. In the upper 600 m the influence of northward Florida Straits velocities is clear. The northward transport of bottom. AAIW is

detected around 1000 m. The southward flow of NADW, is divided into the two lobes of upper and lower NADW, and northward AABW transport is shown at the bottom.

A)

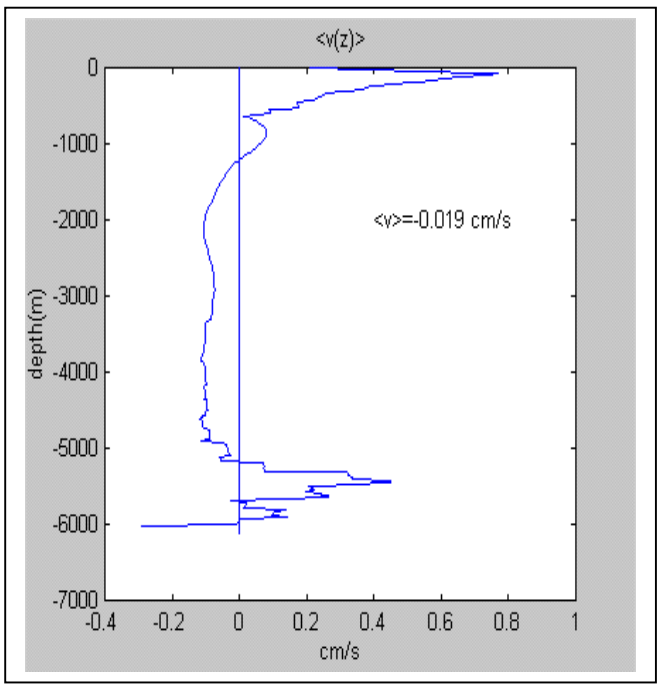

B)

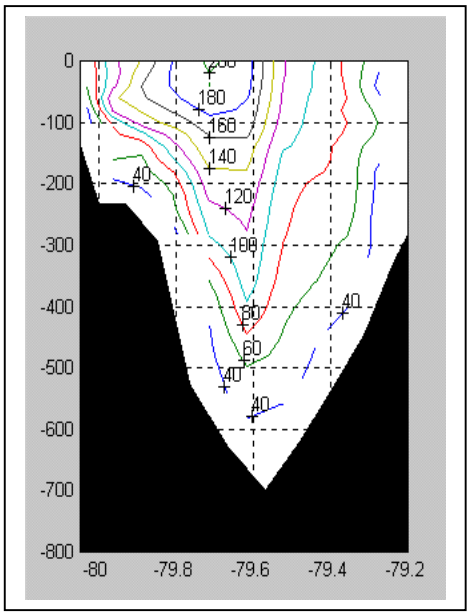

C)

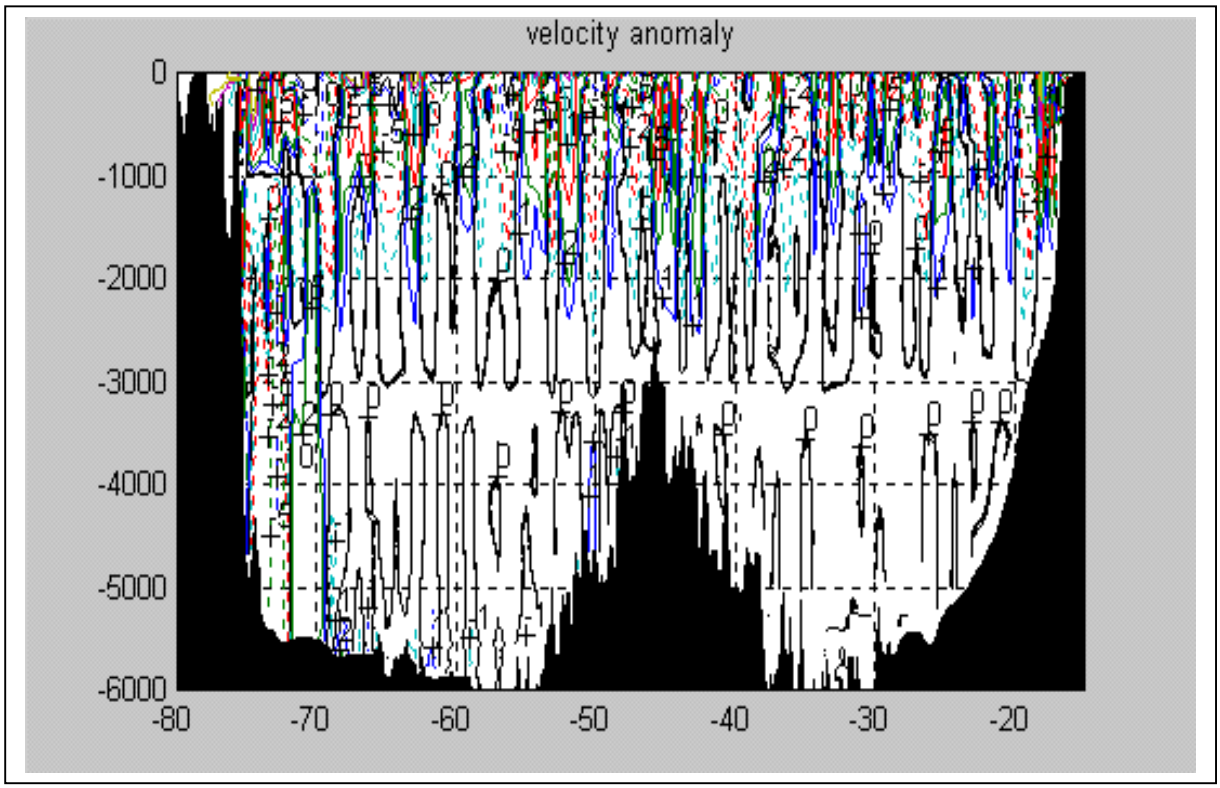

Figure 6.4: Velocity separation: A) zonally average velocity profile <v> superimposed on section averaged velocity <v(z)>, and deviations from zonal average v'(x,z) for B) Florida Straits and C) the total 24.5ºN section.

The distribution of anomalies in velocity presents a complicated view. We have separated the Florida Straits velocities (Fig. 6.4B) from the total section (Fig. 6.4C). Velocities are large in the central part of the Florida Straits reaching anomalies of 2 m s^{-1} at the surface. Principal velocity anomalies for the whole section are located in the upper layers and near the western and eastern boundaries (Fig. 6.4C). The distribution of anomalies in mid-ocean follows the banded pattern of velocities presented in figure 6.2 with bands of positive and negative anomalies in alternation. Zero line is plotted in black. Positive anomaly is plotted in solid contours from blue (1 cm s^{-1}), green (2 cm s^{-1}), red (5 cm s^{-1}) ... Dashed contours represent negative velocity anomalies: light blue (-1 cm s^{-1}), red (-2 cm s^{-1}), green (-5 cm s^{-1}), and higher values.

6.3.1.2 Potential temperature

The separation of potential temperature into components is performed similarly to estimate heat flux components. The baroclinic profile of potential temperature shows warmer temperatures (positive values) in the upper 1300 m and colder temperatures (negative values) below (Fig 6.5A). Schmitz and Richardson (1991) suggest that most of the near-surface flow of water in the Straits of Florida is notably less saline and warmer than surface water at the equivalent latitudes of the North Atlantic and likely originates in the Eastern South Atlantic. Most of the Florida current transport between 12ºC and 24ºC is of North Atlantic origin and a large amount of the remaining transport in the lower temperatures range is from the South Atlantic. The deviation from the averaged values in the Florida Straits is positive (Fig 6.5B) in the upper 200 m mainly in the western part. Anomalies in the lower temperature range are negative, showing the South Atlantic influence. In the upper layers of the mid-ocean section, positive values (solid contours in figure 6.5C) are found in the North America basin and negative (dashed contours) in the Canary basin. In the intermediate water the anomalies are opposite, with negative values in the west and positive in the eastern part. The recirculation area around 70ºW has positive anomaly.

6.3.1.3 Salinity

To calculate the salt and freshwater transport through the section, we have similarly separated salinity values into the three components: The zonally averaged salinity profile

presents a distribution of positive values in the upper 900 m and negative values below, with the 24.5ºN section averaged salinity of 35.17 (Fig. 6.6A). The deviations from the

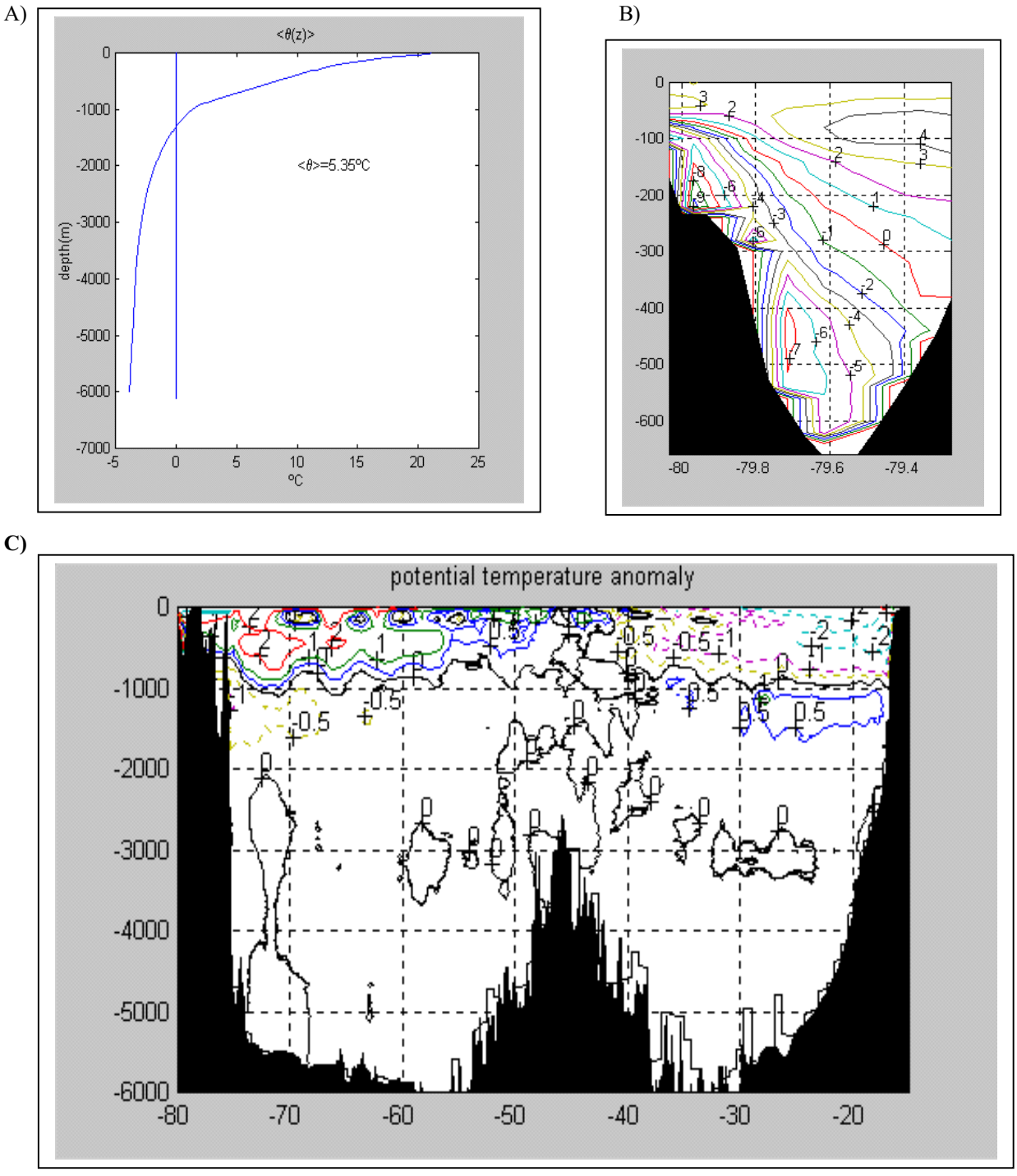

Figure 6.5: Potential temperature separation: A) zonally average potential temperature profile <θ> superimposed on section averaged potential temperature <θ(z)>, and deviations from zonal average θ'(x,z) for B) Florida Straits and C) the total 24.5ºN section.

zonally averaged values in the Florida Straits are negative over most of the section, showing fresher South Atlantic origin water masses (Fig. 6.6B). Only the eastern mid-depth waters of North Atlantic origin exhibit positive values perhaps the results of net

A)

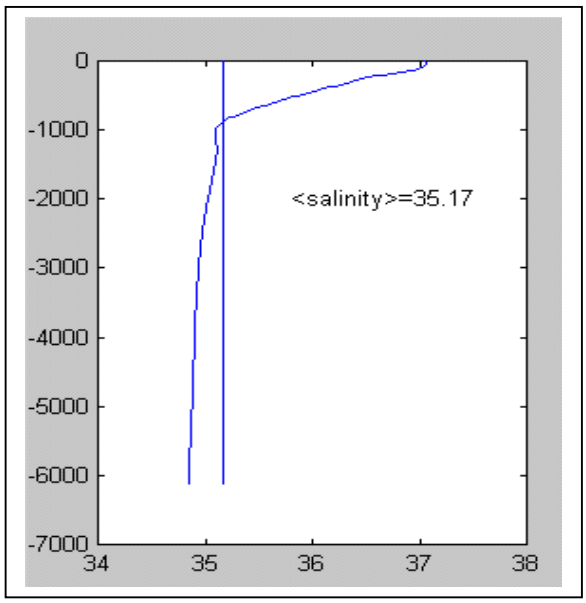

B)

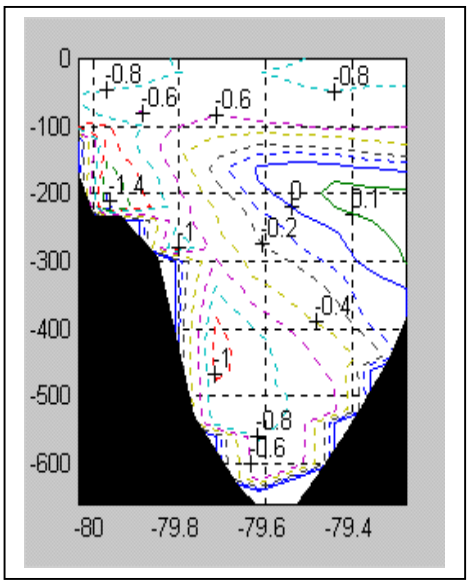

C)

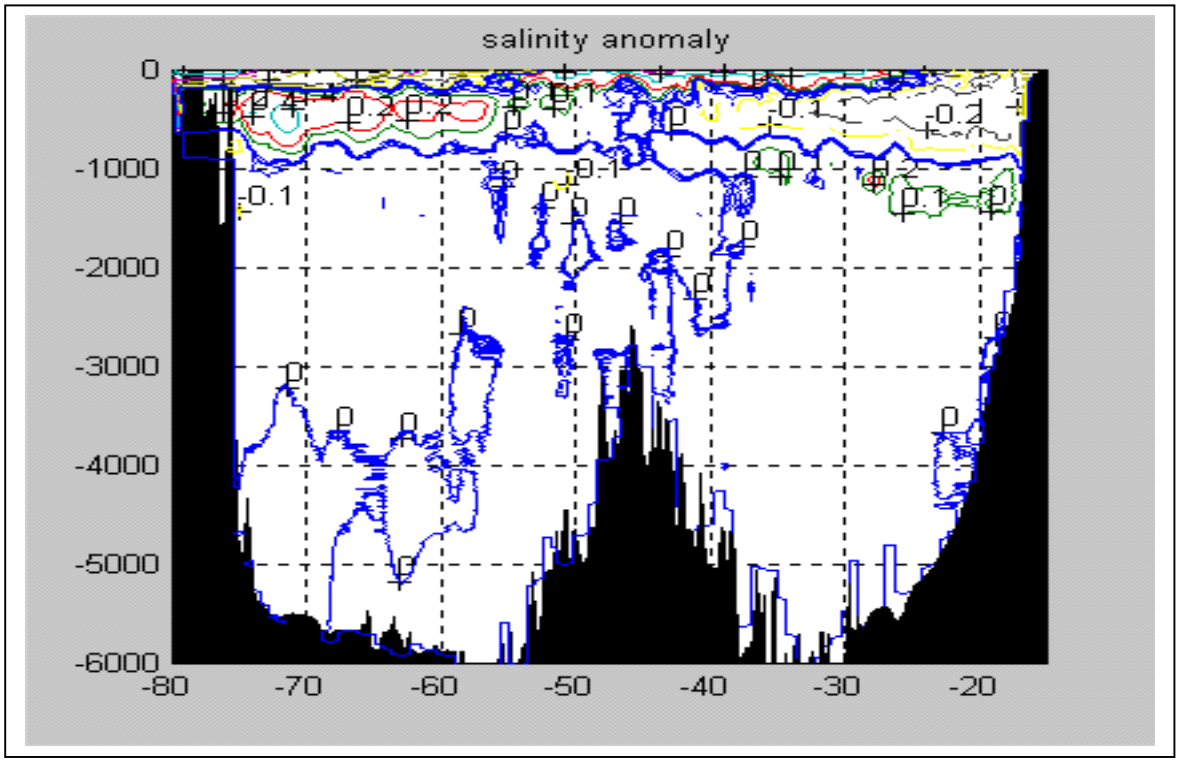

Figure 6.6: Salinity separation: A) zonally averaged salinity profile <salinity (z)> superimposed on section averaged <salinity>, and deviations from zonal average S'(x,z) for B) Florida Straits and C) the total 24.5ºN section.

evaporation over the subtropical gyre. In the mid ocean section upper layers, positive anomalies (saltier water) are found in the North American basin and negatives (fresher water) in the Canary basin (Fig. 6.6C). In the intermediate water the anomalies are opposite, with negative values in the western and positive in the eastern part. Also the LNADW of the North American basin has positive anomaly.

6.3.1.4 Oxygen

For oxygen transport calculation, we have similarly separated oxygen components. The section averaged value is 228.79 μmol kg^{-1}. The baroclinic component present low oxygen water (negative values) in the upper 1500 db and highly oxygenated water (positive values) below (Fig 6.7A). The deviation from the averaged values in the Florida Straits is negative (Fig 6.7B) over most of the section. This low oxygenated waters suggests (Schmitz and Richardson, 1991) an eastern South Atlantic origin for the water mass. In the mid-ocean section upper layers, highly oxygenated water (positive values) are found in the North America basin and low oxygenated water (negatives values) in the Canary basin (Fig. 6.7C). Anomalies are large in the thermocline and intermediate waters. In deep waters, positive anomaly near the western boundary was found showing the recently formed Labrador Sea water (high oxygen concentration) and negative near the eastern boundary and near the MAR where the low oxygenated AABW flows northward.

A)

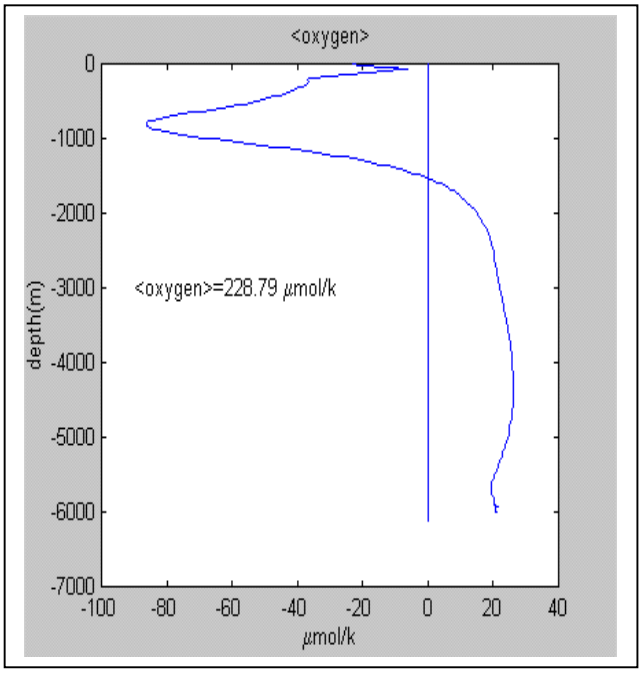

B)

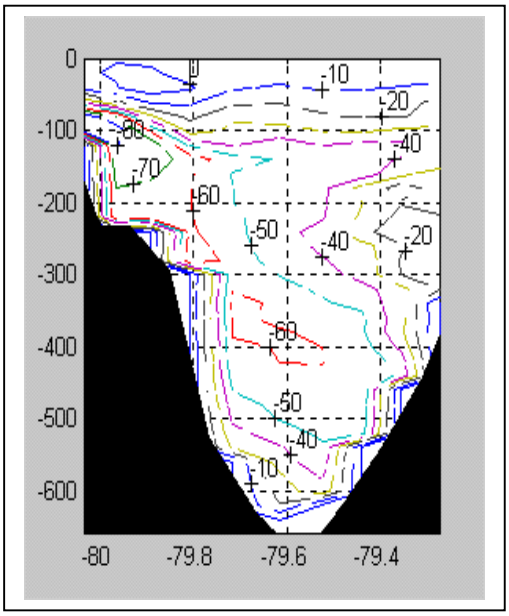

C)

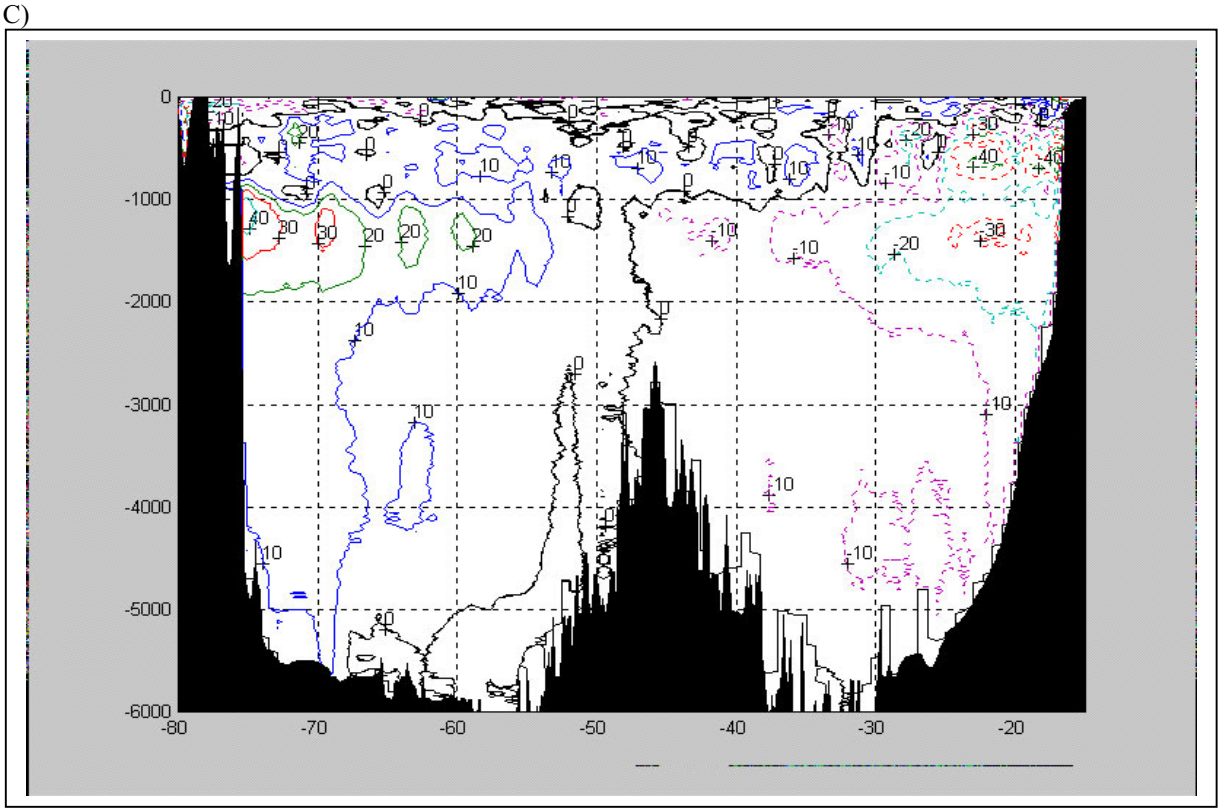

Figure 6.7: Oxygen separation: A) zonally averaged oxygen profile <oxygen (z)> superimposed on section averaged <oxygen>; and deviations from zonal average oxygen'(x,z) for B) Florida Straits and C) the total 24.5ºN section.

6.3.1.5 Silicate

To calculate the silica flux, we have separated similarly the silica components: The section-averaged value of silica concentration is 27.78 μmol kg^{-1}. The baroclinic component follows a nearly strait line from –30 to 30 μmol kg^{-1} from surface to bottom, except around 1000 m depth due to high silica contents in the AAIW (Fig. 6.8A). Low concentration negative values) are located in the upper 2500 m and positive below 2500 m to the bottom. The deviations from the averaged values in the Florida Straits are strong and positive (Fig 6.8B) over most of the section indicating high silica concentration of Antarctic origin in the South Atlantic water. Only the eastern shallow part of the Florida Straits exhibits values near zero. In the mid-ocean section, higher concentration or positive values are found in the Canary basin and deeper waters in the eastern North America basin (showing again AABW influence). Mostly negative values in the North America basin indicate the northern origin of the UNADW and LNADW (Fig 6.8C).

A)

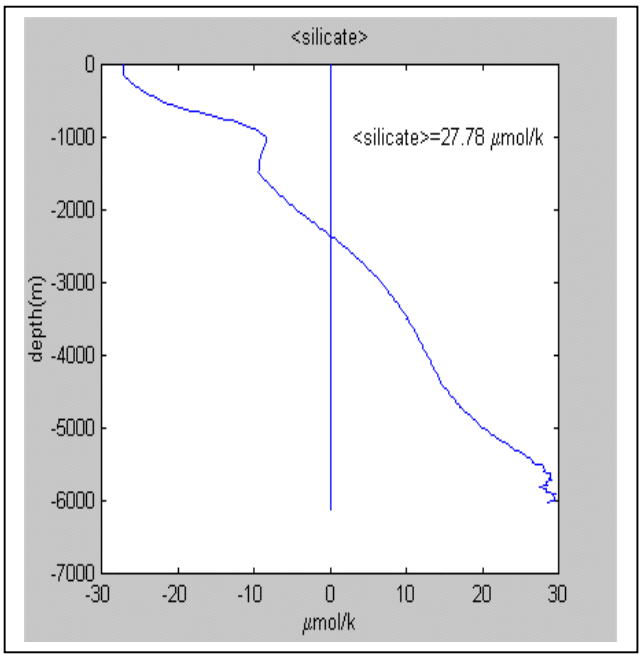

B)

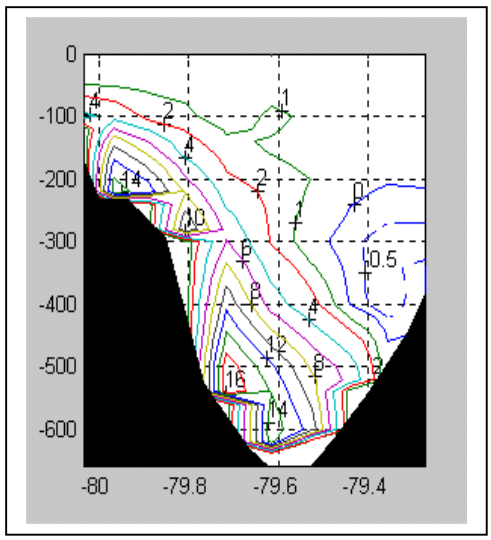

C)

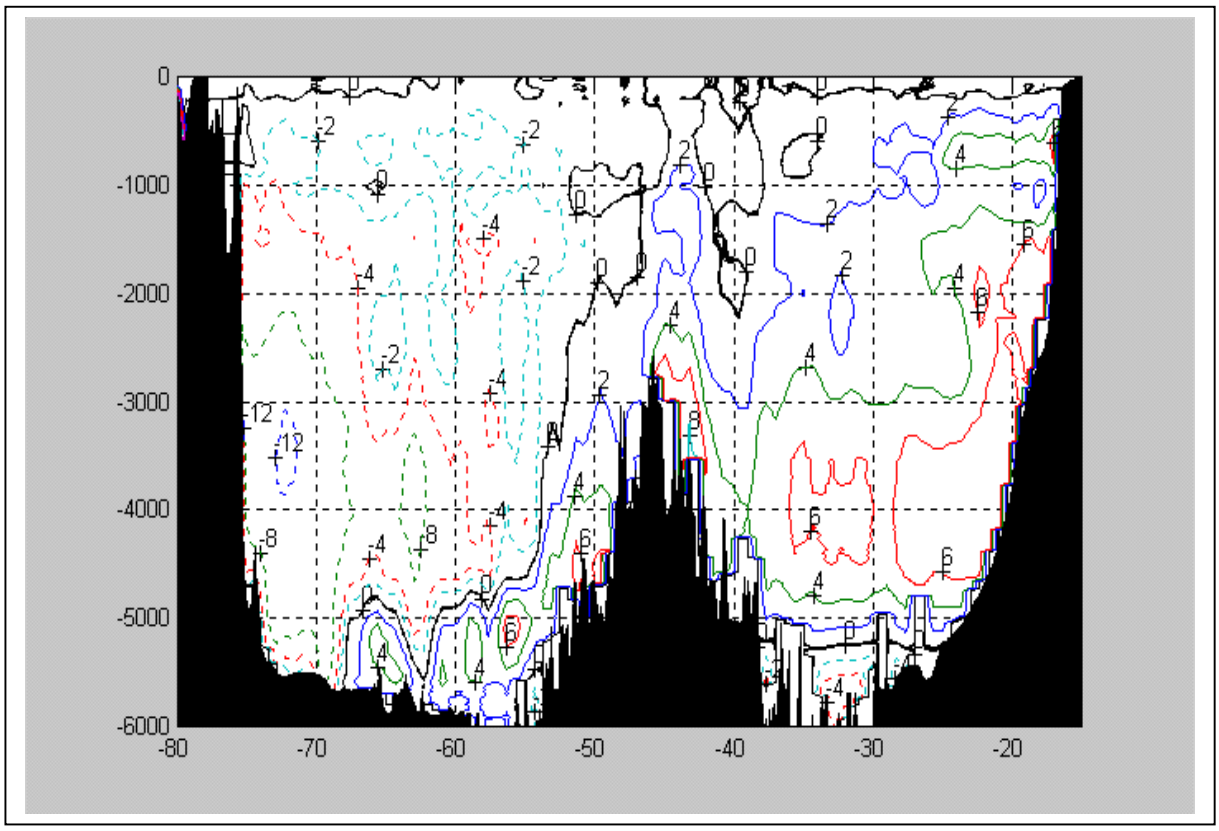

Figure 6.8: Silicate separation: A) zonally average silicates profile < silicate(z) > superimposed on section averaged silicates < silicate >; and deviations from zonal average silicate' (x,z) for B) Florida Straits and C) the total 24.5ºN section.

6.3.1.6 Nitrate

To calculate nitrate flux, nitrate concentrations have been separated in the aforementioned three components. The mean concentration of nitrates all over the section is 19.26 μmol kg^{-1}. The baroclinic component presents very low concentrations (negative values) in the upper 700 m and high concentration (positive values) below (Fig. 6.9A). The strong positive values near 1000 m depth are a signature of AAIW. The deviation from the averaged values in the Florida Straits is strong and positive (Fig 6.9B) over most of the section showing again the southern Atlantic influence, only the eastern shallow region exhibits nearly zero values. In the mid ocean section, high concentrations or positive values are found in the Canary basin and deeper eastern part of the North America basin (AABW signal) with mostly low concentrations or negative values in the North America basin. Anomalies are larger in the thermocline water around 700 m, in the eastern boundary and around 1000 m all over the section due to the high nitrate content of AAIW. At the western boundary, lower content of LSW is evident in the upper layers and of DSOW at lower layers (Fig. 6.9C).

A)

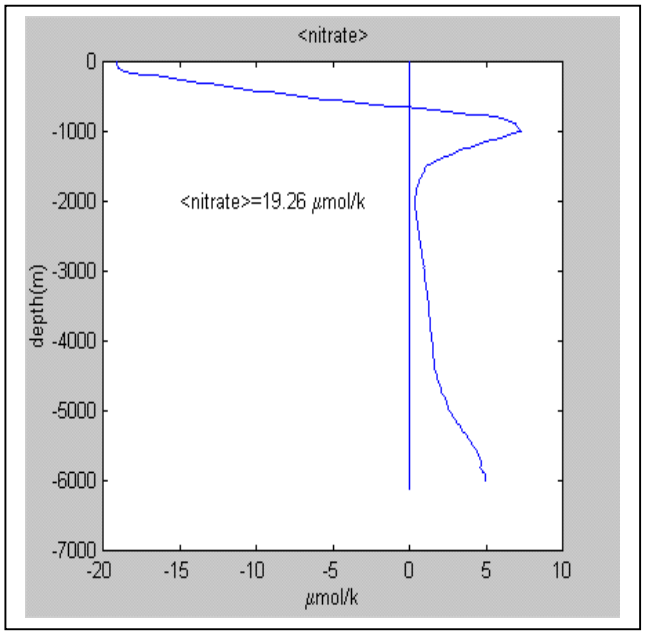

B)

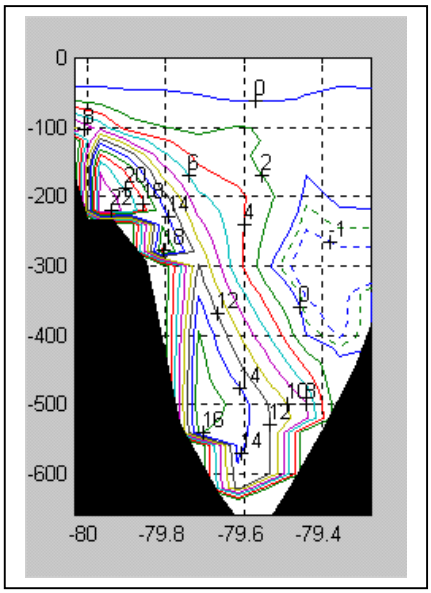

C)

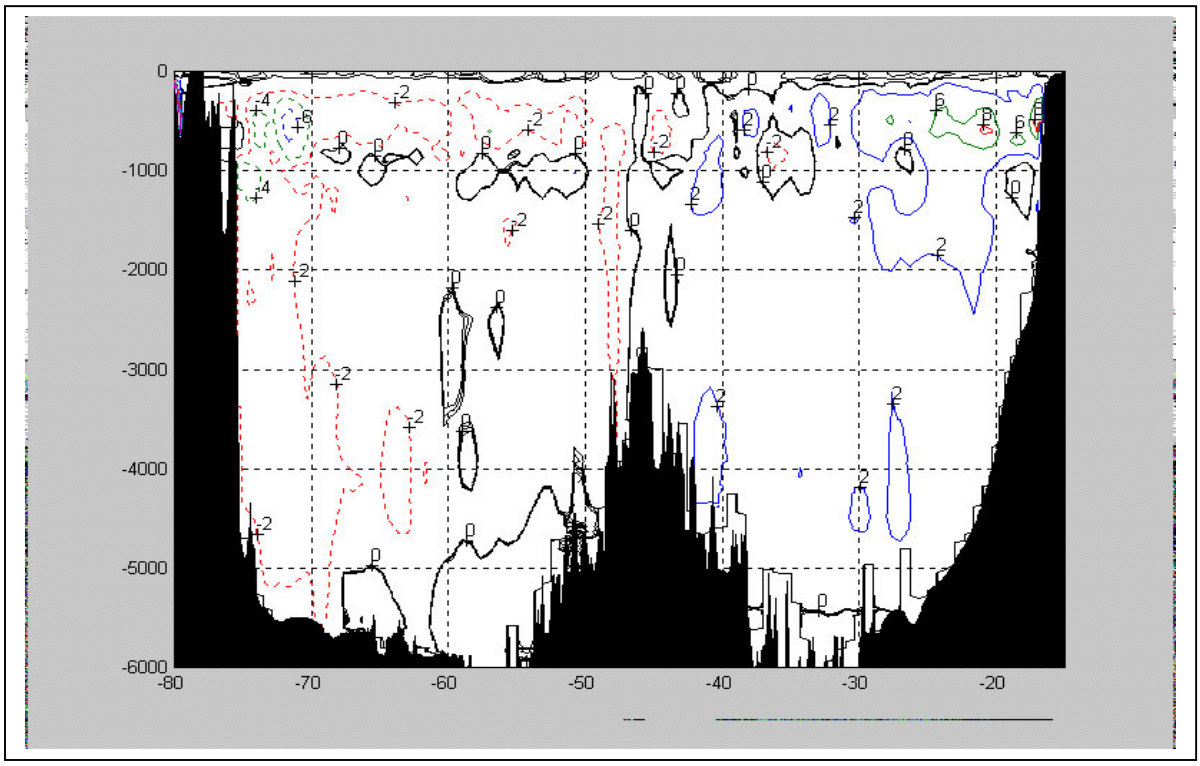

Figure 6.9: Nitrate separation: A) zonally average nitrate profile < nitrate(z) > superimposed on section averaged nitrate < nitrate >; and deviations from zonal average nitrate's (x,z) for B) Florida Straits and C) the total 24.5ºN section.

6.3.1.7 Phosphate

To study the mechanism of the phosphate fluxes, we have separated phosphate concentrations again in three components. The section averaged concentration is 1.23 μmol kg^{-1}. The baroclinic distribution is similar to nitrates. Low concentrations (negative values) are found in the upper 700 db and positive values below (Fig. 6.10A). The deviation from the averaged values in the Florida Straits is strong and positive (Fig. 6.10B) over most of the section, only the eastern shallow region exhibits nearly zero values. In the mid-ocean section positive values are found in the Canary basin and in the deeper eastern waters of the North American basin (AABW signal) with mostly negative values in the North American basin. Anomalies are larger in the thermocline water around 700 m in the eastern boundary and around 1000 m all over the section due to the high phosphate content of AAIW. In the western boundary, lower content of Labrador Sea water is evident in the upper layers and of DSOW at lower layers and its recirculation (Fig. 6.10C).

A)

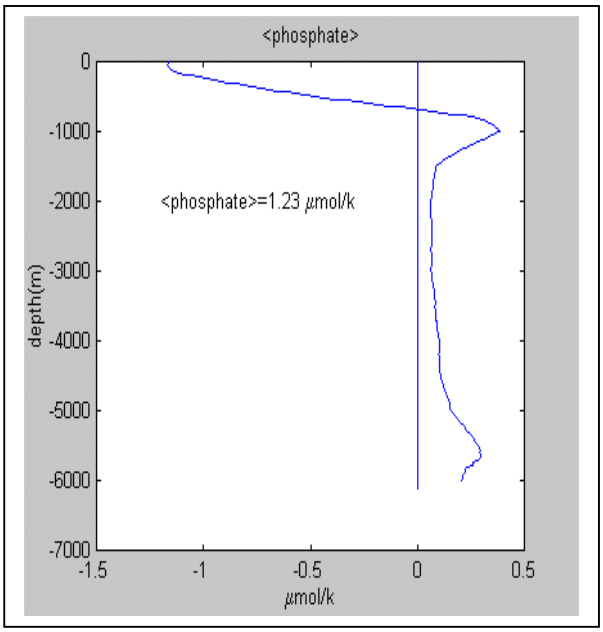

B)

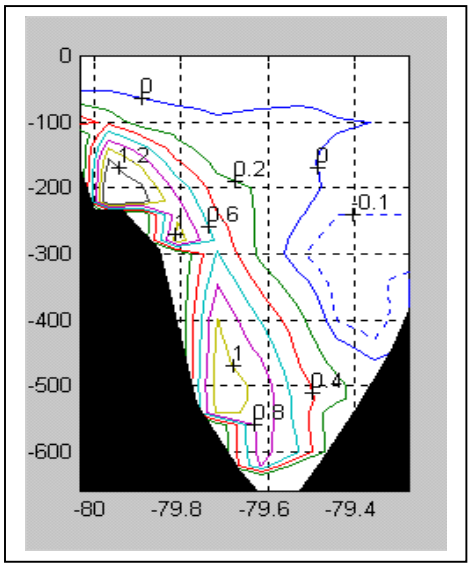

C)

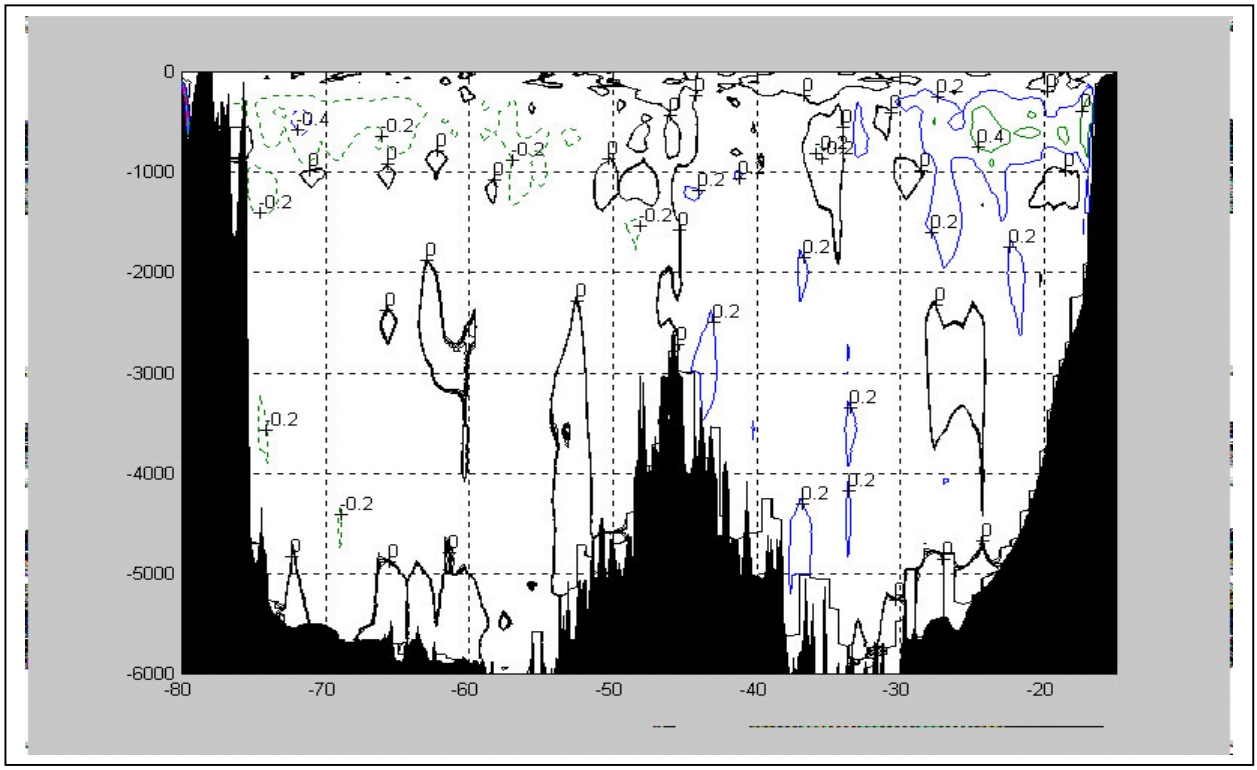

Figure 6.10: Phosphate separation: A) zonally average phosphate < phosphate(z) > superimposed on section averaged phosphate < phosphate >; and deviations from zonal average phosphate's (x,z) for B) Florida Straits and C) the total 24.5ºN section.

6.3.2 Components of the heat, salt, oxygen, silica, nitrate and phosphate fluxes

Following Bryden (1998), the different components of heat transport will be separated. After decomposition of the variables velocity and potential temperature into components by eq. (6.3) and (6.4), the geostrophic component of heat transport can be broken up into 3 parts:

1. The barotropic part due to the net transport across the 24.5ºN section to balance the ageostrophic Ekman transport. At 24.5ºN, the Ekman volume transport was calculated by eq. (5.3). The barotropic transport to balance the Ekman flow then must be:

$$\rho \langle \bar{v} \rangle \int L(z) dz = \int (\tau^x / f \quad \rho) \, dx = 5.4 \; Sv \qquad (6.5)$$

where L(z) is the width of the section at each depth and $\int L(z)\, dz$ is the area of the section thus, a mean velocity <v>= -1.9 10^{-4} m s^{-1} is required to balance the Ekman flow.

The Ekman heat transport was calculated by eq. (5.4) at the surface mean temperature of 25.95ºC; barotropic heat transport is calculated by

$$\rho \, C_p \langle \bar{v} \rangle \langle \bar{\theta} \rangle \int L(z) \, dz \qquad (6.6)$$

at the section average temperature of 5.35ºC.

The Ekman heat transport and its associated barotropic heat flow amounts to

$$\rho \, C_p \, 5.4 (\theta_E - \langle \bar{\theta} \rangle) = \rho \, C_p 5.4 (25.95 - 5.35) = +0.45 \, PW \qquad (6.7)$$

2. The baroclinic heat flux due to the zonally averaged geostrophic vertical-meridional circulation, is

$$\int \rho \, C_p \langle v \rangle (z) \langle \theta \rangle (z) \, L(z) \, dz = +0.93 \, PW \qquad (6.8)$$

and is due to warm surface water flowing northward and cold deep water flowing southward across 24.5ºN with no overall mass transport.

3. The horizontal heat flux due to large-scale gyre circulation, is

$$\int dz \int dx \, \rho \, C_p v'\theta' = +0.13 \, PW \quad (6.9)$$

in which at each depth warm waters flow northward at the Florida Straits (upper 200 m) and return southward colder in the eastern part of the section at the same depth.

The same separation has been performed for the other variables: salt, oxygen, silicates, nitrates and phosphates, the numerical results are given in table 6.2.

The heat transport calculated through the section is higher than the calculated in the previous chapter (see table 5.4). In the previous calculation we have used mean annual values in the Florida Straits for the velocity weighted average temperature (Larsen, 1992) and here we have used the 1992 cruise data. The August temperatures are about 1ºC higher than the annual average (20.29 versus 19.1 we cited in the chapter 5) and so the heat transport is about 29.5 Sv x 1.2ºC = .14 PW higher than the annual average.

Transport	Heat (PW)	Salt (10^6kg s^{-1})	Oxygen (kmol s^{-1})	Silicate (kmol s^{-1})	Nitrate (kmol s^{-1})	Phosphate (kmol s^{-1})
Ekman	0.45	10.1	-107	-150	-106	-6.5
Baroclinic	0.93	23.0	-852	-411	-210	-13.6
Horizontal	0.13	-14.1	-1662	307	186	7.5
Net	1.51	19.0	-2621	-254	-130	-12.6

Table 6.2: Transport of heat (PW), salt (10^6 kg s^{-1}), oxygen (kmol s^{-1}), silicate (kmol s^{-1}), nitrate (kmol s^{-1}) and phosphate (kmol s^{-1}) separated by components: Ekman and its barotropic compensation, baroclinic, horizontal, and net transport

6.4 Freshwater fluxes

6.4.1 Introduction

Freshwater flux provides important information on water mass circulation and sinking (Stommel, 1980) and can be calculated from hydrographic data independent from estimates of evaporation, precipitation, river runoff, etc. The freshwater flux is here calculated based on an integration point at the Bering Straits that connects the Pacific and the Atlantic Ocean via the Arctic Ocean. From long-term measurements Coachman and Aagaard (1988) reported that a flow of 0.8 x 10^6 m^3 s^{-1} of relatively fresh water leaves the North Pacific through the Bering Strait and enters the Arctic Ocean. Since oceanic salinities are typically 35, only 3.5% of the oceanic mass transport is salt transport, with the remaining 96.5% being freshwater transport.

The ocean exchanges freshwater with the atmosphere via evaporation at the surface of the ocean and precipitation both marine and terrestrial which enters as river runoff. Because of this exchange, the steady-state mass divergence in oceanic volumes will not be precisely zero. The zonally integrated meridional transport following Wijffels *et al.* (1992), will be calculated as

$$\frac{\delta}{\delta y}\iint \rho v dx dz = \int_{y}^{Boundary} F(x,y)\, dy \quad (6.10)$$

where x, y and z are the zonal, meridional, and vertical coordinates respectively, v the meridional oceanic flow and ρ the density of seawater. F(x,y) is the net gain of mass at the ocean surface due to precipitation (P), evaporation (E) and land runoff (R) respectively ***F(x,y)=P-E+R***

Since there are no salt pathway in the atmosphere, salt must be conserved:

$$\frac{\delta}{\delta y}\iint \rho v S dx dz = 0 \quad (6.11),$$

where S is the salinity of seawater. The freshwater balance is the difference between (6.10) and (6.11):

$$\frac{\delta}{\delta y}\iint \rho v(1-S) dx dz = \int F(x,y) dx \quad (6.12),$$

For a basin considered to be the Arctic and North Atlantic north of 24.5ºN together, mass conservation is as follows

$$-\rho F = \rho T_{BS} + \rho T_{FS} + \rho T_E + \rho T_M + \rho T_B \quad (6.13)$$

where F is now the net gain of mass at the ocean surface over the North Atlantic area between the 24.5ºN section and Bering Strait and the salt conservation equation:

$$\rho T_{BS} S_{BS} + \rho T_{FS} S_{FS} + \rho T_E S_E + \rho T_M S_M + \rho T_B S_B = 0 \quad (6.14)$$

where T_{BS}, T_{FS}, $T_{E,}$ $T_{M,}$ T_B represent the Bering Strait, Florida Straits, Ekman, Mid-ocean and barotropic transports and S_{BS}, S_{FS}, $S_{E,}$ $S_{M,}$ S_B the Bering Strait, Florida Straits, Ekman, Mid-ocean and barotropic velocity-weighted average salinities.

The zonally averaged mid-ocean transport T_M and the velocity-weighted salinity S_M for the Mid-ocean component is calculated from

$$\int v \; dx \; dz = T_M \quad (6.15)$$

and

$$\int < v > \; < S > \; dx \; dz = T_M \; S_M \quad (6.16)$$

so,

$$\frac{\int \rho < v > < S > \quad dx \quad dz}{\int \rho \quad < v > \quad dx \quad dz} = S_M \quad (6.17)$$

Defining a section salinity average $\overline{S}$, and deviation from zonal average, S' as above $\overline{S}(z) = \int S\,dx / \int dx$, $S'(x,z) = S(x,z) - \overline{S}(z)$; similarly for $\overline{v}$ and v' and neglecting density variations, the mid-ocean salt flux $\rho \, T_M \, S_M$ could be written as: $\rho(\overline{v}\,\overline{S} + \overline{v'\,S'})$; this separation has also been applied to the Florida Straits flow.

Multiplying the mass conservation eq.(6.13) by $\overline{S}$, we get

$$T_{FS}\left(S_{FS} - \overline{S}\right) + T_M\left(S_M - \overline{S}\right) - \iint_M v'\,S'\,dz\,dx + T_E\left(S_E - \overline{S}\right) + \iint_{FS} v'\,S'\,dz\,dx + T_{BS}\left(S_{BS} - \overline{S}\right) = -F\overline{S} \quad (6.18)$$

the barotropic term disappear because the salinity of any barotropic flow equals the average salinity $S_B = \overline{S}$.

Using the estimated values for $\overline{S}$=35.171, S_M=35.825, S_{Ek}=37.062, S_{FS}= 36.159 and $v'S'_M = +1.76$, $v'S'_{FS} = +0.54$ with S_{BS} taken to be 32.5, the freshwater convergence F is -0.47 10^6 m^3 s^{-1}. Since F=P-E+R, there is a divergence of freshwater over the region, which indicates that precipitation and runoff must exceed evaporation in the area north of 24.5ºN. From mass conservation eq.(6.13)

$-0.47 = 0.8 + 29.5 + 5.4 - 34.9 + T_B$, so that

$T_B = -0.47 - 0.8 = -1.27$ Sv

and the barotropic transport amounts to -1.27 Sv.

The freshwater part of the barotropic transport corresponds to a 96.5% of this calculated southward flow of 1.27 Sv, then the freshwater barotropic transport through the 24.5ºN section amounts for -1.23 10^6 m^3 s^{-1} (Sv), and the barotropic salt transport is – 44.6 10^6 kg s^{-1}.

6.4.2 Salt fluxes by components

Following the previous separation of velocity and salinity for the 24.5º North Atlantic section, we have calculated the Ekman and its compensating interior barotropic flow, baroclinic and horizontal salt flux components over the 24.5º N section, the salt balance has been calculated to be 19.0 x 10^6 kg s^{-1} (Table 6.2). The different contribution of the Ekman flow and its barotropic balancing interior, the baroclinic component and the horizontal component as functions of depth has been plotted in figure 6.11. The largest is the baroclinic component that amounts to 23.0 x 10^6 kg s^{-1}, this flow is due to northward flow of high salinity waters in the upper layers and southward flow of low salinity waters in the deep layers. Horizontal salt flux amounts to –14.1x10^6 kg s^{-1} and it is due to the large scale gyre, with northward velocities and negative anomalies in the Florida Straits and southward velocities and positive anomalies in the Canary basin in the uppers layers.

The Ekman flow of high salinity surface water and its compensating barotropic return flow at the section-average salinity amounts for 10.1 x 10^6 kg s^{-1}. As salt must be balanced in the ocean, northward salt transport across the 24.5ºN section makes Bering Strait flow saltier as it transits the North Atlantic. However, there is still excess salinity flux into the region north of 24.5ºN and this must be compensated by a net precipitation over the Arctic and North Atlantic north of 24.5ºN. Mass and salt conservation has been solved to get a barotropic freshwater transport of 1.23 Sv needed for the salt budget.

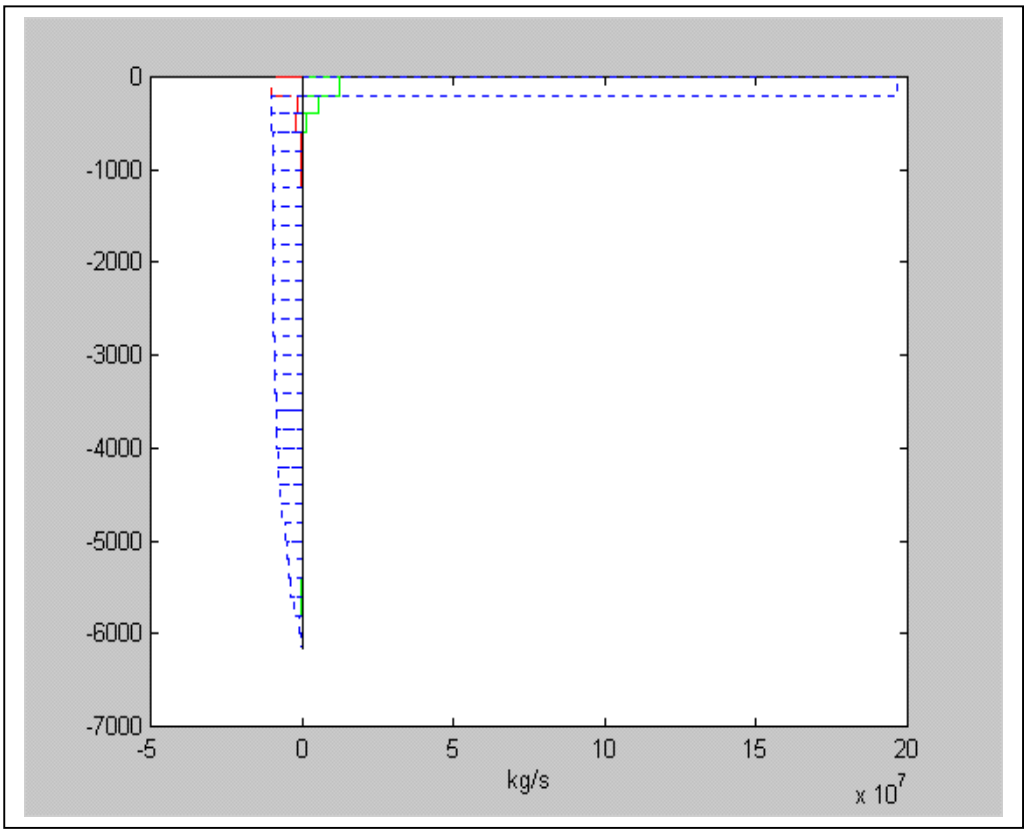

Figure 6.11. Salt fluxes by components: barotropic flow balancing Ekman flow, Bering Strait flow and net precipitation (blue --), baroclinic (green —), horizontal (red — —).

6.4.3 Discussion

The net precipitation obtained is surprising, because the Atlantic is generally known as an evaporative basin. In this case, not only the Atlantic but both oceans Arctic and Atlantic together north of 24.5ºN are considered. For the net gain or loss of freshwater by

the oceans, Baumgartner and Reichel (1975) estimated from air-sea exchange of freshwater and coastal runoff the net precipitation for the world ocean. The Arctic and North Atlantic north of 45ºN gives a net precipitation. South of 45ºN, evaporation prevails, in such amount that at 25ºN it compensates all the reported precipitation and runoff north of 45ºN (Hall and Bryden, 1982; Wijffels *et al*., 1992). At this latitude the freshwater transport should thus be the same than through the Bering Strait.

But the unquestionable fact is that the water flowing northward in the Florida Straits and Ekman layer is saltier than the water coming southward through the section: there must be a net precipitation to freshen the sea water and to balance the salt. This occurs even when we have included basins as the Mediterranean Sea where evaporation surely excess precipitation and high salinity water of Mediterranean origin pours into the Atlantic in the area we are studying.

The flow through the Bering Straits carries 26.7 (±3.3) x 10^6 kg s^{-1} of salt northward out of the Pacific into the Arctic and then into the northern Atlantic. To maintain salt conservation an equal amount of salt should be transported southward through the Atlantic (Wijffels *et al*., 1992). The net barotropic salt flux across 24.5ºN advects – 44.6 x 10^6 kg s^{-1} of salt, a quantity larger than the required -26.7 x 10^6 kg s^{-1}. The flow through the 24.5ºN section composed by the Ekman and its compensating interior, baroclinic and horizontal circulation amounts a salt transport of 19.0 x 10^6 kg s^{-1} (Table 6.2) without a net mass transport. Then the salt flow through the 24.5ºN section amounts to –25.6 x 10^6 kg s^{-1}, not different (within the precision of our calculations) from the quantity required by Wijffels *et al*. (1992) for all the sections through the Oceans.

6.5 Fluxes by Ekman, baroclinic and horizontal components

In this section we will analyse the different contribution of each of the separated components of the transport: Ekman and its barotropic compensation, baroclinic and horizontal component. All of them have been plotted by depth classes of 200 m depth.

6.5.1 Heat fluxes

Baroclinic heat transport is the largest component of the heat transport. It amounts to 0.93 PW and is due to the overturning circulation, northward velocities (positive and larger in the upper 500 m) of the upper layers multiplied by positives values of mean baroclinic potential temperature (from surface to 1200 m) amounts for around 0.8 PW. The rest of the baroclinic contribution is due to negative (southward) velocities in the NADW multiplied by negative baroclinic temperatures with a small negative contribution from the AABW, due to positive velocities and negative baroclinic potential temperatures. Thus, the baroclinic heat transport due to large temperature differences and velocities towards the north in the upper layer and south in the lower layers is the main component of the heat transport at 24.5ºN. Horizontal transport due to large scale gyre is northward in the upper 200 m due to warmer waters flowing northward in the Florida Straits and western boundary upper layer and colder waters flowing southward over the rest of the section. Deeper than 200 m, Florida Straits potential temperatures are actually lower than in the mid-ocean, so horizontal transport is negative. Deeper than 1000 m contributions from the horizontal cell are negligible. The last factor of heat transport is the Ekman transport. Using Trenberth *et al.* (1990) ECMWF climatology, Ekman transport is 5.4 Sv flowing at a mean upper 40 m temperature of 25.9ºC and Ekman heat transport amounts to 0.57 PW. To balance this ageostrophic Ekman transport a barotropic component is required. This flow of 5.4 Sv accounts for a mean velocity of $-1.9\ 10^{-4}$ m s^{-1} at a mean potential temperature of 5.35ºC. The barotropic component is very small (-0.12 PW, only 8% of the total transport) and goes in a southward direction; thus the total Ekman heat transport and its barotropic interior compensation amounts to 5.4 Sv at a difference of temperatures of (25.9ºC-5.35ºC) or a northward heat transport of 0.45 PW. Figure 6.12 shows the components of the transport by depth classes.

There are also small barotropic components for balancing the Bering Strait flux of freshwater and net precipitation over the North Atlantic. This baroclinic flux amounts to 1.23 Sv (0.77 Sv through the Bering Strait and 0.46 Sv of net precipitation). Then:

$$\rho C_p \langle \bar{v} \rangle (z) (\langle \bar{\theta} \rangle - \theta_{BS}) = \rho C_p \ 0.77\ (5.35 - 0) \quad balancing\ \ Bering\ \ Strait$$

$$\rho C_p \ \langle \bar{v} \rangle (z) (\langle \bar{\theta} \rangle - \theta_p) = \rho C_p \ \ 0.46\ (5.35 - 0) \qquad balancing \quad net \quad precipitation$$

Assuming potential temperatures for the Bering Strait and for the precipitation to be close to 0ºC. Those are very small contributions (-0.03 PW), below the accuracy of the heat flux calculations.

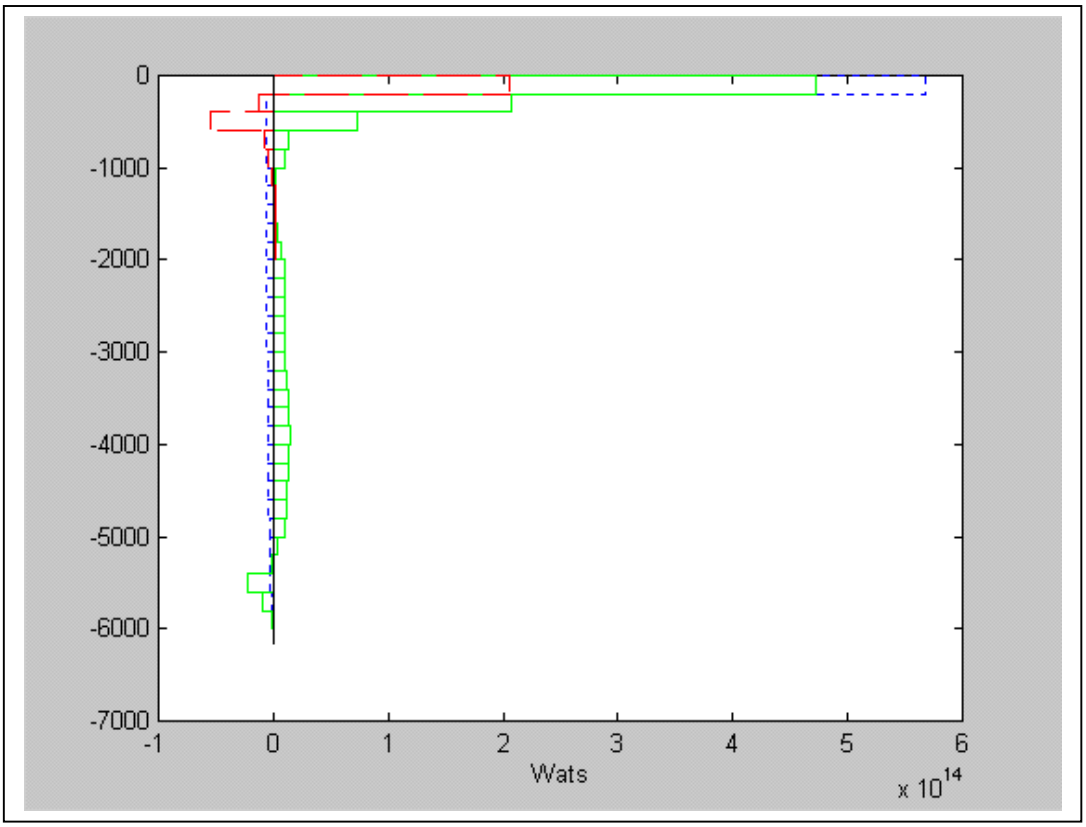

Figure 6.12: Heat fluxes by components: Barotropic balancing Ekman, Bering Strait and net precipitation (blue --), baroclinic (green —), horizontal (red — —).

6.5.2 Oxygen fluxes

The three components of the oxygen transport amount to a large quantity of southward transport. In figure 6.13 the three contributions are presented by depth classes. Ekman northward contribution amounts for 1168 kmol s^{-1}. Due to the mean oxygen concentration (228.8 µmol kg^{-1}), the barotropic compensation to the Ekman oxygen transport is –1275 kmol s^{-1}, hence the net Ekman component is actually a southward oxygen flow of –107 kmol s^{-1}. The baroclinic flux due to the zonally averaged geostrophic vertical-meridional circulation in which warm and poor oxygen upper layer

waters flow northward and deep oxygen-rich waters flow equatorward across 24.5ºN amounts for –852 kmol s^{-1} and is due to the combination of negative baroclinic concentrations and positive velocities (northward) in the upper layers and positive baroclinic concentrations and negative velocities (southward) in the lower layers. The only contribution to the northward transport is due to the AABW flowing northward with oxygen concentration larger than the mean value. The largest contribution to the oxygen transport is due to the large scale gyre circulation. This horizontal circulation amounts to –1661 kmol s^{-1}, mostly in the upper layers due to the relatively low oxygen concentrations in the Florida Straits waters flowing northward relative to higher mid-ocean concentration at the same depth flowing southward. The total southward transport amounts for –2621 kmol s^{-1}, around 10 % less than the calculated by Rintoul and Wunsch, (1991) for the 24.5ºN 1981 section (–2900 kmol s^{-1}). Table 6.2 presents the balance between components. Zonally averaged values of the total section and anomalies over the mid-ocean section and Florida Straits are presented in figure 6.7.

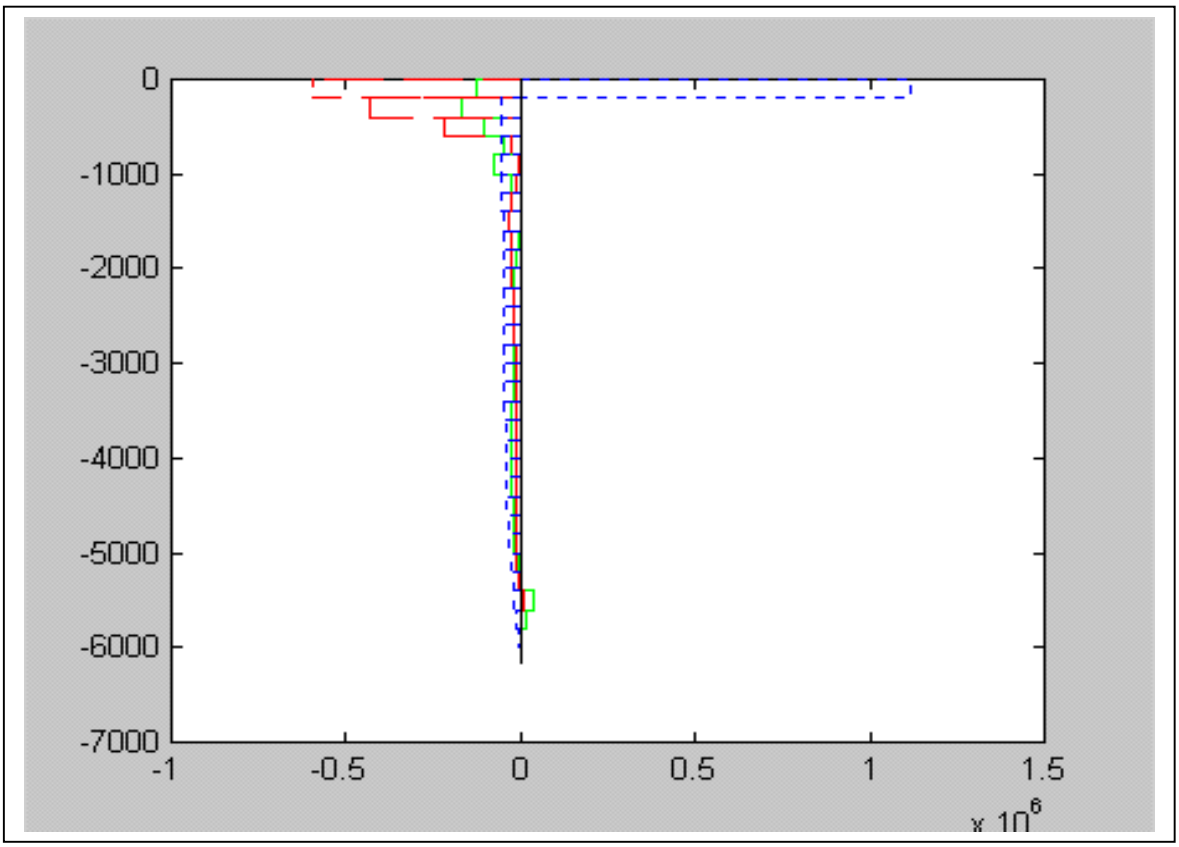

Figure 6.13. Oxygen fluxes by components: Ekman and its compensating barotropic flux (blue --), baroclinic (green —), horizontal (red — —). Units are mol s^{-1}.

The primary mechanism responsible for the southward flux of oxygen is the formation of deep water in the North Atlantic. When low oxygen subsurface water carried north by the Gulf Stream is exposed at the sea surface at higher latitude, it equilibrates with the atmosphere at colder temperatures and forms deep water which returns to the south at depth with a higher oxygen concentration. The higher oxygen concentration is notably found in the deep core of NADW on the DWBC. This highest oxygen concentration led Wust (1935) and Mantyla and Reid (1983) to say that the formation and export of NADW played an important role in the ventilation of the deep ocean. Here we are quantifying this ventilation in estimating that the overturning circulation leads to an oxygen input to the deep waters of 850 kmol s^{-1}.

6.5.3 Silica fluxes

Using the same separation as for oxygen, we have calculated the three contributions. Figure 6.14 presents the contributions by depth classes. Due to low surface concentrations, Ekman silica transport is very small; its compensating barotropic component amounts for –154 kmol s^{-1} and is due to a mean concentration of 27.78 µmol kg^{-1}; the total Ekman component is a southward flux of 150 kmol s^{-1}. The negative baroclinic contribution is greater in the upper layers due to positive velocities and negative baroclinic silica concentrations; small positive contributions are found at intermediate depths when velocities are negative (southward flow) and baroclinic concentrations are also negative. From 2400 m down to AABW, the deep water contribution is again negative due to positive baroclinic concentration and negative velocities. Finally, a small northward transport in the bottom waters is due to positive velocities and high concentrations in the AABW. Thus, the overturning circulation with low concentration in the northward transport and higher concentrations in the southward flowing deep water is responsible for a southward silica flux of –411 kmol s^{-1}. Horizontal circulation is responsible for a northward silica transport of 307 kmol s^{-1} nearly uniform throughout the water column. In the upper layers, concentrations and velocities are higher in the Florida Straits than in the mid-ocean section, in deep water silica concentrations in the Canary basin are higher than in the southward flowing NADW in the North American basin, leading to a net positive contribution. Overall, the net silica transport is toward the south and amounts to –254 kmol s^{-1}. Table 6.2 presents the balance between components. Zonally averaged values of

the total section and anomalies over the mid-ocean section and Florida Straits are presented in figure 6.8.

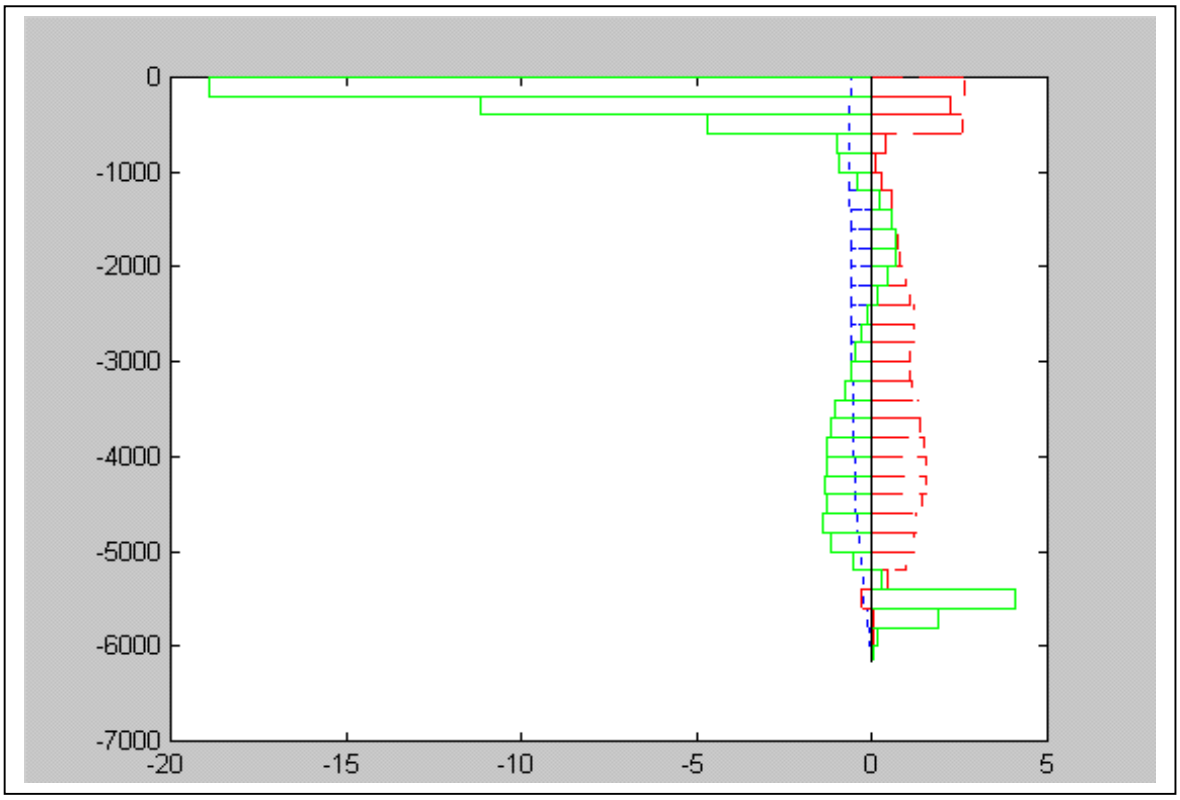

Figure 6.14. Silica flux by components: Ekman and its compensating barotropic flux (blue --), baroclinic (green —), horizontal (red — —). Units are mol s^{-1}.

As Rintoul and Wunsch, (1991) suggested, the overturning cell in the North Atlantic plays an important role in the flux of silica. Because the poleward flux in the upper layers is lower in silica than the equatorward deep flow, the result is a net equatorward flux of silica. Rintoul and Wunsch, (1991) justified his silica flux by the import of silica to the North Atlantic from the Arctic Ocean (Codispoti, 1979) as a net flux toward the Atlantic of 36 kmol s^{-1} of silicate (Anderson *et al*, 1983). River run-off of silicates supply an additional 40 $kmols^{-1}$ (Livingstone, 1963) for a total input of 74 kmol s^{-1} of silicate from different sources in the North Atlantic. Rintoul and Wunsch, (1991) conclude that within the probable uncertainty in both numbers, there is no conflict between the fluxes they found (–152 kmol s^{-1}) and the estimated input of silica into the basin. DeMaster (1980) suggested that the accumulation rates of silica in the Antarctic polar front from the south Atlantic Ocean is around 30%, of the total silicate supply to the world

ocean, which is estimated to be around 35 kmol s^{-1} of silica. The total transport calculated here (–254 kmol s^{-1}) is somewhat higher that the calculated by Rintoul and Wunsch, (1991) and therefore some adjustments of the circulation on the section within constraints on silica transport will be presented later in this chapter.

6.5.4 Nitrate fluxes

Nitrate+nitrite transport contributions have similar distribution to those for silica but with some difference in the baroclinic deep contribution which is very low for nitrates

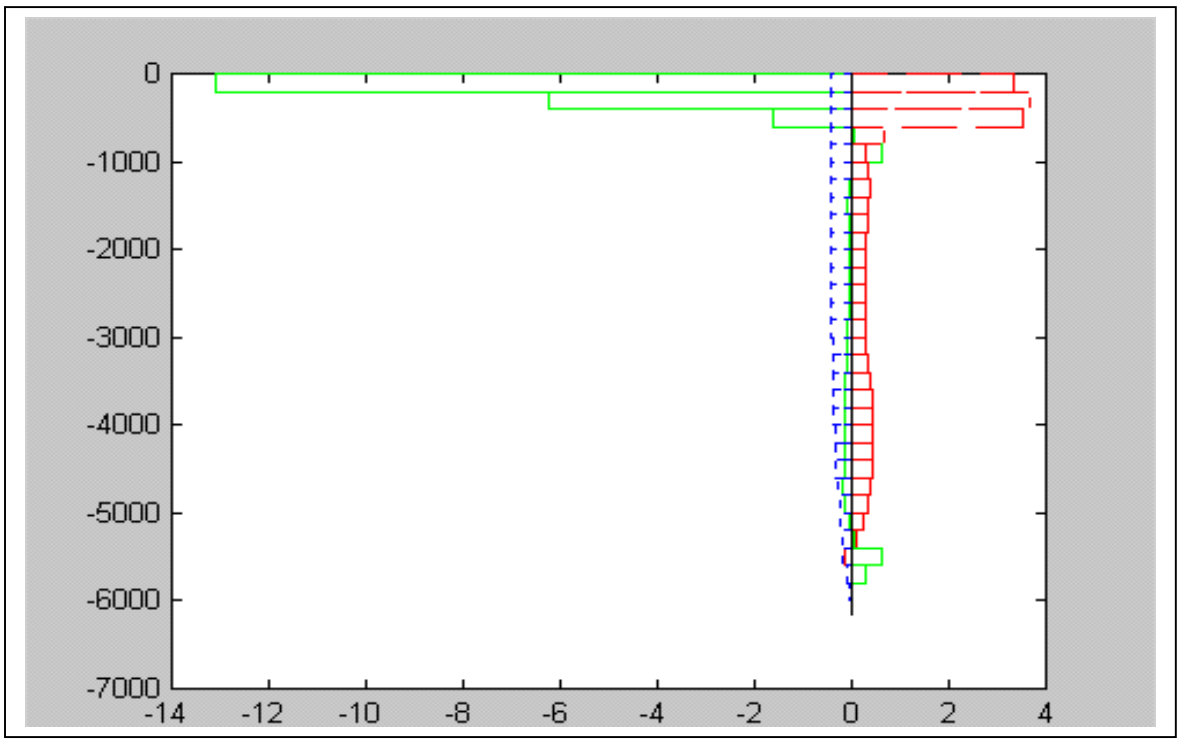

Figure 6.15. Nitrate fluxes by components: Ekman and its compensating barotropic flux (blue --), baroclinic (green —), horizontal (red — —).. Units are mol s^{-1}.

(Fig. 6.15). Ekman contribution is negligible because of low surface concentrations but its barotropic compensation amounts to 107 kmol s^{-1}, due to a mean nitrate concentration of 19.26 µmol kg^{-1}. The baroclinic contribution is large in the upper layers and negligible deeper than 1200 m, only AABW exhibits a small positive contribution. The overturning circulation mechanism with northward transport (positive velocities) in the upper layers with low nitrates (negative baroclinic concentration) gives a negative contribution to baroclinic transport. Small southward (negative) velocities in deep water with concentrations not too different from the mean value (positive) result in small

contributions in deep layers. Overall the baroclinic flux is southward and amounts to 210 kmol s^{-1}. Horizontal contribution is 186 kmol s^{-1} northward, nearly balancing the baroclinic contribution. Larger nitrate concentration in the Florida Straits than in the mid-ocean section is responsible for the positive contribution in horizontal nitrate transport of the upper waters. The small positive contribution all over the NADW depths is due to small differences in nitrates concentration of the North Atlantic basin and the Canary basin.

Table 6.2 presents the balance between components. Zonally averaged values of the total section and anomalies over the mid-ocean section and Florida Straits are presented in figure 6.9. Overall we found an export of nitrate from the North Atlantic of -130 kmol s^{-1}. This amount differs from the Rintoul and Wunsch, (1991) result which gave no meridional transport of nitrate at 24ºN but showed a divergence between 36 and 24º similar in magnitude to the amount found in our calculation.

6.5.5 Phosphate fluxes

Phosphate transport has the same pattern as the nitrate transport as the Redfield ratio of around 15.5 is found for both the Ekman and its barotropic compensation and baroclinic contribution (Fig. 6.16). Ekman contribution to the phosphate flow is negligible but as the mean phosphate concentration is 1.23 μmol kg^{-1}, compensating barotropic transport gives a value of -6.9 kmol s^{-1}. Baroclinic contribution amounts to -13.6 kmol s^{-1}, and is due to low phosphate concentration in the upper layers water flowing northward and higher concentration waters flowing southward in deep waters, as in the nitrate transport. Horizontal contribution amounts to 7.5 kmol s^{-1}, not quite as large as might be expected considering the Redfield ratio with the nitrates. This smaller contribution of the horizontal cell may be due to errors in the concentration determination, which affects individual values rather than the mean values. Table 6.2 presents the balance between components. Zonally averaged values of the total section and anomalies over the mid-ocean section and Florida Straits are presented in figure 6.10. The total export of phosphate from the northern part of the North Atlantic is around -13 kmol s^{-1}. We have no basis for comparison but appears to be an important amount for be exported in steady state.

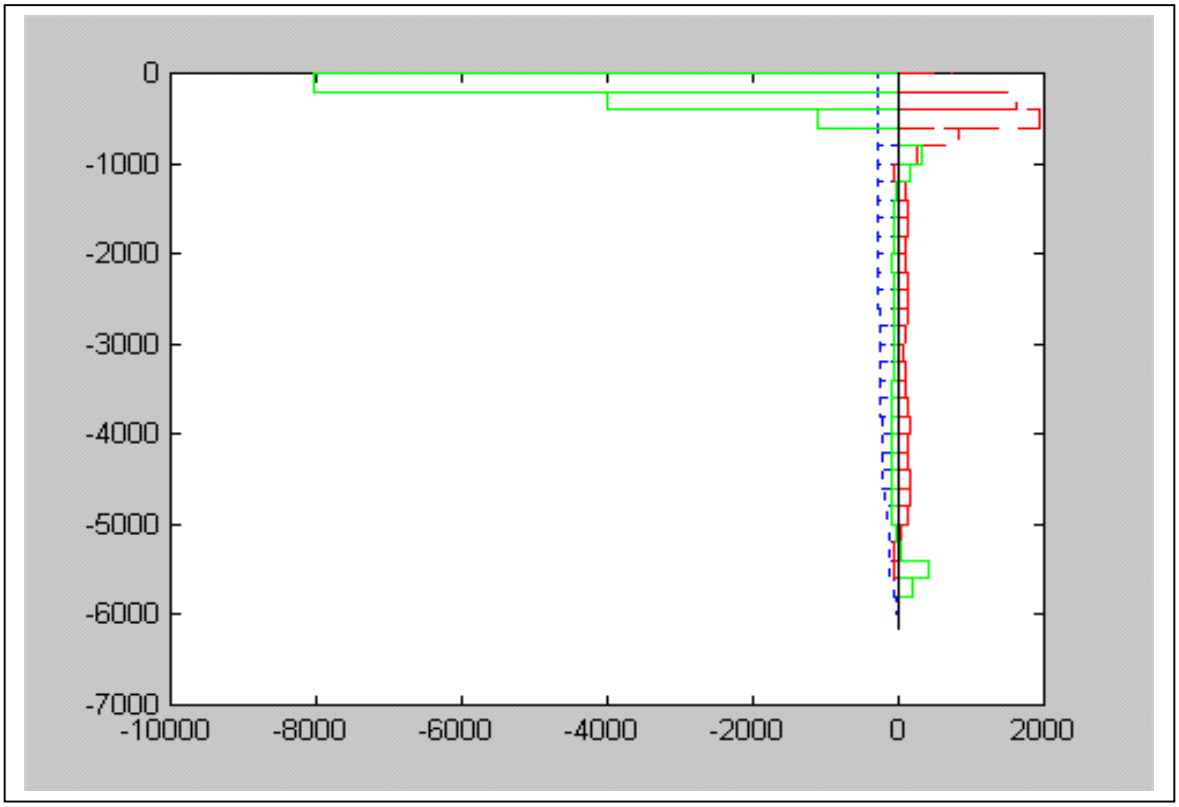

Figure 6.16. Phosphate fluxes by components: Ekman and its compensating barotropic flux (blue --), baroclinic (green —), horizontal (red — —). Units are mol s^{-1}.

- In summary, the baroclinic contribution due to overturning circulation is responsible for the largest amount of heat transport and the Ekman component is the second source of transport. Horizontal transport is the main contribution to southward oxygen flux, and the large scale gyre circulation is responsible for this, mainly in the upper layers where low oxygen water in Florida Straits flows northward and higher oxygen mid-ocean water flows southward. Baroclinic contribution from the overturning circulation is the second factor in importance to the southward oxygen transport. Ekman northward oxygen transport and its compensating barotropic oxygen transport have similar levels but are in a southward direction and contribute a small southward element to the final southward oxygen transport.

- In the case of nutrients, baroclinic transport due to overturning circulation is the main factor for the southward transport of all nutrients, due to low upper water concentrations in the northward flow and higher deep water concentrations in the southward flow. Horizontal northward transport is the second factor due to higher

concentrations in the Florida Straits than in the mid-ocean in the upper layers. The difference of concentrations and velocities in both deep basins: northward flow in the Canary basin and southward flow and lower concentration of recent ventilated water in the deep western boundary current and consequently in the North American basin also contribute to the horizontal transport but in a lesser extent than the upper-layers contribution.

6.6 Flux components: Ekman, mid-ocean and Florida Straits

In this section we will repeat the oxygen and nutrient transport calculations using the components separation we have discussed for heat and freshwater transport previously. Following the chapter 5 calculations on heat transport, once we have determined the three components of the transport: Ekman, mid-ocean and Florida Straits, the fluxes across 24.5ºN latitude of the subtropical North Atlantic can be written by eq. (5.5). Taking a velocity weighted average property value for each of the different components of the transport by

$$C_c = \frac{\int_W^E \int_{-H(x)}^O C\ V\ dx\ dz}{\int_W^E \int_{-H(x)}^O V\ dx\ dz} \quad (6.19)$$

where C denotes the concentrations of the chemical variables and V the velocity of each component. The results are given as follows in table 6.3

The velocity weighted average property gives an idea of the mean concentration over the three components: Oxygen concentrations are higher in the mid-ocean, a little lower in the Ekman layer and very low in the Florida Straits. This very low oxygen concentration in the Florida Straits gives a clear idea of the influence of water masses of distant origin such as Antarctic Intermediate Water and eastern South Atlantic waters. Ekman layer nutrient concentrations are very low. Values in the Florida Straits are surprisingly higher for the shallower depth. The South Atlantic influence in Florida Straits waters (according to Schmitz and Richardson (1991), 45% of water flowing through the Florida Straits is of eastern South Atlantic origin) is again clearly shown in the mean

nutrient concentrations mainly in nitrates. Difference in velocity-weighted average nitrate concentration in the Florida Straits with mid-ocean section is only of 25%. Differences are higher in phosphates at 40% and even higher in the silicates at 70%. The differences in silica are due to the increase of concentrations with depth, since there is a large difference in depth between Florida Straits and the mid-ocean, the difference in silica concentrations is large.

	Mid-ocean	**Ekman**	**Florida Straits**
oxygen (µmol kg^{-1})	245	210	165.2
silicate (µmol kg^{-1})	10.7	0.72	4.2
nitrate+nitrite(µmol kg^{-1})	9.6	0.2	7
phosphate(µmol kg^{-1})	0.7	0.07	0.4

Table 6.3: Velocity weighted average concentration of oxygen, silicate, nitrate+nitrite and phosphate in the Mid-ocean, Ekman layer and Florida Straits. Units are µmol kg^{-1}.

The high nutrient concentration in the shallow layers of the Florida Straits is a very important element in the productivity of the northern North Atlantic. Rintoul and Wunsch (1991) have shown the existence of net northward transport of nitrate through 36ºN; with most due to advection in the Gulf Stream. Pelegrí and Csanady (1991) have shown that (along stream) nutrient transport by Gulf Stream approximately triples between the Florida Straits and 36ºN because of large (cross stream) epipycnal inflow. And Pelegrí *et al.* (1996) conclude that the nutrient stream of the North Atlantic subtropical gyre, or Nutrient Gulf Stream, is responsible for the epipycnal transport of large amounts of nutrients to the northern North Atlantic.

The overall flux can be written as

$$T_{NA} = (FS_T C_{FS} + EK_T C_{EK} + MO_T C_{MO}) \rho \qquad (6.20)$$

where FS_T stands for transport in the Florida Straits and C_{FS} is the velocity-weighted average chemical concentration for this transport, and analogous terms are used for Ekman and geostrophic mid-ocean transport.

Because the mid-ocean transport compensates the other transport MO_T=-FS_T-EK_T, the equation (6.20) can then be written as

$$T_{NA} = \{ FS_T (C_{FS} - C_{MO}) + EK_T (C_{EK} - C_{MO}) \} \rho \quad (6.21)$$

In table 6.4 the transports due to the difference in concentration for the three components are presented.

PROPERTY	COMPONENT	TRANSPORT (SV)	PROPERTY DIFF. WITH MID-OCEAN (μMOL KG^{-1})	NORTHWARD TRANSPORT (KMOL S^{-1})	NET TRANSPORT (KMOL S^{-1})
Oxygen	Ekman layer	5.4	210-245	-195	-2620
	Florida Straits	29.5	165.2-245	-2425	
Silicate	Ekman layer	5.4	0.7-10.7	-56	-254
	Florida Straits	29.5	4.2-10.7	-198	
Nitrate+ nitrite	Ekman layer	5.4	0.2-9.6	-52.3	-130
	Florida Straits	29.5	7-9.6	-77.7	
Phosphate	Ekman layer	5.4	0.07-0.71	-3.5	-12.6
	Florida Straits	29.5	0.4-0.71	-9.1	

Table 6.4: Components of the fluxes of oxygen, silicate, nitrate+nitrite and phosphate, transport, difference of property with Mid-Ocean concentration, transport due to difference of property with Mid-Ocean concentration and with Ekman and Florida Straits transport and total transport given by equation. 6.21.

The transport results obtain in this thesis are compared with previous results from 1957 and 1981 24.5ºN sections. In table 6.5 results of the 1992 cruise from this work, Rintoul and Wunsch (1991) results from the 1981 cruise, Hall and Bryden (1982) results from the 1957 cruise and Brewer *et al*. (1989) results from the 1957 cruise are presented.

Changes in the current structure in the Florida Straits involves a reduction in the total silicate transport from 145 kmol s^{-1} in 1981 to 128 in 1992, the reduction in nitrate was from 244 to 214 and in phosphate from 13.7 to 12 kmol s^{-1}. Those changes are due to the sampling during 1992 being shallower than in 1981, and even though an adjustment in

	1992 SECTION (1)	1981 SECTION(2)	1957 SECTION
heat (PW)	1.36	1.3	1.2 (3)
oxygen (kmol s^{-1})	-2618	-2900	-2084* (4)
silicate (kmol s^{-1})	-254	-152	
nitrate+nitrite(kmol s^{-1})	-130	0	
phosphates (kmol s^{-1})	-12.6		

*Due to a problem with the 1957 Oxygen data (see chapter 2) those values are not used.

Table 6.5: Transport of heat, oxygen, silicate, nitrate+nitrite and phosphate for the three 1992, 1981 and 1957 sections by authors: 1992 results of this work (1), 1981 Rintoul and Wunsch, (1991) results (2), 1957 Hall and Bryden (1982) results (3) and 1957 Brewer *et al,* (1989) results (4).

transport to 29.5 Sv was made, shallow waters have lower concentration of nutrients. This reduction on northward nutrient transports ultimately results in an increase of the overall southward transport mainly for nitrate and phosphate an in a lesser amount for silicate.

6.7 Variability of the calculations

The variability in the transport calculations is discussed here. The first source of uncertainty is given in the Ekman transport. For the calculation of the Ekman transport the climatology of Trenberth *et al*. (1990) that gives a transport of 5.4 ± 0.7 Sv has been chosen (see chapter 5). Helleman and Rosenstein (1983) climatology results in an Ekman transport of 6 ± 2 Sv. To evaluate the variability in the Ekman transport the calculation is repeated again changing 5.4 Sv in +/- 2 Sv.

We conclude that a difference of 2 Sv in the Ekman flow calculations could influence heat transport by ± 0.16 PW, salt by ± 3.9 x 10^6 kg s^{-1}, oxygen by ± 40 kmol s^{-1}, silicate transport by ± 50 kmol s^{-1}, nitrate transport by ± 40 kmol s^{-1} and phosphate by ± 2 $kmols^{-1}$.

In this chapter, 1992 cruise data are used instead of annual means as in the previous chapter for the Florida Straits, so interannual as well as seasonal variability in the fluxes must be taken into account. Variability in the Florida Straits flux amounts to ± 3 Sv (Leaman *et al.,* 1987). This variability therefore and the nutrient transport variability, due to the shallower 1992 sampling, may also affect heat transport by ± 0.16 PW, salt by ± 2.5

x 10^6 kg s^{-1}, oxygen by ± 240 kmol s^{-1}, silicate transport by ± 75 kmol s^{-1}, nitrate transport by ± 45 kmol s^{-1} and phosphate by ± 2.9 $kmols^{-1}$.

Another source of variability is the horizontal cell or eddy contribution along the mid-ocean section. First, the contribution to the heat transport of the horizontal cell was studied. In figure 6.17 the eddy heat flux contribution of each pair of stations (dotted) and the eddy fluxes accumulated from the eastern boundary (solid) is plotted. High variability is found in both basins mainly near the boundaries and low over the Mid Atlantic Ridge. The standard deviation found is 1.8 x 10^{13} W. For error analysis, the standard deviation would accumulate by $\sqrt{N}$, N being the degree of freedom. An estimate of the correlation distance for the section is required. The eddy scale was calculated in Chapter 3 to be about 350 km. Parrilla *et al*. (1994b) estimated 300 km for the eddy scale. The difference is small and so the value that gives greater error (300 km) is used to calculate the uncertainty of calculations. Therefore, for 6000 km zonal width, a total of 20 freedom degrees are considered. The error due to the horizontal cell in heat transport increases on that previously calculated by only about 0.08 PW.

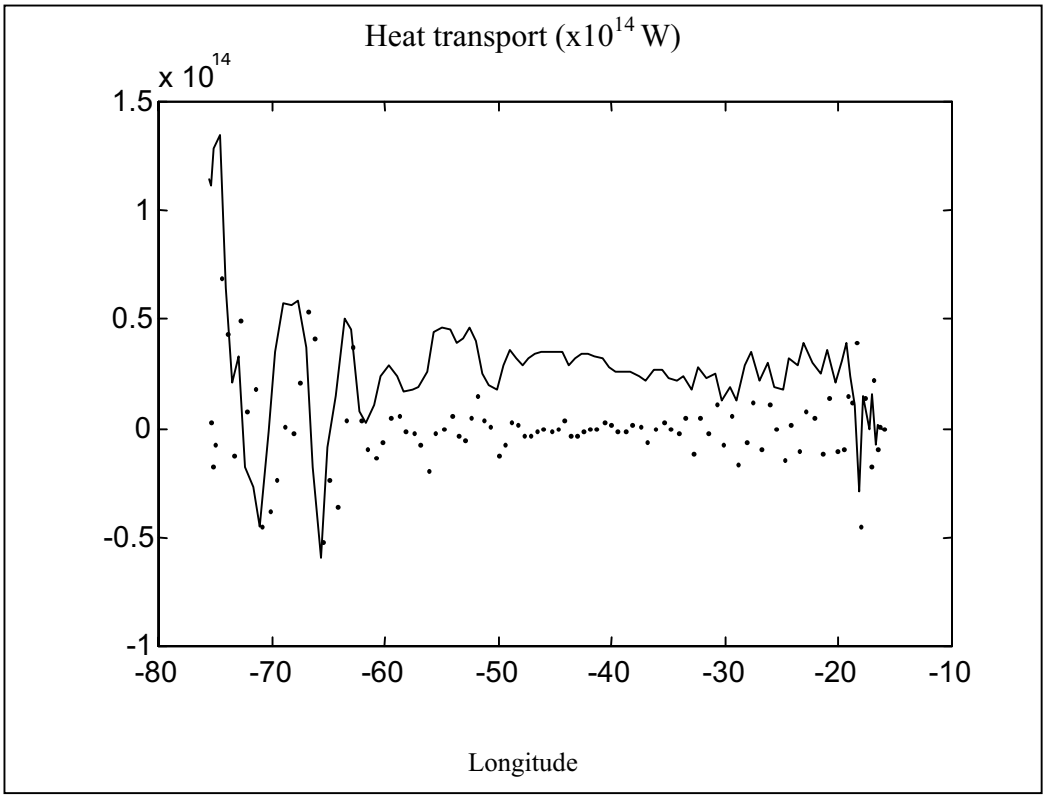

Figure 6.17. Horizontal component of the heat transport on the mid-ocean section calculated for each station pair (dotted) and accumulated (solid) from the eastern end of the section.

Following the same calculation for oxygen (Fig. 6.18), the horizontal cell or eddy contribution gives a southward transport of 200 kmol s^{-1}, which increases in the western boundary to –560 kmol s^{-1}. Standard deviation is 56 kmol s^{-1} and error increases by 250 kmol s^{-1}.

If we consider the horizontal cell by pair of stations and accumulate from the African coast we get the following picture for silica (Fig. 6.19) and nitrate (Fig. 6.20) horizontal cells. Horizontal transport of silica is southward near the Eastern boundary reaching 27ºW. From this longitude silica transport becomes generally northward in the Canary Basin and close to zero in the central regions, so accumulated transport remains at around 50 kmol s^{-1} with a standard deviation of about 9. Near the western boundary great variability in horizontal transport is detected and accumulated transport becomes southward by –140 kmol s^{-1} and then northward again around 230 kmol s^{-1} with a standard deviation of 29. The error in silica transport then increases by 130 kmol s^{-1}. Accumulated horizontal transport of nitrate shows less variability and the total amount is 66 kmol s^{-1}, substantially less than silica. From the eastern boundary southern flow is also found up to around 30ºW, and more or less homogeneous flow to 70ºW. Near the western

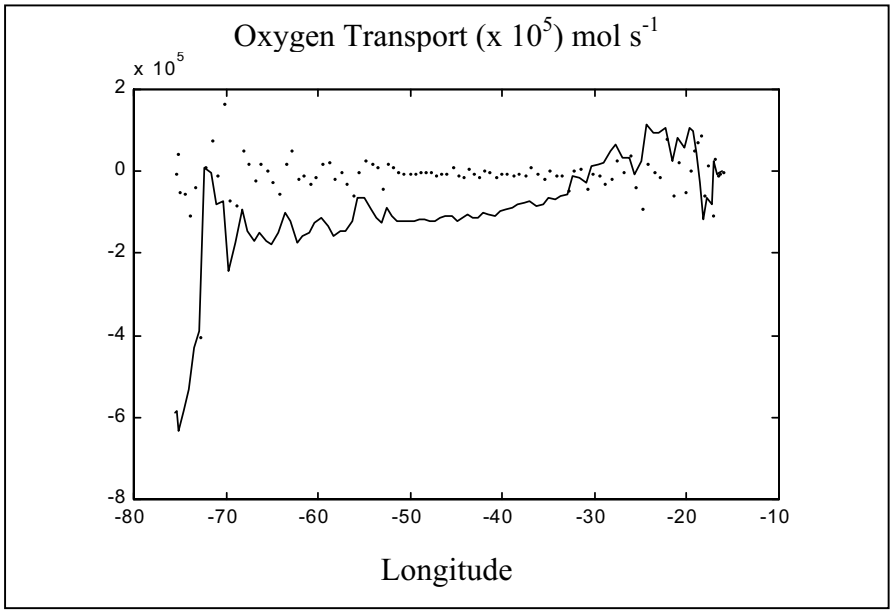

Figure 6.18.- Horizontal component of the Oxygen transport on the mid-ocean section calculated for each stations pair (dotted) and accumulated (solid).

boundary an increase in northward nitrate transport is detected. Total standard deviation is around 9 kmols^{-1} with the corresponding error of 40 kmol s^{-1}. The total standard deviation for phosphate is around 0.6 kmols^{-1} and the error is 2.7 kmol s^{-1}. Relative to salt transport, we should add a variability of 1.8 x 10^{6} kg s^{-1} due to horizontal circulation.

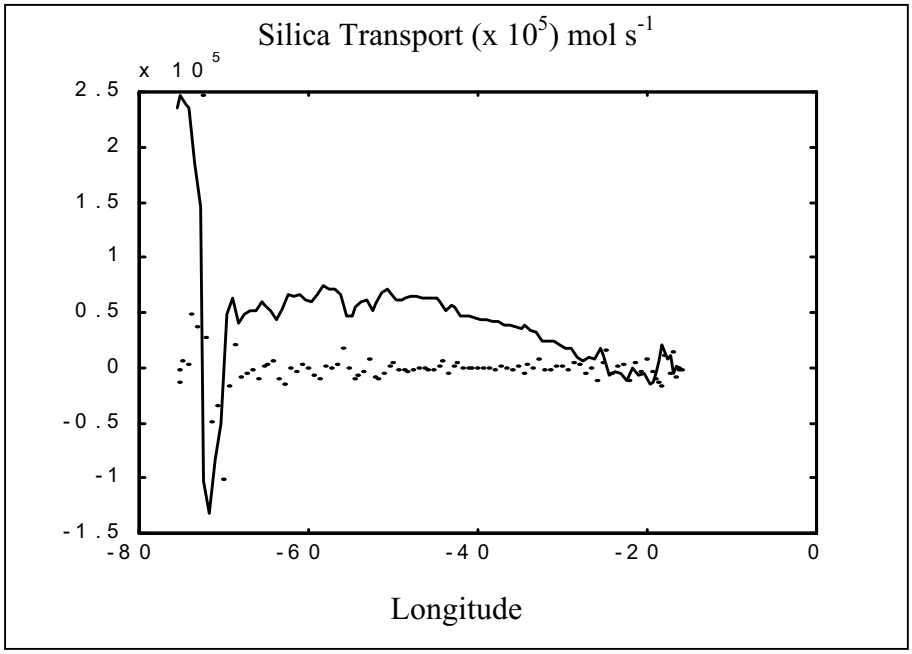

Figure 6.19.- Horizontal component of the silica transport on the mid-ocean section calculated for each stations pair (dotted) and accumulated (solid) from the eastern end of the section.

For the error in transport we have to add such horizontal cell variability to the Ekman and Florida Straits transport variability to account for 1.51 ± 0.40 PW, salt transport of 19.0 ± 8.2 x 10^{6} kg s^{-1}, oxygen –2600 ± 530 kmol s^{-1}, silica –254 ± 250 kmol s^{-1}, nitrate –125 ± 120 kmol s^{-1} and phosphate –12.3 ± 7.6 kmol s^{-1}.

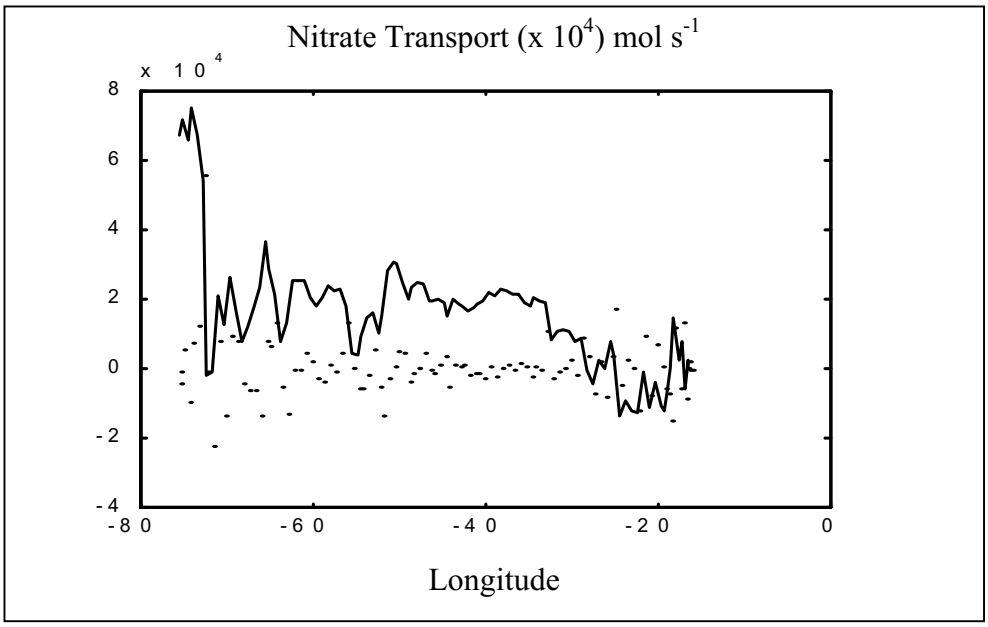

Figure 6.20. Horizontal component of the nitrate transport on the mid-ocean section calculated for each stations pair (dotted) and accumulated (solid) from the eastern end of the section.

6.8 The dissolved silica budget as a constraint on the meridional circulation

In chapter 5, the circulation was estimated based on geostrophic analysis of the observed density field. A startling feature of the circulation analysis is an unexpectedly large dissolved silicate exportation from the North Atlantic (see Robbins and Toole, (1997) for a similar case in the Indian Ocean). Considerations previously presented and high uncertainty in silica transport have lead us to reconsider the circulation evaluated in chapter 5 to yield a circulation scheme that conserves the silicate more closely. This modification requires changes in the geostrophic reference levels.

First, however, it is necessary estimate how near pure conservation it is reasonable to expect the Atlantic Ocean silica budget to be. An attempt has been made to estimate the magnitude of the sources and sinks of silicates in the North Atlantic. DeMaster (1981) estimates the rate of dissolved silica supplied to the global ocean as 320 ± 32 kmol s^{-1} of which two-thirds is due to riverine input and the remaining one-third due to hydrothermal

vents. The best estimate of the total global loss of silicate to sedimentation and burial on the ocean floor is 200 ± 32 kmol s^{-1}. Thus the rate of cycling silica in and out the world ocean is between 200 and 300 kmol s^{-1}. Considering the Rintoul and Wunsch (1991) justification for silica conservation and that DeMaster also stated that the South Atlantic accumulation rates of sink silicates is around 30% of the world ocean, for the purpose of the analysis, two solutions will be checked: For the first one we will assume the ocean is in balance, so that no net flux of silica occurs through the 24.5ºN section. The second solution gives some amount of southward transport that accounts for the rivers and hydrothermal sources, and the Pacific flow through the Bering Straits (Coachman and Aagard, 1988); it has been considered half of the calculated transport to amount -127 kmol s^{-1}. This silica flux is similar (within the error calculation) to the silica flux calculated by Rintoul and Wunsch (1991) for the section (-138 kmol s^{-1}).

The circulation discussed in chapter 5 is based on a reference level and a barotropic velocity for all stations calculated to conserve mass together with Florida Straits and Ekman transport. Although the reference levels are based on a careful study of the water masses, it is reasonable to expect ambiguity in the precise choice of the reference level. Some constraints will be defined to solve the new system: the first one, as in the previous model, is conservation of mass and the second one, conservation of silica (null transport or the amount previously selected). No other constraints are imposed.

The equations of conservation of mass and silica are:

$$\sum \rho A v_b = 0 \quad (6.22)$$

CASE 1

$$\sum \rho A v_b C_{si} = 127 \quad (6.23)$$

or CASE 2

$$\sum \rho A v_b C_{si} = 254 \quad (6.24)$$

where ρ is sea water density, A is the area between stations, v_b is the reference level velocity and C_{si} is silica concentration for each pair of stations, both sums extend to all pairs of stations (from stations 1-2 to 100-101):

$$A = \begin{pmatrix} A_{1-2} \\ A_{2-3} \\ . \\ . \\ . \\ A_{100-101} \end{pmatrix},\ v_b = \begin{pmatrix} v_{b1} \\ v_{b2} \\ . \\ . \\ . \\ v_{b100} \end{pmatrix} \text{ and } C_{si} = \begin{pmatrix} C_{s1} \\ C_{s2} \\ . \\ . \\ . \\ C_{s100} \end{pmatrix}$$

and $C_{si} = \langle C_{sii} \rangle$ is the station-pair averaged silica concentration

The system has two equations (6.22 and 6.23 for Case 1) or (6.22 and 6.24 for Case 2) and 100 unknown reference levels velocities (v_b) to solve. The system of equations is solved using the singular value decomposition (SVD) (Wunsch, 1996), which obtains the simplest model consistent with observations and with silica conservation. Here, simplest refers to the solution which minimises variance in the reference level velocities. By adding mass and silica conservation the sensitivity of the results to the assumed reference level is removed (Roemmich and Wunsch, 1985). In figure 6.21 the two series of reference level velocities obtained by the resolution of the system of equations for Case 1 and Case 2 is presented.

The new barotropic velocities adjustment increases southward transport near the western boundary where silica is relatively low and reduces northward transport over the Mid-Atlantic ridge. It increases northward transport over the central Canary basin where silica is relatively high and reduces northward transport near the eastern boundary. In general, the solution has imposed southward corrections in the shallow regions near the boundaries and the Mid-Atlantic ridge where silica concentrations are low, and northward corrections in the deep basins, mainly in the Canary basin, where silica concentrations are high. The volume transport in the two cases, silica transport = 127 kmol s^{-1}, and silica transport =0 are presented in table 6.6 as they are in table 6.1 for the following layers: upper layers, thermocline, UNADW, LNADW and AABW. To separate the influence of the adjustment, this transport has been calculated in four regions: Western Boundary (from 75ºW to 69ºW), North American basin (from 69ºW to 45ºW), Canary basin (45 to 25ºW) and the eastern part of the Canary basin (from 25ºW to 16ºW). Table 6.1 gives the same information without any constraints (case 0, as was deduced from chapter 5 calculations).

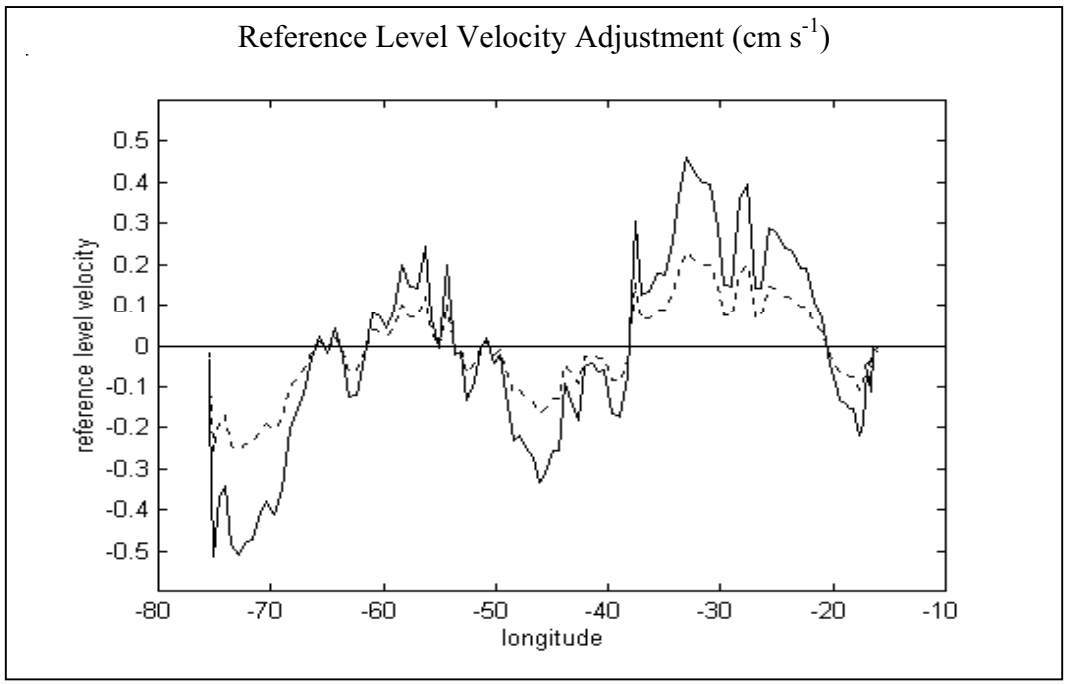

Figure 6.21. Barotropic velocity adjustment added to the previously discussed circulation to create an adjustment of 127 kmol s^{-1} of southward silica transport (Case 1: dotted red line) and a silica-conserving scheme (Case 2: solid blue line). Maximum adjustments are only around 0.2 cm s^{-1} in the first case and of 0.5 cm s^{-1} for the second case.

A large increase in the southward transport near the western boundary is detected; from 27.4 Sv (Case 0) to 35.3 Sv (Case 1) and finally 43.4 Sv (Case 2). In the Canary basin, the increase in flow of deep water (deeper than 1200 m) is from 1.8 Sv to 9.1 Sv to 16.6 Sv for the three cases. Increase in the southward flow of the DWBC is compensated by intensification of the northward flow of the Canary basin. These changes produce intensification in the horizontal or eddy flux (water flowing south in the western boundary current and northward in the Canary basin at the same depth) and the transport associated with that cell. Changes in the horizontal transport are due to correlation between velocities and silica concentration anomalies: increase in negative anomalies in velocity in the DWBC multiplied by negative anomalies (low silica concentration in the DWBC) and increase in positive anomalies in velocity in the Canary basin multiplied by positive anomalies on silica concentration in this basin. Both are positive contributions to the horizontal cell. The velocity field in the upper ocean is hardly affected by the changes as velocities in the upper layers are much greater (as shown in the figure 6.1A) than the adjustment velocities calculated by our models. The most significant change in the current structure occurs in the Canary basin where the deep flow increases from no motion to weakly northwards. Changes in the deep ocean (below 3000 m depth) are larger due the

slow geostrophic flow with the exception of the western boundary. This deep northward transport increases in the Canary basin from 0.6 Sv to 4.2 Sv and 7.8 Sv in our model.

A)

Transport (Sv) Silica tr=127 kmol/s	West Boundary (75ºW-69ºW)	N.American B (69ºW-45ºW)	Canary B. (45ºW-25ºW)	E. Canary B. (25ºW-16ºW)	Florida Straits	Ekman layer
Upper (0-600m)	-2.9	-2.2	-8.9	-3.4	29.2	5.4
Thermocl.(600-1200)	-3.2	5.2	-1.3	0.1	0.3	
UNADW(1200-3000)	-14.4	0.4	3.1	0.3		
LNADW(3000-4900)	-13	-1.0	3.2	1.0		
AABW(4900-bottom)	-1.8	2.3	1.3	0.2		

B)

Transport (Sv) Not silica transport	West Boundary (75ºW-69ºW)	N.American B (69ºW-45ºW)	Canary B. (45ºW-25ºW)	E. Canary B. (25ºW-16ºW)	Florida Straits	Ekman layer
Upper (0-600m)	-3.8	-2.4	-8.2	-3.3	29.2	5.4
Thermocl.(600-1200)	-4.1	4.9	-0.6	0.3	0.3	
UNADW(1200-3000)	-17.1	-0.3	5.3	0.8		
LNADW(3000-4900)	-15.8	-1.1	6.1	1.7		
AABW(4900-bottom)	-2.6	2.5	2.4	0.3		

Table 6.6: Transport (Sv) by classes of depth (0-600, 600-1200, 1200-3000, 3000-4900, 4900-bottom) and for different regions: Western Boundary (75ºW-69ºW), North American basin (68ºW-45ºW), Canary basin (45ºW-25ºW), East Canary basin (25ºW-16ºW), Florida Straits and Ekman layer; for A) Silica adjustment to 127 kmol s^{-1} and B) not silica transport. Table 6.1 gives similar information without any constraints.

Table 6.7 summarises the 24.5ºN transport by depth classes for the three cases. The meridional overturning circulation is practically the same. A flow of 19 Sv of northward warm upper layers (shallower than 1200 m depth), a return southward flow of NADW of 20.4 Sv and a bottom AABW flow of 1.3 Sv in the mass conservation only case, slight changes of upper layer flow to 18.3 and 17.7 Sv for Cases 1 and 2, similar NADW flow and a small increase of AABW flow to 2 and 2.6 Sv respectively.

Transport (Sv)	Mass Conservation only	Silica tr=127 kmol s^{-1}	No silica transport
Upper (0-600m)	17.6	17.2	16.9
Thermocl.(600-1200)	1.4	1.1	0.8
UNADW(1200-3000)	-9.8	-10.6	-11.3
LNADW(3000-4900)	-10.6	-9.8	-9.1
AABW(4900-bottom)	1.3	2	2.6

Table 6.7: Transport (Sv) by classes of depth (0-600, 600-1200, 1200-3000, 3000-4900, 4900-bottom) for the three cases: case 0: mass conservation only, case 1: silica transport = 127 kmol s^{-1} and case 2: no silica transport.

In table 6.8 the Ekman and its barotropic compensation, baroclinic, and horizontal component of the new adjustment in the heat, salt, oxygen, and nutrients flow for both cases are presented (same information with only mass conservation constraint is presented in table 6.2). The net transport for the three cases are presented in table 6.9.

The differences on the extreme cases 0 and 2 (mass conservation only constraint and no silica transport) are now described. There is no change in the Ekman or compensating barotropic part, and only small changes in the amount of the baroclinic transport of heat (8%), oxygen (15%), silicate (20%), nitrate (5%) and phosphate (6%). All these changes decrease the northward heat and salt transports, reduce southward transports of nitrate, phosphate and freshwater but increase southward oxygen transport.

The changes in the horizontal components are larger than in the baroclinic part in most instances. For the horizontal heat transport, changes are very small. In oxygen, an increase of 25% in the horizontal southward transport is found. For nutrients the changes amount to 58, 40 and 51% for silica, nitrate and phosphate, all tending to increase northward (or decrease southward) transport due to the horizontal cell. Thus, a large change has occurred in the horizontal component of the fluxes which is more important for the nutrients.

The main result of these adjustments is to decrease the North Atlantic heat transport by 5%, to decrease the northward salt transport by 7% and to decrease the southward freshwater flux by 3%, to increase the southward oxygen flux by 11%, to cancel the silicate flux (as imposed), and to reduce the nitrate and phosphate fluxes in a 70 and 40 %,

A)

Transport Silica =127	Heat (PW)	Salt (10^6kg s^{-1})	Oxygen (kmol s^{-1})	Silica (kmol s^{-1})	Nitrate (kmol s^{-1})	Phosphate (kmol s^{-1})
Ekman	0.45	10.1	-107	-151	-106	-6.5
Baroclinic	0.89	22.3	- 790	-369	-205	-13.2
Horizontal	0.13	-14.0	-1866	395	224	9.4
Net	1.47	18.4	-2763	-125	- 87	-10.3

B)

Not Silica Transport	Heat (PW)	Salt (10^6kg s^{-1})	Oxygen (kmol s^{-1})	Silica (kmol s^{-1})	Nitrate (kmol s^{-1})	Phosphate (kmol s^{-1})
Ekman	0.45	10.1	-107	-151	-106	-6.5
Baroclinic	0.86	21.5	- 728	-327	-199	-12.8
Horizontal	0.12	-13.9	-2071	484	261	11.3
Net	1.43	17.7	-2906	6	- 44	-8.0

Table 6.8: Ekman and its barotropic compensation, baroclinic, horizontal and net transport for Heat, Salt, Oxygen, Silica, Nitrate, and Phosphate for A) silica transport of 127 kmol s^{-1} and B) no silica transport. Same information with only mass conservation constraint (case 0) is given in table 6.2.

Transport	Heat (PW)	Salt (x10^6 kg s^{-1})	Freshwater (10^6 m^3 s^{-1})	Oxygen (kmol s^{-1})	Silica (kmol s^{-1})	Nitrate (kmol s^{-1})	Phosphate (kmol s^{-1})
Mass Conservat.	1.51	19.0	-1.23	-2621	-254	-130	-12.6
Silica tr=127	1.47	18.4	-1.21	-2763	-125	- 87	-10.3
Not silica trans.	1.43	17.7	-1.19	-2906	6	- 44	-8.0

Table 6.9: Total transport for Heat, Salt, Freshwater, Oxygen, Silica, Nitrate and Phosphate for the three cases: mass conservation only, silica transport of 127 kmol s^{-1} and not silica transport.

respectively. The mechanism of reduction of the southward flux of silica is based on reducing the southward flux on the Canary basin where the silica concentration is higher and increasing the deep western boundary current where silica concentration is lower. Nevertheless, the addition of the velocity adjustment only significantly modifies the deep flow in the Canary basin. Northward heat transport decreases by 0.08 PW, northward salt transport through the section reduces by 1.3 x 10^6 kg s^{-1}, southward oxygen transport increases by 285 kmol s^{-1}, transport of nitrate is reduced by 86 kmol s^{-1} (reaching a level of

-44 kmol s^{-1}), and phosphate flow is reduced by 4.6 kmol s^{-1} across the 24.5ºN section (Table 6.9). For the intermediate adjustment results are coherent with these showed tendencies. The heat transport reduction is around 0.04 PW, and half of the values described for the other parameters.

Silica adjustment mainly affects the silica distribution and results in changes to the horizontal cell (70%) but only 30 % in the baroclinic cell. Changes in the other components are quite small. Baroclinic southward transport is reduced but the increase in northward horizontal transport is three times as large. For nitrate, changes in baroclinic distribution are small, but the increase in the horizontal cell is important. Finally, for phosphate fluxes, changes are due to increases in baroclinic and horizontal transports.

6.9 Discussion

The major change in circulation resulting from imposition of silica conservation constraints is the large increase in northward deep water transport in the Canary basin. Here an attempt is made to decide whether such substantial northward flow is realistic.

Measurements of abyssal temperatures in the eastern Atlantic show a marked variation with latitude at a depth of 5000 m. Near 10ºN the potential temperature is 1.8ºC (McCartney *et al.,* 1991); at the same depth near 50ºN it is 2.1ºC (Maillard, 1986). The northward warming of the bottom water throughout the entire Atlantic, including that within the Eastern Basin, results from its northward movement and mixing with the overlaying warmer water (Warren, 1981).

Saunders (1987) at 37ºN gave a small northward transport of cold water (potential temperature less than 2.05ºC) from the Canary basin to the Iberian basin in a narrow gap (Discovery gap) in the East Azores Fracture Zone. He considered that the cold water arrives from the south along the eastern margin; its hydrographic signal is the 'piling up' of isotherms against the lower continental rise. Near 32ºN the signal is small, he proposed that just south of this latitude the eastern boundary current ends. The signal is detected in our section against the western flank of the MAR, with potential temperatures lower than 1.9ºC below the 5200 m between 33ºW and 38ºW.

McCartney *et al,* (1991) have studied the flow through the Romanche and Vema fracture zones, near the Equator and at 11ºN respectively and the influence on the property distributions in the Eastern North Atlantic. They found a geostrophic transport through the Vema of 2.1 to 2.3 Sv of water colder than 2.0ºC (around 4500 m depth at 24.5ºN). This current bifurcates and a northward western boundary current along the flank of the Mid Atlantic Ridge transports between 1.8 and 3.9 Sv towards the Canary basin.

Schlitzer *et al.* (1985) in a study of deep water in the northeastern Atlantic basins based on ^{14}C and ^{39}Ar concentrations from stations along a meridional section (8ºS to 45ºN) through the Romanche trench and along the northeast Atlantic basins found a turnover time of about 30 years for the waters below the depth of the ^{14}C minimum (~4250 m). Converting this turnover into a water flow taking into account the volume of the layer of North Eastern Atlantic Deep Water (NEADW) below 4250 m, they obtained an approximate northward deep water flow of 4.8 Sv.

Schmitz and McCartney (1993), in a broad description of the North Atlantic circulation, suggest 2 Sv of upwelled water from deep water to shallow layers flowing northward over the Eastern basins. Deeper than 4250 m, a flow of 0.6, 2.8 and 5.3 Sv for the three models in the Canary basin is calculated in this thesis. Of these amounts the intermediate value, 2.8 Sv, is in reasonable agreement with silica conservation as well as with the deep northward transport evaluated in the Canary basin by the previously mentioned authors.

Consideration of the physical mechanism of silica transport at 24.5ºN in the North Atlantic in conjunction with the silica budget of the Atlantic Ocean basin requires modification of the geostrophic reference levels. The resulting overturning meridional circulation composed of northward flowing shallow waters returning south at lower levels is practically the same as previously calculated. The divergence of heat transport through the 24.5ºN section is calculated to be 1.47 ± 0.40, the salt transport of $18.4 \pm 8.2 \times 10^6$ kg s^{-1}, the oxygen transport -2760 ± 530 kmol s^{-1}, the silica transport -125 ± 250 kmol s^{-1}, the nitrate transport -87 ± 120 kmol s^{-1} and the phosphate transport of -10.3 ± 7.6 kmol s^{-1}. Adding the influence of the inflow of water from the Bering Straits and net precipitation,

which increases the barotropic freshwater transport to –1.23 Sv, then for the final North Atlantic budget, the salt transport changes to –26.2 ±11.5 x10^6 kg s^{-1}. For the heat, oxygen and nutrients fluxes, the Bering Strait flow, precipitation minus evaporation and its baroclinic compensation transport are under the uncertainty of the calculations. An amount of 0.14 PW in the heat transport may be considered due to the effect of seasonal sampling of the 1992 section across the Florida Straits in August.

Chapter 7

Conclusions, contributions and future work

7.1 Conclusions

In this thesis hydrographic data have been used to calculate and examine the fluxes across the 24.5ºN section in the subtropical North Atlantic, its trends and decadal changes in oceanographic characteristics. To map data for the comparison two methods of data interpolation were used: spline interpolation and objective mapping. There is a high degree of similarity between cubic spline smoothing with a gaussian filter and objective mapping methods. The results of the two methods are within the expected error in all regions except near the boundaries. Cubic spline is simpler to use, but the advantage of calculating expected errors makes objective mapping the most suitable method of data interpolation for this analysis.

Comparison of the 1981 and 1957 surveys had revealed that the ocean waters along 24.5ºN had warmed appreciably down to 3000 m depth over the 24-year period (Roemmich and Wunsch, 1984). The same result was also found here and shows that the dominant feature in the temperature difference is a large region of strong warming extending down to 4000 m depth in the central North American basin, with temperature increases as large as 0.75ºC in the main thermocline. From 1981 to 1992, the warming along 24.5ºN in the Atlantic continued. The entire Canary basin warmed significantly over those 11 years. In the North American basin, the region of strong warming from 1957 to 1981, cooled from 1981 to 1992; just to the west of this cooling, there is a region of approximately equal warming. There appears to be a new type of large-scale, long-term variability in these temperature differences with zonally alternating regions of warming and cooling in the western basin of the Atlantic.

Over the 35-year period from 1957 to 1992, the 24.5ºN section warmed between 700 and 2500 m depth with a zonal mean maximum of 0.28 $\pm$0.05ºC at 1000 m depth. What is particularly striking in the 35-yr warming is the flatness of the temperature-difference contours, that is to say, the entire zonal extension of the 24.5ºN section warmed

almost uniformly, with maximum warming (up to 0.5ºC) occurring at a depth of ~1000 m. The deeper water, below 3000 m, cooled, with a strong cooling of 0.1ºC appearing just below 3000 m depth in the western boundary where the southward flow of NADW renews the deep water reservoir of the global ocean.

From the long time series of hydrographic stations near Bermuda, Roemmich (1990) showed statistically significant warming of deep waters from 1954 to 1981; Levitus and Antonov (1995) confirmed the remarkable linear warming trend from 1960 to 1990; and Joyce and Robbins (1996) have recently demonstrated that the general warming trend between 1500 and 2500 dbar goes back at least as far as 1922, although there are considerable decadal-scale oscillations in temperature at fixed depth (Levitus *et al,*. 1995) which can obscure the trend in observational periods of over 10 years. Joyce and Robbins (1996) also showed that warming in the deeper waters extended meridionally over the entire subtropical gyre along 66°W in the western basin from 20°N to 35°N.

In terms of the mechanisms for the observed changes along 24.5°N, it is clear that the changes from 1957 to 1981 involved mainly downward displacement of isopycnals with little change in water mass properties below 500 m. Roemmich and Wunsch (1984), Levitus (1989a, 1989b) and Antonov (1993) reached the same conclusion for decadal changes from 1957 through 1981 in the subtropical North Atlantic. The continued descent of isopycnals from 1981 to 1992 has a similar structure, though the maximum downward displacement is only 20 db at about 1500 db depth. The isopycnals in the middle of the water column (1500 to 2000 db) have descended at a rate of 1.5 to 2.5 db per year since 1957. As there is no apparent large-scale zonal structure to these displacements, we cannot associate this deepening with a spin-up of the subtropical gyre which might occur as the result of the increasing wind stress curl noted by Bunker (1980) from 1947 to 1972.

The striking increases in salinity and temperature on isopycnal surfaces in the main thermocline from 1957 to 1981, and through to 1992, suggest that the formation conditions of these recently ventilated waters must be changing. In terms of Bindoff and McDougall's (1994) model, the observed changes in the thermocline are consistent with higher net evaporation at the sea surface in the formation region, leading to higher salinity. The decrease in oxygen from 1981 to 1992 may suggest less vigorous ventilation of the thermocline.

To explain the increases in salinity and temperature on isopycnal surfaces in the intermediate waters, a more sophisticated model is needed in the depth region where waters of Mediterranean and Antarctic origin mix. Is the higher salinity due ultimately to stronger or saltier outflow of Mediterranean Water over the sill at Gibraltar, or to a lesser northward flow of relatively fresh Antarctic Intermediate Waters? While we would have preferred an explanation based on a westward and southward displacement of the Mediterranean Water salt tongue, such lateral movement of the Mediterranean Water tongue is in conflict with the observed decrease in oxygen over time. The source strength or character of Mediterranean Water may be changing and, indeed, deep water in the western Mediterranean basin has exhibited increasing salinity and temperature by over 0.02 and 0.07°C over the period from 1955 to 1989 (Rohling and Bryden, 1992). We know of no information on long-term changes in the strength of the Mediterranean outflow. From comparison of the geostrophic meridional circulation across 24.5°N from the 1957, 1981 and 1992 sections, a decrease in northward flow of Antarctic Intermediate Water over time was appreciated, as described in Chapter 5. Thus, the mixture of low salinity Antarctic Intermediate water may be lesser, which could lead to higher salinities in the intermediate waters. However, such an interpretation has difficulty in explaining why the increase in salinity is minimal over the crest of the Mid-Atlantic Ridge, where the most pronounced Antarctic Intermediate water signature is generally found and, because this water mass has relatively low oxygen concentrations, a weaker source of low oxygen waters also fails to explain the observed decrease in oxygen on isopycnal surfaces from 1981 to 1992. The minimum increase in salinity could be explained because the only notorious patch of AAIW detected in 1992 was located over the MAR (see figure 2.3).

In the deep waters where the changes in isopycnal surfaces are smaller, we can explain the increasing salinities from 1981 to 1992 in the upper core of NADW as the result of a lesser source of low salinity waters formed in the Labrador Sea. The shutdown in production of Labrador Sea Water during the late 1960's and early 1970's is well documented (Lazier, 1980); estimated penetration speeds of over 0.8 cm s^{-1} for the upper core of NADW from CFC measurements (Smethie, 1993) suggest that the Labrador Sea anomalies would take around 15 years to reach 24.5°N, that is after 1981 but before 1992; the lower oxygen levels, particularly in the upper core against the western boundary also suggest a reduced ventilation of this density surface. For the lower core of NADW, the

decreasing salinities with time could be attributed to the freshening of deep waters formed in the Greenland-Iceland-Norwegian Sea, first observed by Brewer *et al.* (1983) in the northern North Atlantic.

More information is certainly needed on the spatial structure of the changes over a basin like the North Atlantic in order to begin to determine the causes of decadal change. The 24.5°N changes, while intriguing, intrinsically suffer from a lack of information at other latitudes. Here, the use of only the highest quality data has been emphasised to determine the changes in water mass characteristics. Clearly, the changes in water mass characteristics are more readily determined using the horizontally dense and vertically continuous CTD stations which have been standardly taken since about 1980. In fact, there was quite a comprehensive hydrographic survey of the North Atlantic during the 1980's and many of these same sections have been repeated during the WOCE time period from 1990 to 1997. Comparison of these North Atlantic surveys a decade apart and the extension of the comparison back to the IGY survey of 1957-58 should establish the large-scale patterns in decadal scale changes of water mass characteristics as well as the changes in depths of the isopycnal surfaces throughout the North Atlantic. In the northern North Atlantic, where variability is higher, some sections have been repeated near yearly during the WOCE period. Surprisingly rapid spreading of newly formed intermediate waters from the deep convection areas (Labrador Sea) across the North Atlantic toward the eastern basin (Sy *et al*., 1997) and to the western basins (Curry *et al.,* 1998) has been detected.

By requiring that the ocean interior transport balances the Gulf Stream transport through the Straits of Florida and the Ekman transport over the Atlantic (Hall and Bryden, 1982), we have performed a heat flux calculation using similar methods on each dataset. Even though temperature and salinity have changed, the three cruises exhibit similar features in the large-scale velocity fields and similar zonally averaged meridional transport. Ocean heat transport founded from similar calculations on the three cruises are indistinguishable, which is the same conclusion reached by Roemmich and Wunsch (1985) in their comparison between the 1957 and 1981 sections based on a number of inverse models.

A comparison of the transport for the three cruises shows quite a similar scheme in the overall vertical structure. The southward flow in the thermocline above 600 m is quite

similar for the three cruises: total transport varies from -17.1 in 1957 to -18.7 in 1981, and -17.4 Sv in 1992. A core of northward flow between 600 and 1200 m depths shows the influence of the AAIW. The transport over this depth interval reduces with time from 2.5 Sv in 1957 to 1.7 Sv in 1981, to only 0.7 Sv in 1992. The NADW appears clearly divided in two lobes, an upper lobe originating in the Labrador Sea and a deeper lobe from the Norwegian-Greenland Sea, as described by Roemmich and Wunsch (1985). The upper lobe appears deeper and stronger in 1992 than in the previous cruises as it takes around 15 years for Labrador Sea Water to reach 24.5ºN (Smethie, 1993; Bryden *et al.*, 1996). 1981 would correspond to the period of lack of deep water convection on the Labrador Sea during the late 1960's (Lazier, 1988) and 1992 would correspond to the following intensification period.

The large increase in the transport of the lower lobe of North Atlantic Deep water which occurred in 1981 was, in 1992, reduced to values lower than in 1957. This variation detected at 24.5ºN was also shown at 36ºN by Dobroliubov *et al*. (1996). The total transport of North Atlantic Deep water over the depth interval from 1200 to 4900 m was 22.6 Sv in 1957, 21.1 Sv in 1981 and 20.8 Sv in 1992. Thus, both the southward flow of North Atlantic Deep water and the northward flow of Antarctic Intermediate water are smallest in 1992, compared with 1981 and 1957. The flow of Antarctic Bottom water is about 3 Sv, the largest value of 3.3 was detected in 1981 and it was reduced in 1992 to 2.7. The water that was flowing between 5000 and 5200 m depth in 1957 has deepened and flowed at around 5500 m for both the 1981 and 1992 cruises. In contrast with the 36ºN results (Dobroliubov *et al*., 1996), the AABW at 24.5ºN flows consistently northward over the whole period but with some changes in the depth of the transport.

The calculated freshwater flux, based on an integration point at the Bering Strait that connects the Pacific and the Atlantic Ocean via the Arctic Ocean, is -1.23 Sv. The associated barotropic salt transport is $-44.6\ 10^6$ kg s^{-1}. The salt transport through the section by the Ekman flow and its compensating barotropic flow, and by baroclinic and horizontal components amounts to 19.0×10^6 kg s^{-1}. Thus, the salt flux balance through the section is $-25.6\ 10^6$ kg s^{-1}, and within the precision of the calculation this is no different from the quantity required by Wijffels *et al.,* (1992) for all the sections through the oceans.

The different components of the fluxes of heat, oxygen and nutrients have been analysed. After the variables are separated into section average, baroclinic profile and anomalies, the fluxes are separated into Ekman and its barotropic compensation, baroclinic and horizontal components. The baroclinic contribution due to overturning circulation is responsible for the largest amount of heat transport with warmer waters flowing poleward and cooler deep water flowing equatorward. The Ekman component and its barotropic compensation is the second source of transport. Horizontal transport is the main contribution to southward oxygen flux, and the large scale gyre circulation is responsible for this, mainly in the upper layers where low oxygen water flows northward in the Florida Straits and higher oxygen mid-ocean water flows southward. Baroclinic contribution from the overturning circulation is the second most important factor for the southward transport. Ekman northward oxygen transport and its compensating barotropic oxygen transport have similar amounts but in the southward direction and yield a small southward contribution to the final southward oxygen transport.

In the case of nutrients, baroclinic transport due to overturning circulation is the main factor for the southward transport of all nutrients, due to low upper water concentrations in the northward flow and higher deep water concentrations in the southward flow. Horizontal northward transport is the second factor due to higher concentrations in the Florida Straits than in the mid-ocean in the upper layers. The difference of concentrations and velocities in both deep basins: higher concentration and northward flow in the Canary basin and southward flow and lower concentration of recent ventilated water in the deep western boundary current and consequently in the North American basin also contribute to the horizontal transport but to a lesser extent than the upper layer contribution.

Consideration of the physical mechanisms of silica transport at 24.5ºN in the North Atlantic in conjunction with the silica budget of the Atlantic Ocean basin requires modification of the geostrophic reference levels. For the purpose of analysis we have tried two solutions: The first one assumes there is no net flux of silica through the 24.5ºN section. The second solution gives some amount of southward transport to account for river input and hydrothermal sources. Deeper than 4250 m, we have calculated a flow of 0.6 Sv in the Canary basin for unconstrained circulation, 2.8 Sv for the intermediate silica transport and 5.3 Sv for the case of no silica transport. Of these amounts we think that the

intermediate value of 2.8 Sv is in a good agreement with the silica conservation as well as with the deep northward transport evaluated in the Canary basin by the previously mentioned authors.

The mechanism of reduction of the southward flux of silica is based on reducing the southward flux on the Canary basin where silica concentration is higher and increasing the deep western boundary current where silica concentration is lower. Then for the final North Atlantic budget, the zonally integrated meridional cell carries a poleward heat flux of 1.47 ± 0.40 PW, equatorial salt transport of –26.2 ± 11.5 x 10^6 kg s^{-1}, and oxygen transport of –2760 ± 530 kmol s^{-1}, an equatorial silica transport of -125 ± 250 kmol s^{-1}, nitrate transport of -87± 120 kmol s^{-1} and phosphate transport of –10.3 ± 7.6 kmol s^{-1}. An amount of 0.14 PW of the heat transport may be considered due to the seasonal effect.

7.2 Contributions

From this thesis, the first contribution is a high quality dataset, due to the instrumentation, calibration and the cruise designed as part of the WOCE program, for researchers and modellers to use together with all of the Atlantic and global dataset.

Together with the dataset and quality control, a series of analysis has been performed together with others cruises data on the same latitude to obtain decadal changes in temperature, salinity and tendencies between 1957 and 1992, and the possible causes of these decadal changes on water masses. Also, a comparison is made between heat transport in the three cruises 1957, 1981 and 1992. Finally fluxes of freshwater, salt, oxygen and nutrients through the section has been calculated from the 1992 dataset. Consideration of the silica budget in the North Atlantic requires modification of the meridional circulation in the subtropical North Atlantic.

Attention is drawn to the quick calibration, analysis and publication of the fist part of this work. Intense dedication on the beginning resulted in a quickly data calibration. Hydrographic data calibration is hard and long time requiring from very specialised people. Changes in temperature and salinity were the first published from the WOCE sampling as well as decadal changes in water masses. A paper on heat transport analysis is in press now.

As conclusions from these contributions, the following are presented:

- The significant warming found in intermediate waters from 700 to 2500 m depth, with a peak value of 0.28 ±0.05 at 1000 m depth. What is particularly striking in the 35-yr warming is the flatness of the temperature-difference contours, that is to say, the entire zonal extension of the 24.5ºN section warmed almost uniformly, with maximum warming (up to 0.5ºC) occurring at a depth of ~1000 m. This result has been widespread throughout the climatic and oceanographic community and have justify the ocean' role in the climatic change.
- In terms of the mechanisms for the observed changes along 24.5°N, it is clear that the changes from 1957 to 1981 involved mainly downward displacement of isopycnals with little change in water mass properties below 500 m. The continued descent of isopycnals from 1981 to 1992 has a similar structure, though maximum downward displacement is only 20 m at about 1500 m depth. The striking increases in salinity and temperature on isopycnal surfaces in the main thermocline from 1957 to 1981, and through to 1992, suggest that the formation conditions of these recently ventilated waters must be changing. The combined effects from 940 to 1890 db of warming on isopycnal surfaces and deepening isopycnals yields the striking warming found from 1981 to 1992 in intermediate waters. Some hypothesis about water masses displacements and increase or decrease of MW and AAIW are discussed.
- Ocean heat transport founded from similar calculations on the three cruises is indistinguishable. Even though temperature and salinity have changed, the three cruises exhibit similar features in the large-scale velocity fields and similar zonally averaged meridional transport. A core of northward flow between 600 and 1200 m depths shows the influence of the AAIW. The transport over this depth interval reduces with time from 2.5 Sv in 1957 to 1.7 Sv in 1981, to only 0.7 Sv in 1992. The NADW appears clearly divided in two lobes, an upper lobe originating in the Labrador Sea and a deeper lobe from the Norwegian-Greenland Sea. The upper lobe appears deeper and stronger in 1992 than in the previous cruises, indicating of the changes that are taking place in the water masses formation areas. The flow of Antarctic Bottom Water has deepened and cooled for both the 1981 and 1992 cruises.
- The different components of the fluxes, Ekman and its barotropic compensation, baroclinic and horizontal, have been evaluated for the fluxes of heat, freshwater,

oxygen and nutrients. The baroclinic contribution due to overturning circulation is responsible for the largest amount of poleward heat transport, with warmer waters flowing poleward and cooler deep water flowing equatorward. The barotropic flow, associated to the Bering Straits, net precipitation and Ekman transport is the main component in the salt transport. Horizontal transport, is the main contribution to southward oxygen flux, and the large scale gyre circulation is responsible for this, mainly in the upper layers where low oxygen water flows northward in the Florida Straits and higher oxygen mid-ocean water flows southward at the same depths. In the case of nutrients, baroclinic transport due to overturning circulation is the main factor for the southward transport of all nutrients, due to low upper water concentrations in the northward flow and higher deep water concentrations in the southward flow. Finally a new circulation model has been elaborated consistent with the silica budget of the Atlantic Ocean basin.

7.3 Future work

Following this work, there are some interesting points to make. One of them is to check heat transport through the 24.5ºN section in a different season. The aim is to evaluate changes in heat transport due to seasonal effects. The three cruises analysed in this research have been performed in late summer and autumn, a recent cruise has sampled the section in January-February 1998. The study of the fluxes using the same methodology will give an idea of the new fluxes and seasonal variability.

Another line of work to follow is the use of inverse models to evaluate the meridional circulation through the 24.5ºN section. In these models properties are conserved in density layers. Vertical velocities and interchange between layers are computed. These models could be applied to calculate fluxes of heat, oxygen, nutrients and carbon.

Another point to study lies in the Gulf Stream through the Straits of Florida or Florida Current. In the present thesis the Florida Straits flow is only used to close the section and make the mass and volume balance. There is a great number of possibilities for working, but they should at least include water masses characteristics and origin of the detected changes in temperature, salinity, oxygen and nutrients.

Adding to the flow of nutrients, it is also interesting to study the flow of chemical conservative parameters as NO or PO (Broecker, 1974) that are not affected by the oxidation of organic matter.

Finally, but also very interesting, would be the provision of a definitive description of the North Atlantic Overturning Circulation. This circulation is compose of northward upper layers transport through the Florida Straits and western part of the section as the Antilles current, and the southward flow mainly by the deep westerly boundary current. The section is well located to give a good description of it and chemical such as oxygen and nutrient concentrations may help in the study. Modellers have a great interest in comparing results and evaluating how well the models reproduce the North Atlantic Overturning. Dr. Bryden suggests it should be done in potential temperature classes, in the same way mid-ocean circulation was presented the in chapter 5, but for the three components: Florida Straits, Ekman layer and mid-ocean and with finer resolution than that presented in chapter 6.

Comparing sections of hydrographic data is the best way to find temperature and salinity trends over time, but these sections are available only at selected times separated by long time intervals. Other measurement systems must be used between hydrographic samples. To examine the structure of climate variability, long time series hydrographic stations like the one at Bermuda are very useful. A project to create a sampling station over time has been proposed during WOCE off the Canary Islands, and it is supported by Instituto Español de Oceanografía, Instituto Canario de Ciencias del Mar, Institut for Meereskunde (Kiel) and Bremen University. Time series in the Eastern North Atlantic would be very helpful to understand the circulation of this area and its influence in the rest of the North Atlantic.

In the contest of recent international agreements to reduce the buildup of CO_2 in the atmosphere, detailed and accurate knowledge of the behaviour of the vast oceanic CO_2 reservoir becomes increasingly important. WOCE and the recent Global Ocean CO_2 Survey provides a base from which to assess the transport, storage and future variability of oceanic CO_2. From the 24.5ºN section, carbon transport has been primarily evaluated. Rosón, Ríos, Lavín, Pérez and Bryden (1998) presented some preliminary results in the

poster 'Carbon fluxes in the North Atlantic Ocean' in the WOCE Conference Ocean Circulation and Climate en Halifax .

One of the objectives of the 24.5ºN section was to calibrate and submit the data to the WOCE data centre to be used by the Physical Oceanography Community. Some models have been run with the WOCE data including the 24.5ºN section. Baks (1998) compared the numerical results of the ocean-atmosphere HAOCME model with heat transport calculation from the 24.5ºN section. Satisfactory results were found in this section but and not such a good agreement in the southern hemisphere.

Ganachaud and Wunsch (1998) from MIT used an inverse model with WOCE data to calculate a globally consistent circulation with flux of heat, salt and nutrients. In the 32 issue of the International WOCE Newsletter Ganachaud and Wunsch (1998) present the new results of the large Scale Oceanic Nutrient and Oxygen Fluxes. In the same issue Reynaud, LeGrand and Mercier (1998) present a new analisis of hydrographic data in the Atlantic and its aplication to an inverse modelling study. The dataset contains 17 one-time WOCE Atlantic sections (A-5 included) and 9 repeated 2 or 3 times. Ekman transporte was calculated using the ERS wind field products (in the same way it was used in chapter 5 to compare old climatology with new satellite wind data). A comparison of estimates of the circulation clearly shows that the new climatology better resolves the main currents.

Moisan and Niiler (1998) presented the seasonal heat budget of the world oceans: net heat and heat storage rates. They calculated the net surface heat flux from temperature profiles from NODC and satellite data.

Sampling requirements for the WOCE program have not been totally completed. The 36ºN section from Cádiz to Cape Hatteras (US) has not yet been covered. It was attempted by some Russian scientists, but equipment failed and the data did not pass the quality control standards established by WOCE. Atlantic models are being run with the 1981 section data, but conditions have changed, as shown in this research. There is a great need to cover this section in order to finish the Atlantic WOCE survey.

After an intense period of ocean observation from 1990 to 1998 the WOCE has entered a new phase, the Analysis, Interpretation, Modelling and Synthesis (AIMS) phase.

WOCE data are distributed to everybody and modellers are trying to validate models and assimilate field and satellite data as well. The 24.5ºN heat transport seems to be indistinguishable over 35 years, and oceanic models need to simulate this extraordinary condition. The 24.5ºN section remains a key for validation of these models. The Meridional Overturning Circulation (MOC) in the North Atlantic is pivotal to the oceans' role in climate and 24.5ºN and 36ºN are located in the central part of the North Atlantic, in privileged positions to monitor the variability of MOC.

There was quite a comprehensive hydrographic survey of the North Atlantic during the 1980's and many of these same sections have been repeated during the WOCE time period from 1990 to 1997. Comparison of these North Atlantic surveys a decade apart and the extension of the comparison back to the IGY survey of 1957-58 should establish the large-scale patterns in decadal scale changes of water mass characteristics as well as the changes in depths of the isopycnal surfaces throughout the North Atlantic. The spatial pattern of observed decadal changes could then be compared with realistic coupled ocean-atmosphere simulations with varying air-sea exchange conditions and wind forcing to understand the causes of the decadal changes. In many respects, a case study in which the magnitude and spatial pattern of decadal changes in ocean water mass characteristics in the North Atlantic are determined would provide a sensitive test-bed through which coupled ocean-atmosphere models could be assessed and developed

The essential contribution of the WOCE project to advancing our understanding of the role of the oceans in the present climate has been to measure the large degree of variability in ocean circulation. Time series stations, repeating hydrographic sections such as 24.5ºN, and satellite observations have quantified the low frequency oceanic variability. It is also clear that the oceans hold the primary memory of the climate system. Wind driven circulation carries deep heat and freshwater anomalies around the ocean basins, which present a slowly changing SST field to the winter atmosphere.

Last May's WOCE Conference marked the end of the 8-year observational phase and, in so doing, marked the completion of the major international ocean observational project. It leaves behind a rich legacy in terms of advances in technology, datasets, understanding and knowledge, as well as a better skilled ocean and climate community. Knowledge gained through WOCE is having a great impact on research into predictability

and prediction at seasonal-to-interannual and shorter time scales, mostly within the Climate Variability and Predictability Program (CLIVAR).

CLIVAR is a component part of the World Climate Research Program (WCRP) sponsored jointly by the World Meteorological Organisation (WMO), the Intergovernmental Oceanographic Commission (IOC) of UNESCO and by the International Council of Scientific Unions (ICSU). CLIVAR is a research programme on climate variability and prediction for the 21st century and aims to address many of the unanswered questions concerning the functioning of the climate system on time scales up to a century, including the human influence on global climate. CLIVAR has been divided into three components: 1.- GOALS: Seasonal-to-Interannual variability and predictability of the Global Ocean Atmospheric Land System, 2.- (DecCen): Decadal-to-Centennial climate variability and predictability studies. 3.- (ACC): Modelling and detection of anthropogenic climate change. The second component includes two important points: North Atlantic Oscillation (NAO), and Atlantic Thermohaline Circulation.

A large part of the climatic variability of the European Atlantic area is driven by the NAO. The low frequency variability of the North Atlantic and the thermohaline circulation are influenced by the NAO. The thermohaline circulation is fundamental for the European climate system. The study of the antrophogenic climate change, its detection and prediction is an important part of CLIVAR. The increase in knowledge must be on regional and local scales. These represent one of the main goals for future work in physical oceanography and climate research for European oceanographers.

References

Ahlberg, A. J., E. N. Nilson and J. L. Walsh, 1967. *The theory of splines and their applications*. New York Academic Press, 284 pp.

Anderson, L., D. W. Dryssen, E. P. Jones and M. G. Lowing, 1983. Inputs and outputs of salt, freshwater, alkalinity and silica in the Arctic Ocean. *Deep-Sea Research.* **30,** 87-94.

Antonov, J. I., 1993: Linear trends of temperature at intermediate and deep layers of the North Atlantic and the North Pacific Oceans: 1957-1981. *Journal of Climate*, **6**, 1928-1942.

Baks, H., 1998. Aspects of Ocean Circulation and Heat Transport in a Coupled Climate model. Abstract for Talks and Posters at the 1998 Conference of the World Ocean Circulation Experiment, Halifax, Canada, 24-29 May 1998. Poster. Page 59.

Barber, C. R., 1969. The International Practical Temperature Scale of 1968. *Meteorologia* **5**, (2), 35-44

Baumgartner, A. and E. Reichel, 1975. *The World Water Balance.* Elsevier. 179 pp.

Bevington, P. R., and D. K. Robinson, 1992. *Data reduction and error analysis for the physical sciences*. McGraw-Hill, Inc. 328 pp.

Bindoff, N. L., and T. J. McDougall, 1994. Diagnosing climate change and ocean ventilation using hydrographic data. *Journal of Physical Oceanography*, **24**, 1137-1152.

Böning, C. W., R. Doscher, and H. J. Isemer, 1991. Monthly Mean Wind Stress and Sverdrup transports in the North Atlantic: A Comparison of the Hellerman-Rosenstein and Isemer-Hasse Climatologies. *Journal of Physical Oceanography*, **21**, 221-235.

Bretherton, F. P., R. E. Davis and C. B. Fandry, 1976. A technique for objective analysis and design of oceanographic experiments applied to MODE-73. *Deep-Sea Research*, **23**, 559-582.

Brewer, P. G., W. S. Broecker, W. J. Jenkins. P. B. Rhines, C. G. Rooth, J. H. Swift, T. Takahashi, and R. T. Williams, 1983: A climatic freshening of the deep North Atlantic (north of 50°N) over the past 20 years. *Science*, **222**, 1237-1239.

Brewer, P.G., C. Goyet and D. Dyrssen, 1989. Carbon Dioxide Transport by Ocean Currents at 25 Latitude in the Atlantic Ocean. *Science*, **240**. (Reports), 477-479.

Brown, N. L., 1974. A precision CTD microprofiler. IEEE Conference on Engineering in the Ocean Environment, **2**, 270-278

Broecker, W.S, 1974. "NO," a conservative water-mass tracer. *Earth Planet. Sci. Lett*., **23,** 100-107.

Bryan, K., 1962. Measurements of meridional heat transport by ocean currents. *Journal of Geophysical Research*, **67**, 3403-3414.

Bryden, H. L., 1993. Ocean heat transport across 24ºN latitude. In: *Interaction Between Global Climate Subsystems: The Legacy of Hann* (G. A, McBean and M. Hantel, editors) Geophysical Monographs, **75**, 65-75.

Bryden, H. L., 1998. Ocean Heat Flux, Abstract for Talks and Posters at the 1998 Conference of the World Ocean Circulation Experiment, Halifax, Canada, 24-29 May 1998. Plenary abstract, 12-13.

Bryden, H. L. and M. M. Hall, 1980. Heat Transport by Currents Across 25ºN Latitude in the Atlantic Ocean. *Science*, **207**, 884-886.

Bryden, H. L., D. H. Roemmich, and J. A. Church, 1991. Heat transport across 24ºN in the Pacific. *Deep-Sea Research*, **38**, (3), 297-324

Bryden, H. L., M. J. Griffiths, A. Lavín, R. C. Millard, G. Parrilla and W. Smethie, 1996. Decadal changes in water masses characteristics at 24ºN in the Subtropical North Atlantic Ocean. *Journal of Climate,* **9**, 12, 3162-3186.

Bunker, A. F., 1976. Computations of Surface Energy Flux and Annual Air-Sea Interaction Cycles of the North Atlantic Ocean. *Monthly Weather Review,* **104**, (9) 1122-1140.

Bunker, A. F., 1980. Trends of variables and energy fluxes over the Atlantic Ocean from 1948 to 1972. *Monthly Weather Review*, **108**, 720-732.

Carissimo, B. C., H Oort. and T. H. Vonder Haar, 1985. Estimates of the meridional energy transports in the atmosphere and ocean. *Journal of Physical Oceanography,* **15,** 82-91

Coachman, L.K. and K. Aagaard, 1988. Transports through Bering Strait: Annual and interannual variability. *Journal of Geophysical Research,* **93**, 15535-15539.

Codispoti L.A., 1979. Arctic ocean processes in relation to the dissolved silicon content of the Atlantic. *Marine Science communications,* **5,** 361-368

Cooper L.H.N., 1952. Factors affecting the distribution of silicate in the North Atlantic Ocean and the formation of North Atlantic Deep Water. *Journal of the Marine Biological Association of the United Kingdom,* **30,** 511-526.

Curry, R. G., M. S. McCartney and T. M. Joyce, 1998. Oceanic transport of subpolar climate signals to mid-depth subtropical waters. *Nature,* **391**, 575-577.

DeMaster, D. J., 1981. The supply and accumulation of silica in the marine environment. *Geochimica et Cosmochimica Acta.* **45,** 1715-1732.

Dickson, R., J. Lazier, J. Meincke, P. Rhines and J. Swift, 1996. Long term coordinated changes in the convective activity of the North Atlantic. *Progress in Oceano*graphy, **38**, 241-295.

Dobroliubov, S. A., V. P. Tereschenkov and A. V. Sokov, 1996. Water mass transport and heat flux changes at 36ºN in the Atlantic Ocean ICES C.M. 1996/O:1

Finlen, J. R, 1966. Transport investigations in the northwest Providence Channel, Sc M. thesis, Univ. of Miami, Coral Gables, Fla., 110 pp.

Fofonoff, N.F. and H. L. Bryden, 1975. Specific gravity and density of seawater at atmospheric pressure. *Journal of Geophysical Research,* **33**, Supplement, 69-82.

Fuglister, F. C. 1960. Atlantic Ocean Atlas of temperature and salinity profiles and data from the International Geophysical Year of 1957-1958. *Woods Hole Oceanographic Institution Atlas Series* 1, 209 pp.

Fukumori, I. F. Martel and C. Wunsch, 1991. The Hydrography of the North Atlantic in the early 80s. An Atlas. *Progress in Oceanography,* **27**, 1-110.

Fukumori, I and C. Wunsch, 1991. Efficient representation of the North Atlantic hydrographic and chemical distributions. *Progress in Oceanography,* **27**, 111-195.

Ganachaud, A. and C. Wunsch, 1998a. The Oceanic Nutrient Fluxes. Abstract for Talks and Posters at the 1998 Conference of the World Ocean Circulation Experiment, Halifax, Canada, 24-29 May 1998. Poster. Page 61.

Ganachaud, A. and C. Wunsch, 1998b. Large Scale Oceanic Nutrient and Oxygen Fluxes. *International WOCE Newsletter*, **32**, 12-15.

Hall, M. M. and H. L. Bryden, 1982. Direct estimates and mechanisms of ocean heat transport. *Deep-Sea Research*, **29** (3), 339-359.

Hellerman, S. and M. Rosenstein, 1983. Normal monthly wind stress over the world Ocean with error estimates. *Journal of Physical Oceanography,* **13**, 1093-1104.

Hsiung, J. and T. Houghtby, 1989. The annual cycle of oceanic heat storage in the world ocean. *Quart. J. Roy Meteor. Soc ,* **115**, 1-28.

IFREMER, 1996. Mean Wind Field ERS-1 Scatterometer data processed by CERSAT V1. 91/08/05 to 94/04/02.

Isemer, H. J. and L. Hasse, 1987. The Bunker climate atlas of the North Atlantic Ocean. Vol 2. *Air-Sea Interactions*, Springer-Verlag, 218 pp.

Joyce, T.M., and P. Robbins, 1996. The long-term hydrographic record at Bermuda. *Journal of Climate,* **9,** 3121-3131.

Larsen, J. C., 1992. Transport and heat flux of the Florida Current at 27ºN derived from cross-stream voltages and profiling data: theory and observations. *Phil. Trans. R. Soc. Lond.* A 338, 169-236.

Lavín, A. M., 1993: Climatic changes in temperature and salinity in the subtropical North Atlantic. M.S. Thesis, Department of Earth, Atmospheric and Planetary Sciences, Massachusetts Institute of Technology, 126 pp.

Lavín, A., G. Parrilla, H. Bryden, C. Wunsch, R. Millard and M. J. García, 1993. Comparison over time of Temperature and Salinity at 24.5ºN in the Atlantic. *ICES* C.M. 1993/C:40

Lavín, A., H. Bryden, M. J. García and G. Parrilla, 1994. Decadal time changes in the circulation at 24°N in the Atlantic Ocean. *ICES C.M.* 1994/ S**:3**, 16pp.

Lavín, A., H. L. Bryden and G. Parrilla*,* 1998. Meridional transport and heat flux variations in the subtropical North Atlantic. *The Global Atmosphere and Ocean System,* **6**, 269-293.

Lavín, A., H. Bryden, G. Parrilla, R. Millard and M. J. García. 1998. Trends, decadal changes and fluxes at 24.5ºN in the subtropical North Atlantic. Abstract for Talks and Posters at the 1998 Conference of the World Ocean Circulation Experiment, Halifax, Canada, 24-29 May 1998. Poster. Page 65.

Lazier, J. R. N., 1980. Oceanographic conditions at Ocean Weather Ship *Bravo*, 1964-1974. *Atmosphere-Ocean*, **18**, 227-238.

Lazier, J., 1988. Temperature and salinity changes in the deep Labrador Sea, 1962-1986, *Deep-Sea Research*, **35**, 1247-1253.

Lazier, J. R. N. 1995. The Salinity Decrease in the Labrador Sea over the Past Thirty, *Natural Climate Variability on Decadal-to-Century Time Scales. National Research*, 295-302.

Leaman, K. D., R. L. Molinari, and P. S. Vertes, 1987. Structure and Variability of the Florida Current at 27ºN:April 1982 - July 1984. *Journal of Physical Oceanography,* **17**, 565-583.

Lee, T. N., W. E. Johns, R. J. Zantopp and E. V. Fillenbaum, 1996. Moored Observations of Western Boundary Current Variability and Thermohaline Circulation at 26.5º N in the Subtropical North Atlantic. *Journal of Physical Oceanogr*aphy, **26**, 962-983.

Leetmaa, A. and A. Bunker, 1978. Updated charts of the mean annual wind stress convergences in the Ekman layers and Sverdrup transport in the North Atlantic. *Journal of Marine Research*, **36**, 311-322.

Levitus, S., 1989a. Interpentadal variability of temperature and salinity at intermediate depths of the North Atlantic Ocean, 1970-1974 versus 1955-1959. *Journal of Geophysical Research*, **94**, 6091-6131.

Levitus, S., 1989b. Interpentadal variability of temperature and salinity in the deep North Atlantic, 1970-1974 versus 1955-1959. *Journal of Geophysical Research*, **94**, 16125-16131.

Levitus, S., and J. Antonov, 1995. Observational evidence of interannual to decadal-scale variability of the subsurface temperature-salinity structure of the world ocean. *Climatic Change*, **31**, 495-514.

Levitus, S., J. Antonov, X. Zhou, H. Dooley, K. Selemenov, V. Tereschenkov, and T. Michaels, 1996. Observational evidence of decadal-scale variability of the North Atlantic

Ocean. In *Natural Climate Variability on Decade-to-Century Time Scales*, National Academy Press, Washington, D.C.

Liebelt, P. B., 1967. *An introduction to Optimal Estimation,* Addison-Wesley, Reading, Mass., 273 pp.

Livingston, D. A., 1963. The data of geochemistry. *USGS professional paper,* **440-6**, 64 pp.

Lozier, M. S., W. B. Owens and R. G. Curry, 1995: The climatology of the North Atlantic, *Progress in Oceanography*, **36**, 1-44.

Macdonald A., 1995. Oceanic fluxes of mass, heat and freshwater: a global estimate and perspective. PhD dissertation, Mass. Inst. of Techn.- Woods Hole Oceanographic Institution Joint Program. 326 pp.

Maillard, C., 1986. Atlas hydrologique de l' Atlantique nord-est. Brest:IFREMER, 32 pp, 133 pls.

Mamayev, O. I., 1975: *Temperature-Salinity Analysis of World Ocean Waters*. Elsevier Oceanography Series, **11**, 374 pp.

Mamayev, O., H. Dooley, B. Millard and K. Taira, 1991. Processing of oceanographic station data. Joint panel on Oceanographic Tables and Standards (JPOTS). UNESCO, 138 pp.

Mantyla, A. W., 1994. The treatment of inconsistencies in Atlantic deep water salinity data. *Deep Sea Research, Part 1,* **41** , 1387-1405.

Mantyla, A. W. and J. L. Reid, 1983. Abyssal characteristics of the World Ocean waters. *Deep-Sea Research*, **30**, 805-833

McCartney, M. S., 1997. The North Atlantic Atmosphere-Ocean Oscillation. US. WOCE Implementation Report, **9**, 55-60

McCartney, M. S. and L. D. Talley, 1982. The subpolar mode water of the North Atlantic Ocean. *Journal of Physical Oceanography,* **12**, 1169-1188.

McCartney, M. S. and L. D. Talley, 1984. Warm to cold water conversion in the northern North Atlantic Ocean. *Journal of Physical Oceanography,* **14**, 922-935.

McCartney M. S., S. L. Bennet and M. E. Woodgate-Jones, 1991. Eastward Flow through the Mid-Atlantic Ridge at 11ºN and its influence on the Abyss of the Eastern Basin. *Journal of Physical Oceanography*, **21**, 1089-1121.

Millard, R. C., Jr, 1982. CTD calibration and data processing techniques at WHOI using the 1978 practical scale. Marine Technology Society Conference paper.

Millard, R. C., W. B. Owens and N. P. Fofonoff, 1990. On the calculation of the Brunt-Väisala frequency. *Deep-Sea Research*, **37**, (1), 167-181.

Millard, R. C., G. Bond and J. Toole, 1993. Implementation of a Titanium Strain Gauge Pressure Transducer for CTD Applications. *Deep-Sea Research*, **40**, (5), 1009-1021.

Millard, R. C. and K. Yang, 1993. CTD Calibration and Processing Methods used at Woods Hole Oceanographic Institution. Woods Hole Oceanographic Technical report WHOI 93-44. 104 pp.

Moisan, J. R. and P. P. Niiler, 1998. The Seasonal Heat Budget of the World Oceans. Abstract for Talks and Posters at the 1998 Conference of the World Ocean Circulation Experiment, Halifax, Canada, 24-29 May 1998. Poster. Page 70.

Molinari, R. L., E. Johns, and J. F. Festa, 1990. The Annual Cycle of Meridional Heat Flux in the Atlantic Ocean at 26.5ºN. *Journal of Physical Oceanography,* **20,** 476-482.

Newell, R. E., J. W. Kindson, D. G. Vincent, and G. J. Boer, 1974. The General Circulation of the Tropical Atmosphere and Interaction with Extratropical latitudes. Vol 2 MIT Press 68 pp.

Niiler, P. P. and W. S. Richardson, 1973. Seasonal Variability of the Florida Current *Journal of Marine Research*, **31**, (3), 144-167.

Oort, A. and Vonder Haar, T. H., 1976. On the Observed Annual Cycle in the Ocean-Atmosphere Heat Balance Over the Northern Hemisphere. *Journal of Physical Oceanography,* **6**, (6), 781-800.

Parrilla, G., A. Lavín, H. L. Bryden, M. J. García and R. Millard, 1994a. Rising temperatures in the subtropical North Atlantic Ocean over the past 35 years. *Nature* **369**, 48-51.

Parrilla, G., M. J. García, H. L. Bryden and R. Millard, 1994b. Informe de la Campaña HE06 (A-5, WOCE, 1992) Instituto Español de Oceanografía. 110 pp.

Parrilla, G., H. Bryden, A. Cruzado, M. J. García, J. Hernandez-Brito, A. Lavín, R. Millard, A. Rios, G. Rosón, W. Smethie, 1998. Inventory of the A-5 WOCE Section Data. Abstract for Talks and Posters at the 1998 Conference of the World Ocean Circulation Experiment, Halifax, Canada, 24-29 May 1998. Poster. Page 208.

Pelegrí, J. L. and G. T. Csanady, 1991. Nutrient transport and mixing in the Gulf Stream. *Journal of Geophysical Research,* **96,** 2577-2583

Pelegrí, J. L., G. T. Csanady and A. Martins, 1996. The North Atlantic Nutrient Stream. *Journal of Oceanography,* **52**. 275-299.

Pickart, R. S., 1992: Water mass components of the North Atlantic deep western boundary current. *Deep-Sea Research,* **39**, 1553-1572.

Pickart, R. S. and D. R. Watts, 1990. Deep western boundary current variability at Cape Hatteras. *Journal of Marina Research,* **48,** 765-791.

Pickart, R. S. and W. M. Smethie, 1993. How does the deep western Boundary Current cross the Gulf Stream. *Journal of Physical Oceanography,* **23,** 2602-2616.

Pingree, R. D., 1972: Mixing in the deep stratified ocean. *Deep-Sea Research*, **19**, 549-561.

Read, J. F., and W. J. Gould, 1992: Cooling and freshening of the subpolar North Atlantic Ocean since the 1960s. *Nature*, **360**, 55-57.

Reynaud T., LeGrand P., H. Mercier and B. Barnier, 1998. A new Analysis of hydrographic data in the Atlantic and its application to an inverse modelling study. *International WOCE Newsletter*, **32**, 29-31.

Rintoul, S.R and C. Wunsch, 1991. Mass, heat, oxygen and nutrient fluxes and budgets in the North Atlantic Ocean. *Deep-Sea Research,* **38** Suppl 1, S619-S644.

Robbins, P. E. and J. M. Toole, 1997. The dissolved silica budget as a constraint on the meridional overturning circulation of the Indian Ocean. *Deep Sea Research,* **44,** 5, 879-906.

Roemmich, D., 1980. Estimation of meridional heat flux in the North Atlantic by inverse methods *Journal of Physical Oceanography,* **10**, 1972-1983.

Roemmich, D., 1983. Optimal Estimation of Hydrographic Station Data and Derived Fields. *Journal of Physical Oceanography,* **13,** 1544-1549.

Roemmich, D., 1990. Sea level and the thermal variability of the ocean. In *Sea-Level Change*, National Academy Press, Washington, D.C., 208-217.

Roemmich, D., and C. Wunsch, 1984: Apparent changes in the climatic state of the deep North Atlantic Ocean. *Nature,* **307**, 447-450.

Roemmich, D. and Wunsch, C., 1985. Two transatlantic sections: Meridional circulation and heat flux in the subtropical North Atlantic Ocean. *Deep-Sea Research*, **32**, 619-664.

Rohling, E. J., and H. L. Bryden, 1992. Man-induced salinity and temperature increases in western Mediterranean deep water. *Journal of Geophysical Research*, **97**, 11191-11198.

Rosón, G., A. F. Ríos, A. Lavín, F. F. Pérez and H. L. Bryden. Carbon fluxes in the North Atlantic Ocean. Abstract for Talks and Posters at the 1998 Conference of the World Ocean Circulation Experiment, Halifax, Canada, 24-29 May 1998. Poster. Page 46.

Saunders, P.M., 1981. Practical conversion of pressure to depth. *Journal of Physical Oceanogaphy,* **11**, (4), 573-574.

Saunders, P. M., 1982. Circulation in the eastern North Atlantic. *Journal of Marine Research*, **40**, suppl. 641-657.

Saunders, P. M., 1986: The accuracy of measurement of salinity, oxygen and temperature in the deep oceans. *Journal of Physical Oceanography*, **16**, 189-195.

Saunders, P. M., 1987. Flow through Discovery Gap. *Journal of Physical Oceanography,* **17,** 631-543

Schmitt, R. W., P. S. Bogden, and C. E. Dorman, 1989: Evaporation minus precipitation and density fluxes for the North Atlantic. *Journal of Physical Oceanography,* **19**, 1208-1221.

Schmitz W. J. and W. S. Richardson, 1991. On the transport of the Florida Current. *Deep-Sea Research,* **15**, 679-693

Schmitz, W. J., and P. L. Richardson, 1992: On the sources of the Florida Current. *Deep-Sea Research*, **38,** (Suppl.) S379-S409.

Schmitz W. J., J. D. Thompson and J. R. Luyten, 1992. The Sverdrup Circulation for the Atlantic along 24º N. *Journal of Geophysical Research,* **97**, (C5), 7251-7256.

Schmitz, W. J. Jr., J. R. Luyten, and R. W. Schmitt, 1993: On the Florida Current T/S envelope. *Bulletin of Marine Science,* **53**, 1048-1065.

Schmitz, W. J. and M. S. McCartney, 1993. On the North Atlantic Circulation. *Reviews of Geophysics*, **31**, (1), 29-49.

Schlitzer, R., W. Roether, U. Weidmann, P. Kalt and H. H. Loosli, 1985. A meridional ^{14}C and ^{39}Ar section in northeast Atlantic deep water. *Journal of Geophysical Research,* **90**, C4, 6945-6952

Smethie, W. M., 1993. Tracing the thermohaline circulation in the western North Atlantic using chlorofluorocarbons. *Progress Oceanography*, **31**, 51-99

Speer, K. G. and M. S. McCartney, 1991. Tracing Lower North Atlantic Deep Water Across the Equator. *Journal of Geophysical Research,* 96, 20443-20448.

Stommel, H., 1980. Asymmetry of interoceanic fresh-water and heat fluxes. *Proc. Natt. Acad. Sci. USA*. **77,** 2377-2381.

Sy, A. and K. P. Koltermann, 1996. Cooling of the Intermediate layer in the Northern North Atlantic Ocean. *ICES C.M*. 1996/ O:**9**

Sy, A., M. Rhein, J. R. N. Lazier, K. P. Koltermann, J. Meincke, A. Putzka and M. Bersch, 1997. Surprisingly rapid spreading of newly formed intermediate waters across the North Atlantic Ocean. *Nature*, **386**, 675-679.

Thompson, W. J., 1984. *Computing in Applied Science*, Willey, New York.

Trenberth, K. E., W. G. Large, and J. G. Olson, 1990. The Mean Annual Cycle in Global Wind Stress. *Journal of Physical Oceanogaphy,* **20**, 1742-1760.

UNESCO, 1981: Background papers and supporting data on the Practical Salinity Scale 1978. *UNESCO Technical Papers in Marine Science*,. **37**, 144pp.

UNESCO, 1991: *Processing of Oceanographic Station Data*. UNESCO, 138pp.

Vonder Haar, T. H. and A. H. Oort, 1973. New Estimate of Annual Poleward Energy Transport by Northern Hemisphere Oceans. *Journal of Physical Oceanogaphy,* **2**, 169-172.

Warren B. A., 1981. Deep circulation of the world ocean. *In Evolution of Physical Oceanography*, B. A. Warren and C. Wunsch, Eds., MIT press. 6-41.

Whitledge, T. E., S. C. Malloy, C. J. Patton and C. D. Wirick., 1981. Automated nutrient analysis in seawater. Brookhaven National Laboratory, U.S. Dept. of Energy and Environment, Upton, NY. 216 pp.

Wijffels S. E., R. W. Schmitt, H. L. Bryden and A. Stigebrandt, 1992. Transport of freshwater by the oceans. *Journal of Physical Oceanography.* **22**, 155-162.

World Ocean Implementation Plan, 1988. *WMO/TD*, **242**.

Worthington, L. V., 1976. On the North Atlantic Circulation. The *John Hopkins Oceanographic Studies*, **6**, 110 pp.

Wright, W. R., and L. V. Worthington, 1970: *The Water Masses of the North Atlantic Ocean: A Volumetric Census of Temperatures and Salinity*. Serial Atlas of the Marine Environment, Folio 19, American Geographical Society, 88 pp and 7 plates.

Wunsch, C., 1978. The North Atlantic General Circulation West of 50ºW Determined by Inverse Methods. *Reviews of Geophysics and space physics*, **16**, (4) 583:620.

Wunsch, C., 1980. Meridional heat flux of the North Atlantic Ocean *Proceeding of the National Academy of Science*, **77**, 5043-5047.

Wunsch, C., 1985. Can a Tracer Field Be Inverted for Velocity?. *Journal of Physical Oceanogaphy,* **15**, 1521-1531.

Wunsch, C., 1989. Tracer inverse problems. Oceanic Circulation Models: Combining Data and Dynamics 1-77 pp. D.L.T. Anderson and J. Willebrand (eds.), Kluwer Academic Publishers.

Wunsch, C., 1996. The ocean Circulation Inverse Problem. Cambridge U. Press, 437 pp

Wüst, G., 1935. Schichtung und Zirkulation des Atlantischen Ozeans. Die Stratosphäre. In: Wissenschaftliche Ergebnisse der Deutschen Atlantischen Expedition auf dem Forschungsund Vermessungsschiff "Meteor" 1925-1927 **6** (2), 180 pp. (The Stratosphere of the Atlantic Ocean, W.J. EMERY, editor, 1978. Amerind, New Delhi, 112 pp.)